

## INFORMATION TO USERS

This manuscript has been reproduced from the microfilm master. UMI films the text directly from the original or copy submitted. Thus, some thesis and dissertation copies are in typewriter face, while others may be from any type of computer printer.

**The quality of this reproduction is dependent upon the quality of the copy submitted.** Broken or indistinct print, colored or poor quality illustrations and photographs, print bleedthrough, substandard margins, and improper alignment can adversely affect reproduction.

In the unlikely event that the author did not send UMI a complete manuscript and there are missing pages, these will be noted. Also, if unauthorized copyright material had to be removed, a note will indicate the deletion.

Oversize materials (e.g., maps, drawings, charts) are reproduced by sectioning the original, beginning at the upper left-hand corner and continuing from left to right in equal sections with small overlaps. Each original is also photographed in one exposure and is included in reduced form at the back of the book.

Photographs included in the original manuscript have been reproduced xerographically in this copy. Higher quality 6" x 9" black and white photographic prints are available for any photographs or illustrations appearing in this copy for an additional charge. Contact UMI directly to order.

# UMI

A Bell & Howell Information Company  
300 North Zeeb Road, Ann Arbor MI 48106-1346 USA  
313/761-4700 800/521-0600



RICE UNIVERSITY

**Dynamic Response of Hazardous Liquid-Waste  
Storage Tanks used in Nuclear Facilities**

by

**Shivakumar Padmanaban**

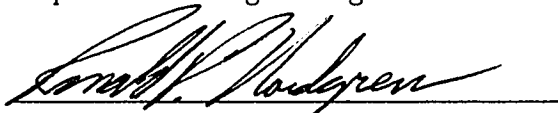
A THESIS SUBMITTED  
IN PARTIAL FULFILLMENT OF THE  
REQUIREMENTS FOR THE DEGREE

**Doctor of Philosophy**

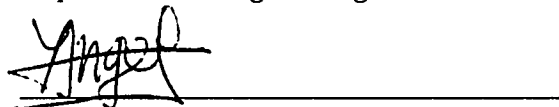
APPROVED, THESIS COMMITTEE:



Dr. Anestis Veletsos, Chairman  
Brown and Root Professor  
Dept. of Civil Engineering



Dr. Ronald Nordgren  
Hermann and George R. Brown Professor  
Dept. of Civil Engineering



Dr. Yves Angel  
Associate Professor  
Dept. of Mechanical Engineering and  
Material Science

Houston, Texas

April, 1996

**UMI Number: 9631083**

---

**UMI Microform 9631083**  
**Copyright 1996, by UMI Company. All rights reserved.**  
**This microform edition is protected against unauthorized**  
**copying under Title 17, United States Code.**

---

**UMI**  
**300 North Zeeb Road**  
**Ann Arbor, MI 48103**



# **Dynamic Response of Hazardous Liquid-Waste Storage Tanks used in Nuclear Facilities**

Shivakumar Padmanaban

## **Abstract**

This dissertation presents a comprehensive study of the dynamic response of storage tanks containing high-level radioactive wastes in nuclear facilities. Of the many issues that are peculiar to these systems, four important ones have been studied. Accordingly, the study is presented in four parts :

The first part deals with the dynamic response of flexible tanks that are placed inside concrete vaults and are attached to the vaults both at the top and the bottom. The tanks are presumed to be fixed at the base and supported by either a roller or a hinge at the top. The response quantities examined include the natural frequencies of vibration, the hydrodynamic pressures and the induced tank forces. The general trends are established by comparing the response quantities for the top-constrained systems with those for base-excited cantilever systems.

The second part deals with the response of rigid and flexible tanks containing stratified liquids. The liquid is considered to be arranged in layers with varying layer thicknesses and mass densities, or to be inhomogeneous with a continuously varying mass density. In addition to the free vibrational sloshing characteristics of the liquid, the responses examined include the vertical displacements at the free surface, and the impulsive and convective components of the hydrodynamic wall pressures and associated tank forces. A simplified analytical procedure that estimates the response quantities for the layered systems from corresponding solutions for homogeneous systems is also presented.

The third part presents an exploratory study for assessing the effects of tank-base flexibility on the response of vertically excited liquid storage tanks. A suitable model of the tank-liquid-foundation-soil system is considered, and the natural frequencies, the associated damping ratios and the induced pressures are studied for a wide range of base-flexibility values.

The final part estimates the effects induced by the impact of the sloshing liquid on the tank roof. Consideration is given not only to the effects that are induced on the roof but also to the effects that are transferred to the side-wall. Both rectangular and cylindrical systems are considered and the effect of changing the slope of the roof on the induced impact effects is also studied.

## Acknowledgments

It is with great pleasure that I acknowledge the encouragement and assistance provided by various people in the course of my doctoral studies.

First and foremost, I would like to express my deepest gratitude to my advisor, Dr. Anestis Veletsos. His guidance and advice at each juncture have been crucial to the development of this thesis. By giving me an opportunity to work on various exciting problems and by helping with suggestions and ideas whenever I was stuck, he provided an ideal environment for doing research.

Special thanks are due to Dr. Ronald Nordgren and Dr. Yves Angel for serving on my thesis committee and for their patience and understanding during the course of my research.

To Adel, I am grateful for our many conversations ranging from academics to politics to philosophy. To Kotax, my Latex Guru, for always being there to help me with any computer problem. To the 'Common Pool' for so many pleasant memories of the Rice experience. To Arati, for enriching my life in so many ways, and to my family, for their understanding and unequivocal support of all my decisions.

Finally, this research work was sponsored in part by Rice University and in part by Brookhaven National Laboratory. I am grateful for this financial support.

# Contents

Abstract	ii
Acknowledgments	iv
List of Tables	x
List of Illustrations	xiv
<b>1 Introduction</b>	<b>1</b>
1.1 Overview . . . . .	1
1.2 Objectives . . . . .	2
1.3 Scope of Work . . . . .	3
1.3.1 Response of Top-Constrained Tank-Liquid Systems . . . . .	3
1.3.2 Response of Layered/Inhomogeneous Tank-Liquid Systems . .	3
1.3.3 Effects of Tank-Base Flexibility . . . . .	5
1.3.4 Effects of Roof-liquid Impact . . . . .	5
<b>2 Dynamic Response of Top-Constrained Tanks</b>	<b>7</b>
2.1 Introduction . . . . .	7
2.2 System Considered . . . . .	8
2.3 Method of Analysis . . . . .	8
2.3.1 Natural Frequencies . . . . .	8
2.3.2 Impulsive Pressures . . . . .	10
2.3.3 Tank Forces . . . . .	11
2.4 Numerical Solutions . . . . .	12
2.4.1 Natural Frequencies . . . . .	12
2.4.2 Impulsive Pressures . . . . .	13
2.4.3 Tank Forces . . . . .	13
2.5 Conclusions . . . . .	16
<b>3 Sloshing Response of Layered Liquids in Rigid Tanks</b>	<b>29</b>
3.1 Introduction . . . . .	29

3.2	Systems Considered . . . . .	30
3.3	Fundamental Relations . . . . .	30
3.4	General Approach . . . . .	32
3.4.1	Solution for $\chi_j$ . . . . .	33
3.4.2	Solution for $\psi_j$ . . . . .	33
3.4.3	Equations of Motion for System . . . . .	35
3.5	Free Vibration . . . . .	37
3.5.1	Two-Layered System . . . . .	38
3.5.2	Numerical Solutions for Sloshing Frequencies and Modes . . .	39
3.6	Forced Vibration . . . . .	43
3.6.1	Sloshing Displacement Coefficients . . . . .	46
3.6.2	Hydrodynamic Pressures . . . . .	48
3.7	Numerical Example . . . . .	48
3.8	Conclusions . . . . .	49
<b>4</b>	<b>Hydrodynamic Effects in Rigid Tanks containing Layered Liquids</b>	<b>63</b>
4.1	Introduction . . . . .	63
4.2	Method of Analysis . . . . .	63
4.2.1	Hydrodynamic Pressures . . . . .	63
4.2.2	Tank Forces . . . . .	67
4.3	Presentation and Analysis of Numerical Solutions . . . . .	70
4.3.1	Hydrodynamic Wall Pressures . . . . .	70
4.3.2	Tank Forces . . . . .	74
4.4	Conclusions . . . . .	76
<b>5</b>	<b>Simplified Analysis of Layered Tank-Liquid Systems</b>	<b>93</b>
5.1	Introduction . . . . .	93
5.2	Background . . . . .	94
5.2.1	Rigid Tanks . . . . .	94
5.2.2	Flexible Tanks . . . . .	94
5.3	Flexible Layered Systems . . . . .	95
5.3.1	Approximate Evaluation of Fundamental Natural Frequency .	95
5.3.2	Approximate Evaluation of Second Natural Frequency . . . .	97

5.3.3	Exact Evaluation of Natural Frequencies of Vibration . . . . .	98
5.3.4	Numerical Results . . . . .	99
5.3.5	Extension to Tall Tanks . . . . .	100
5.4	Rigid Layered Systems . . . . .	101
5.4.1	Proposed Method of Analysis . . . . .	101
5.4.2	Adjustment to Proposed Method . . . . .	103
5.4.3	Other Approximate Methods . . . . .	105
5.5	Conclusions . . . . .	106

## **6 Dynamic Response of Rigid Tanks with Inhomogeneous Liquids 122**

6.1	Introduction . . . . .	122
6.2	System Considered . . . . .	123
6.3	Governing Equations . . . . .	123
6.3.1	Background Information . . . . .	123
6.3.2	Equation of Motion in Terms of a Single Unknown . . . . .	124
6.4	Free Vibration . . . . .	126
6.5	Forced Vibration . . . . .	130
6.5.1	Vertical Sloshing Displacements . . . . .	131
6.5.2	Hydrodynamic Pressures . . . . .	132
6.5.3	Tank Forces . . . . .	134
6.6	Numerical Solutions . . . . .	136
6.6.1	Sloshing Frequencies and Modes . . . . .	137
6.6.2	Sloshing Displacement Coefficients . . . . .	138
6.6.3	Hydrodynamic Pressures . . . . .	139
6.6.4	Hydrodynamic Tank Forces . . . . .	140
6.7	Approximation of Continuous Systems with Layered Systems . . . . .	141
6.7.1	Numerical Comparisons . . . . .	141
6.8	Conclusions . . . . .	143

## **7 Effects of Basemat Flexibility for Vertically Excited Liquid Storage Tanks 164**

7.1	Introduction . . . . .	164
7.2	System Considered . . . . .	165

7.2.1	Model Considered . . . . .	165
7.3	Method of Analysis . . . . .	165
7.3.1	Deflection Configuration . . . . .	166
7.3.2	Strain Energy . . . . .	167
7.3.3	Kinetic Energy . . . . .	167
7.3.4	External Work . . . . .	168
7.3.5	Equations of Motion . . . . .	168
7.4	Free Vibration . . . . .	170
7.4.1	Numerical Solutions . . . . .	170
7.4.2	Further Simplification . . . . .	172
7.5	Forced Vibration . . . . .	173
7.5.1	Hydrodynamic Pressure . . . . .	174
7.5.2	Numerical Solutions . . . . .	175
7.5.3	Implication of Results . . . . .	176
7.6	Incorporation of Damping . . . . .	177
7.6.1	Outline of method . . . . .	177
7.6.2	Damping for fundamental mode of vibration . . . . .	179
7.6.3	Damping for second mode of vibration . . . . .	181
7.6.4	Implication of results . . . . .	183
7.7	Conclusions . . . . .	183
<b>8</b>	<b>Effects of Roof-Liquid Impact</b>	<b>200</b>
8.1	Introduction . . . . .	200
8.2	System Considered . . . . .	201
8.3	Background . . . . .	202
8.4	Method of Analysis . . . . .	203
8.4.1	Fundamental Relations and Assumptions . . . . .	204
8.4.2	Impact Effects for Flat Roofs . . . . .	205
8.4.3	Impact Effects for Sloping Roofs . . . . .	213
8.5	Numerical Solutions . . . . .	216
8.5.1	Impact Effects for Flat Roofs . . . . .	216
8.5.2	Impact Effects for Sloping Roofs . . . . .	221
8.6	Conclusions . . . . .	224
	<b>Bibliography</b>	<b>238</b>

<b>A Hydrodynamic Effects for Rigid Layered Systems</b>	<b>246</b>
A.1 Derivation of Equation (4.12) . . . . .	246
A.2 Derivation of Equation (4.40) . . . . .	246
<b>B Modal Masses for Flexible Layered Systems</b>	<b>248</b>
<b>C Vertically Excited Systems with Flexible Base</b>	<b>252</b>
C.1 Velocity potential function $\phi$ . . . . .	252
C.2 Kinetic Energy . . . . .	253
C.3 Free Vibration of Equivalent Plate : Exact Solution . . . . .	254
C.3.1 Case 1 : $(C^*)^2 < 1$ . . . . .	255
C.3.2 Case II : $(C^*)^2 > 1$ . . . . .	255
<b>D Effects of Roof-Liquid Impact</b>	<b>257</b>
D.1 Background Information . . . . .	257
D.2 Wetting Correction Factor . . . . .	258
D.3 Virtual Liquid Mass . . . . .	259
D.4 Wall Pressures . . . . .	259
D.4.1 Rectangular Tanks . . . . .	259
D.4.2 Cylindrical Tanks . . . . .	261



## Tables

2.1	Values of frequency coefficients for first three modes of vibration for different values of $H/R$ and top-support conditions; Systems with $h/R = 0.001$ , $\nu = 0.3$ and $\rho_l/\rho = 0.127$ . . . . .	18
2.2	Values of coefficients $\alpha_1$ and $\alpha_{e1}$ in expressions for impulsive and convective components of base shear in top-constrained steel tanks; Systems with $h/R = 0.001$ , $\nu = 0.3$ and $\rho_l/\rho = 0.127$ . . . . .	19
2.3	Values of impulsive and convective moment coefficients at critical sections of cantilever and top-constrained steel tanks; Systems with $h/R = 0.001$ , $\nu = 0.3$ and $\rho_l/\rho = 0.127$ . . . . .	20
3.1	Surface-displacement coefficients for two-layered long rectangular and cylindrical systems . . . . .	51
3.2	Surface-displacement coefficients for three-layered cylindrical system with $H/R = 1$ and $H_1 = H_2 = H_3$ . . . . .	52
3.3	Natural frequencies and surface-displacement coefficients for system considered in numerical example . . . . .	53
3.4	Maximum values of surface displacements of liquid along tank wall for system considered in numerical example . . . . .	54
4.1	Values of coefficients in expression for hydrodynamic wall pressure at selected sections of two-layered systems with different $H/R$ and $H_2/H_1$ . . . . .	77
4.2	Normalized values of effective masses in expression for base shear of two-layered systems with different $H/R$ and $H_2/H_1$ . . . . .	79
4.3	Normalized values of coefficients in expression for overturning moment at a section immediately above tank base of two-layered systems with different $H/R$ and $H_2/H_1$ . . . . .	80
4.4	Normalized values of coefficients in expression for foundation moment of two-layered systems with different $H/R$ and $H_2/H_1$ . . . . .	81

4.5	Normalized values of effective masses in expression for base shear of three-layered systems with different $H/R$ and $H_1 = H_2 = H_3 = H/3$ .	82
4.6	Normalized values of coefficients in expression for overturning moment at a section immediately above tank base of three-layered systems with different $H/R$ and $H_1 = H_2 = H_3 = H/3$ . . . . .	83
4.7	Normalized values of coefficients in expression for foundation moment of three-layered systems with different $H/R$ and $H_1 = H_2 = H_3 = H/3$	84
5.1	Frequency coefficients for fundamental mode of vibration of two-layered systems with different $H/R$ and $H_2/H_1$ ; Systems with $h/R = 0.001$ , $\rho_2/\rho = 0.127$ and $\nu = 0.3$ . . . . .	108
5.2	Frequency coefficients for second mode of vibration of two-layered systems with different $H/R$ and $H_2/H_1$ ; Systems with $h/R = 0.001$ , $\rho_2/\rho = 0.127$ and $\nu = 0.3$ . . . . .	109
5.3	Frequency coefficients for first two modes of vibration of three-layered systems with different $H/R$ and $H_1 = H_2 = H_3 = H/3$ ; systems with $h/R = 0.001$ , $\rho_3/\rho = 0.127$ and $\nu = 0.3$ . . . . .	110
5.4	Ratios of approximate to exact values of impulsive component of base shear, base moment and foundation moment for rigid two-layered systems with different $H/R$ and $H_1/H$ . . . . .	111
5.5	Ratios of approximate to exact values of impulsive component of base shear, base moment and foundation moment for rigid three-layered systems with different $H/R$ and $H_1 = H_2 = H_3 = H/3$ . . . . .	112
6.1	Values of $\gamma_{mn}$ for systems with different $H/R$ and $\rho_1/\rho_o$ . . . . .	145
6.2	Surface displacement coefficients for systems with different $H/R$ and $\rho_1/\rho_o$ . . . . .	146
6.3	Normalized values of effective masses in expression for base shear of systems with different $H/R$ and $\rho_1/\rho_o$ . . . . .	147
6.4	Normalized values of coefficients in expression for overturning moment at a section immediately above tank base of systems with different $H/R$ and $\rho_1/\rho_o$ . . . . .	148
6.5	Normalized values of coefficients in expression for foundation moment of systems with different $H/R$ and $\rho_1/\rho_o$ . . . . .	149

6.6	Values of frequency coefficients $C_{mn}$ for layered and continuous systems with $H/R = 1$ and $\rho_1/\rho_o = 0.25$ . . . . .	150
6.7	Values of surface displacement coefficients $d_{mn}$ for layered and continuous systems with $H/R = 1$ and $\rho_1/\rho_o = 0.25$ . . . . .	150
6.8	Normalized values of effective masses in expression for base shear of a continuous system with $H/R = 1$ , $\rho_1/\rho_o = 0.25$ and its N-layered approximation . . . . .	150
6.9	Normalized values of coefficients in expression for overturning moment at a section immediately above tank base for a continuous system with $H/R = 1$ , $\rho_1/\rho_o = 0.25$ and its N-layered approximation . . . . .	151
6.10	Normalized values of coefficients in expression for foundation moment of a continuous system with $H/R = 1$ , $\rho_1/\rho_o = 0.25$ and its N-layered approximation . . . . .	151
7.1	Values of frequency coefficients for fundamental mode of vibration for different values of $H/R$ , $\beta_{em}$ and $D_p/kR^4$ ; $\beta_p = 0.1$ . . . . .	185
7.2	Values of frequency coefficients for second mode of vibration for different values of $H/R$ , $\beta_{em}$ and $D_p/kR^4$ ; $\beta_p = 0.1$ . . . . .	186
7.3	Comparison of approximate fundamental frequency coefficients to corresponding exact solutions for elastically supported equivalent plate; $\beta_{em} = 0.5$ . . . . .	187
7.4	Comparison of approximate frequency coefficients for second mode of vibration with corresponding exact solutions for elastically supported equivalent plate; $\beta_{em} = 0.5$ . . . . .	187
7.5	Values of wall pressure coefficients for fundamental mode of vibration for different values of $H/R$ , and $D_p/kR^4$ ; $\beta_{em} = 0.3$ , $\beta_p = 0.1$ . . . .	188
7.6	Values of wall pressure coefficients for fundamental mode of vibration for different values of $H/R$ , and $D_p/kR^4$ ; $\beta_{em} = 0.5$ , $\beta_p = 0.1$ . . . .	189
7.7	Values of radii of equivalent ring foundation for fundamental mode of elastically supported flexible plate; $\beta_{em} = 1.0$ . . . . .	190
7.8	Values of effective damping $\zeta_1$ for fundamental mode of vibration for different values of $H/R$ , $\beta_{em}$ and $D_p/kR^4$ ; $\beta_p = 0.1$ , $\nu_p = 0.17$ . . . .	191
7.9	Values of effective damping $\zeta_2$ for second mode of vibration for different values of $H/R$ , $\beta_{em}$ and $D_p/kR^4$ ; $\beta_p = 0.1$ , $\nu_p = 0.17$ . . . .	192

8.1	Values of maximum roof impact effects for flat-roofed cylindrical tanks with different values of $d_o/d_{max}$ . . . . .	226
8.2	Values of maximum wall impact force for flat-roofed cylindrical tanks with different values of $H/R$ and $d_o/d_{max}$ . . . . .	227
8.3	Values of maximum wall impact moment for flat-roofed cylindrical tanks with different values of $H/R$ and $d_o/d_{max}$ . . . . .	228
8.4	Comparison of maximum impact effects for representative flat-roofed cylindrical tanks with associated impulsive and convective effects . . .	229
8.5	Comparison of impact pressures corresponding to time of occurrence of maximum wall forces with maximum impulsive and convective pressures . . . . .	229
8.6	Values of maximum roof and wall impact effects for representative cylindrical tanks with sloping roofs with different values of $\alpha$ and $d_o/d_{max}$ . . . . .	230

## Illustrations

1.1	Types of underground tank-liquid systems used . . . . .	6
2.1	Top-constrained tank-liquid system considered . . . . .	21
2.2	Natural frequency coefficients for first three modes of vibration of roofless steel tanks filled with water; $h/R = 0.001$ , $\nu = 0.3$ , $\rho_l/\rho = 0.127$	22
2.3	Displacement configurations for fundamental mode of vibration of water-filled steel tanks with $H/R = 0.5$ supported differently at top; $h/R = 0.001$ , $\rho_l/\rho = 0.127$ , $\nu = 0.3$ . . . . .	23
2.4	Displacement configurations for fundamental mode of vibration of water-filled steel tanks with $H/R = 3.0$ supported differently at top; $h/R = 0.001$ , $\rho_l/\rho = 0.127$ , $\nu = 0.3$ . . . . .	24
2.5	Comparison of impulsive wall-pressure distribution functions for rigid tanks with fundamental modal pressure distribution functions for flexible tanks; latter systems with $h/R = 0.001$ , $\nu = 0.3$ , $\rho_l/\rho = 0.127$	25
2.6	Comparison of impulsive base-pressure distribution functions for rigid tanks with fundamental modal pressure distribution functions for flexible tanks;latter systems with $h/R = 0.001$ , $\nu = 0.3$ , $\rho_l/\rho = 0.127$	26
2.7	Total impulsive load for rigid tanks compared with corresponding load for the fundamental mode of vibration of flexible tanks; flexibility-independent convective load associated with fundamental sloshing mode also shown . . . . .	27
2.8	Heightwise distribution of fundamental impulsive moment coefficient $d_i(\eta)$ for steel tanks with different support conditions at top; $h/R =$ $0.001$ , $\rho_l/\rho = 0.127$ and $\nu = 0.3$ . . . . .	28
3.1	Systems considered . . . . .	55
3.2	Frequency coefficients $C_{1n}$ for fundamental horizontal mode of vibration of two-layered liquids in long rectangular tanks . . . . .	56

3.3	Frequency coefficients $C_{1n}$ for fundamental horizontal mode of vibration of two-layered liquids in cylindrical tanks . . . . .	57
3.4	Ratio of natural frequencies of two-layered and homogeneous liquids in cylindrical tanks . . . . .	58
3.5	Vertical displacement configuration for the fundamental horizontal mode of vibration of two-layered liquids in cylindrical tanks with $H/R = 0.5$ . . . . .	59
3.6	Vertical displacement configuration for the fundamental horizontal mode of vibration of two-layered liquids in cylindrical tanks with $H/R = 2.0$ . . . . .	60
3.7	Frequency coefficient $C_{1n}$ for the fundamental horizontal mode of vibration of three-layered liquids in cylindrical tanks and associated vertical displacement configurations for systems with $H/R = 1$ ; $H_1 = H_2 = H_3$ and $\rho_3/\rho_2/\rho_1 = 1/2/3$ . . . . .	61
3.8	Design response spectrum considered in numerical example . . . . .	62
4.1	Interrelationship of coefficients for impulsive and convective components of wall pressure for two-layered systems with $H/R = 1$ , $H_2/H_1 = 1$ and $\rho_2/\rho_1 = 0.5$ . . . . .	85
4.2	Interrelationship of coefficients for impulsive and convective components of wall pressure for three-layered system with $H/R = 1$ , $H_1 = H_2 = H_3 = H/3$ and $\rho_3/\rho_2/\rho_1 = 1/2/3$ . . . . .	86
4.3	Effect of $\rho_2/\rho_1$ on impulsive and fundamental convective pressure distributions for $H/R = 1.0$ , $H_2/H_1 = 1$ . . . . .	87
4.4	Effect of $H_2/H_1$ on convective pressure coefficient $c_{1n}(\eta)$ as $\rho_2/\rho_1$ tends to zero; system with $H/R = 1.0$ . . . . .	88
4.5	Impulsive and fundamental convective masses for two-layered systems with $H_2/H_1 = 1$ . . . . .	89
4.6	Normalized values of coefficients for impulsive and fundamental convective component of base moment for two-layered systems with $H_2/H_1 = 1$ . . . . .	90
4.7	Normalized values of coefficients for impulsive and fundamental convective component of foundation moment for two-layered systems with $H_2/H_1 = 1$ . . . . .	91

4.8	Convective masses for first two horizontal and two vertical modes of vibration of two-layered systems with $H_2/H_1 = 1$ . . . . .	92
5.1	Proposed procedure for representing a three-layered system in terms of three homogeneous sub-systems A, B and C . . . . .	113
5.2	Frequency coefficients for fundamental mode of vibration of two-layered steel tanks with $H_1 = H_2 = H/2$ , $\rho_2/\rho = 0.127$ , $h/R = 0.001$ , $\nu = 0.3$ . . . . .	114
5.3	Proposed approximate procedure for evaluating the impulsive wall-pressure distribution for a three-layered system in terms of those for its homogeneous sub-systems . . . . .	115
5.4	Approximate and exact impulsive wall-pressure distributions for two-layered system with $H/R = 1$ , $H_1 = H_2 = H/2$ , $\rho_2/\rho_1 = 0.5$ and for three-layered system with $H/R = 1$ , $H_1 = H_2 = H_3 = H/3$ , $\rho_3/\rho_2/\rho_1 = 1/2/3$ . . . . .	116
5.5	Ratios of approximate and exact impulsive base forces for two-layered systems with equal layer thicknesses; Approximate values computed by unadjusted proposed procedure . . . . .	117
5.6	Approximate, adjusted and exact impulsive pressure distributions for two-layered system with $H/R = 1$ , $H_1 = H_2 = H/2$ , $\rho_2/\rho_1 = 0.5$ and for three-layered system with $H/R = 1$ , $H_1 = H_2 = H_3 = H/3$ , $\rho_3/\rho_2/\rho_1 = 1/2/3$ . . . . .	118
5.7	Ratios of approximate and exact impulsive base forces for two-layered systems with equal layer thicknesses; Approximate values computed by adjusted proposed procedure . . . . .	119
5.8	Ratios of approximate and exact impulsive base forces for two-layered systems with equal layer thicknesses; Approximate values computed for a uniform liquid of the same average mass density . . . . .	120
5.9	Ratios of approximate and exact impulsive base forces for two-layered systems with equal layer thicknesses; Approximate values computed by using Method II . . . . .	121
6.1	System considered . . . . .	152
6.2	Vertical variations of liquid density for different values of $\rho_1/\rho_o$ and $\beta$ . . . . .	153

6.3	Frequency coefficients $C_{1n}$ for the fundamental horizontal mode of vibration of systems with different values of $H/R$ and $\rho_1/\rho_o$ . . . . .	154
6.4	Vertical modes of vibration associated with fundamental horizontal mode of systems with $H/R = 1$ . . . . .	155
6.5	Surface displacement coefficients for fundamental horizontal mode of vibration of systems with different values of $H/R$ and $\rho_1/\rho_o$ . . . . .	156
6.6	Effect of liquid density ratio $\rho_1/\rho_o$ on coefficients for impulsive and convective components of wall pressure for systems with $H/R = 1.0$ .	157
6.7	Coefficients $\bar{c}_o(\eta)$ and $\bar{c}_{11}(\eta)$ in expressions for impulsive and fundamental convective components of wall pressure for systems with $H/R = 1.0$ . . . . .	158
6.8	Normalized values of impulsive and fundamental convective masses for systems with different $H/R$ and $\rho_1/\rho_o$ . . . . .	159
6.9	Normalized values of coefficients for impulsive and fundamental convective components of base moment for systems with different $H/R$ and $\rho_1/\rho_o$ . . . . .	160
6.10	Normalized values of coefficients for impulsive and fundamental convective components of foundation moment for systems with different $H/R$ and $\rho_1/\rho_o$ . . . . .	161
6.11	Configurations of vertical modal displacements for $m=1$ and $n = 1, 2, 3$ for continuous system and its layered approximation; $H/R = 1$ , $\rho_1/\rho_o = 0.25$ , $N = 10$ . . . . .	162
6.12	Comparison of wall pressure distributions for continuous system with $H/R = 1$ and $\rho_1/\rho_o = 0.25$ with those of its layered approximation .	163
7.1	System considered . . . . .	193
7.2	Frequency coefficients for first two modes of vibration for elastically supported flexible base plate hinged at edge; $H/R = 1$ , $\beta_p = 0.1$ , $\nu_p = 0.17$ . . . . .	194
7.3	Frequency coefficients for first two modes of vibration for elastically supported flexible base plate clamped at edge; $H/R = 1$ , $\beta_p = 0.1$ , $\nu_p = 0.17$ . . . . .	195
7.4	Modal displacement amplitudes for first two modes of vibration of elastically supported flexible plate; $H/R = 1$ , $\beta_p = 0.1$ , $\nu_p = 0.17$ , $D_p/kR^4 = 0.02$ . . . . .	196



7.5	Modal displacement amplitudes for first two modes of vibration of elastically supported flexible plate; $H/R = 1$ , $\beta_p = 0.1$ , $\nu_p = 0.17$ , $D_p/kR^4 = 0.001$ . . . . .	197
7.6	Wall and base pressure distributions for first two modes of vibration; Systems with $H/R = 1$ , $\beta_p = 0.1$ , $\nu_p = 0.17$ , $D_p/kR^4 = 0.02$ . . . . .	198
7.7	Wall and base pressure distributions for first two modes of vibration; Systems with $H/R = 1$ , $\beta_p = 0.1$ , $\nu_p = 0.17$ , $D_p/kR^4 = 0.001$ . . . . .	199
8.1	System considered . . . . .	231
8.2	Impacted roof areas for different values of $d_o/d_{max}$ . . . . .	232
8.3	Variation of normalized roof impact force with time for flat-roofed rectangular and cylindrical systems with $d_o/d_{max} = 0.5$ . . . . .	233
8.4	Variation of wall impact response coefficients with time for flat-roofed cylindrical systems; $H/R = 1$ , $d_o/d_{max} = 0.5$ . . . . .	234
8.5	Wall pressure distributions corresponding to time of occurrence of maximum wall forces for different values of $H/R$ and $d_o/d_{max}$ . . . . .	235
8.6	Comparison of roof impact forces for rectangular and cylindrical systems with different angles of roof slope $\alpha$ ; Tank-liquid system considered is System 2; $H = R = 35$ ft, $d_{max} = 3.8$ ft, $v_{max} = 5.2$ ft/s, $d_o = 0.5d_{max}$ . . . . .	236
8.7	Comparison of wall impact response coefficients for cylindrical systems with different angles of roof slope $\alpha$ ; Tank-liquid system considered is System 2; $H = R = 35$ ft, $d_{max} = 3.8$ ft, $v_{max} = 5.2$ ft/s, $d_o = 0.5d_{max}$ . . . . .	237

# Chapter 1

## Introduction

### 1.1 Overview

Deeply embedded and underground tanks storing high-level radioactive wastes are critical components in nuclear facilities, and it is important that they be designed to withstand safely the earthquakes to which they may be subjected. Failure of these systems, which may typically contain up to a million gallons of waste, may have catastrophic consequences, and their safety is of major concern at the present time.

There are two types of underground tanks currently in use, as shown in Fig. 1.1 : the *single-shell tank* which is composed of a steel liner adjoining a concrete vault; and the *double-shell system* which is composed of a steel tank embedded in a nearly rigid concrete vault. The tank in the latter case may be either free-standing or constrained by the surrounding vault at the top.

Current understanding of the seismic response of liquid-containing upright cylindrical tanks is mainly derived from analyses of ground-supported, base-excited cantilever systems that contain homogeneous liquids. For a detailed account of this knowledge, the reader is referred to the state-of-the art report by Veletsos [65] and to the references of more recent publications by Haroun et al, [17, 18, 19], Lau and Zeng [36], Veletsos et al [67, 69, 70] and Malhotra et al [40]. The rational analysis of the underground tanks that are of current interest requires the solution of a number of special problems :

1. Being embedded in the ground, the effects of soil-structure interaction may be important and must be considered. For the single-shell tanks, the interaction effects of interest are those of the liquid-tank system with the surrounding soil, whereas for the double-shell systems, provision must also be made for the interaction of the concrete vault with the enclosed steel tank.
2. Many of the steel tanks in the double-shell systems are connected at the top to the surrounding concrete vault. The top constraint may affect significantly the

magnitude and distribution of the resulting hydrodynamic forces in the tank and must be considered.

3. The contents of many of these tanks cannot adequately be modeled as homogeneous liquids but must be approximated as layered liquids with varying layer thicknesses and mass densities or as inhomogeneous liquids with continuously varying mass densities. The effects of this density stratification on the hydrodynamic effects may be important and need to be assessed.
4. The base plate of the tank-liquid system is usually assumed to be rigid. This may not be true in many cases, particularly when the base-plate to soil stiffness is small and the distribution of the superposed tank and liquid inertias is non-uniform. It is necessary to evaluate the adequacy of the rigid-base assumption and assess the effects of base-flexibility on the induced hydrodynamic response.
5. Surface-waves, with displacement amplitudes larger than the available free-board, will impact the tank-roof. The impact pressures and forces that are then transmitted to the side-wall of the tank can be significant and need to be evaluated.

The embedded tank-liquid systems of current interest have also been the subject of parallel studies at Rice University, [73, 74, 75]. Some of the issues related to item 1 have been addressed by these studies. Many of the remaining issues are addressed in this dissertation.

## 1.2 Objectives

The principal aim of this study is to provide valuable insight into the various issues governing the dynamic response of tanks storing high-level radioactive liquid wastes in nuclear facilities. The specific objectives of this study are :

1. To determine the hydrodynamic response of top-constrained systems and highlight the interrelationship of such systems with the corresponding response of cantilever systems.
2. To assess the effects of density stratification on the hydrodynamic response through comprehensive studies of both rigid and flexible systems containing layered and inhomogeneous liquids.
3. To evaluate the effects of foundation flexibility on the hydrodynamic response of vertically excited liquid storage tanks.

4. To evaluate the effects of surface waves impacting the tank-roof, with special attention given to the magnitude and distribution of the resulting wall pressures and tank forces.

The tanks are presumed to be of circular cross-section, uniform wall thickness and to be fully anchored to a horizontally moving rigid base. The contained liquid is considered to be incompressible, irrotational and inviscid, and only linear actions are examined.

The focus of the proposed study is to formulate methods of analysis and to generate information and concepts with which the effects of the factors enumerated may be evaluated rationally and cost-effectively. It is expected that the results of the proposed studies will prove of value in the evaluation of the seismic safety of existing tanks as well as in the design of new tanks. The scope is outlined briefly in the following section.

## **1.3 Scope of Work**

### **1.3.1 Response of Top-Constrained Tank-Liquid Systems**

Chapter 2 deals with the hydrodynamic effects induced in tank-liquid systems that are constrained at the top and excited simultaneously and similarly at the top and bottom. The tanks are presumed to be fixed at the base and supported by either a roller or a hinge at the top. The response quantities examined include the natural frequencies of vibration, the hydrodynamic pressures and the induced tank forces. The procedures formulated are used for evaluating both impulsive and convective components of the tank forces. Extensions of procedures originally developed for cantilever systems are used for this purpose. The general trends are established by comparing the response quantities for the top-constrained systems with those for base-excited cantilever systems.

### **1.3.2 Response of Layered/Inhomogeneous Tank-Liquid Systems**

The response studies for these systems are presented in Chapters 3, 4, 5 and 6.

In Chapter 3, the sloshing action of layered liquids in rigid cylindrical and long rectangular tanks is investigated considering both their free vibrational characteristics and their response to a horizontal component of base shaking. Special attention is given to the maximum surface displacement induced by the base motion. The analysis

is formulated for systems with  $N$  superimposed layers of different thicknesses and densities, and it is illustrated by a numerical example. In addition, comprehensive numerical data are presented for two-layered and some three-layered systems which elucidate the underlying response mechanisms and the effects and relative importance of the numerous parameters involved.

In Chapter 4, the hydrodynamic wall pressures and the associated tank forces induced by horizontal ground shaking in rigid, vertical, circular cylindrical tanks containing liquid layers of different thicknesses and mass densities are examined, and comprehensive numerical solutions are presented for two-layered and some three-layered systems. Both the impulsive and convective actions are studied.

Chapter 5 presents a simplified analytical procedure to assess the dynamic response of both rigid and flexible layered tank-liquid systems. A simple concept is proposed to estimate the natural frequencies of the dominant modes of vibration of the flexible layered systems. The layered system in the proposed approach is represented as a series of sub-systems containing uniform, homogeneous liquids of different heights and densities, and frequency expressions based on the Dunkerley procedure are developed. The approximate frequency solutions are compared with rigorously computed exact solutions over a wide range of parameters. The underlying concept is then extended to rigid layered systems and the associated impulsive response coefficients are estimated by superposing corresponding solutions for the homogeneous sub-systems.

In Chapter 6, a study of the response to horizontal ground shaking of rigid cylindrical tank containing an inviscid liquid with a continuous vertical variation in density is presented. In addition to the free vibrational sloshing characteristics of the liquid, the responses examined include the vertical displacements at the free surface, and the impulsive and convective components of the hydrodynamic wall pressures and associated tank forces. The equations of motion for the system are formulated for an arbitrary variation in liquid density but the solutions presented are for a density that increases exponentially from top to bottom. Comprehensive numerical data are included which elucidate the underlying response mechanisms and the effects and relative importance of the various parameters involved. The solution for the continuous density variation considered are also compared with the solutions previously reported in Chapters 3 and 4, in which the liquid was modeled as a multi-layered, discrete system.

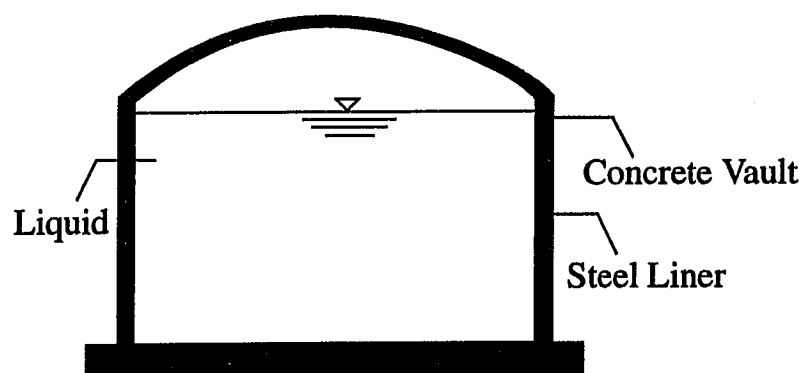
### 1.3.3 Effects of Tank-Base Flexibility

In Chapter 7, an exploratory study for assessing the effects of tank-base flexibility on the response of vertically excited liquid storage tanks is presented. The foundation is modeled as a flexible circular plate supported on a soil represented by Winkler springs. The effects of the tank wall, roof and participating soil inertias are represented by a mass distributed along the periphery of the plate. Different conditions of rotational constraint are considered at the junction of the wall and plate, including the limiting cases of hinged and fixed edge-supports. The response quantities of interest include the natural frequencies of the system, the associated mode shapes, the modal damping ratios, and the hydrodynamic pressures that are induced on the tank-wall and base. Results are obtained over a wide range of parameters to assess the effects of the base-flexibility.

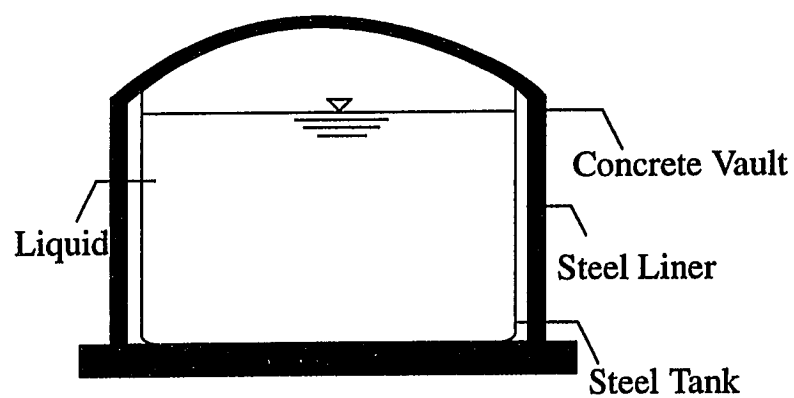
### 1.3.4 Effects of Roof-liquid Impact

The objective of Chapter 8 is to estimate the effects induced by the impact of the sloshing liquid on the tank roof and those that are then transmitted to the side-wall. The emphasis of the effort is to obtain conservative, yet realistic estimates of the impact effects. The study is initially confined to two-dimensional motions in long, rectangular tanks and the results are then used to obtain conservative estimates of the corresponding effects in cylindrical tanks.

The kinematics of a design impact wave are defined such that the wave can be presumed to produce the maximum impact effects during the time history of the liquid sloshing. The magnitude and temporal variation of the roof impact force due to the design wave are then derived by using an impulse-momentum relation. The added hydrodynamic mass of the impacted length of the roof plate is used in this computation. The effects are evaluated for both flat and sloping roofs and the validity of the results is established by comparing them with limited experimental/empirical data available in the literature [31, 64]. Procedures are then formulated for evaluating the impact pressures and forces transmitted to the tank wall. Comprehensive numerical solutions are finally presented for the roof and wall impact effects and their importance is ascertained by comparing them with previously established impulsive and convective effects.



(a) Single-Shell Tank



(b) Double-Shell Tank

Figure 1.1 : Types of Underground Tank-Liquid Systems Used

## Chapter 2

# Dynamic Response of Top-Constrained Tanks

### 2.1 Introduction

Many tanks used to store liquid radioactive wastes in nuclear facilities are underground and are embedded in vaults. Furthermore, they are attached to the vaults in such a manner that during an earthquake, they are excited simultaneously at the top and base. Fundamental to the analysis and design of the inner tank of these double-shell systems is a thorough understanding of the hydrodynamic effects in constrained systems. The objectives of this chapter are :

- To highlight the nature of the hydrodynamic effects induced in tanks that are supported at the top and experience the same input motion at that level as at the base; and
- To establish the interrelationship of the response of the top-constrained systems to the well-established response of free-standing, cantilever systems.

The governing expressions are presented in a form similar to those for the cantilever systems, and the effects of the top-constraint on the associated response coefficients are assessed by suitably using/modifying existing methods and programs for cantilever systems.

The response quantities of interest include the natural frequencies of the vibrating tank-liquid system, the impulsive pressures exerted against the tank wall and base, the shears at the top and the base, the base moment and the foundation moment. Both impulsive and convective components of the induced tank forces are considered. Selected numerical data are presented in order to elucidate the action of the top-constraint, and the effects and relative importance of the numerous parameters that influence the response.



## 2.2 System Considered

The system investigated is as shown in Fig. 2.1. It is an upright, circular, cylindrical tank of radius  $R$  and is filled with liquid to a height  $H$ . The tank is presumed to be bonded to a moving rigid base and to be supported by either a roller or a hinge at the top. While a roller support allows axial displacement and prevents the tangential and radial displacements, a hinge support does not permit displacements in any direction. The liquid is considered to be incompressible and inviscid. Only linear actions are examined. The mass densities of the tank and liquid are denoted by  $\rho$  and  $\rho_l$ , and the modulus of elasticity and Poisson's ratio for the tank material are denoted by  $E$  and  $\nu$ , respectively. Points for the tank and contained liquid are defined by the cylindrical coordinate system,  $r$ ,  $\theta$  and  $z$ , as shown in Fig. 2.1.

The system is presumed to be excited by a uniform horizontal motion directed along the  $\theta = 0$  coordinate axis. The constrained system is excited simultaneously and similarly at the base and at the level of the top-support. The acceleration of the ground motion at any time  $t$  is denoted by  $\ddot{x}_g(t)$ . The corresponding velocity and displacement is denoted by  $\dot{x}_g(t)$  and  $x_g(t)$  respectively.

## 2.3 Method of Analysis

Since the convective component is associated with motions of significantly lower frequencies than the natural frequencies of the tank-liquid system or the dominant frequencies of the excitation, the sloshing frequencies and the convective pressures remain practically unaffected by the flexibility of the tank wall or by the condition of top-support and can be conveniently evaluated from well-established expressions for rigid tanks, [65]. Hence it is only necessary to assess the impulsive frequencies and the impulsive component of the hydrodynamic pressure for the constrained tank-liquid systems. These are deduced herein by extending existing methods for flexible cantilever systems, [82]. Both impulsive and convective components of the induced shears and moments in the tank are, however, affected by the condition of top-support and the methods developed in the study cater to both response components.

### 2.3.1 Natural Frequencies

The constrained system is replaced by a cantilever system that possesses springs of large finite stiffnesses,  $k$ , per unit circumferential length of the shell at the top. The

number of springs are taken equal to the number of displacement components that are curtailed at that level : 2 for a roller support and 3 for a hinge support.

The analysis then follows well-established principles for cantilever systems, ([55, 82]). The fundamental principles are briefly summarized here and the reader is referred to [55, 82] for more details. The basic scheme used is the Rayleigh Ritz method in combination with Lagrange's equations of motion. The axial, radial and tangential components of displacement,  $u$ ,  $v$ , and  $w$ , respectively, are expressed as linear combinations of the natural modes of vibration of a uniform, cantilever beam,  $\psi(z)$ , or of the first derivatives of the modes,  $\psi'(z)$ .

$$u = \sum_{i=1}^{N_1} U_i(t) \psi'(z) \cos\theta \quad v = \sum_{i=1}^{N_2} V_i(t) \psi(z) \sin\theta \quad w = \sum_{i=1}^{N_3} W_i(t) \psi(z) \cos\theta \quad (2.1)$$

where  $U_i(t)$ ,  $V_i(t)$  and  $W_i(t)$  are time-dependent coefficients with units of length indicating the degree of participation of each mode;  $N_1$ ,  $N_2$  and  $N_3$  are the number of terms used in the series expressions.

Using the above expressions for the displacement components, the strain energy of the shell is evaluated in a manner consistent with Flugge's theory for cylindrical shells. For the top-constrained systems considered, due consideration is also provided for the strain energy,  $S_s$ , stored in the springs located at the top of the tank,

$$S_s = \frac{1}{2} \int_0^{2\pi} k w(H)^2 R d\theta = \frac{\pi}{2} k R \sum_{i=1}^{N_3} \sum_{j=1}^{N_3} W_i(t) W_j(t) \psi_i(H) \psi_j(H) \quad (2.2)$$

The total kinetic energy of the system which includes the contributions of the shell and the liquid is then evaluated. The distributed inertia force of the shell and the impulsive pressure on the wall of a rigid tank, are used to compute the virtual work performed by the external forces. The differential equations of motion are then obtained by repeated application of Lagrange's equation and can be expressed in matrix form as

$$[M]\{\ddot{q}\} + [K_c]\{q\} = -\{P\}\ddot{x}_g(t) \quad (2.3)$$

where  $[M]$  and  $[K_c]$  represent the mass and stiffness matrices respectively, and  $\{P\}$  represents the loading vector.  $\{q\}$  is the vector of displacement coefficients given by

$$\{q\} = \{U_1, U_2, \dots, U_{N_1}, V_1, V_2, \dots, V_{N_2}, W_1, W_2, \dots, W_{N_3}\}^T \quad (2.4)$$

While  $[M]$  and  $\{P\}$  remain unchanged for the cantilever and spring-supported systems,  $[K_c]$  for the top-constrained system is established as the sum of two matrices :  $[K]$  for the cantilever tank and a matrix representing the effect of the top-support.

Now, on neglecting the right hand side and expressing  $\{q(t)\}$  in the form,

$$\{q\} = \{\hat{q}\}e^{i\omega t} \quad (2.5)$$

and substituting in equation (2.3), one obtains

$$[K_c]\{\hat{q}\} = \omega^2[M]\{\hat{q}\} \quad (2.6)$$

This free-vibration problem is then solved to obtain the natural frequencies,  $f_k$ , and the corresponding modes of vibration,  $\hat{q}_k$ .

### 2.3.2 Impulsive Pressures

With the natural frequencies and modes established, the impulsive pressures are evaluated by using the modal superposition method. The steps followed are identical to those for the cantilever systems, [55], and are not repeated here. The pressures exerted on the wall and base of the constrained tank,  $p_i(z, \theta, t)$  and  $p_i(r, \theta, t)$  respectively, are finally expressed in the form

$$p_i(z, \theta, t) = \sum_{n=1}^{\infty} c_n(z) \rho_l R A_n(t) \cos\theta \quad (2.7)$$

and

$$p_i(r, \theta, t) = \sum_{n=1}^{\infty} c_n(r) \rho_l R A_n(t) \cos\theta \quad (2.8)$$

where  $c_n(z)$  and  $c_n(r)$  are dimensionless functions that define, respectively, the height-wise and radial variations of the impulsive pressure component associated with the  $n$ th natural mode of vibration of the constrained system;  $A_n(t)$  is the instantaneous pseudoacceleration of a similarly excited single-degree-of-freedom (SDOF) oscillator with natural frequency and damping equal to those of the  $n$ th natural mode of vibration of the tank-liquid system and is given by

$$A_n(t) = \frac{\omega_n}{\sqrt{1 - \zeta_n^2}} \int_0^t \ddot{x}_g(\tau) \exp[-\zeta_n \omega_n(t - \tau)] \sin[\bar{\omega}_n(t - \tau)] \quad (2.9)$$

The quantities  $\omega_n$  and  $\bar{\omega}_n$  in equation (2.9) are the  $n$ th undamped and damped circular natural frequencies of the constrained system, respectively;  $\zeta_n$  represents the damping factor for the  $n$ th mode of vibration; and  $\tau$  is a dummy time variable. The maximum values of  $A_n(t)$  are the quantities normally displayed in a response spectrum.

### 2.3.3 Tank Forces

With the hydrodynamic pressures established, the induced tank forces can be computed by means of a pseudo-static analysis. The maximum pressure is evaluated and is applied as a static load, and the resulting tank forces can be computed by means of an appropriate shell theory using any one of a number of existing computer programs. Alternatively, the support reactions and internal forces at critical sections may be computed by use of the beam and ring theories in a manner analogous to that normally employed for cantilever tanks. The latter approach is used in the present study. This requires the evaluation of the reactions at the level of the top-support. The *method of consistent deformation* is applied herein to evaluate the top-support reactions.

The top-constraint is removed so as to render the tank free at the top and the spectral value of the impulsive pressure that was computed in the previous section is applied as a static load on the cantilever system. The resulting displacements at the top that were initially constrained by the top-support are then given by

$$\{\Delta_i\} = [K]^{-1} \{f_i\} \quad (2.10)$$

where  $\{\Delta_i\}$  is the vector of top displacements associated with the impulsive load: it comprises of the  $v$  and  $w$  displacement components for the roller case, and  $u$ ,  $v$  and  $w$  displacement components for the hinged case;  $[K]$  is the stiffness matrix for the cantilever system; and  $\{f_i\}$  is the load vector due to the applied impulsive pressure.

Unit loads along the circumferential length of the shell at the top are then successively applied in each of the directions that were initially constrained and the resulting displacement matrix,  $[\delta]$ , is evaluated. The vector of top-support reactions,  $\{r_i\}$ , is then evaluated from

$$\{r_i\} = [\delta]^{-1} \{\Delta_i\} \quad (2.11)$$

With  $\{r_i\}$  established, the shear and moment distributions along the tank-wall are easily established from equilibrium considerations.

The top-reactions and the associated shears and moment distributions induced by the convective pressure can be evaluated in a similar manner. The convective pressure, evaluated herein from well-established rigid-tank expressions, is applied as a static load on the cantilever system and the top displacement vector  $\{\Delta_c\}$  is evaluated. The vector of associated top-support reactions is then given by

$$\{r_c\} = [\delta]^{-1} \{\Delta_c\} \quad (2.12)$$

## 2.4 Numerical Solutions

### 2.4.1 Natural Frequencies

The natural frequency in cycles per second of the  $n$ th mode of vibration of the tank-liquid system,  $f_n$ , is conveniently expressed in the form

$$f_n = \frac{C_n}{2\pi H} \sqrt{\frac{E}{\rho}} \quad (2.13)$$

where  $C_n$  is a dimensionless coefficient that depends on  $H/R$ ,  $h/R$ ,  $\nu$ ,  $\rho_l/\rho$  and the condition of top-support.

The frequency coefficients for the first three modes of vibration are plotted in Fig. 2.2 as a function of  $H/R$  for three conditions of top-support. For these solutions,  $h/R = 0.001$ ,  $\nu = 0.3$  and  $\rho_l/\rho = 0.127$ . The associated values of the frequency coefficients are also listed in Table 2.1. The following trends can be observed:

- The effect of the top constraint is negligibly small for broad tanks with values of  $H/R$  of the order of 0.3 to 0.5. The effect, however, increases in importance for tall, slender tanks.
- The effect of the top constraint is greatest for the fundamental natural frequency of the system, and of decreasing importance for the higher frequencies.
- There is practically no difference in the results obtained for the roller and hinge conditions of top support.

Additional results for tanks having clamped top-boundaries (fixed against rotation) have been presented in [66] and again it has been demonstrated that the natural frequency coefficients are quite insensitive to the degree of top-constraint.

Further insight into the greater importance of the top-constraint on the fundamental natural frequencies of tanks of higher slenderness ratios may be obtained from an examination of the natural modes of vibration. Figs. 2.3 and 2.4 show the configurations of the displacement components,  $u$ ,  $v$  and  $w$ , for cantilever and top-constrained tanks with  $H/R = 0.5$  and  $3.0$  respectively. It is seen that the broad cantilever tanks exhibit shear-beam type behavior and the top displacements are quite small. On the other hand, tanks with higher slenderness ratios exhibit flexural-beam type behavior and the top displacements are substantial. The introduction of a top constraint could, therefore, be expected to have inconsequential effects on the natural modes and associated frequencies for broad tanks. On the other hand, it could affect the corresponding quantities for slender tanks appreciably.

### 2.4.2 Impulsive Pressures

The distribution functions for the impulsive pressures,  $c_n(z)$  and  $c_n(r)$ , are a function of  $H/R$ ,  $h/R$ ,  $\rho_l/\rho$ ,  $\nu$  and the condition of support at the top. In the following discussion, the contribution of only the fundamental mode of vibration will be considered. Based on previous studies of cantilever systems, this simplification is deemed to be totally acceptable for realistic tanks with values of  $H/R \leq 1$ .

The function  $c_1(z)$  for the fundamental impulsive mode of vibration of tanks with either a roller or a hinge at the top are compared with those for cantilever tanks in Fig. 2.5. Results for rigid tanks are also shown in the figure. Three values of  $H/R$  in the range between 0.5 and 3.0 are considered. Similar results for  $c_1(r)$  are presented in Fig. 2.6. The following trends are worthy of note:

- There is no significant difference in the results obtained for the roller and hinge conditions of support. In fact, the curves for the two cases are practically indistinguishable from each other.
- For broad tanks with values of  $H/R$  of the order of 0.5, the wall pressure distributions are practically independent of the degree of the top-constraint and the pressure distributions for all three conditions of top-support and for rigid tanks are essentially the same. On the other hand, for tall, slender tanks with  $H/R$  of the order of 3.0, the pressure values for tanks with free and constrained top boundaries are significantly different.
- The solutions for the top-constrained tanks are closer to the rigid tank solutions than those of the cantilever tanks. It follows that the impulsive pressure distributions for the flexible constrained tanks may be approximated by those of rigid tanks over a wider range of  $H/R$  values than is acceptable for flexible cantilever tanks.

### 2.4.3 Tank Forces

#### Total Force

The instantaneous value of the total hydrodynamic force exerted against the tank wall,  $P(t)$ , may be expressed by the sums of a series of impulsive and convective components as

$$P(t) = \sum_{n=1}^{\infty} m_n A_n(t) + \sum_{n=1}^{\infty} m_{cn} A_{cn}(t) \quad (2.14)$$

where  $m_n$  represents the effective mass of the tank-liquid system vibrating in its  $n$ th impulsive mode and  $m_{cn}$  is the mass associated with the  $n$ th sloshing mode of vibration of the liquid.

The values of  $m_1$  normalized with respect to the total liquid mass,  $m_l = \rho_l \pi R^2 H$ , are plotted in Fig. 2.7 for water-filled steel tanks constrained, respectively, by a roller and hinge at the top. Normalized values of  $m_{c1}$  obtained by integrating the corresponding rigid tank pressure distributions are also shown in the figure. For the impulsive component, it is seen that there are no significant differences in the results for the two conditions of top-support. Furthermore, the results are relatively independent of wall-flexibility and of the condition of top-support for the broad tanks, while for taller tanks, the values for the top-constrained systems are closer to the values of  $m_o$  for rigid tanks than the corresponding cantilever systems.

### Base Shear

The instantaneous value of the base shear,  $Q_b(t)$ , may be expressed in the form

$$Q_b(t) = \sum_{n=1}^{\infty} \alpha_n m_n A_n(t) + \sum_{n=1}^{\infty} \alpha_{cn} m_{cn} A_{cn}(t) \quad (2.15)$$

in which  $\alpha_n$  and  $\alpha_{cn}$  are dimensionless factors representing the contributions of the  $n$ th impulsive and convective modes respectively.

The values of  $\alpha_1$  and  $\alpha_{c1}$  for the water-filled steel tanks of current interest are presented in Table 2.2 for both roller and hinge conditions of top-support. It is seen that  $\alpha_1$  is approximately 0.60 indicating that, for both conditions of top-support, the fundamental impulsive component of the base shear is roughly 60 percent of the corresponding component of the total force exerted on the tank wall. Similarly, the values of  $\alpha_{c1}$  indicate that the fundamental convective component of the base shear varies from 20 percent to 50 percent of the corresponding component of the total force. The shear at the top is clearly equal to the difference between the total hydrodynamic wall force and the base shear.

### Moments

The instantaneous value of the wall moment,  $M(\eta, t)$ , may be expressed in the form

$$M(\eta, t) = \sum_{n=1}^{\infty} d_n(\eta) m_l H A_n(t) + \sum_{n=1}^{\infty} d_{cn}(\eta) m_l H A_{cn}(t) \quad (2.16)$$

in which  $d_n(\eta)$  and  $d_{cn}(\eta)$  are dimensionless factors representing the heightwise distributions of the  $n$ th impulsive and convective wall moments respectively.

The instantaneous value of the foundation moment,  $M'(t)$ , may be similarly expressed as

$$M'(t) = \sum_{n=1}^{\infty} d'_n m_l H A_n(t) + \sum_{n=1}^{\infty} d'_{cn} m_l H A_{cn}(t) \quad (2.17)$$

in which  $d'_n$  and  $d'_{cn}$  are the  $n$ th impulsive and convective foundation moment coefficients respectively.

Values of the fundamental impulsive and convective moment coefficients at critical sections of cantilever and top-constrained tanks are presented in Table 2.3. Three values of  $H/R$  in the range from 0.5 to 3.0 are considered. The moment coefficients at the top and base, the maximum values (denoted by the subscript  $m$ ) and their associated locations  $H_m$ , and the foundation moment coefficients are presented in the table. Additionally, the heightwise distributions of  $d_1(\eta)$  for the systems are compared in Fig. 2.8 for the cantilever and top-supported systems. The values presented, like those in Tables 2.1 and 2.2, are for steel tanks with  $h/R = 0.001$ ,  $\rho_l/\rho = 0.127$ , and  $\nu = 0.3$ . Examination of the data presented reveals the following:

- The maximum values of the wall moment coefficients for tanks with a roller support at the top are, as might be expected, smaller than those for similarly excited cantilever tanks of the same proportions. By contrast, for broad tanks, the corresponding values for hinged tanks are either of the same order of magnitude or significantly larger than those for cantilever tanks.
- The heightwise distributions of the bending moments for the top-constrained tanks are more nearly uniform than for the corresponding cantilever tanks. Furthermore, whereas the absolute maximum values of the moment for the cantilever tanks occur at the base, those for the top-constrained tanks occur at or close to mid height.
- For a prescribed direction of the hydrodynamic wall pressure, the maximum bending moments in top-constrained tanks act in a direction opposite to that for the corresponding cantilever tanks. This fact is indicated by the opposite signs of the data presented in Table 2.3.

Large moment coefficients for broad tanks that are hinge supported at the top are Poisson's ratio related, and may be explained as follows. Because of the Poisson's ratio effect, a tensile circumferential (hoop) force in the tank wall tends to induce axial



shortening of the wall, whereas a compressive circumferential force tends to induce axial extension. For a tank that is fully constrained against axial movements, these displacements naturally cannot occur. As a result, the circumferential tensile forces caused by the hydrodynamic wall pressures over half of the tank induce tensile axial forces over that half, and the circumferential compressive forces over the opposite half induce compressive axial forces in that half. The net effect of these axial forces is a bending moment over sections normal to the tank axis. Furthermore, the direction of this moment is opposite to that of the moment induced in a similarly excited cantilever tank.

It should be realized that, for axially constrained tanks, Poisson's ratio-related axial forces also develop under hydrostatic loads, and that these forces must be considered in assessing the consequences of the axial forces induced by the hydrodynamic actions. For the tank proportions and intensities of ground shaking normally encountered in practice, the uniform axial tensile forces induced by the hydrostatic wall pressures are generally larger than the corresponding tensile and compressive forces induced by the hydrodynamic pressures. The net effect under these conditions would be a reduction in the magnitudes of the compressive axial forces compared to those developed in a free-standing cantilever tank, and a consequent reduction in the tendency for wall buckling.

## 2.5 Conclusions

The constrained tanks differ from the cantilever tanks in three respects:

- They are stiffer systems, with higher natural frequencies and different modes of vibration. The increased frequencies affect the ratios of the maximum response pseudoaccelerations to the maximum ground acceleration, and, hence, the magnitudes of the resulting hydrodynamic pressures and tank forces.
- The distributions of the hydrodynamic pressures also are different in the two cases. However, these differences are not significant for broad tanks with values of  $H/R$  of the order of unity or less.
- Whereas the hydrodynamic pressures for cantilever tanks are resisted entirely at the base, those for the constrained systems are resisted partly at the top and partly at the base. In particular, the top support may reduce significantly the magnitudes of the base forces which typically control the design of cantilever

systems. These reductions will, in turn, decrease the tendencies for wall buckling and base uplifting.

**Table 2.1: Values of frequency coefficients for first three modes of vibration for different values of  $H/R$  and top-support conditions; Systems with  $h/R = 0.001$ ,  $\nu = 0.3$  and  $\rho_l/\rho = 0.127$**

$H/R$	Values of $C_1$			Values of $C_2$			Values of $C_3$		
	Free	Roller	Hinge	Free	Roller	Hinge	Free	Roller	Hinge
0.3	0.0600	0.0613	0.0634	0.1035	0.1048	0.1051	0.1344	0.1351	0.1353
0.4	0.0666	0.0690	0.0712	0.1171	0.1196	0.1200	0.1521	0.1528	0.1531
0.5	0.0719	0.0758	0.0781	0.1285	0.1326	0.1330	0.1690	0.1701	0.1703
0.6	0.0762	0.0820	0.0843	0.1381	0.1440	0.1444	0.1843	0.1859	0.1862
0.7	0.0799	0.0880	0.0901	0.1462	0.1542	0.1545	0.1981	0.2003	0.2007
0.8	0.0829	0.0937	0.0957	0.1534	0.1634	0.1637	0.2106	0.2135	0.2139
0.9	0.0855	0.0993	0.1011	0.1598	0.1718	0.1720	0.2220	0.2257	0.2262
1.0	0.0875	0.1047	0.1062	0.1657	0.1795	0.1796	0.2324	0.2370	0.2376
1.2	0.0903	0.1148	0.1158	0.1765	0.1932	0.1933	0.2509	0.2575	0.2582
1.4	0.0916	0.1239	0.1243	0.1864	0.2054	0.2054	0.2667	0.2756	0.2764
1.6	0.0917	0.1316	0.1317	0.1956	0.2165	0.2165	0.2803	0.2918	0.2926
1.8	0.0910	0.1379	0.1379	0.2040	0.2268	0.2268	0.2920	0.3064	0.3073
2.0	0.0897	0.1430	0.1431	0.2115	0.2365	0.2365	0.3024	0.3197	0.3206
2.2	0.0879	0.1468	0.1474	0.2180	0.2456	0.2457	0.3117	0.3319	0.3328
2.4	0.0859	0.1496	0.1508	0.2233	0.2542	0.2543	0.3201	0.3432	0.3440
2.6	0.0838	0.1515	0.1536	0.2275	0.2622	0.2623	0.3280	0.3537	0.3545
2.8	0.0815	0.1527	0.1557	0.2304	0.2696	0.2697	0.3355	0.3636	0.3643
3.0	0.0792	0.1533	0.1574	0.2323	0.2764	0.2765	0.3426	0.3729	0.3736

**Table 2.2: Values of coefficients  $\alpha_1$  and  $\alpha_{c1}$  in expressions for impulsive and convective components of base shear in top-constrained steel tanks; Systems with  $h/R = 0.001$ ,  $\nu = 0.3$  and  $\rho_l/\rho = 0.127$**

$H/R$	Top-Support Condition			
	Roller		Hinge	
	$\alpha_1$	$\alpha_{c1}$	$\alpha_1$	$\alpha_{c1}$
0.3	0.567	0.449	0.622	0.499
0.4	0.569	0.438	0.623	0.489
0.5	0.571	0.428	0.624	0.478
0.6	0.573	0.418	0.624	0.465
0.7	0.575	0.407	0.623	0.452
0.8	0.577	0.395	0.622	0.437
0.9	0.579	0.383	0.620	0.423
1.0	0.581	0.372	0.618	0.408
1.2	0.585	0.348	0.612	0.377
1.4	0.588	0.326	0.606	0.348
1.6	0.590	0.306	0.599	0.321
1.8	0.592	0.287	0.590	0.295
2.0	0.593	0.270	0.582	0.272
2.2	0.595	0.255	0.576	0.252
2.4	0.596	0.242	0.568	0.233
2.6	0.598	0.230	0.562	0.216
2.8	0.600	0.218	0.554	0.200
3.0	0.601	0.208	0.548	0.186

**Table 2.3: Values of impulsive and convective moment coefficients at critical sections of cantilever and top-constrained steel tanks; Systems with  $h/R = 0.001$ ,  $\nu = 0.3$  and  $\rho_l/\rho = 0.127$**

Coeff.	$H/R = 0.5$			$H/R = 1.0$			$H/R = 3.0$		
	Top-support condition								
	Free	Roller	Hinge	Free	Roller	Hinge	Free	Roller	Hinge
	Impulsive Component								
$d_1(1)$	0	0	0.310	0	0	0.110	0	0	-0.051
$d_1(0)$	-0.115	0.015	0.310	-0.224	0.021	0.111	-0.371	-0.041	-0.050
$(d_1)_m$	-0.115	0.048	0.349	-0.224	0.084	0.183	-0.371	0.094	0.065
$\frac{H_{1,m}}{H}$	0	0.40	0.45	0	0.40	0.45	0	0.50	0.50
$d_1'$	-0.434	-0.304	-0.009	-0.399	-0.155	-0.064	-0.389	-0.059	-0.069
	Convective Component								
$d_{c1}(1)$	0	0	0.697	0	0	0.090	0	0	-0.004
$d_{c1}(0)$	-0.352	0.026	0.681	-0.262	0.010	0.085	-0.124	-0.004	-0.005
$(d_{c1})_m$	-0.352	0.094	0.774	-0.262	0.056	0.139	-0.124	0.013	0.010
$\frac{H_{c1,m}}{H}$	0	0.50	0.55	0	0.55	0.55	0	0.70	0.70
$d_{c1}'$	-1.030	-0.653	0.002	-0.338	-0.066	0.009	-0.125	-0.005	-0.005

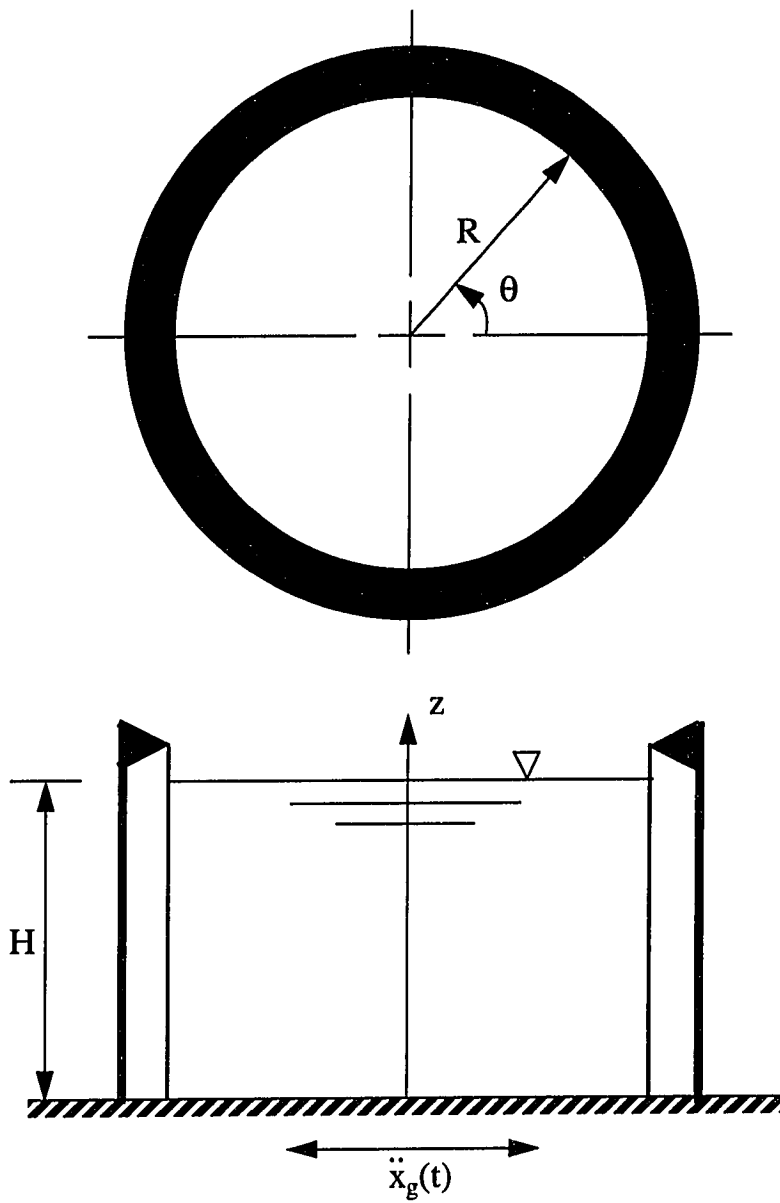


Figure 2.1 : Top-constrained tank-liquid system considered

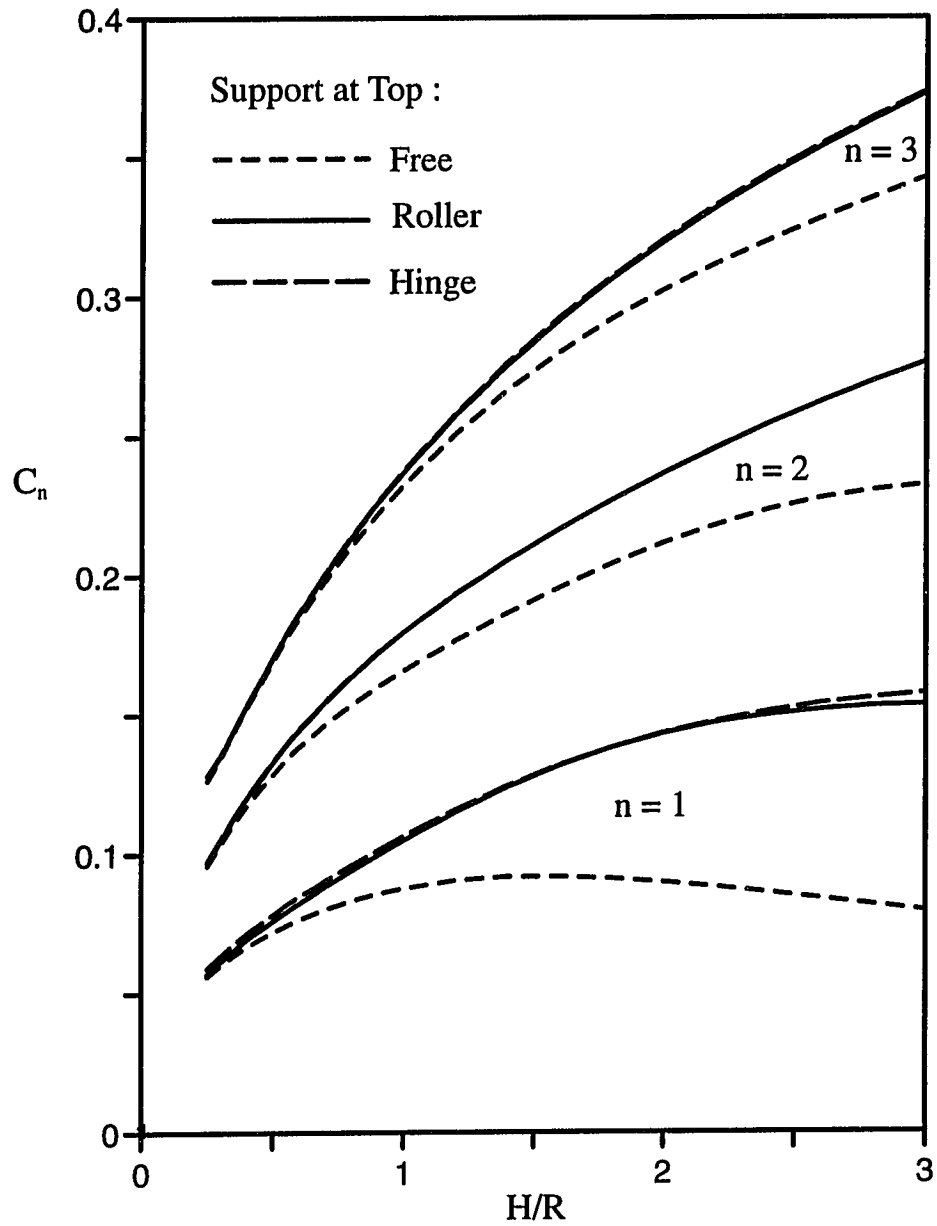


Figure 2.2 Natural frequency coefficients for first three modes of vibration of roofless steel tanks filled with water;  $h/R = 0.001$ ,  $\nu = 0.3$ ,  $\rho_l/\rho = 0.127$

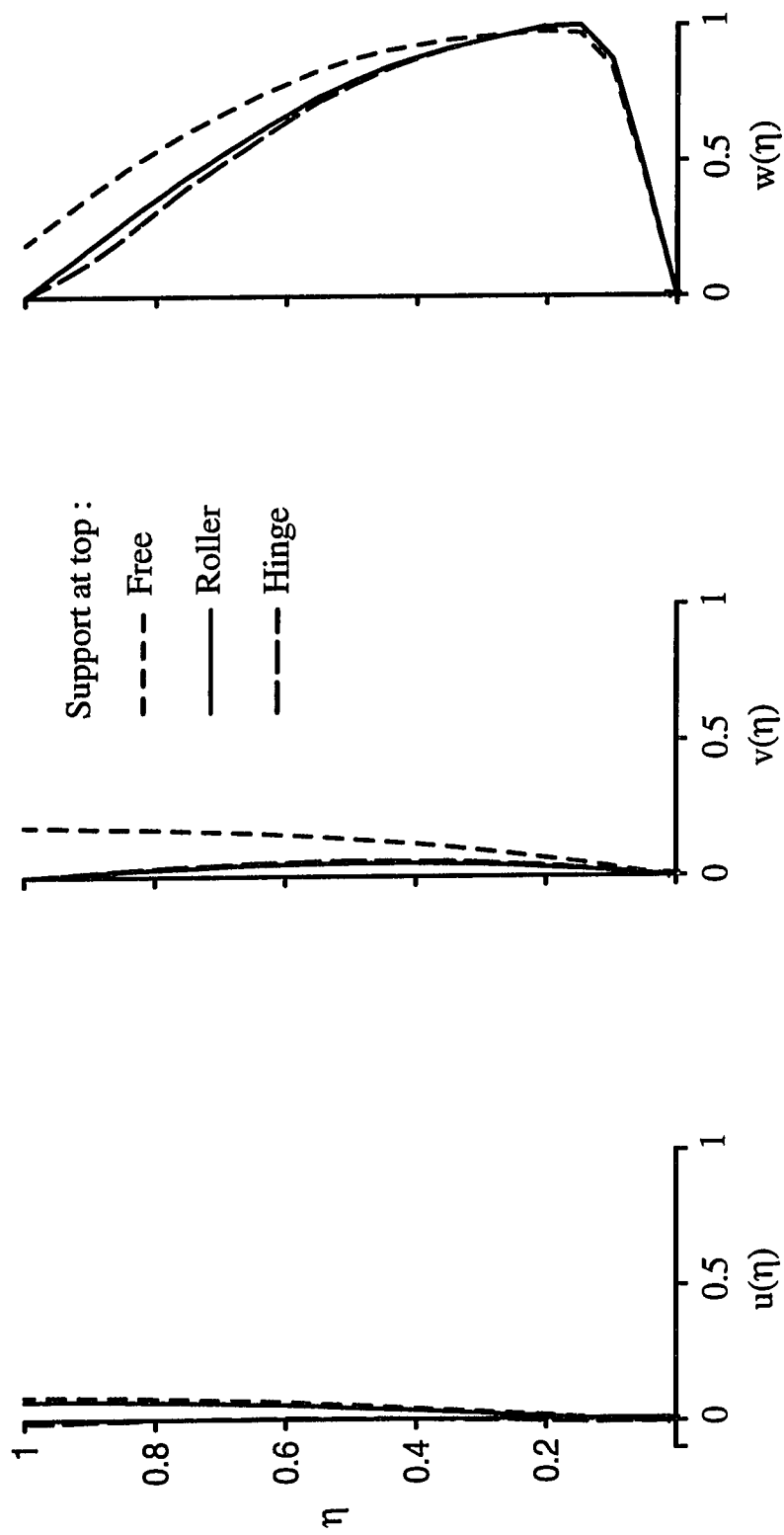


Figure 2.3 Displacement configurations for fundamental mode of vibration of water-filled steel tanks with  $H/R = 0.5$  supported differently at the top;  $h/R = 0.001$ ,  $\rho_l/\rho = 0.127$ ,  $\nu = 0.3$



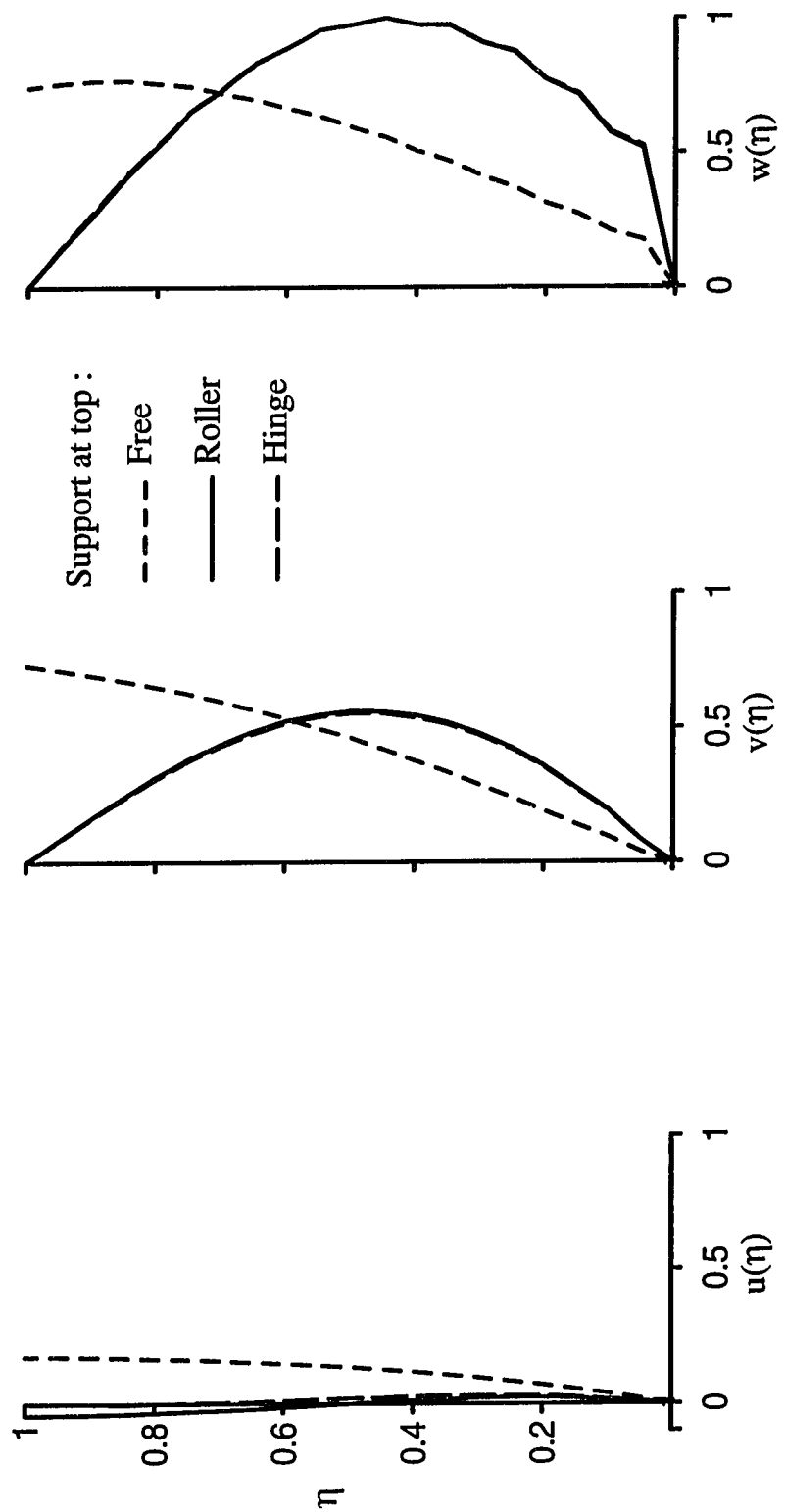


Figure 2.4 Displacement configurations for fundamental mode of vibration of water-filled steel tanks with  $H/R = 3.0$  supported differently at the top;  $h/R = 0.001$ ,  $\rho_l/\rho = 0.127$ ,  $\nu = 0.3$

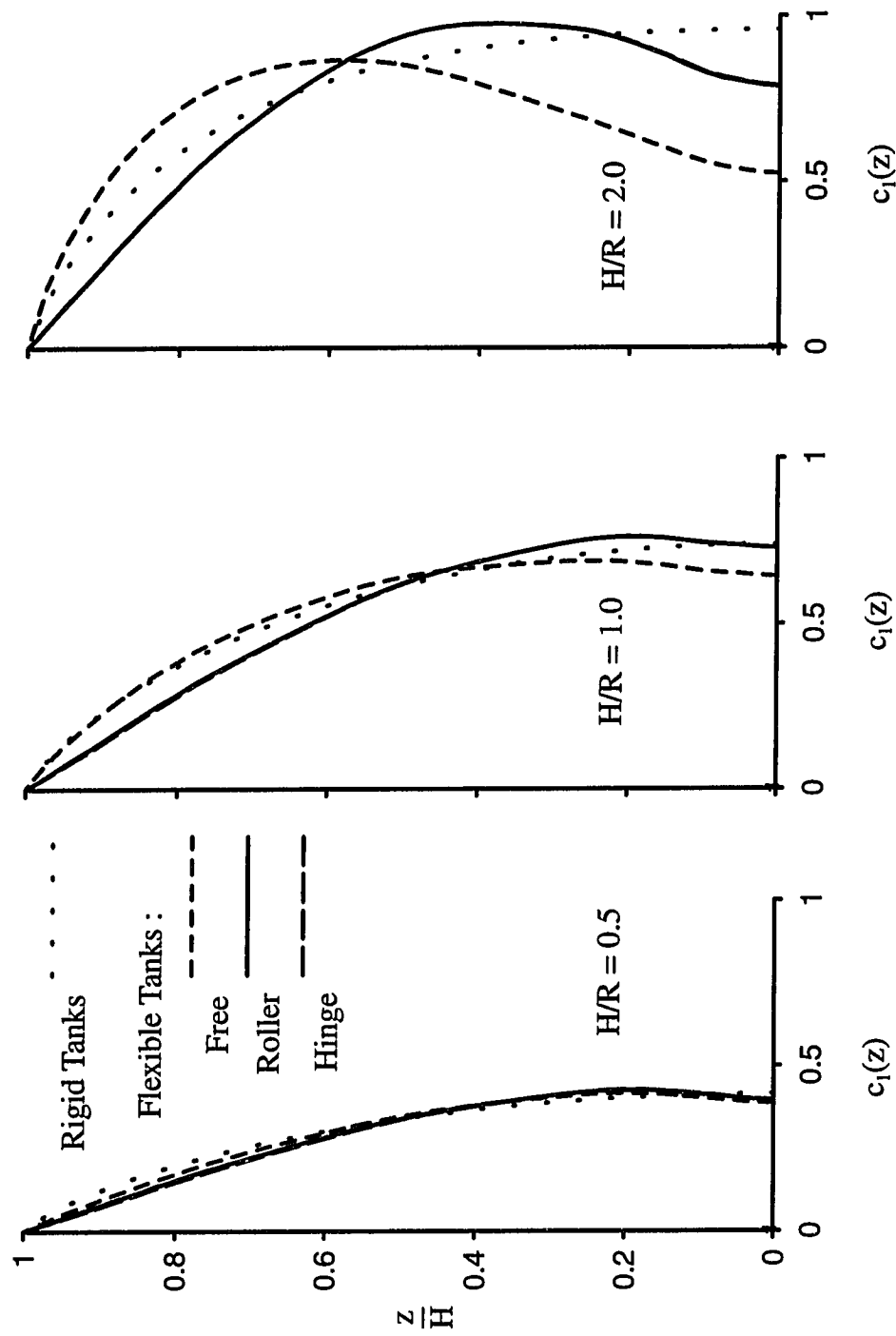


Figure 2.5 Comparison of impulsive wall-pressure distribution functions for rigid tanks with fundamental modal pressure distribution functions for flexible tanks; latter systems with  $h/R = 0.001$ ,  $\nu = 0.3$ ,  $\rho_l/\rho = 0.127$

Rigid Tanks . . . . .

Flexible Tanks :

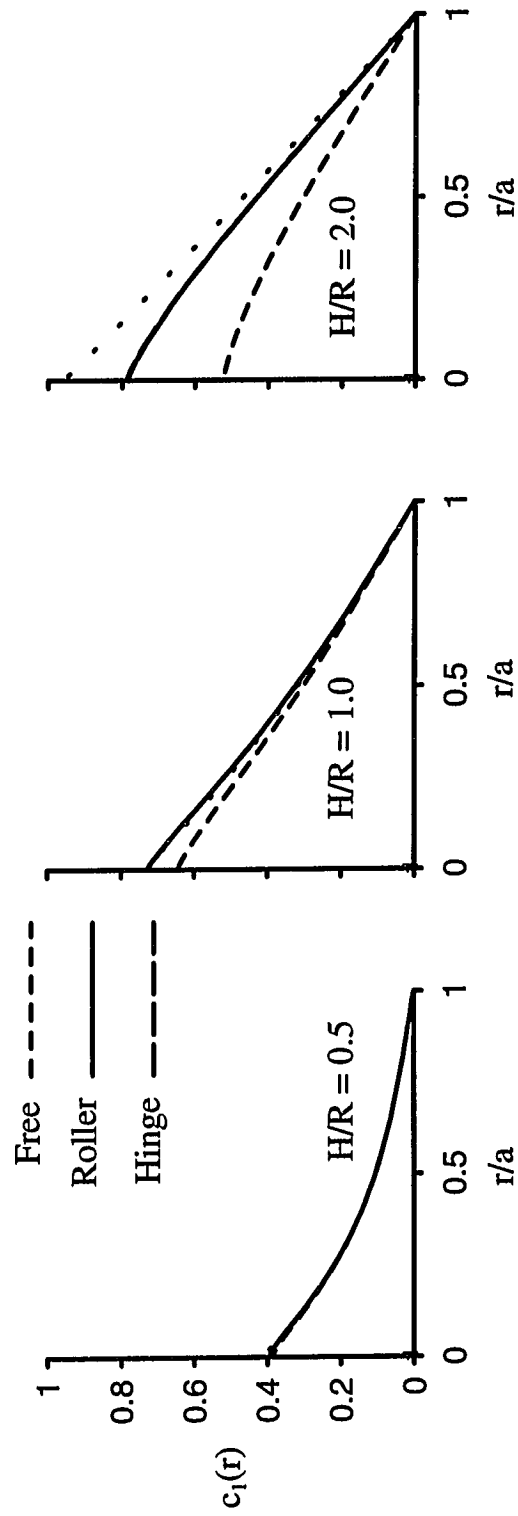


Figure 2.6 Comparison of impulsive base-pressure distribution functions for rigid tanks with fundamental modal pressure distribution functions for flexible tanks; latter systems with  $h/R = 0.001$ ,  $\nu = 0.3$ ,  $\rho_l/\rho = 0.127$

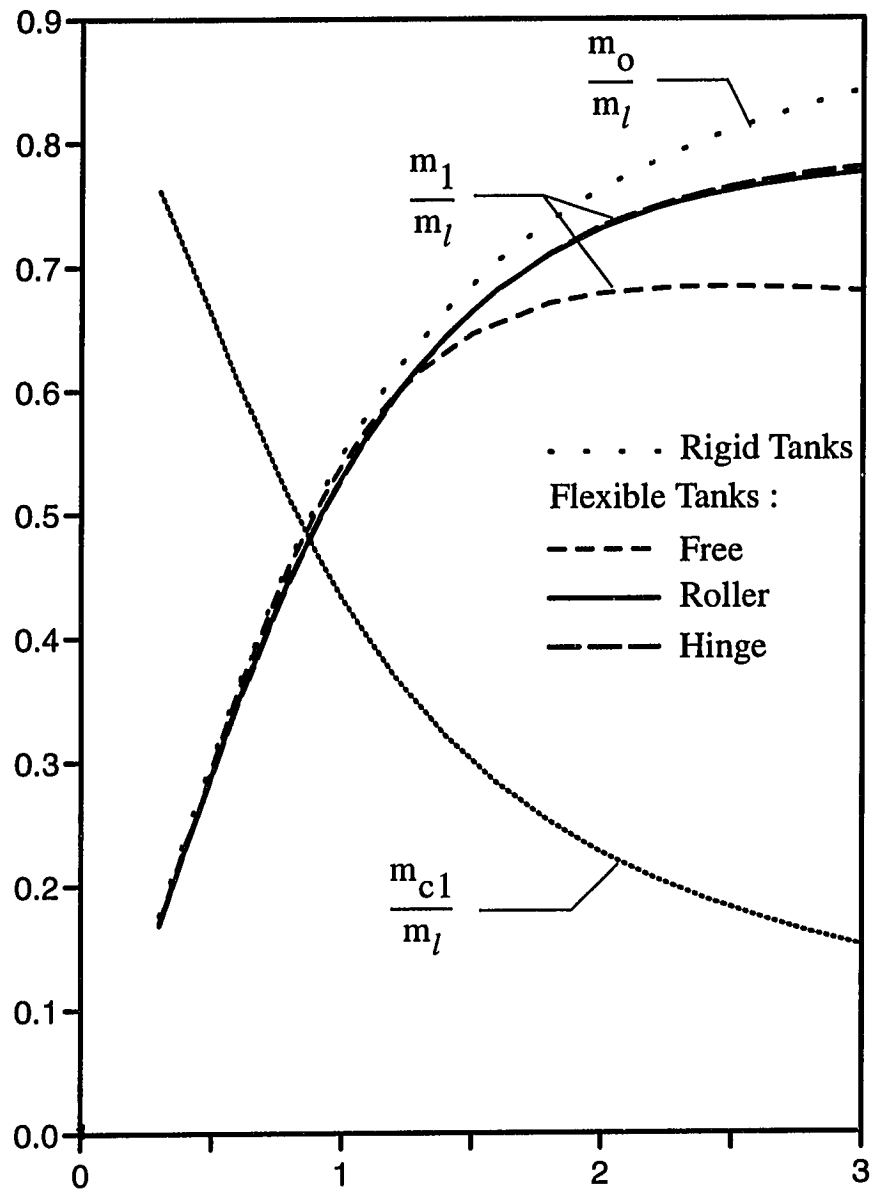


Figure 2.7 Total impulsive load for rigid tanks compared with corresponding load for the fundamental mode of vibration of flexible tanks; flexibility-independent convective load associated with fundamental sloshing mode also shown.

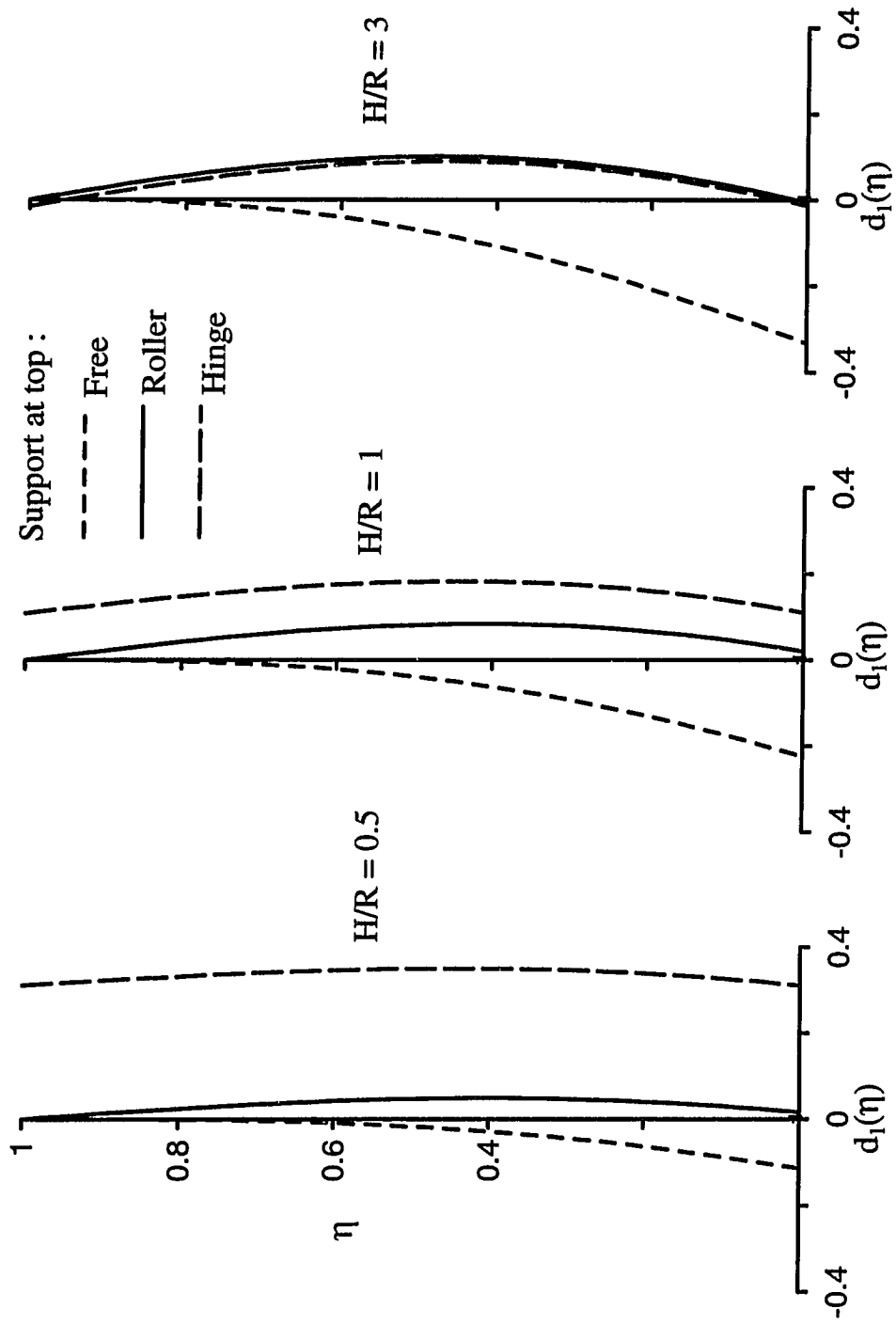


Figure 2.8 Heightwise distribution of fundamental impulsive moment coefficient  $d_1(\eta)$  for steel tanks with different support conditions at top;  $h/R = 0.001$ ,  $\rho_l/\rho = 0.127$  and  $v = 0.3$

## Chapter 3

# Sloshing Response of Layered Liquids in Rigid Tanks

### 3.1 Introduction

Current interest in the response of tanks with layered liquids is motivated by two factors: (1) Many waste storage tanks in nuclear facilities contain two or more layers of liquid or liquid-like material of different densities; and (2) recent processing for the recovery and decontamination of discharge fuel materials is typically carried out in tanks containing two-layered liquids, [8].

Prior to the present study, the only known study of the sloshing response of tanks with layered liquids was the one reported by Tang et al [60], who examined the free vibrational characteristics and the surface sloshing action of a two-layered liquid in a rigid, circular cylindrical tank subjected to a horizontal component of base shaking. The solutions presented, however, have been based on an incorrect characterization of the pressure condition at the interface of the two liquids, and the accuracy of the reported expressions and numerical results is questionable.

The objectives of this chapter are: (1) To reformulate the analysis for the sloshing response, considering the general case of a system with  $N$  homogeneous liquid layers of different thicknesses and mass densities; and (2) Through comprehensive parametric studies of systems with two and three layers, to elucidate the underlying response mechanisms and the effects and relative importance of the parameters involved.

In addition to circular cylindrical tanks, long rectangular tanks are examined, and the interrelationship of the responses of the two systems is identified. The response quantities investigated include the natural modes of vibration of the liquid, the associated frequencies, and the sloshing motions induced by a horizontal component of base shaking.

For all the solutions reported, the tanks are presumed to be rigid. However, inasmuch as the sloshing action of the liquid is normally associated with significantly longer periods of vibration than the dominant periods of the earthquake ground mo-

tions, based on previous analyses of tanks with a homogeneous liquid [65, 69], the results are expected to be also applicable to flexible tanks that are either rigidly or flexibly supported at the base.

### 3.2 Systems Considered

The systems investigated are shown in Fig. 3.1. They are rigid, vertical tanks that are filled to a height  $H$  with two or more layers of liquid of different thicknesses and densities. The tanks are either rectangular, of width  $2R$  in one direction and infinite extent in the normal direction as shown in part (a) of the figure, or cylindrical, with a circular cross section of radius  $R$  as shown in part (b) of the figure, and they are presumed to be anchored to a rigid moving base. The liquids are considered to be incompressible, irrotational and inviscid, and only linear actions are examined.

The liquid layers are numbered sequentially starting with 1 at the lowermost or bottom layer and terminating with  $N$  at the uppermost or top layer. The mass density and height of the  $j$ th layer are denoted by  $\rho_j$  and  $H_j$ , respectively. The values of  $\rho_j$  are considered to decrease with increasing  $j$ . Points within the  $j$ th layer of the long rectangular system are defined by the local Cartesian coordinates,  $x$  and  $z_j$ , shown in part (a) of Fig. 3.1, and those for the cylindrical system are defined by the cylindrical coordinates,  $r$ ,  $\theta$ ,  $z_j$ , shown in part (b) of the figure.

The ground motion is considered to be horizontal and uniform and to be directed along the  $x$ - or  $\theta = 0$  coordinate axis. The acceleration of the ground motion at any time,  $t$ , is denoted by  $\ddot{x}_g(t)$ , and the corresponding velocity and displacement are denoted by  $\dot{x}_g(t)$  and  $x_g(t)$ , respectively.

### 3.3 Fundamental Relations

The flow field in the  $j$ th layer must satisfy Laplace's equation,

$$\nabla^2 \phi_j = 0 \quad (3.1)$$

in which  $\phi_j$  = a velocity potential function of time and the position coordinates, and the operator  $\nabla^2$  is defined by

$$\nabla^2 = \frac{\partial^2}{\partial x^2} + \frac{\partial^2}{\partial z_j^2} \quad (3.2)$$

in the rectangular coordinate system, and by

$$\nabla^2 = \frac{\partial^2}{\partial r^2} + \frac{1}{r} \frac{\partial}{\partial r} + \frac{1}{r^2} \frac{\partial^2}{\partial \theta^2} + \frac{\partial^2}{\partial z_j^2} \quad (3.3)$$

in the cylindrical coordinate system. If  $v_{jn}$  is the instantaneous value of the velocity of an arbitrary particle in the  $j$  th layer in the direction of a generalized  $n$ -coordinate, then

$$v_{jn} = -\frac{\partial \phi_j}{\partial n} \quad (3.4)$$

and the corresponding hydrodynamic pressure is

$$p_j = \rho_j \frac{\partial \phi_j}{\partial t} \quad (3.5)$$

The solution of equation (3.1) must satisfy the following boundary conditions:

1. At the tank base, the vertical component for the liquid velocity must vanish; accordingly,

$$\left( \frac{\partial \phi_1}{\partial z_1} \right)_{z_1=0} = 0 \quad (3.6)$$

2. Along the tank wall, the radial or normal velocity component of both the tank and liquid must equal the corresponding component of the ground motion. For the long rectangular system, this requires that

$$\left( -\frac{\partial \phi_j}{\partial x} \right)_{x=\pm R} = \dot{x}_g(t) \quad (3.7)$$

whereas for the cylindrical system, it requires that

$$\left( -\frac{\partial \phi_j}{\partial r} \right)_{r=R} = \dot{x}_g(t) \cos \theta \quad (3.8)$$

3. At the free liquid surface, the following linearized pressure boundary condition must be satisfied

$$(\dot{\phi}_N - g d_N)_{z_N=H_N} = 0 \quad (3.9)$$

where  $d_N$  represents the vertical surface displacement, a dot superscript denotes differentiation with respect to time, and  $g$  = the gravitational acceleration. The origin of this equation is identified under item 4.



4. At the interface of a pair of layers, the vertical velocity of the liquid must be continuous; accordingly,

$$\left(\frac{\partial \phi_j}{\partial z_j}\right)_{z_j=H_j} = \left(\frac{\partial \phi_{j+1}}{\partial z_{j+1}}\right)_{z_{j+1}=0} \quad (3.10)$$

Additionally, the total pressure (hydrodynamic plus the increment due to the vertical displacement at the interface) must be continuous. If  $d_j$  represents the instantaneous vertical displacement of an arbitrary point at the upper interface of the  $j$ th layer measured from the position of static equilibrium, then assuming that the displacements are small and that the inertia of the interfacial wave is negligible, the pressure condition may be written in the form indicated in Lamb [35], as

$$\rho_j \left(\dot{\phi}_j\right)_{z_j=H_j} - \rho_j g d_j = \rho_{j+1} \left(\dot{\phi}_{j+1}\right)_{z_{j+1}=0} - \rho_{j+1} g d_j \quad (3.11)$$

Equation (3.9) may be deduced from equation (3.11) merely by letting  $j = N$  and  $\rho_{j+1} = 0$ .

It is clear from equation (3.11) that while the total pressures are continuous, the hydrodynamic components are discontinuous at the interfaces of layers of different densities. In the studies of Tang et al [56, 60], the contribution of the pressure increment due to the interfacial displacement was not considered, and the hydrodynamic component of the pressure was taken as continuous. The consequences of this approximation are identified in later sections.

### 3.4 General Approach

The solution of equation (3.1) is obtained in a manner analogous to that employed by Abramson [1] and Bauer [5] in their studies of tanks containing a homogeneous liquid, by the superposition of two component solutions as

$$\phi_j = \chi_j + \psi_j \quad (3.12)$$

In this expression,  $\chi_j$  = a velocity potential function associated with the rigid body motion of the tank walls, and  $\psi_j$  = a corresponding function providing for the relative motion of the contained liquid and the tank walls. The function  $\chi_j$  represents the solution obtained when both the upper and lower surfaces of the  $j$ th liquid layer are rigidly capped, whereas  $\psi_j$  represents a corrective solution which accounts for the

difference between the actual and fully constrained conditions at these boundaries. It is important to realize that these component solutions are different from the so-called impulsive and convective solutions used by Housner [24], Veletsos et al [65, 72] and Haroun and Housner [20] in their studies of tanks with homogeneous liquids.

### 3.4.1 Solution for $\chi_j$

For the long rectangular system,

$$\frac{\partial \chi_j}{\partial x} = -\dot{x}_g(t) \quad (3.13)$$

whereas for the cylindrical system,

$$\frac{\partial \chi_j}{\partial r} = -\dot{x}_g(t) \cos \theta \quad (3.14)$$

On integrating these expressions, one obtains

$$\chi_j = -\dot{x}_g(t) x \quad (3.15)$$

for the rectangular system, and

$$\chi_j = -\dot{x}_g(t) r \cos \theta \quad (3.16)$$

for the cylindrical system.

It is observed that the functions  $\chi_j$  are independent of the physical properties of the liquid layers, and will henceforth be denoted by  $\chi$ . Furthermore, considering that equations (3.15) and (3.16) are independent of the vertical coordinates  $z_j$ , it follows from equations (3.4) and (3.5) that  $\chi$  is associated with no vertical velocities or displacements but represents simply a finite-sized pressure field which increases linearly in the horizontal direction.

### 3.4.2 Solution for $\psi_j$

The function  $\psi_j$  must satisfy Laplace's equation (3.1), the solution of which may be obtained by the method of separation of variables as follows. For the long rectangular system,

$$\psi_j = Z(z_j) X(x) T(t) \quad (3.17)$$

and for the cylindrical system,

$$\psi_j = Z(z_j) \tilde{R}(r) T(t) \cos \theta \quad (3.18)$$

in which  $X$ ,  $\tilde{R}$ ,  $Z$  and  $T$  are functions of  $x$ ,  $r$ ,  $z_j$  and  $t$ , respectively.

Inasmuch as the boundary conditions along the walls are satisfied exactly by the potential function  $\chi$ , the corresponding conditions for  $\psi_j$  are zero at these boundaries. On substituting equations (3.17) and (3.18) into Laplace's equation and making use of the homogeneous boundary conditions along the walls, the following expressions are obtained for  $\psi_j$ . For the long rectangular system,

$$\psi_j = \sum_{m=1}^{\infty} [P_{m,j}(t) \cosh \lambda_m \eta_j + Q_{m,j}(t) \sinh \lambda_m \eta_j] \sin \lambda_m \xi \quad (3.19)$$

in which  $\xi = x/R$ ,  $\eta_j = z_j/R$ ,

$$\lambda_m = (2m - 1) \frac{\pi}{2} \quad (3.20)$$

and  $P_{m,j}(t)$  and  $Q_{m,j}(t)$  are time-dependent coefficients that must be determined from the conditions at the lower and upper boundaries of the  $j$ th layer. These boundaries will henceforth be referred to as the  $(j - 1)$ th and  $j$ th interfaces, respectively. The corresponding expression for the cylindrical tank is

$$\psi_j = \sum_{m=1}^{\infty} [P_{m,j}(t) \cosh \lambda_m \eta_j + Q_{m,j}(t) \sinh \lambda_m \eta_j] J_1(\lambda_m \xi) \cos \theta \quad (3.21)$$

in which  $\xi$  now stands for the normalized radial distance,  $r/R$ ;  $J_1$  = the Bessel function of the first kind and first order; and  $\lambda_m$  = the  $m$ th zero of the first derivative of  $J_1$ , i.e., the  $m$ th root of  $J_1'(\lambda) = 0$ . The first three of these roots are

$$\lambda_1 = 1.841 \quad \lambda_2 = 5.331 \quad \lambda_3 = 8.536 \quad (3.22)$$

Note that the meaning of  $\xi$  and the values of  $\lambda_m$ ,  $P_{m,j}(t)$  and  $Q_{m,j}(t)$  are different in equations (3.19) and (3.21).

Before proceeding to the formulation of the equations of motion, it should be noted that if equation (3.12) is substituted into equation (3.11) and the resulting terms are rearranged and normalized with respect to  $\rho_1$ , the pressure condition for the  $j$ th interface may be expressed in terms of the potential functions  $\psi_j$  and  $\chi$  as

$$\frac{\rho_j}{\rho_1} \dot{\psi}_j - \frac{\rho_{j+1}}{\rho_1} \dot{\psi}_{j+1} - \left[ \frac{\rho_j}{\rho_1} - \frac{\rho_{j+1}}{\rho_1} \right] g d_j = - \left[ \frac{\rho_j}{\rho_1} - \frac{\rho_{j+1}}{\rho_1} \right] \dot{\chi} \quad (3.23)$$

### 3.4.3 Equations of Motion for System

In formulating the equations of motion for the multi-layered system, it is desirable to use as generalized coordinates the modal values of the vertical displacements at the junctions of the tank wall and the interfaces of the liquid layers, rather than the quantities  $P_{m,j}$  and  $Q_{m,j}$ . To this end, let  $D_{m,j}(t)$  be the displacement at the junction of the wall and the  $j$ th interface when the system is vibrating in its  $m$ th horizontal mode of vibration. For the cylindrical tanks, for which these displacements are functions of the circumferential coordinate  $\theta$ ,  $D_{m,j}(t)$  refers to the value at  $\theta = 0$ . The sloshing displacement  $d_j(\xi, t)$  for an arbitrary point at the  $j$ th interface may then be expressed as

$$d_j(\xi, t) = \sum_{m=1}^{\infty} D_{m,j}(t) \frac{\sin \lambda_m \xi}{\sin \lambda_m} \quad (3.24)$$

for the long rectangular system, and as

$$d_j(\xi, \theta, t) = \sum_{m=1}^{\infty} D_{m,j}(t) \frac{J_1(\lambda_m \xi)}{J_1(\lambda_m)} \cos \theta \quad (3.25)$$

for the cylindrical system. That the functions of the  $\xi$ -coordinate in these expressions are the same as those in the corresponding expressions for  $\psi_j$  follows from the fact that  $d_j(\xi, t)$  is the time integral of the velocity  $v_j(\xi, t)$ , which, in turn, is related to  $\psi_j$  through equation (3.4). The normalizing functions  $\sin \lambda_m$  and  $J_1(\lambda_m)$  are needed so that, when evaluated at  $\xi = 1$  and  $\theta = 0$ , the component terms in equations (3.24) and (3.25) reduce to  $D_{m,j}(t)$ . It should be recalled that the values of  $\lambda_m$  for the rectangular system are defined by equation (3.20), whereas those for the cylindrical system are defined by the roots of  $J_1'(\lambda) = 0$ .

In order to relate  $P_{m,j}(t)$  and  $Q_{m,j}(t)$  to  $D_{m,j}(t)$ , the vertical velocities of the liquid at the  $j$ th and  $(j-1)$ th interfaces evaluated from equation (3.4) are equated to those obtained by differentiating with respect to time the interfacial displacements defined by equations (3.24) and (3.25). On solving the resulting equations and back substituting, the potential function  $\psi_j$  may be rewritten as

$$\psi_j = - \sum_{m=1}^{\infty} \frac{R}{\lambda_m} \left[ \frac{\dot{D}_{m,j}(t) \cosh \lambda_m \eta_j - \dot{D}_{m,j-1}(t) \cosh \lambda_m (\alpha_j - \eta_j)}{\sinh \lambda_m \alpha_j} \right] \frac{\sin \lambda_m \xi}{\sin \lambda_m} \quad (3.26)$$

for the long rectangular system, and as

$$\psi_j = - \sum_{m=1}^{\infty} \frac{R}{\lambda_m} \left[ \frac{\dot{D}_{m,j}(t) \cosh \lambda_m \eta_j - \dot{D}_{m,j-1}(t) \cosh \lambda_m (\alpha_j - \eta_j)}{\sinh \lambda_m \alpha_j} \right] \frac{J_1(\lambda_m \xi)}{J_1(\lambda_m)} \cos \theta \quad (3.27)$$

for the cylindrical system. In these expressions,  $\alpha_j = H_j/R$ .

The equation of motion for the  $j$  th interface of the rectangular system may now be derived from equation (3.23) by substituting the expressions for  $\chi$ ,  $d_j$  and  $\psi_j$  defined by equations (3.15), (3.24) and (3.26), respectively. The left-hand member of the expression obtained in this manner involves an infinite sum of horizontal sinusoidal modes. On multiplying both sides of this expression by  $\sin \lambda_m \xi$  and integrating from 0 to 1, all but one of the terms on the left side cancel because of the orthogonality of the trigonometric functions involved, and the equation reduces to

$$\mathcal{A}_{j,j-1} \ddot{D}_{m,j-1} + \mathcal{A}_{j,j} \ddot{D}_{m,j} + \mathcal{A}_{j,j+1} \ddot{D}_{m,j+1} + \frac{\lambda_m g}{R} \mathcal{B}_{j,j} D_{m,j} = -\epsilon_m \lambda_m s_j \ddot{x}_g(t) \quad (3.28)$$

where

$$\mathcal{A}_{j,j} = \frac{\rho_j}{\rho_1} \coth \lambda_m \alpha_j + \frac{\rho_{j+1}}{\rho_1} \coth \lambda_m \alpha_{j+1} \quad (3.29)$$

$$\mathcal{A}_{j,j-1} = -\frac{\rho_j}{\rho_1} \frac{1}{\sinh \lambda_m \alpha_j} \quad (3.30)$$

$$\mathcal{A}_{j,j+1} = -\frac{\rho_{j+1}}{\rho_1} \frac{1}{\sinh \lambda_m \alpha_{j+1}} \quad (3.31)$$

$$\mathcal{B}_{j,j} = s_j = \frac{\rho_j}{\rho_1} - \frac{\rho_{j+1}}{\rho_1} \quad (3.32)$$

and  $\epsilon_m$  is a dimensionless factor defined by

$$\epsilon_m = \frac{2}{\lambda_m^2} \quad (3.33)$$

It is shown later that the factor  $\epsilon_m$  appears in the expression for the surface sloshing motion of a homogeneous liquid, and to highlight its meaning, is kept separately from  $\lambda_m$ . Note that  $D_{m,0} = 0$ ; hence, both  $D_{m,j-1}$  and  $\ddot{D}_{m,j-1}$  in equation (3.28) vanish for  $j = 1$ .

The equation of motion for the  $j$  th interface of the cylindrical system is obtained similarly by substituting equations (3.16), (3.25) and (3.27) into equation (3.23). The two sides of the resulting expression are then multiplied by  $\xi J_1(\lambda_m \xi) d\xi$  and integrated from 0 to 1. Because of the orthogonality of the Bessel functions, the infinite summation of terms again reduces to equation (3.28) with  $\mathcal{A}_{j,j-1}$ ,  $\mathcal{A}_{j,j}$ ,  $\mathcal{A}_{j,j+1}$ ,  $\mathcal{B}_{j,j}$  and  $s_j$  defined, as before, by equations (3.29) through (3.32), except that the values of  $\lambda_m$  are different in the two cases. Additionally, the factor  $\epsilon_m$  for the cylindrical system is given by

$$\epsilon_m = \frac{2}{\lambda_m^2 - 1} \quad (3.34)$$

rather than by equation (3.33).

The complete set of equations for the multilayered system is obtained by repeated application of equation (3.28) to all interfaces. The resulting set of equations may be written as

$$[\mathcal{A}] \{\ddot{D}_m\} + \frac{\lambda_m g}{R} [\mathcal{B}] \{D_m\} = -\epsilon_m \lambda_m \{s\} \ddot{x}_g(t) \quad (3.35)$$

where  $\{D_m\}$  and  $\{s\}$  are vectors of size  $N$ , the  $j$ th elements of which are  $D_{m,j}$  and  $s_j$ , respectively;  $[\mathcal{A}]$  is a tri-diagonal, symmetric matrix of size  $(N \times N)$ , for which the elements of the  $j$ th row are given by equations (3.29), (3.30) and (3.31);  $[\mathcal{B}]$  is a diagonal matrix of the same size, with its  $j$ th element given by equation (3.32); and  $\epsilon_m$  is defined by equation (3.33) for the long rectangular system and by equation (3.34) for the cylindrical system.

### 3.5 Free Vibration

The equations for free vibration are deduced from equation (3.35) by setting its right-hand member equal to zero. The solution of these equations is obtained in the usual manner by letting

$$\{D_m(t)\} = \{\hat{D}_m\} e^{i\omega_m t} \quad (3.36)$$

and solving the resulting characteristic value problem,

$$[\mathcal{B}] \{\hat{D}_m\} = \frac{\omega_m^2 R}{\lambda_m g} [\mathcal{A}] \{\hat{D}_m\} \quad (3.37)$$

in which  $i = \sqrt{-1}$ , and  $\omega_m$  = the circular frequency associated with the  $m$ th horizontal mode of vibration. For the long rectangular system, the latter mode is defined by the function  $\sin \lambda_m \xi$ , whereas for the cylindrical system, it is defined by the function  $J_1(\lambda_m \xi)$ .

It is clear from equation (3.37) that, for each horizontal mode of vibration, there exist  $N$  vertical modes, each associated with a distinct frequency. This fundamental fact was not revealed in the solutions presented by Tang et al [60], which led to a single frequency and a single vertical mode of vibration for each value of  $m$ .

The  $n$ th circular natural frequency of the system for the  $m$ th horizontal mode of vibration is denoted by  $\omega_{mn}$ , the corresponding vector of interfacial displacement amplitudes is denoted by  $\{\hat{D}_{mn}\}$ , and the  $j$ th element of the latter vector is denoted by  $\hat{D}_{mn,j}$ . The ordering of these frequencies and modes is identified later. The

characteristic vectors are real-valued and satisfy the orthogonality relations

$$\{\hat{D}_{mr}\}^T [\mathcal{A}] \{\hat{D}_{ms}\} = 0 \quad (3.38)$$

and

$$\{\hat{D}_{mr}\}^T [\mathcal{B}] \{\hat{D}_{ms}\} = 0 \quad (3.39)$$

for  $r \neq s$ . Furthermore, both  $[\mathcal{A}]$  and  $[\mathcal{B}]$  can be shown to be positive definite, ensuring that all natural frequencies are real and positive. The positive definiteness of  $[\mathcal{A}]$  and  $[\mathcal{B}]$  follow from the fact that these matrices are symmetric and diagonally dominant. For the definition of diagonal dominance, the reader is referred to Golub and Van Loan [16].

### 3.5.1 Two-Layered System

For the special case of a two-layered system, for which the matrices  $[\mathcal{A}]$  and  $[\mathcal{B}]$  in equation (3.37) are of size  $2 \times 2$ , the resulting frequency equation, after multiplying through by  $\tanh \lambda_m \alpha_1 \tanh \lambda_m \alpha_2$ , becomes

$$\begin{aligned} \left(1 + \frac{\rho_2}{\rho_1} \tanh \lambda_m \alpha_1 \tanh \lambda_m \alpha_2\right) \omega_m^4 - (\tanh \lambda_m \alpha_1 + \tanh \lambda_m \alpha_2) \frac{\lambda_m g}{R} \omega_m^2 \\ + \left(1 - \frac{\rho_2}{\rho_1}\right) \left(\frac{\lambda_m g}{R}\right)^2 \tanh \lambda_m \alpha_1 \tanh \lambda_m \alpha_2 = 0 \end{aligned} \quad (3.40)$$

With the natural frequencies of the system,  $\omega_{m1}$  and  $\omega_{m2}$ , determined from this equation, the ratio of the interfacial to the surface modal displacement amplitudes for the  $(mn)$ th mode of vibration is determined from equation (3.37) to be

$$\frac{\hat{D}_{mn,1}}{\hat{D}_{mn,2}} = \cosh \lambda_m \alpha_2 - \frac{\lambda_m g}{\omega_{mn}^2 R} \sinh \lambda_m \alpha_2 \quad (3.41)$$

Finally, the orthogonality relation defined by equation (3.39) can be written as

$$\left(1 - \frac{\rho_2}{\rho_1}\right) \hat{D}_{m1,1} \hat{D}_{m2,1} + \frac{\rho_2}{\rho_1} \hat{D}_{m1,2} \hat{D}_{m2,2} = 0 \quad (3.42)$$

Provided one uses the appropriate values of  $\lambda_m$  as previously indicated, equations (3.40), (3.41) and (3.42) are applicable to both the long rectangular and the cylindrical systems. Incidentally, with the appropriate reinterpretation of the meaning of the various symbols, equations (3.40) and (3.41) can be shown to be identical to those

presented by Lamb [35] for the sloshing frequencies and the associated modal ratios of two superposed liquids flowing in a long rectangular channel.

For a homogeneous liquid with  $\rho_2/\rho_1 = 1$ , on neglecting the trivial solution of zero frequency, equation (3.40) yields the well known expression for the  $m$ th circular natural frequency of sloshing motion,

$$\omega_m = C_m \sqrt{\frac{\lambda_m g}{R}} \quad (3.43)$$

in which

$$C_m = \sqrt{\tanh\left(\frac{\lambda_m H}{R}\right)} \quad (3.44)$$

Furthermore, for the limiting case of  $\rho_2/\rho_1 = 0$ , which corresponds either to a system without the upper layer or to one with a very heavy, practically immobile lower layer, the two frequencies reduce, as they should, to those obtained from equation (3.43) for homogeneous liquids with depths  $H_1$  and  $H_2$ , respectively.

### 3.5.2 Numerical Solutions for Sloshing Frequencies and Modes

The circular natural frequency corresponding to the  $m$ th horizontal and  $n$ th vertical mode of vibration may conveniently be expressed in a generalized form of equation (3.43) as

$$\omega_{mn} = C_{mn} \sqrt{\frac{\lambda_{mn} g}{R}} \quad (3.45)$$

in which  $C_{mn}$  is a dimensionless factor that depends on the tank shape and slenderness,  $H/R$ , the number, relative thicknesses and relative densities of the liquid layers, and, of course, on the order of the frequency or mode under consideration. As already indicated, the values of  $\lambda_m$  in this expression are defined by equation (3.20) for the long rectangular system, and by equation (3.22) for the cylindrical system.

### Two-Layered Systems

The frequency coefficients  $C_{11}$  and  $C_{12}$  for two-layered liquids in long rectangular tanks are presented in Fig. 3.2, and those for the corresponding cylindrical systems are shown in Fig. 3.3. The results are plotted as a function of the slenderness ratio,  $H/R$ , for two values of the layer thickness ratio,  $H_2/H_1$ , and several values of the density ratio,  $\rho_2/\rho_1$ . These coefficients and the associated natural frequencies and



modes of vibration are numbered in reverse order, starting with  $n = 1$  for the highest frequency and terminating with  $n = N = 2$  for the lowest frequency. The rationale for this convention is that the higher numbered modes are associated with a higher order of waviness (larger number of points of zero crossings) in the vertical direction. The explanation for the decrease in the values of the associated natural frequencies with increasing modal order is examined later in this section. It is observed that both the frequency coefficients and the associated natural frequencies for the cylindrical tanks are larger than those for the corresponding rectangular tanks; however, the differences are not significant, and the general trends of the results for the two systems are quite similar. Incidentally, the corresponding plots for the second horizontal mode of vibration,  $m = 2$ , also exhibit the same general trends and are not shown.

The uppermost curves in Figs. 3.2 and 3.3 are for a homogeneous liquid with a depth  $H$  equal to the total depth of the layered system. It is noteworthy that both frequency coefficients for the layered system are smaller than that for the associated homogeneous system. The effect of the heavier bottom layer is to decrease the effective total depth of the layered system and, as would be expected from equations (3.43) and (3.44), this reduction leads to a corresponding reduction in the values of the frequency coefficient and of the associated natural frequency.

The interrelationship of the natural frequencies of the layered and the homogeneous systems can more clearly be seen in Fig. 3.4, in which the frequencies  $\omega_{11}$  and  $\omega_{12}$  for the cylindrical systems examined in Fig. 3.3 are plotted normalized with respect to  $\omega_1$ , the fundamental natural frequency for a homogeneous liquid of the same total depth. It is observed that the results, particularly those corresponding to the lower values of  $H/R$ , are substantially less than unity and that those for  $\omega_{12}$  tend to zero as  $\rho_2/\rho_1$  approaches unity. In general, when the densities of the individual layers in a multi-layered system become equal to each other, all but one of the natural frequencies corresponding to each horizontal mode tend to zero. These limiting values represent trivial solutions and may be disregarded. The interfacial sloshing displacements are caused solely by density discontinuities across interfaces and cease to exist for a homogeneous liquid.

The dotted curves in Figs. 3.2 and 3.3, which refer to systems of  $\rho_2/\rho_1 = 0$ , also represent the frequency coefficients for homogeneous liquids with depths  $H_1$  and  $H_2$  when they are considered to act independently. For the systems with equal layer thicknesses considered in the left-hand plots, there is naturally a single such curve, whereas for the systems with unequal depths considered in the right-hand plots, there

are two distinct curves. Note that the highest natural frequency of the layered system is higher than the higher of these curves, whereas the lowest frequency is lower than the lower curve. This result is consistent with the well known interrelationship of the natural frequencies of systems having one and two degrees of freedom. If a single-degree-of-freedom system with a natural frequency  $f_1$  is augmented by the addition of another such system, it is well known that the natural frequencies of the resulting two-degree-of-freedom system lie on either side of  $f_1$ . Since the systems in the right-hand plots of Figs. 3.2 and 3.3 may be formed either from the lower layer by the addition of an upper layer, or from the upper layer by the insertion of a lower layer, their natural frequencies must lie on either side of the pair of dotted curves, and there will be no frequencies in the region between.

Further insight into the free-vibrational characteristics of the two-layered systems may be gained by examining the distributions of the modal displacement amplitudes of the liquid throughout its depth. Denoted by  $\hat{D}_{mn}(\eta)$ , where  $\eta = z/H$  and  $z$  = the vertical distance measured from the tank base, these amplitudes are shown in Figs. 3.5 and 3.6 for cylindrical systems with two values of  $H/R$ , two values of  $H_2/H_1$  and several values of  $\rho_2/\rho_1$ . The interfacial values of these amplitudes constitute the vector  $\{\hat{D}_{mn}\}$ . The values of  $\hat{D}_{mn}(\eta)$  at elevations between the liquid interfaces are evaluated by substituting equation (3.36) for the mode under consideration into equation (3.27), differentiating the resulting expression with respect to  $\eta_j$  and integrating the resulting modal velocity with respect to time. The modes on the left correspond to the first or higher of the two natural frequencies and are normalized with respect to the free-surface displacement, whereas those on the right correspond to the second or lower natural frequency and are normalized with respect to the interfacial displacement. Note that the first or fundamental mode is associated with no zero crossings, while the second mode is associated with a single such crossing. The interfacial ordinates of these modal configurations naturally satisfy both the orthogonality relation defined by equation (3.42) and the somewhat more involved relation defined by equation (3.38). For a multi-layered system, the  $n$ th vertical mode of vibration is associated with  $n - 1$  zero crossings.

It is noteworthy that, for the fundamental mode of vibration, the displacement amplitude at the interface of the two layers for the layered system is lower than that for the homogeneous system, the difference increasing with decreasing values of  $\rho_2/\rho_1$ . This result confirms the earlier statement to the effect that the larger density

of the lower layer decreases the effective total depth of the layered system leading to a reduction in frequency.

The very low frequency values of the second natural modes may also be explained by the location of the sections of zero modal amplitudes (points of zero crossings) near the top. Since the vertical motion of the liquid is zero at these sections, the natural frequency of the system for this mode must be equal to that of a homogeneous liquid with a depth equal to the distance from the free surface to the section of zero amplitude. As an illustration, it is noted that for the cylindrical system with values of  $H/R = 0.5$ ,  $H_2/H_1 = 1$  and  $\rho_2/\rho_1 = 0.5$  considered in Fig. 3.5, the section of zero crossing for the second mode of vibration is located at a distance  $0.140 H$  from the top. This leads to an effective depth-to-radius ratio for the homogeneous liquid of 0.070. If this ratio is substituted into equation (3.44), the value of the resulting frequency coefficient turns out to be  $C_1 = 0.358$ , which is precisely the value of  $C_{12}$  reported in Fig. 3.3.

In concluding this section on two-layered systems, it should be noted that the frequency coefficients for the systems with  $H_2/H_1 = 2$  considered in the right-hand plots of Figs. 3.2 and 3.3 also apply to systems with  $H_1/H_2 = 2$ . This follows from equation (3.40), which shows that interchanging the dimensionless thicknesses  $\alpha_1$  and  $\alpha_2$  does not alter the equation. However, the natural modes are different in the two cases, as may well be appreciated from equation (3.41).

### Three-Layered Systems

As an illustration of the free vibrational characteristics of systems with more than two layers, in Fig. 3.7 are shown the natural frequency coefficients for the fundamental horizontal mode of vibration,  $m = 1$ , of a cylindrical system with three layers of identical depths. The mass densities of the layers are presumed to increase from top to bottom in proportion to 1:2:3, and a range of  $H/R$  values is considered. Also shown are the natural modes of the system for the special case of  $H/R = 1$ , with each mode normalized to a unit maximum amplitude. The values of the modal amplitudes for sections between layer interfaces are computed in a manner analogous to that indicated earlier for the two-layered system. The dashed curves in this figure represent the corresponding results for a homogeneous system with a depth equal to the total depth of the layered system.

It is observed that all three frequencies are lower than that of the associated homogeneous system, that the highest frequency is associated with a vertical mode of vibration which has no zero crossing and is similar to that of the associated homogeneous system, whereas the modes of the next two lower frequencies have one and two zero crossings, respectively.

### 3.6 Forced Vibration

With the natural frequencies and modes of vibration of the system established, its response to an arbitrary lateral excitation may be obtained by the modal superposition method. In this approach, the vector  $\{D_m(t)\}$  of the interfacial vertical displacements of the liquid along the tank wall is expressed as a linear combination of the characteristic vectors,  $\{\hat{D}_{mn}\}$ , as

$$\{D_m(t)\} = \sum_{n=1}^N \{\hat{D}_{mn}\} q_{mn}(t) \quad (3.46)$$

in which  $q_{mn}(t)$  is a generalized time-dependent coordinate corresponding to the  $m$ th horizontal and  $n$ th vertical mode of vibration. On substituting equation (3.46) into equation (3.35), premultiplying the resulting expression by  $\{\hat{D}_{mr}\}^T$ , and making use of equation (3.37) and of the orthogonality properties of the natural modes defined by equations (3.38) and (3.39), the resulting system of equations is uncoupled, leading to

$$\ddot{q}_{mn}(t) + \omega_{mn}^2 q_{mn}(t) = -\lambda_m \epsilon_m \frac{\{\hat{D}_{mn}\}^T \{s\}}{\{\hat{D}_{mn}\}^T [\mathcal{A}] \{\hat{D}_{mn}\}} \ddot{x}_g(t) \quad (3.47)$$

It is convenient to replace the tri-diagonal matrix  $[\mathcal{A}]$  on the right-hand member of this expression by the diagonal matrix  $[\mathcal{B}]$ . On making use of equation (3.37), equation (3.47) may be rewritten as

$$\ddot{q}_{mn}(t) + \omega_{mn}^2 q_{mn}(t) = -\epsilon_m \omega_{mn}^2 \Gamma_{mn} R \frac{\ddot{x}_g(t)}{g} \quad (3.48)$$

in which  $\Gamma_{mn}$  is a dimensionless factor given by

$$\Gamma_{mn} = \frac{\{\hat{D}_{mn}\}^T \{s\}}{\{\hat{D}_{mn}\}^T [\mathcal{B}] \{\hat{D}_{mn}\}} \quad (3.49)$$

The solution of equation (3.48) is then given by

$$q_{mn}(t) = -\epsilon_m \Gamma_{mn} R \frac{A_{mn}(t)}{g} \quad (3.50)$$

in which  $A_{mn}(t)$  represents the pseudoacceleration function defined by

$$A_{mn}(t) = \omega_{mn} \int_0^t \ddot{x}_g(\tau) \sin \omega_{mn}(t - \tau) d\tau \quad (3.51)$$

For a base-excited single-degree-of-freedom oscillator with a circular frequency  $\omega_{mn}$ , the pseudoacceleration  $A_{mn}(t)$  represents the product of the square of  $\omega_{mn}$  and the deformation of the oscillator,  $U_{mn}(t)$ . The maximum value of  $A_{mn}(t)$  is the quantity displayed on a pseudoacceleration response spectrum.

The interfacial displacements at arbitrary points are finally determined from equation (3.24) or (3.25) by making use of equations (3.46) and (3.50). For the long rectangular system, they are given by

$$\{d(\xi, t)\} = -R \sum_{m=1}^{\infty} \sum_{n=1}^N \{d_{mn}\} \frac{\sin \lambda_m \xi}{\sin \lambda_m} \frac{A_{mn}(t)}{g} \quad (3.52)$$

and for the cylindrical system, by

$$\{d(\xi, \theta, t)\} = -R \sum_{m=1}^{\infty} \sum_{n=1}^N \{d_{mn}\} \frac{J_1(\lambda_m \xi)}{J_1(\lambda_m)} \frac{A_{mn}(t)}{g} \cos \theta \quad (3.53)$$

where

$$\{d_{mn}\} = \epsilon_m \Gamma_{mn} \{\hat{D}_{mn}\} \quad (3.54)$$

It must be recalled that the factors  $\lambda_m$  and the expressions for  $\epsilon_m$  are different for the two systems. The same is also true of  $\{\hat{D}_{mn}\}$ ,  $\Gamma_{mn}$ ,  $\{d_{mn}\}$ ,  $\omega_{mn}$  and  $A_{mn}(t)$ .

For a single-layered system with a homogeneous liquid, the only interfacial displacements are those at the surface. In this case,  $\{D_{mn}\}$  and  $\{d_{mn}\}$  reduce to the scalars  $D_m$  and  $d_m$ ;  $\{d\}$  reduces to the surface displacement,  $d(\xi, \theta, t)$ ; the matrix  $[\mathcal{B}]$  and vector  $\{s\}$  become unit scalars; and the product  $\Gamma_{mn} \{\hat{D}_{mn}\}$  in equation (3.54) reduces to unity. It can then be concluded from equation (3.54) that the factors  $\epsilon_m$ , which are defined by equation (3.33) for the long rectangular system and by equation (3.34) for the cylindrical system, represent the displacement coefficients for the surface sloshing motion along the tank wall of the homogeneous liquid. The latter factors can be shown to satisfy the relation

$$\sum_{m=1}^{\infty} \epsilon_m = 1 \quad (3.55)$$

Because of their special meaning, these factors were not absorbed into the  $\Gamma_{mn}$  factors but were retained as multipliers in the expressions for the layered systems as well.

The surface displacement of the uniform system may then be determined from the following specialized forms of equations (3.52) and (3.53), of which the second has been reported previously, e.g., Reference 1:

$$d(\xi, t) = -R \sum_{m=1}^{\infty} \epsilon_m \frac{\sin \lambda_m \xi}{\sin \lambda_m} \frac{A_m(t)}{g} \quad (3.56)$$

and

$$d(\xi, \theta, t) = -R \sum_{m=1}^{\infty} \epsilon_m \frac{J_1(\lambda_m \xi)}{J_1(\lambda_m)} \frac{A_m(t)}{g} \cos \theta \quad (3.57)$$

In these expressions,  $A_m(t)$  represents the instantaneous pseudoacceleration of a simple oscillator with a natural frequency equal to that of the  $m$ th sloshing mode of vibration of the actual system when it is subjected to the prescribed ground motion.

If the contribution of only the fundamental mode of vibration is considered, the surface displacement along the tank wall,  $d_w$ , for a homogeneous liquid in a cylindrical tank reduces to the well known expression

$$d_w(\theta, t) = 0.837 R \frac{A_1(t)}{g} \cos \theta \quad (3.58)$$

On replacing  $A_1(t)$  by  $\omega_1^2 U_1(t)$ , where  $U_1(t)$  = the instantaneous deformation of the single-degree-of-freedom oscillator, and making use of equation (3.45), equation (3.58) can also be written as

$$d_w(\theta, t) = 1.54 C_1^2 U_1(t) \cos \theta \quad (3.59)$$

in which  $C_1$  is the dimensionless frequency coefficient defined by equation (3.44).

For a multi-layered system, it can be shown that

$$\sum_{n=1}^N \{d_{mn}\} = \epsilon_m \{1\} \quad (3.60)$$

and by virtue of equation (3.55), it can further be concluded that

$$\sum_{m=1}^{\infty} \sum_{n=1}^N \{d_{mn}\} = \{1\} \quad (3.61)$$

Equation (3.60) is proved in the following by examining the hydrodynamic pressure difference at the  $j$ th interface of the system,  $\Delta p_j$ . The instantaneous value of this difference is determined from equation (3.11), by making use of equation (3.5), to be

$$\Delta p_j(\xi, t) = (\rho_j - \rho_{j+1}) g d_j(\xi, t) \quad (3.62)$$

in which  $d_j$  is defined by equation (3.52) for the long rectangular system, and by equation (3.53) for the cylindrical system. For the latter system, equation (3.62) may thus be written as

$$\Delta p_j(\xi, \theta, t) = (\rho_j - \rho_{j+1}) R \sum_{m=1}^{\infty} \sum_{n=1}^N d_{mn,j} \frac{J_1(\lambda_m \xi)}{J_1(\lambda_m)} A_{mn}(t) \cos \theta \quad (3.63)$$

Now, if the natural frequencies of the system are very high compared to the dominant frequency of the ground motion, all the pseudoacceleration functions  $A_{mn}(t)$  will reduce to the ground acceleration  $\ddot{x}_g(t)$ , the liquid will respond as a rigid body, and the resulting expression for  $\Delta p_j$  will reduce to the pressure induced by the inertia of a rigid disk which has unit depth, radius  $r$ , mass density  $\rho_j - \rho_{j+1}$  and is subjected to a horizontal motion with acceleration  $\ddot{x}_g(t)$ . The latter pressure is given by

$$\Delta p_j(\xi, \theta, t) = (\rho_j - \rho_{j+1}) r \ddot{x}_g(t) \cos \theta \quad (3.64)$$

On equating the right-hand members of equations (3.63) and (3.64) and cancelling the common terms, one obtains

$$\sum_{m=1}^{\infty} \sum_{n=1}^N d_{mn,j} \frac{J_1(\lambda_m \xi)}{J_1(\lambda_m)} = \xi \quad (3.65)$$

Finally, on multiplying through by  $\xi J_1(\lambda_m \xi) d\xi$  and integrating from 0 to 1, by virtue of the orthogonality of the Bessel functions, the double summation on the left-hand side reduces to a single summation over  $n$  only, and the final expression reduces to the  $j$ th element of equation (3.60). The validity of equation (3.60) for the long rectangular system can be demonstrated in a similar manner working with trigonometric rather than Bessel functions.

### 3.6.1 Sloshing Displacement Coefficients

Of special interest in practice is the sloshing motion of the liquid at its free surface, as the maximum surface displacement is needed to define the freeboard that must be provided to prevent the liquid from overflowing or impacting the roof. This displacement is defined by the top elements of equations (3.52) and (3.53).

In Table 3.1 are listed the surface values of the displacement coefficients  $d_{mn,2}$  for two-layered, long rectangular and cylindrical tanks. Systems with two different slenderness ratios,  $H/R$ , two liquid thickness ratios,  $H_2/H_1$ , and several mass density ratios,  $\rho_2/\rho_1$ , are considered. Results for the first two horizontal modes of vibration,

$m = 1$  and 2, and for each of the two vertical modes are presented. The following trends are worth noting:

1. The results for the two vertical modes of vibration are of opposite signs, and their numerical values increase with decreasing  $\rho_2/\rho_1$ ; the increase is particularly large for the lower values of  $H/R$ , especially for  $H_2/H_1 = 1$ , for which the natural frequencies of the individual layers are equal. The larger displacement coefficients for the fundamental vertical mode of vibration of the layered systems are attributed to the fact that, in addition to being excited laterally, the upper layers of these systems are excited at their base by the rocking motion of the interfacial sloshing.
2. For a specified horizontal mode of vibration, the sum of the displacement coefficients for the two vertical modes is equal to that obtained for a homogeneous liquid of the same total depth. This is in agreement with equation (3.60).
3. The values of the coefficients for the second horizontal mode of vibration,  $m = 2$ , are significantly smaller than those for the fundamental mode,  $m = 1$ .
4. Provided a sufficiently large number of horizontal modes of vibration is considered, the algebraic sum of the coefficients is unity, in agreement with equation (3.61).
5. The results for the long rectangular and cylindrical systems are very similar.

In Table 3.2, the top values of the displacement coefficients,  $d_{mn}$ , for the two horizontal modes of vibration of the three-layered cylindrical system examined in the right part of Fig. 3.7 are compared with those obtained for a homogeneous liquid of the same total depth. As before, the larger numerical values are obtained for the layered system, and the reported values satisfy both equations (3.60) and (3.61).

Notwithstanding the importance of the displacement coefficients, it must be realized that the relative contribution of the various modes of vibration to the total response depends also on the relative values of the pseudoaccelerations,  $A_{mn}(t)$ . The latter quantities depend, in turn, on the characteristics of the ground motion and the natural frequencies of the system itself. This matter is considered further in the following section.



### 3.6.2 Hydrodynamic Pressures

The main focus of this chapter has been on the sloshing motion of the system. With the information presented, however, it is also possible to determine the magnitude and distribution of the hydrodynamic pressures induced by the ground shaking. The hydrodynamic pressure at any point in the  $j$ th layer may be evaluated from equation (3.5) making use of the expression for the velocity potential function  $\phi_j$  defined by equation (3.12). The functions  $\chi$  and  $\psi_j$  in the latter equation may be evaluated from equations (3.15) and (3.26) for the long rectangular system and from equations (3.16) and (3.27) for the cylindrical system. The final expressions, along with numerical solutions that elucidate the interrelationship of the hydrodynamic pressures for layered and homogeneous systems, will be presented in the next chapter.

## 3.7 Numerical Example

The surface sloshing displacements induced by the lateral component of an earthquake ground motion are evaluated for two-layered liquids in a cylindrical tank of 60-ft radius. The depths of the lower and upper layers are taken as 12 ft and 24 ft, respectively, and several different values are used for the relative mass densities of the two layers. System damping for each mode of vibration is considered to be of the viscous type, and is taken as 0.5 percent of the critical value.

The ground motion is specified by the response spectrum shown in Fig. 3.8, which refers to viscously damped single-degree-of-freedom systems with the designated amount of damping. The spectrum is displayed in a tripartite logarithmic format with the abscissa representing the natural frequency of the system,  $f$ , and the pseudoacceleration,  $A$ , plotted on the right-hand diagonal scale. The vertical scale represents the pseudovelocity of the system,  $V$ , and the left-hand diagonal scale represents the associated deformation,  $U$ . The three spectral quantities are interrelated by

$$A = 2\pi fV = 4\pi^2 f^2 U \quad (3.66)$$

The maximum values of  $A$ ,  $V$  and  $U$  are  $1.68g$ ,  $61 \text{ in./sec}$  and  $31 \text{ in.}$ , respectively, and the maximum values of the acceleration, velocity and displacement of the ground are  $0.33g$ ,  $15.9 \text{ in./sec}$  and  $10.2 \text{ in.}$ , respectively. The response spectrum considered is the same as that used for the illustrative example in Reference 1.

The cyclic natural frequencies of the liquid for the first two horizontal and each of the two vertical modes of vibration are listed in Table 3.3 along with the corresponding

values of the surface displacement coefficients,  $d_{mn,2}$ . Several values of  $\rho_2/\rho_1$  in the range between unity and 0.10 are considered. Note that all frequency values fall in the left-hand, displacement-sensitive region of the response spectrum, and that, for all cases considered, the frequencies  $f_{11}$  and  $f_{21}$  fall within the segment for which the deformation  $U$  attains its maximum value. Note further that the largest displacement coefficients are associated with the fundamental mode of vibration,  $m = n = 1$ .

Table 3.4 lists the maximum values of the components of the surface displacements along the tank wall contributed by each of the four modes of vibration. The results are normalized with respect to the maximum ground displacement,  $(x_g)_{max}$ . Also listed are the corresponding values of the total displacement computed by taking the square root of the sum of the squares (SRSS value) of the component terms. The following trends are worth noting:

1. The displacements of the layered liquid are larger than those of the homogeneous liquid of the same total depth. However, as would be expected from the information presented in the preceding sections, the increase is not particularly significant for values of  $\rho_2/\rho_1 \geq 0.5$ .
2. The fundamental mode of vibration, which corresponds to values of  $m = n = 1$ , is the dominant contributor to the response. The contribution of the remaining modes is minor due to the smallness either of the relevant displacement coefficients or of the associated pseudoaccelerations or both.
3. The response contributed by the mode corresponding to  $m = 2$  and  $n = 1$  is greater than that contributed by the mode corresponding to  $m = 1$  and  $n = 2$ .

### 3.8 Conclusions

With the information presented herein, the free vibrational characteristics and the sloshing action of base-excited, layered liquids both in long rectangular and in cylindrical tanks may be evaluated readily and accurately. The comprehensive numerical data that have been presented provide valuable insights into the underlying response mechanisms and into the effects and relative importance of the numerous parameters involved. The principal conclusions of the study may be summarized as follows:

1. For a liquid with  $N$  homogeneous layers, there is an infinite number of horizontal natural modes of vibration, and corresponding to each such mode, there are  $N$  distinct vertical modes. The latter modes have from zero to  $N - 1$  points of zero

crossings, and their frequencies are lower than the corresponding frequency of a uniform liquid of the same total depth.

2. For a specified horizontal mode of vibration, the natural frequencies of a two-layered system are, respectively, higher and lower than those computed considering the two liquid layers to act independently.
3. The natural modes of the layered liquid satisfy simple orthogonality relations that are identified in the text.
4. The maximum surface sloshing displacement of a layered system is typically greater than that of a homogeneous system of the same total depth. The increase is significant, however, only when the densities of individual layers differ substantially. The increased response is associated with the fact that, in addition to the lateral component of shaking, the base of the top layer is subjected to the rocking motion induced by the sloshing action of the interface.
5. For large-capacity tanks subjected to earthquake-ground motions, the mode of vibration corresponding to  $m = n = 1$  is the dominant contributor to the surface sloshing displacements of the liquid. Furthermore, the contribution of the mode corresponding to  $m = 2$  and  $n = 1$  is typically greater than that of the mode corresponding to  $m = 1$  and  $n = 2$ .
6. For the 2-layered system considered in the illustrative example, the maximum surface displacement along the tank wall was found to range from 3.96 times the maximum ground displacement when the densities of the two layers were considered to be equal, to 5.3 times the maximum ground displacement when the density of the top layer was taken as one-tenth that of the lower layer.

**Table 3.1: Surface-displacement coefficients for two-layered long rectangular and cylindrical systems**

$H/R$	$\rho_2/\rho_1$	Values of $d_{mn,2}$ for long rectangular systems				Values of $d_{mn,2}$ for cylindrical systems					
		$m = 1$		$m = 2$		$m = 1$		$m = 2$			
		$n = 1$	$n = 2$	$n = 1$	$n = 2$	$n = 1$	$n = 2$	$n = 1$	$n = 2$		
0.5	1.0	0.811		0.090	$(a) \ H_2/H_1 = 1$	0.837		0.073			
		0.75	0.873	-0.062		0.096	-0.006	0.901	-0.064	0.077	-0.004
		0.50	0.978	-0.167		0.106	-0.016	1.009	-0.172	0.085	-0.012
		0.25	1.215	-0.405		0.132	-0.042	1.254	-0.417	0.105	-0.032
		0.10	1.687	-0.876		0.184	-0.094	1.741	-0.904	0.148	-0.075
		0.01	4.458	-3.647		0.494	-0.404	4.602	-3.765	0.399	-0.326
		2.0	1.0	0.811			0.090		0.837		0.073
0.75	0.853			-0.042	0.090	0.000	0.873	-0.036	0.073	0.000	
0.50	0.932			-0.121	0.091	-0.001	0.942	-0.105	0.073	0.000	
0.25	1.138			-0.327	0.092	-0.002	1.130	-0.293	0.074	-0.001	
0.10	1.598			-0.787	0.097	-0.007	1.579	-0.742	0.076	-0.003	
0.01	4.415			-3.604	0.168	-0.078	4.507	-3.670	0.108	-0.035	
0.5	1.0			0.811		0.090	$(b) \ H_2/H_1 = 2$	0.837		0.073	
		0.75	0.863	-0.052	0.094	-0.004		0.890	-0.053	0.076	-0.003
		0.50	0.944	-0.133	0.101	-0.011		0.973	-0.136	0.081	-0.008
		0.25	1.099	-0.289	0.115	-0.025		1.132	-0.295	0.091	-0.018
		0.10	1.303	-0.493	0.137	-0.047		1.342	-0.505	0.109	-0.036
		0.01	1.573	-0.762	0.173	-0.083		1.623	-0.786	0.139	-0.066
		2.0	1.0	0.811		0.090			0.837		0.073
0.75	0.836			-0.025	0.090	0.000	0.857	-0.020	0.073	0.000	
0.50	0.881			-0.070	0.090	0.000	0.893	-0.056	0.073	0.000	
0.25	0.986			-0.176	0.091	-0.001	0.983	-0.146	0.073	0.000	
0.10	1.170			-0.360	0.092	-0.002	1.156	-0.319	0.074	-0.001	
0.01	1.533			-0.722	0.104	-0.014	1.560	-0.723	0.078	-0.005	

**Table 3.2:** Surface-displacement coefficients for three-layered cylindrical system with  $H/R = 1$  and  $H_1 = H_2 = H_3$

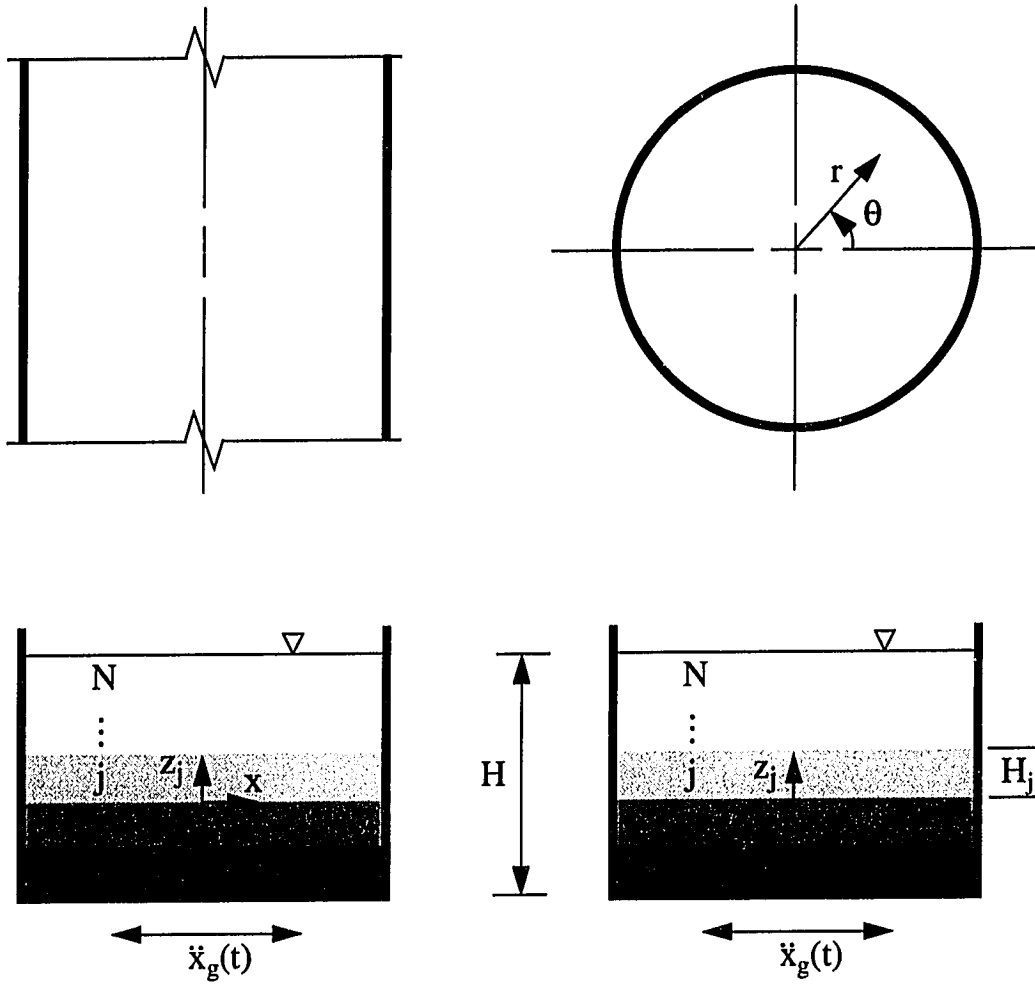
$\rho_3/\rho_2/\rho_1$	Values of $d_{mn,3}$					
	$m = 1$			$m = 2$		
	$n = 1$	$n = 2$	$n = 3$	$n = 1$	$n = 2$	$n = 3$
1/1/1	0.837			0.073		
1/2/3	1.101	-0.295	0.031	0.085	-0.013	0.001

**Table 3.3: Natural frequencies and surface-displacement coefficients for system considered in numerical example**

$\rho_2/\rho_1$	Natural frequency, $f_{mn}$ in cps				Surface-displacement coefficients, $d_{mn,2}$			
	$f_{11}$	$f_{12}$	$f_{21}$	$f_{22}$	$d_{11,2}$	$d_{12,2}$	$d_{21,2}$	$d_{22,2}$
1.00	0.142		0.269		0.837		0.073	
0.75	0.140	0.039	0.269	0.094	0.888	-0.051	0.075	-0.002
0.50	0.137	0.058	0.268	0.142	0.970	-0.133	0.079	-0.006
0.25	0.133	0.075	0.268	0.188	1.127	-0.290	0.088	-0.015
0.10	0.129	0.086	0.267	0.217	1.337	-0.500	0.105	-0.032

**Table 3.4: Maximum values of surface displacements of liquid along tank wall for system considered in numerical example**

$\rho_2/\rho_1$	Values of $(d_w)_{max}/(x_g)_{max}$				
	Component contributed by				Total computed by SRSS rule
	$m = 1$		$m = 2$		
	$n = 1$	$n = 2$	$n = 1$	$n = 2$	
1.00	3.775		1.181		3.956
0.75	3.893	0.006	1.213	0.004	4.078
0.50	4.071	0.047	1.269	0.028	4.265
0.25	4.459	0.263	1.414	0.119	4.687
0.10	4.975	0.706	1.673	0.337	5.307



(a) Long rectangular system

(b) Cylindrical system

Figure 3.1 Systems considered



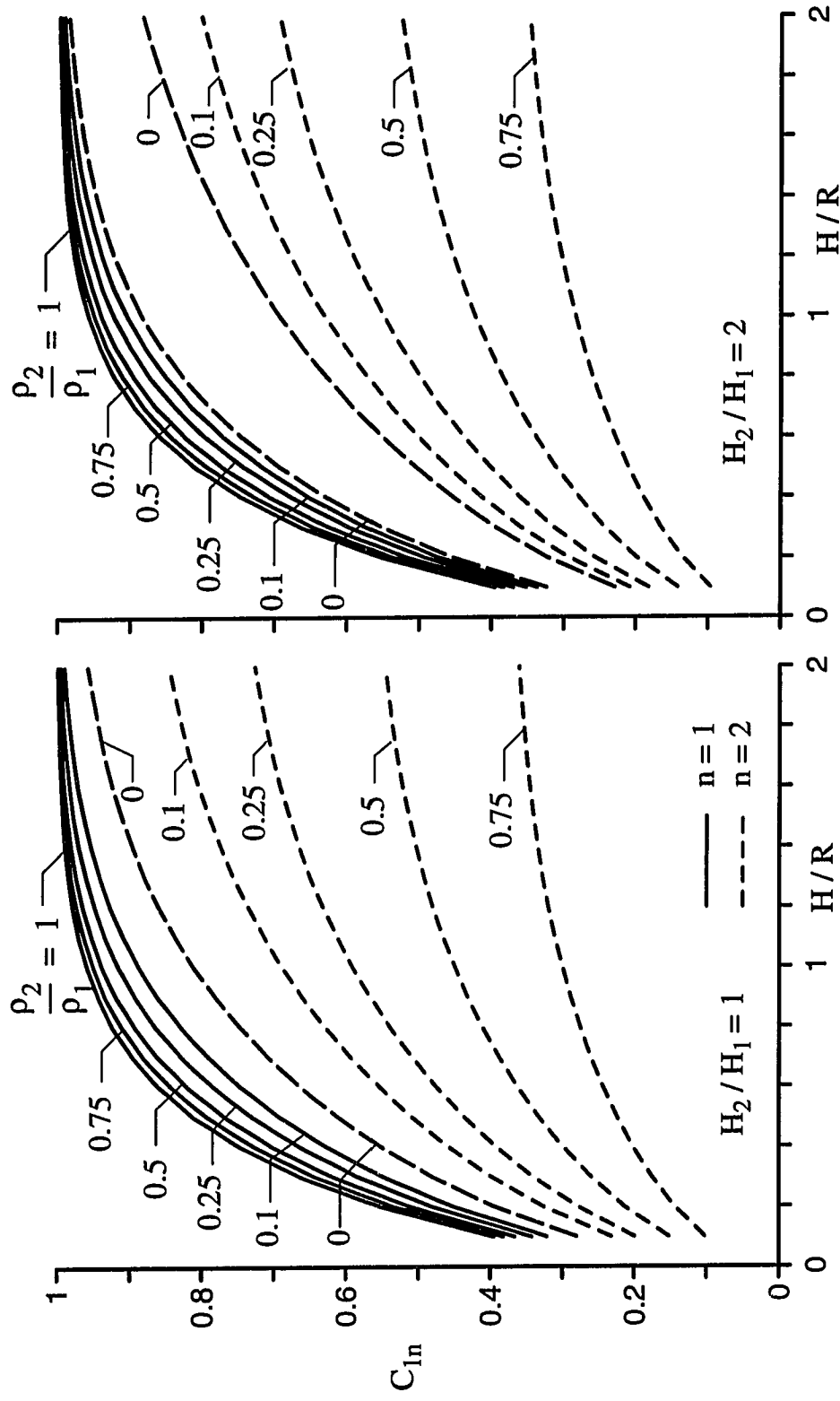


Figure 3.2 Frequency coefficients  $C_{1n}$  for fundamental horizontal mode of vibration of two-layered liquids in long rectangular tanks

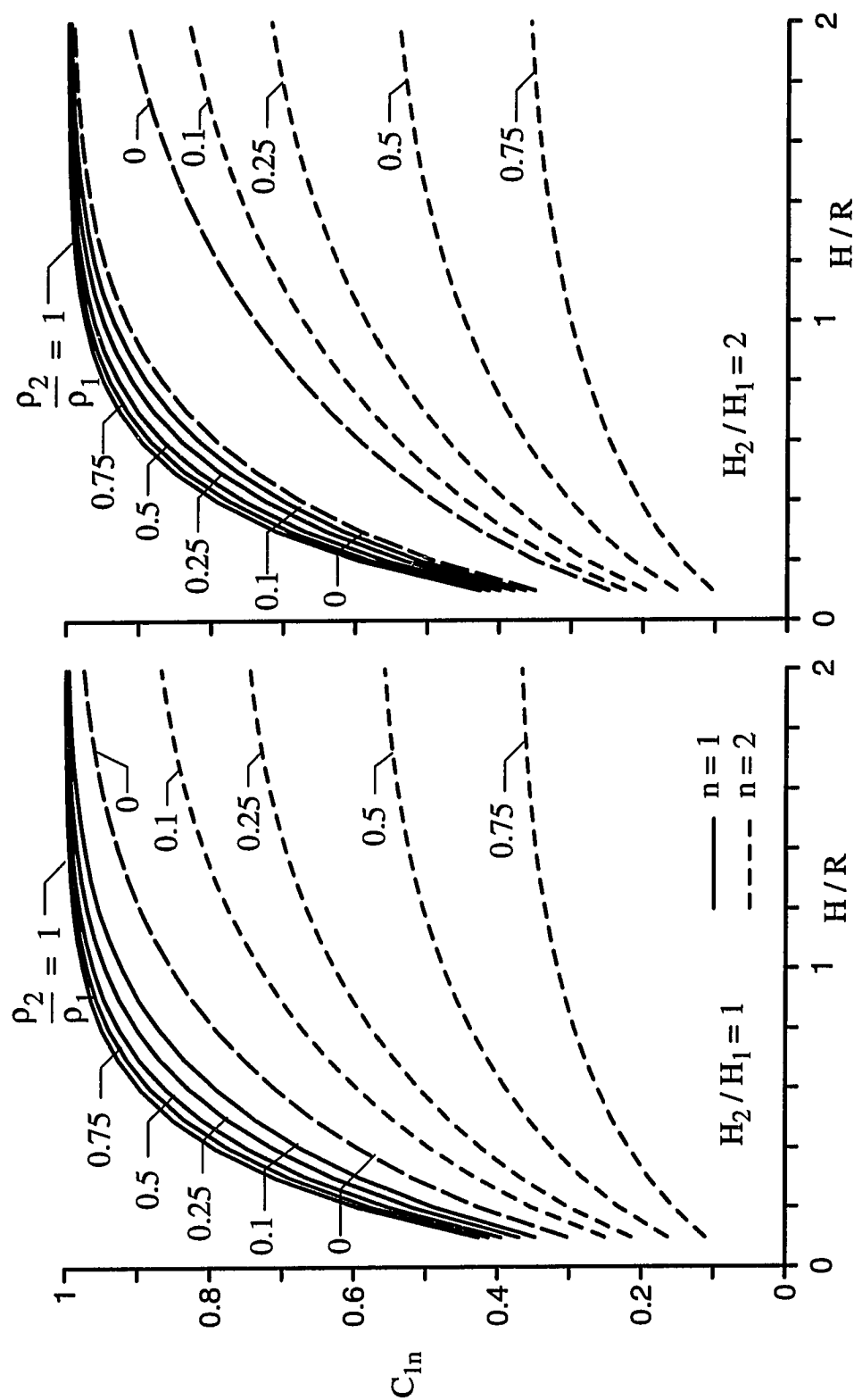


Figure 3.3 Frequency coefficients  $C_{1n}$  for fundamental horizontal mode of vibration of two-layered liquids in cylindrical tanks

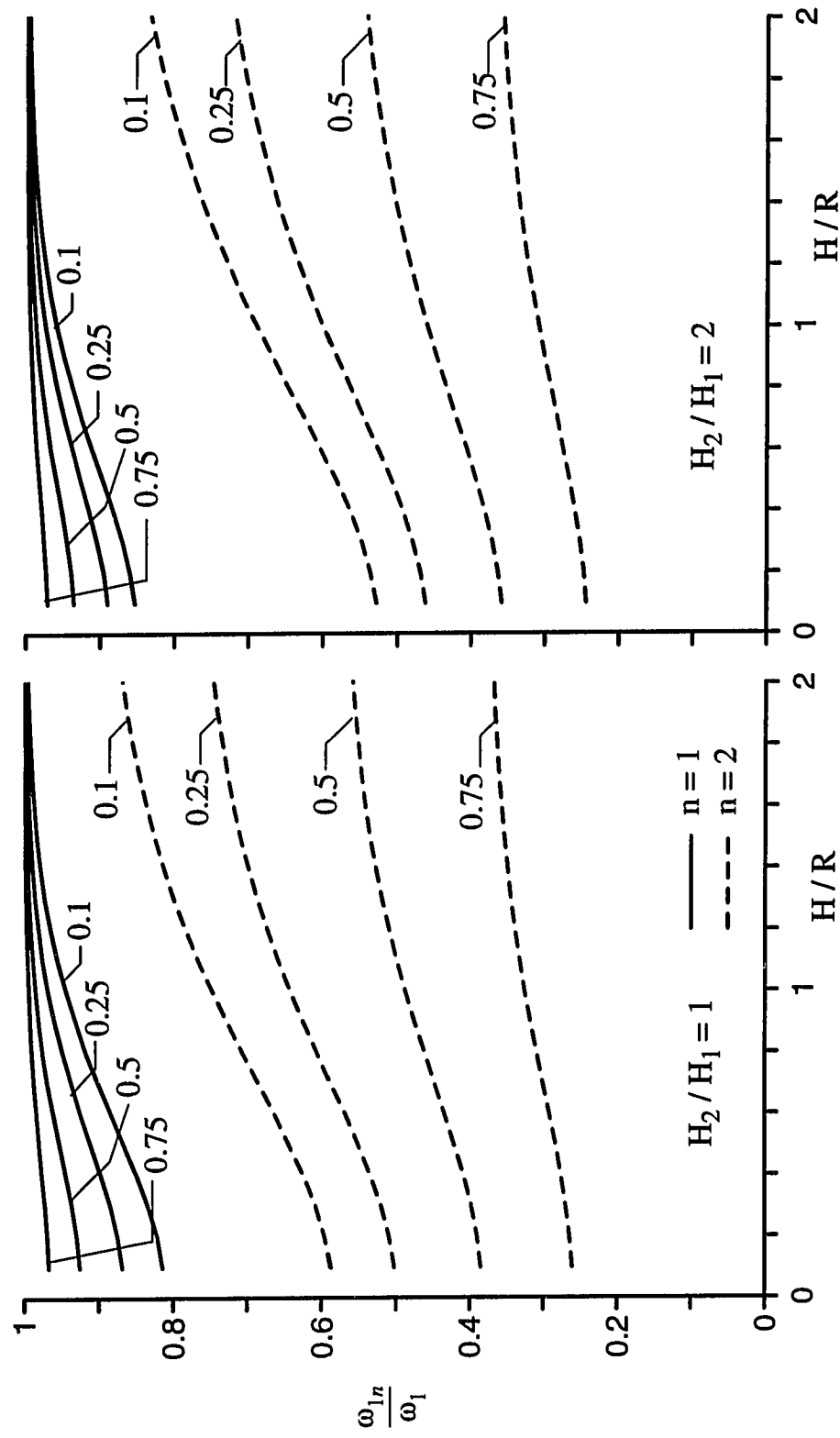


Figure 3.4 Ratio of natural frequencies of two-layered and homogeneous liquids in cylindrical tanks

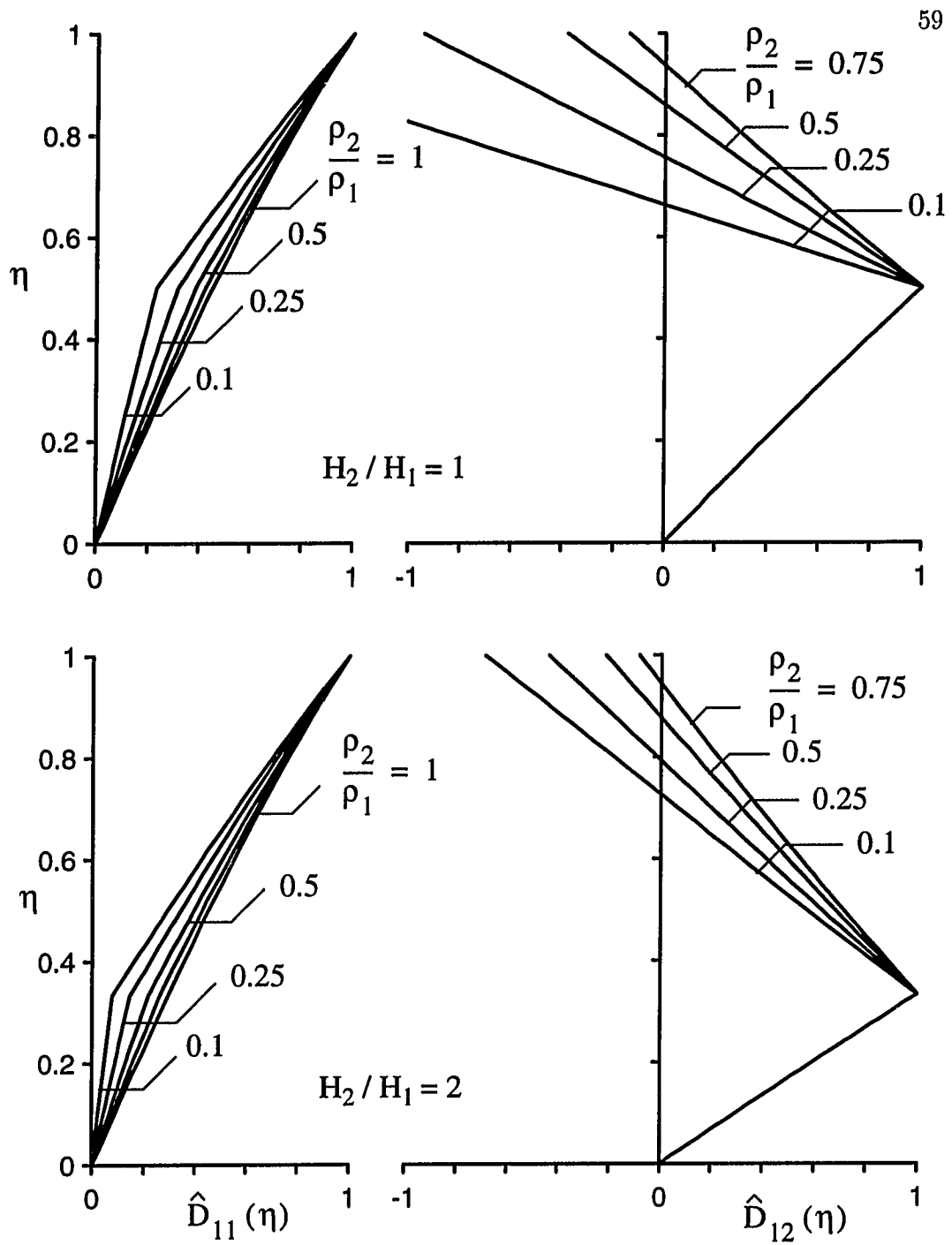


Figure 3.5 Vertical displacement configuration for the fundamental horizontal mode of vibration of two-layered liquids in cylindrical tanks with  $H/R = 0.5$

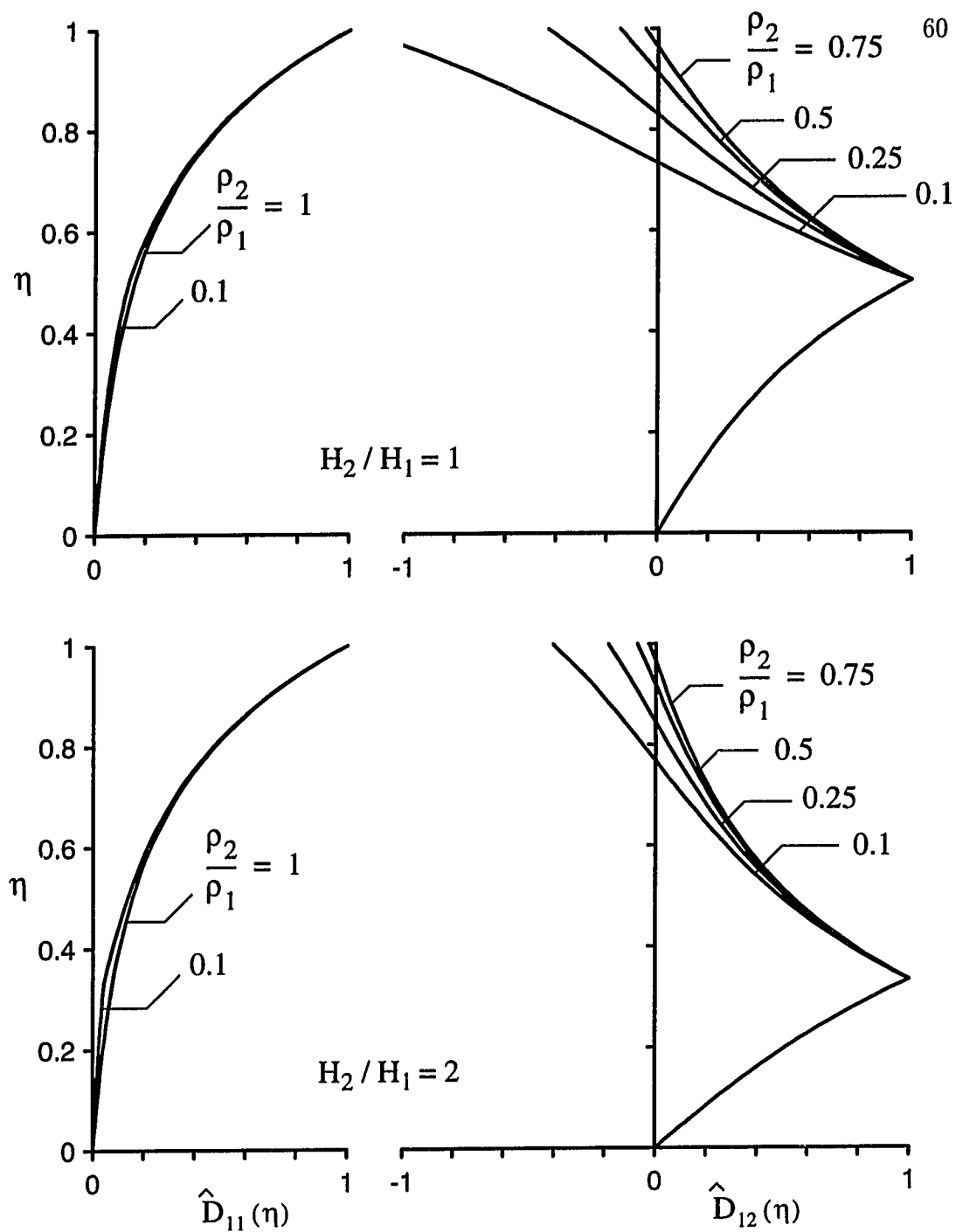


Figure 3.6 Vertical displacement configurations for the fundamental horizontal mode of vibration of two-layered liquids in cylindrical tanks with  $H/R = 2.0$

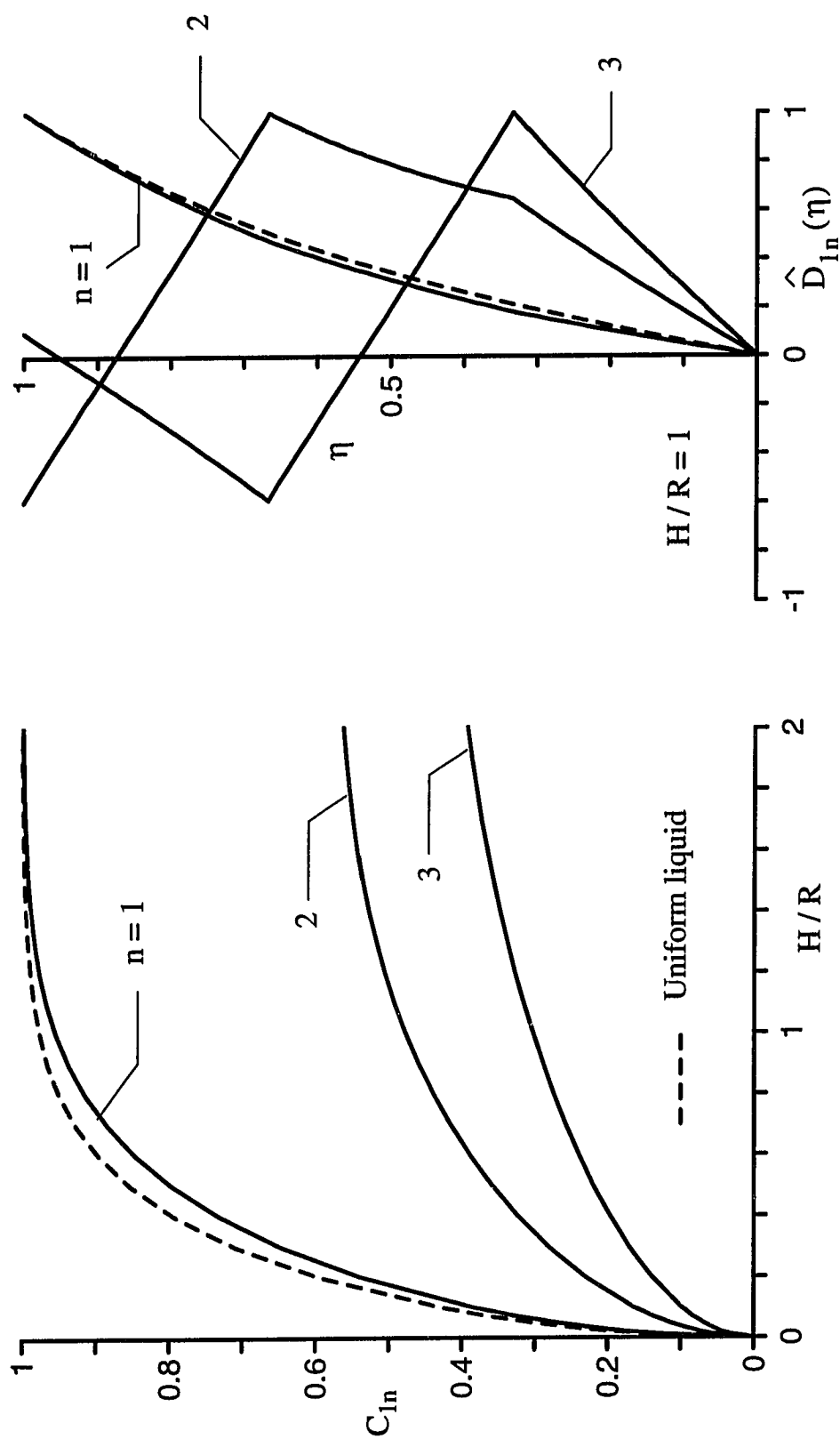


Figure 3.7 Frequency coefficient  $C_{1n}$  for the fundamental horizontal mode of vibration of three-layered liquids in cylindrical tanks and associated vertical displacement configurations for systems with  $H/R = 1$ ;  $H_1 = H_2 = H_3$  and  $\rho_3/\rho_2/\rho_1 = 1/2/3$

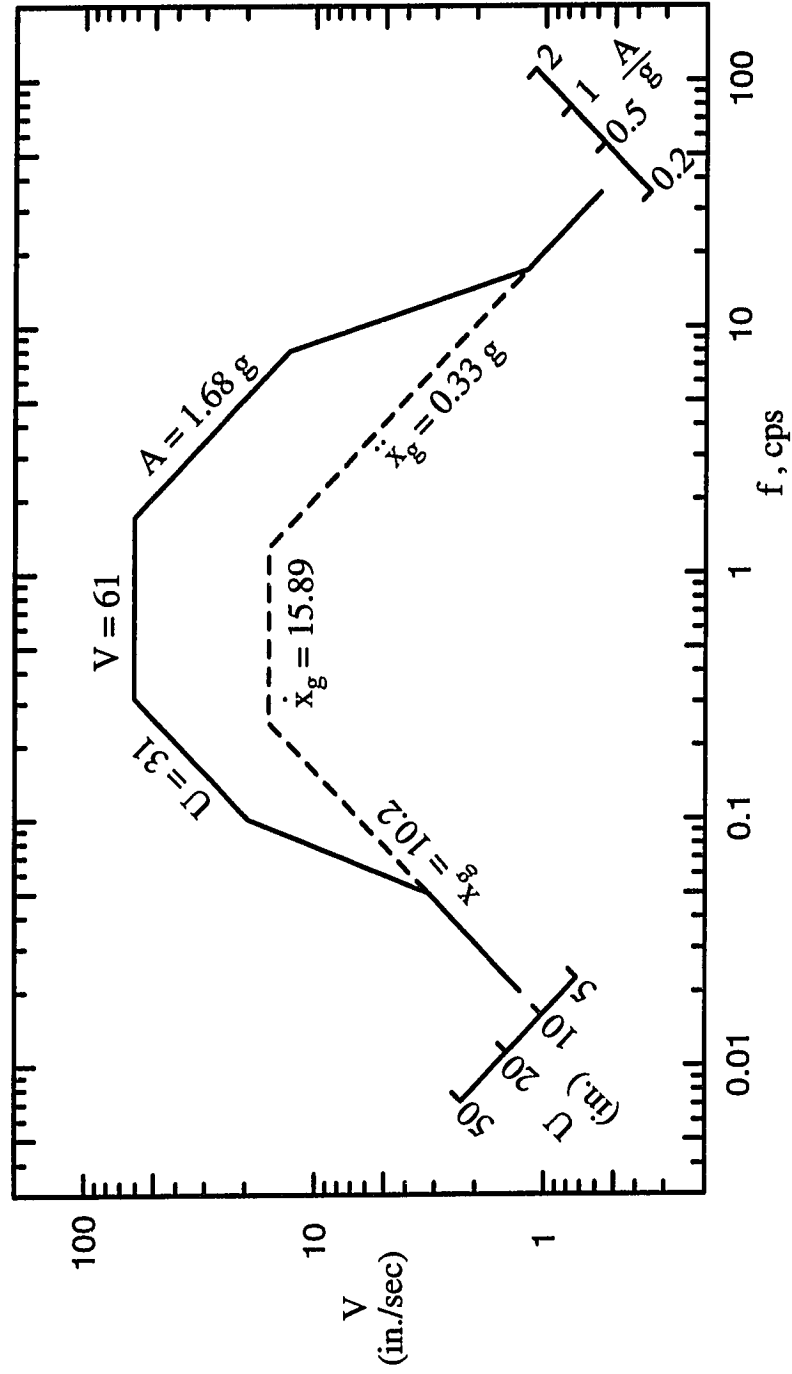


Figure 3.8 Design response spectrum considered in numerical example

## Chapter 4

# Hydrodynamic Effects in Rigid Tanks containing Layered Liquids

### 4.1 Introduction

The study described herein is a sequel to the one reported in Chapter 3. It deals with the evaluation of the hydrodynamic effects induced in rigid tanks containing layered liquids. The objectives are to elucidate the response mechanisms of the systems referred to, and to provide information and concepts with which the effects of the primary parameters may be evaluated rationally and conveniently for design purposes. The response quantities examined include the hydrodynamic wall pressures, the associated base shears, and the bending moments at sections immediately above and below the tank base. Both the impulsive and convective actions are examined. Related studies for rigid two-layered systems have also been presented recently by Tang et al [56, 59, 60]. The earlier of these studies were based on an inaccurate representation of the layered system and the consequences of this approximation have been identified in Chapter 3.

Only the cylindrical system is considered here. The system is the same as that shown in Fig. 3.1 (b).

### 4.2 Method of Analysis

#### 4.2.1 Hydrodynamic Pressures

On substituting equations (3.16) and (3.27) into equation (3.12) and making use of equation (3.5), the hydrodynamic pressure in the  $j$ th layer,  $p_j(\xi, \eta_j, \theta, t)$ , may be expressed as

$$p_j = - \left\{ \xi \ddot{x}_g(t) + \sum_{m=1}^{\infty} \left[ \frac{\ddot{D}_{m,j}(t) \cosh \lambda_m \eta_j - \ddot{D}_{m,j-1}(t) \cosh \lambda_m (\alpha_j - \eta_j)}{\lambda_m \sinh \lambda_m \alpha_j} \right] \frac{J_1(\lambda_m \xi)}{J_1(\lambda_m)} \right\} \rho_j R \cos \theta \quad (4.1)$$



in which  $\ddot{D}_{m,j}$  and  $\ddot{D}_{m,j-1}$  are obtained by double differentiating with respect to time the expression

$$\{D_m(t)\} = -R \sum_{n=1}^N \{d_{mn}\} \frac{A_{mn}(t)}{g} \quad (4.2)$$

which in turn is obtained by substituting equation (3.50) into equation (3.46) and by making use of equation (3.54) for the vector of dimensionless displacement coefficients,  $\{d_{mn}\}$ .  $A_{mn}(t)$  is the instantaneous modal pseudoacceleration function given by equation (3.51). On recalling that  $A_{mn}(t)$  is related to the deformation  $U_{mn}(t)$  of a base-excited single-degree-of-freedom system by

$$A_{mn}(t) = -\omega_{mn}^2 U_{mn}(t) \quad (4.3)$$

and that the second time derivative of  $U_{mn}(t)$  may be determined from the equation of motion for such a system to be

$$\ddot{U}_{mn}(t) = -\ddot{x}_g(t) - \omega_{mn}^2 U_{mn}(t) = -\ddot{x}_g(t) + A_{mn}(t) \quad (4.4)$$

equation (4.2) leads to

$$\{\ddot{D}_m(t)\} = -R \sum_{n=1}^N \omega_{mn}^2 \{d_{mn}\} \left( \frac{\ddot{x}_g(t)}{g} - \frac{A_{mn}(t)}{g} \right) \quad (4.5)$$

Finally, on substituting the expressions for  $\ddot{D}_{m,j}(t)$  and  $\ddot{D}_{m,j-1}(t)$  into equation (4.1), making use of equation (3.45) for  $\omega_{mn}^2$ , and grouping together all terms that are proportional to the ground acceleration, equation (4.1) may be rewritten as the sum of an impulsive component and a convective component as

$$p_j(\xi, \eta_j, \theta, t) = p_j^i(\xi, \eta_j, \theta, t) + p_j^c(\xi, \eta_j, \theta, t) \quad (4.6)$$

The impulsive component, which represents the effect of the part of the liquid that may be considered to move as a rigid body with the tank wall and hence experiences the same acceleration as the ground, is given by

$$p_j^i(\xi, \eta_j, \theta, t) = - \left[ \xi - \sum_{m=1}^{\infty} \sum_{n=1}^N c_{mn,j}(\eta_j) \frac{J_1(\lambda_m \xi)}{J_1(\lambda_m)} \right] \rho_j R \cos \theta \ddot{x}_g(t) \quad (4.7)$$

whereas the convective component, which represents the effect of the sloshing action of the liquid, is given by

$$p_j^c(\xi, \eta_j, \theta, t) = - \left[ \sum_{m=1}^{\infty} \sum_{n=1}^N c_{mn,j}(\eta_j) \frac{J_1(\lambda_m \xi)}{J_1(\lambda_m)} A_{mn}(t) \right] \rho_j R \cos \theta \quad (4.8)$$

in which

$$c_{mn,j}(\eta_j) = C_{mn}^2 \left[ \frac{d_{mn,j} \cosh \lambda_m \eta_j - d_{mn,j-1} \cosh \lambda_m (\alpha_j - \eta_j)}{\sinh \lambda_m \alpha_j} \right] \quad (4.9)$$

In the latter expression,  $d_{mn,j}$  represents the  $j$ th element of  $\{d_{mn}\}$ ;  $C_{mn}$  represents the dimensionless frequency coefficient in equation (3.45); and the terms with the factors  $d_{mn,j-1}$  and  $d_{mn,j}$  represent the effect of the sloshing or rocking actions of the lower and upper interfaces, respectively. It should be clear from equation (4.8) that there is an infinite number of horizontal sloshing modes of vibration; that for each such mode, there exist  $N$  vertical modes; and that associated with each horizontal and vertical mode, there is a distinct pseudoacceleration function,  $A_{mn}(t)$ . The summations on  $m$  in equations (4.7) and (4.8) represent the contributions of the horizontal modes, while those on  $n$  represent the contributions of the vertical modes.

### Simplification of solution for impulsive pressures

In the form presented so far, the evaluation of the impulsive component of response requires the prior evaluation of the convective components. The impulsive component can also be evaluated independently of the convective as follows : On letting

$$\{e_m\} = \sum_{n=1}^N C_{mn}^2 \{d_{mn}\} \quad (4.10)$$

equation (4.7) may be rewritten as a single series as

$$p_j^i(\xi, \eta_j, \theta, t) = - \left\{ \xi - \sum_{m=1}^{\infty} \left[ e_{m,j} \frac{\cosh \lambda_m \eta_j}{\sinh \lambda_m \alpha_j} - e_{m,j-1} \frac{\cosh \lambda_m (\alpha_j - \eta_j)}{\sinh \lambda_m \alpha_j} \right] \frac{J_1(\lambda_m \xi)}{J_1(\lambda_m)} \right\} \rho_j R \cos \theta \ddot{x}_g(t) \quad (4.11)$$

in which  $e_{m,j}$  is the  $j$ th element of  $\{e_m\}$ . It is shown in Appendix A that the vector  $\{e_m\}$  also represents the solution of the system of algebraic equations

$$[\mathcal{A}] \{e_m\} = \epsilon_m \{s\} \quad (4.12)$$

in which  $[\mathcal{A}]$  and  $\{s\}$  are the matrices appearing in equation (3.35). With the values of  $\{e_m\}$  determined in this manner, the impulsive pressures may be evaluated from equation (4.11) without prior knowledge of the sloshing frequencies and the associated modes of vibration of the system. The numerical solutions reported herein have been obtained by this approach.

It may be of interest to observe that equation (4.12) is merely a statement of the fact that the impulsive pressures are continuous at the  $N$  liquid interfaces. If the dimensionless distance coordinate  $\xi$  in equation (4.11) is expanded in the form

$$\xi = \sum_{m=1}^{\infty} \epsilon_m \frac{J_1(\lambda_m \xi)}{J_1(\lambda_m)} \quad (4.13)$$

the  $j$  th component of equation (4.12) is obtained simply by equating the expressions for the impulsive component of the pressure on either side of the  $j$  th interface.

### Wall pressure

The hydrodynamic wall pressure for the  $j$  th layer may be written in the form

$$p_j(1, \eta_j, \theta, t) = - \left[ c_{o,j}(\eta_j) \ddot{x}_g(t) + \sum_{m=1}^{\infty} \sum_{n=1}^N c_{mn,j}(\eta_j) A_{mn}(t) \right] \rho_j R \cos \theta \quad (4.14)$$

where  $c_{o,j}(\eta_j)$  is a dimensionless function, obtained from the expression within the braces in equation (4.11) by letting  $\xi = 1$ , i.e.,

$$c_{o,j}(\eta_j) = 1 - \sum_{m=1}^{\infty} \left[ e_{m,j} \frac{\cosh \lambda_m \eta_j}{\sinh \lambda_m \alpha_j} - e_{m,j-1} \frac{\cosh \lambda_m (\alpha_j - \eta_j)}{\sinh \lambda_m \alpha_j} \right] \quad (4.15)$$

From equations (4.9), (4.10) and (4.15), it now follows that

$$c_{o,j}(\eta_j) + \sum_{m=1}^{\infty} \sum_{n=1}^N c_{mn,j}(\eta_j) = 1 \quad (4.16)$$

It is important to note that the pressure in equation (4.14) is expressed in terms of the density of the layer under consideration rather than that of some reference layer.

### Specialized expressions for wall pressure

For a single-layered, homogeneous system,  $[A] = \coth \lambda_m H/R$ ,  $\{s\} = 1$ , equation (4.12) yields

$$e_m = \epsilon_m \tanh \lambda_m H/R \quad (4.17)$$

and equation (4.15) reduces, as it should, to the well-known expression

$$c_o(z) = 1 - \sum_{m=1}^{\infty} \epsilon_m \frac{\cosh \lambda_m z/R}{\cosh \lambda_m H/R} \quad (4.18)$$

where  $z$  is the vertical distance from the tank base, and the  $m$ th term of the summation represents the dimensionless function  $c_m(z)$  in the expression for the convective component of the pressure.

For a two-layered system, the solution of equation (4.12) yields

$$e_{m,1} = \epsilon_m \frac{[(1 - \rho_2/\rho_1) \cosh \lambda_m \alpha_2 + \rho_2/\rho_1] \sinh \lambda_m \alpha_1}{\cosh \lambda_m \alpha_1 \cosh \lambda_m \alpha_2 + (\rho_2/\rho_1) \sinh \lambda_m \alpha_1 \sinh \lambda_m \alpha_2} \quad (4.19)$$

and

$$e_{m,2} = \frac{\epsilon_m \sinh \lambda_m \alpha_2 + e_{m,1}}{\cosh \lambda_m \alpha_2} \quad (4.20)$$

On substituting these expressions for  $e_{m,j}$  into equation (4.15) and recalling that  $e_{m,j-1}$  for  $j = 1$  is zero, the resulting expressions can be shown to reduce to those presented in [56]. The corresponding expressions for the convective pressure components are given by equation (4.9), in which  $d_{mn,j-1}$  for  $j = 1$  must be taken as zero,  $d_{mn,j}$  for  $j = 1$  and 2 must be determined from equation (3.54) and  $C_{mn}^2$  must be evaluated from equation (3.40). The results obtained in this manner can again be shown to agree with those obtained from expressions presented in [59].

## 4.2.2 Tank Forces

### Base shear

The instantaneous value of the base shear or total hydrodynamic force acting on the tank-wall,  $Q_b(t)$ , is given by

$$Q_b(t) = \sum_{j=1}^N \int_0^{H_j} \int_0^{2\pi} p_j(1, z_j, \theta, t) R \cos \theta d\theta dz_j \quad (4.21)$$

which, on expressing the wall pressure by equation (4.14) and performing the indicated integrations, can be written as

$$Q_b(t) = m_o \ddot{x}_g(t) + \sum_{m=1}^{\infty} \sum_{n=1}^N m_{mn} A_{mn}(t) \quad (4.22)$$

with  $m_o$  and  $m_{mn}$  given by

$$m_o = \sum_{j=1}^N m_{o,j} = \sum_{j=1}^N m_{l,j} \left( 1 - \sum_{m=1}^{\infty} \frac{e_{m,j} - e_{m,j-1}}{\lambda_m \alpha_j} \right) \quad (4.23)$$

and

$$m_{mn} = \sum_{j=1}^N m_{mn,j} = \sum_{j=1}^N m_{l,j} \left( \frac{C_{mn}^2 d_{mn,j} - C_{mn}^2 d_{mn,j-1}}{\lambda_m \alpha_j} \right) \quad (4.24)$$

The quantity  $m_{l,j}$  in the preceding two equations represents the mass of the  $j$ th layer,  $\rho_j \pi R^2 H_j$ ;  $m_{o,j}$  represents the portion of  $m_{l,j}$  that acts impulsively; and  $m_o$  represents the total impulsive mass. Similarly,  $m_{mn}$  represents the total liquid mass participating in the  $m$ th horizontal and  $n$ th vertical sloshing mode of vibration, and  $m_{mn,j}$  represents the part that is contributed by the  $j$ th layer. From equations (4.23) and (4.24), and with the aid of equation (4.10), it can finally be shown that

$$m_o + \sum_{m=1}^{\infty} \sum_{n=1}^N m_{mn} = \sum_{j=1}^N m_{l,j} = m_l \quad (4.25)$$

That is, the sum of the impulsive mass and all convective masses equals the total mass of the liquid,  $m_l$ .

### Moment above base

The instantaneous value of the hydrodynamic moment induced across a section of the tank immediately above the base is given by

$$M(t) = \sum_{j=1}^N \int_0^{H_j} \int_0^{2\pi} p_j(1, z_j, \theta, t) [L_{j-1} + z_j] R \cos \theta \, d\theta \, dz_j \quad (4.26)$$

where

$$L_{j-1} = \sum_{k=1}^{j-1} H_k \quad (4.27)$$

refers to the height of the  $(j-1)$ th liquid interface measured from the tank base. On substituting equation (4.14) for the wall pressure into equation (4.26) and integrating, one obtains

$$M(t) = m_o h_o \ddot{x}_g(t) + \sum_{m=1}^{\infty} \sum_{n=1}^N m_{mn} h_{mn} A_{mn}(t) \quad (4.28)$$

in which the quantity  $m_o h_o$  for the impulsive component of response is given by

$$m_o h_o = \sum_{j=1}^N \left\{ m_{l,j} H_j \left[ \frac{1}{2} - \sum_{m=1}^{\infty} \left( \frac{(e_{m,j} + e_{m,j-1})(1 - \cosh \lambda_m \alpha_j)}{\lambda_m^2 \alpha_j^2 \sinh \lambda_m \alpha_j} + \frac{e_{m,j}}{\lambda_m \alpha_j} \right) \right] + m_{o,j} L_{j-1} \right\} \quad (4.29)$$

and the quantity  $m_{mn}h_{mn}$  for the convective component associated with the  $m$ th horizontal and  $n$ th vertical mode of vibration is given by

$$m_{mn}h_{mn} = \sum_{j=1}^N \left\{ m_{lj}H_j \left[ C_{mn}^2 \left( \frac{(d_{mnj} + d_{mnj-1})(1 - \cosh \lambda_m \alpha_j)}{\lambda_m^2 \alpha_j^2 \sinh \lambda_m \alpha_j} + \frac{d_{mnj}}{\lambda_m \alpha_j} \right) \right] + m_{mnj}L_{j-1} \right\} \quad (4.30)$$

The quantity  $h_o$  in these expressions represents the height at which the mass  $m_o$  must be concentrated to yield the impulsive component of the base moment, and  $h_{mn}$  represents the height at which  $m_{mn}$  must be concentrated to yield the convective component of the corresponding moment associated with the  $m$ th horizontal and  $n$ th vertical mode of vibration. From equations (4.29) and (4.30) and with the aid of equations (4.10) and (4.25), it can be shown that

$$m_o h_o + \sum_{m=1}^{\infty} \sum_{n=1}^N m_{mn} h_{mn} = \sum_{j=1}^N m_{lj} \left( L_{j-1} + \frac{H_j}{2} \right) = m_l h_l \quad (4.31)$$

where  $h_l$  represents the height of the center of gravity of the total liquid mass from the tank base.

### Foundation moment

In addition to the moment  $M(t)$ , the foundation moment,  $M'(t)$ , includes the effect of the hydrodynamic pressures exerted on the tank base. The latter moment is given by,

$$M'(t) = M(t) + \int_0^R \int_0^{2\pi} p_1(r, 0, \theta, t) r^2 \cos \theta \, d\theta \, dr \quad (4.32)$$

which, on expressing  $M(t)$  by equation (4.28), replacing  $p_1$  by the sum of equations (4.7) and (4.8) with  $j = 1$ , and integrating, can be written as

$$M'(t) = m_o h_o' \ddot{x}_g(t) + \sum_{m=1}^{\infty} \sum_{n=1}^N m_{mn} h'_{mn} A_{mn}(t) \quad (4.33)$$

with

$$m_o h_o' = m_o h_o + m_{l,1} H_1 \left( \frac{1}{4\alpha_1^2} - \sum_{m=1}^{\infty} \frac{e_{m,1}}{\alpha_1^2 \lambda_m^2 \sinh \lambda_m \alpha_1} \right) \quad (4.34)$$

and

$$m_{mn} h'_{mn} = m_{mn} h_{mn} + m_{l,1} H_1 \left( \frac{C_{mn}^2 d_{mn,1}}{\alpha_1^2 \lambda_m^2 \sinh \lambda_m \alpha_1} \right) \quad (4.35)$$

From the latter two expressions and equations (4.10) and (4.31), one finally obtains

$$m_o h'_o + \sum_{m=1}^{\infty} \sum_{n=1}^N m_{mn} h'_{mn} = m_l h_l + m_{l,1} H_1 \frac{1}{4\alpha_1^2} = m_l h'_l \quad (4.36)$$

where the term on the extreme right represents the foundation moment induced by an unit acceleration when the entire liquid is presumed to act as a rigid mass, and the term involving  $m_{l,1}$  represents the component of this moment contributed by the base pressure. The latter pressure increases linearly from zero at the center of the tank base to  $\rho_1 R \cos\theta$  at the junction of the base and the wall.

### 4.3 Presentation and Analysis of Numerical Solutions

#### 4.3.1 Hydrodynamic Wall Pressures

##### Normalization of Wall Pressures

In examining their variations with height, it is desirable to express the hydrodynamic wall pressures in terms of the density of some reference liquid layer rather than in the form of equation (4.14), in terms of the density of the layer being considered. In the remainder of this paper, all pressures are expressed in terms of the mass density of the heaviest or bottom layer,  $\rho_1$ , as

$$p(1, \eta, \theta, t) = - \left[ c_o(\eta) \ddot{x}_g(t) + \sum_{m=1}^{\infty} \sum_{n=1}^N c_{mn}(\eta) A_{mn}(t) \right] \rho_1 R \cos\theta \quad (4.37)$$

where  $\eta = z/H$  is the normalized vertical position coordinate, and  $c_o(\eta)$  and  $c_{mn}(\eta)$  are dimensionless functions defining the vertical distributions of the various pressure components.

For a value of  $z$  corresponding to the  $j$ th layer (i.e.,  $L_{j-1} \leq z \leq L_j$ ), the functions  $c_o(\eta)$  and  $c_{mn}(\eta)$  are related to the functions  $c_{o,j}(\eta_j)$  and  $c_{mn,j}(\eta_j)$  in equation (4.14) by

$$c_o(\eta) = \frac{\rho_j}{\rho_1} c_{o,j}(\eta_j) \quad \text{and} \quad c_{mn}(\eta) = \frac{\rho_j}{\rho_1} c_{mn,j}(\eta_j) \quad (4.38)$$

Accordingly, equation (4.16) may be rewritten as

$$c_o(\eta) + \sum_{m=1}^{\infty} \sum_{n=1}^N c_{mn}(\eta) = \frac{\rho_j}{\rho_1} \quad \text{for } L_{j-1} \leq z \leq L_j \quad (4.39)$$

It is shown in Appendix A that the  $c_{mn}(\eta)$  functions are discontinuous at the layer interfaces, and that, for each horizontal mode of vibration, the sum of the discontinuities at an interface for all the vertical modes of vibration satisfy the relation

$$\sum_{n=1}^N \left\{ c_{mn}^- - c_{mn}^+ \right\} = \epsilon_m \{s\} \quad (4.40)$$

in which the  $-$  and  $+$  superscripts identify sections immediately below and above the interface under consideration. For two-layered systems, equation (4.40) reduces to

$$\sum_{n=1}^2 \left( c_{mn}^{1-} - c_{mn}^{1+} \right) = \epsilon_m \left( 1 - \frac{\rho_2}{\rho_1} \right) \quad (4.41)$$

for the first or lower interface, and to

$$\sum_{n=1}^2 c_{mn}^{2-} = \epsilon_m \left( \frac{\rho_2}{\rho_1} \right) \quad (4.42)$$

for the second or top interface.

### Representative Wall Pressures

Fig. 4.1 shows the heightwise distributions of the components of wall pressure for a tank with  $H/R = 1$  containing a two-layered liquid with  $\rho_2/\rho_1 = 0.5$  and  $H_2 = H_1 = 0.5 H$ . Part (a) of the figure shows the dimensionless function  $c_o(\eta)$  for the impulsive component of the pressure, whereas part (b) shows the functions  $c_{mn}(\eta)$  for the convective components associated with the first two horizontal modes of vibration. It should be recalled that there is an infinite number of horizontal modes, and that to each such mode there correspond  $N$  (two for a two-layered system) vertical modes. The  $c_{mn}(\eta)$  functions for the third and higher horizontal modes are negligibly small and are not included. Also shown in part (c) of the figure is the distribution function  $c_l(\eta)$  computed on the assumption that the entire liquid mass acts impulsively.

Similar plots are given in Fig. 4.2 for a three-layered liquid with equal layer thicknesses and values of  $\rho_j$  increasing from top to bottom in the ratio 1/2/3. In this case, only the convective pressure distributions corresponding to the fundamental horizontal mode of vibration are given.

The following trends are worth noting in Figs. 4.1 and 4.2 :

1. As is true of a homogeneous liquid, the impulsive pressures increase from zero at the top to a maximum at the base. The distributions of these pressures are continuous, but exhibit slope discontinuities or cusps at the layer interfaces.



2. The convective pressure components are discontinuous at the layer interfaces and, for a given horizontal mode of vibration, the sum of the discontinuities at an interface for all the vertical modes satisfies equation (4.40).
3. Irrespective of the order of the horizontal mode of vibration, the convective pressure associated with the  $n$ th vertical mode exhibits  $(n - 1)$  changes in sign. These changes are consistent with those noted in Chapter 3 for the corresponding modal displacements, and are associated with the relative sloshing or rocking actions of successive interfaces.
4. The algebraic sum of the impulsive and of all the convective pressure distribution functions satisfies equation (4.39); it is, therefore, equal to the function obtained by considering the entire liquid to act as a rigid mass.

In assessing the relative importance of the various convective pressure components, it should be kept in mind that their contributions depend not only on the values of the dimensionless distribution functions  $c_{mn}(\eta)$  but also on those of the corresponding pseudoacceleration functions  $A_{mn}(t)$ . The latter functions depend, in turn, on the characteristics of the ground motion, and on the natural frequency and damping of the mode of vibration being considered.

As an illustration, consider the two-layered system examined previously in Chapter 3, for which  $H = 36$  ft (10.98 m),  $R = 60$  ft (18.29 m),  $H_2 = 2H_1 = 2H/3$  and  $\rho_2 = 0.5\rho_1$ . The instantaneous value of the normalized hydrodynamic wall pressure at a section just below the interface of the two layers in this case is given by

$$\frac{p(1, \frac{1}{3}, \theta, t)}{\gamma_1 R \cos \theta} = 0.265 \frac{\ddot{x}_g(t)}{g} + 0.431 \frac{A_{11}(t)}{g} + 0.239 \frac{A_{12}(t)}{g} + 0.009 \frac{A_{21}(t)}{g} + 0.023 \frac{A_{22}(t)}{g} + \dots \quad (4.43)$$

in which  $\gamma_1 = \rho_1 g$  is the unit weight of the lower layer. Further, let the ground motion be specified by the design response spectrum presented in Fig. 3.8, which corresponds to a maximum ground acceleration  $\ddot{x}_g = 0.33g$  and a coefficient of viscous damping of 0.5 percent critical. Using the natural sloshing frequency values listed in Table 3.3, the maximum or spectral values of the first four pseudoacceleration functions  $A_{mn}(t)$ , denoted by  $A_{mn}$ , are found to be

$$A_{11} = 0.059g \quad A_{12} = 0.005g \quad A_{21} = 0.228g \quad A_{22} = 0.064g \quad (4.44)$$

On substituting these values along with  $\ddot{x}_g = 0.33g$  into equation (4.43), the maximum values of the impulsive and the first four convective terms become

Impulsive Term	Convective Terms			
	m=1		m=2	
	n=1	n=2	n=1	n=2
0.0875	0.0259	0.0012	0.0021	0.0015

Finally, when computed approximately by adding to the maximum value of the impulsive component the square root of the sum of squares of the convective components, the maximum value of the total hydrodynamic wall pressure at the elevation considered becomes  $0.114\gamma_1 R$ .

It should be noted that, whereas the coefficient of the term involving the  $A_{12}(t)$  function is much larger than of the term involving the  $A_{21}(t)$  function, the opposite is true of the relative magnitudes of these two terms. Note further that the maximum component of the convective pressure is contributed by the fundamental sloshing mode of vibration ( $m = n = 1$ ), that the contributions of the higher modes are negligibly small, and that the total convective pressure is small compared to the corresponding impulsive pressure. These results are representative of those that can be expected for large capacity tanks of normal proportions subjected to earthquakes.

### Wall Pressures for Two-Layered Systems

In the left part of Fig. 4.3, the  $c_o(\eta)$  function for the impulsive component of the wall pressure for the two-layered system examined previously in Fig. 4.1 is compared with those obtained for several other values of the density ratio  $\rho_2/\rho_1$ . Also shown are the corresponding functions  $c_{11}(\eta)$  and  $c_{12}(\eta)$  for the first horizontal sloshing mode of vibration. As would be expected, the impulsive pressure coefficients decrease with decreasing  $\rho_2/\rho_1$ , and for the limiting case of  $\rho_2/\rho_1 = 0$ , they reduce to the values applicable to a tank that is half-full with a homogeneous liquid of density  $\rho_1$ . By contrast, the convective pressures in the lower layer increase with decreasing  $\rho_2/\rho_1$ , and as  $\rho_2/\rho_1$  tends to zero,  $c_{11}(\eta)$  and  $c_{12}(\eta)$  become proportional to each other and their sum tends to the corresponding function for the half-full tank. The latter function is associated with a value of 0.837 at the tank mid-height and a value of 0.575 at the tank base.

The limiting behavior of the convective pressure distributions referred to above is strictly valid only for systems with  $H_1 = H_2 = 0.5 H$ , for which the uncoupled natural frequencies of the two layers (i.e., the frequencies computed considering the two layers

to act independently) are equal. For systems with unequal layer thicknesses, as  $\rho_2/\rho_1$  tends to zero, the convective pressure distribution for the tank containing only the lower layer is reached by the function  $c_{1n}(z)$  for which the associated frequency of vibration is closest to the uncoupled natural frequency of the lower layer. This is demonstrated in Fig. 4.4, where the distributions of  $c_{11}(\eta)$  and  $c_{12}(\eta)$  for a tank with  $H/R = 1$  and  $\rho_2/\rho_1 = 0.1$  are shown for two values of  $H_2/H_1$ . Note that for  $H_2 = 0.5H_1$ , for which the fundamental uncoupled natural frequency of the lower layer is higher than that of the upper (see, for example, equation 3.44), it is the  $c_{11}(\eta)$  function that approaches the distribution of the partially filled tank, while  $c_{12}(\eta)$  becomes negligibly small. By contrast, for  $H_2 = 2H_1$ , for which the uncoupled natural frequency of the bottom layer is the lower of the two, it is the  $c_{12}(\eta)$  function that approaches the distribution of the partially filled tank while  $c_{11}(\eta)$  tends to zero.

The impulsive and convective pressure coefficients for additional two-layered systems are listed in Table 4.1. The tabulated results are for the free-surface, for sections immediately above and below the interface (denoted by  $I+$  and  $I-$ , respectively), and for the tank base of systems with  $H/R = 0.5, 1$  and  $2$ , and  $H_2/H_1 = 0.5$  and  $2$ . The general trends of these data are similar to those of the data displayed in Figs. 4.3 and 4.4.

### 4.3.2 Tank Forces

#### Two-layered systems

Fig. 4.5 shows the masses  $m_o$  and  $m_{11}$  in the expression for base shear of systems with equal layer thicknesses and density ratios  $\rho_2/\rho_1$  in the range between 0.1 and 1. The results are plotted as a function of the total liquid height to tank radius ratio,  $H/R$ , and they are normalized with respect to  $m_l$ , the total liquid mass of the system being considered. Normalized values of the corresponding base moment coefficients,  $m_o h_o$  and  $m_{11} h_{11}$ , and of the foundation moment coefficients,  $m_o h'_o$  and  $m_{11} h'_{11}$ , are presented in Figs. 4.6 and 4.7, respectively. The normalizing quantities in these plots are those obtained by considering the entire liquid to act as a rigid mass, and are naturally different for tanks of different proportions and contents.

The normalized values of  $m_o$  and  $m_{11}$  for additional two-layered systems, along with the corresponding values of  $m_{12}$ ,  $m_{21}$  and  $m_{22}$ , are presented in Table 4.2, and the associated moment coefficients are presented in Tables 4.3 and 4.4. Examination of these data and of those displayed in the figures reveals the following trends :

1. For values of  $\rho_2/\rho_1$  between 0.5 and 1, the *normalized* values of the liquid masses  $m_o$ ,  $m_{11}$  and  $m_{21}$  may, for all practical purposes, be considered to be same over the entire range of  $H/R$  considered. The same is also true of the corresponding moment coefficients, although the ranges of  $\rho_2/\rho_1$  and  $H/R$  over which the results may be considered to be the same are somewhat different in the two cases. Incidentally, these quantities are the ones most likely to affect significantly the seismic response of practical systems. It follows that, within the indicated range of  $\rho_2/\rho_1$  values, the solutions for layered systems may be obtained with reasonable accuracy from well-established solutions [65] for tanks with homogeneous liquids. It should be recalled, however, that the normalizing quantities are different in the two cases.
2. For values of  $\rho_2/\rho_1$  smaller than 0.5, the proportion of the total liquid acting impulsively may be substantially lower for the layered system than for the homogeneous system. The large interfacial discontinuity in liquid density increases the sloshing or convective actions of the system, and this increase, in turn, leads to a corresponding diminution of the impulsive effects.
3. While the increase in the convective action of systems with the large changes in liquid density does not necessarily increase the normalized values of the response components for  $n = 1$ , it does increase the sum of the corresponding components for  $n = 1$  and  $n = 2$ . This is true for each horizontal mode of vibration and is demonstrated in Fig. 4.8 for the convective masses associated with the first and second horizontal modes of vibration (i.e.,  $m = 1$  and  $m = 2$ ). It can be seen that, in each case, the sum of the convective masses for the layered system is indeed higher than the corresponding mass for the homogeneous system.

### Three-layered systems

Numerical data similar to those presented in the preceding section for two-layered systems are given in Tables 4.5, 4.6 and 4.7 for three-layered systems with equal layer thicknesses. Three different values of  $H/R$  and two different ratios of layer densities are considered. As before, the results are normalized with respect to those computed on the assumption that the entire liquid mass acts rigidly.

The tabulated data satisfy equations (4.25), (4.31) and (4.36), and the interrelationships of the impulsive and convective results are generally similar to those for the two-layered systems examined in previous sections.

## 4.4 Conclusions

With the information presented herein, the response to horizontal base shaking of rigid, vertical, circular cylindrical tanks containing an arbitrary number of uniform liquid layers of varying thicknesses and densities may be evaluated rationally and effectively. The comprehensive numerical solutions that have been presented elucidate the underlying response mechanisms, as well as the effects and relative importance of the numerous parameters involved. The principal conclusions of the study are as follows :

1. The response of an  $N$ -layered system may be expressed as the sum of an impulsive component and an infinite number of horizontal convective or sloshing components, each associated with  $N$  vertical modes of vibration.
2. The convective component of the pressure associated with any horizontal and the  $n$ th vertical mode of vibration exhibits  $(n - 1)$  changes in sign. These changes are due to the in-phase or out-of-phase sloshing actions of the interfaces.
3. The impulsive pressure component is continuous and increases from zero at the top to a maximum at the base, whereas the convective pressure components are discontinuous at the layer interfaces, the magnitude of the discontinuity being a function of the tank proportions and of the relative densities and thicknesses of the layers.
4. When normalized with respect to the pressures computed on the assumption that the entire liquid acts as a rigid mass, the coefficients for the impulsive and all convective components of the hydrodynamic wall pressures add up to unity. The same is also true of the corresponding coefficients for base shear and base moments in the tank.
5. The impulsive component of response may be evaluated either as the difference between the response computed on the assumption that the entire liquid acts as a rigid mass and the sum of all convective components of response or, independently, without the prior evaluation of the convective effects.
6. For two-layered systems with ratios of mass densities in the range between 0.5 and 1.0, the base shear and base moments may be related simply to those obtained from well-established solutions for homogeneous systems.

**Table 4.1: Values of coefficients in expression for hydrodynamic wall pressure at selected sections of two-layered systems with different  $H/R$  and  $H_2/H_1$**

$\frac{\rho_2}{\rho_1}$	$\eta$	$H_2/H_1 = 0.5$					$H_2/H_1 = 2$				
		$c_o$	$c_{11}$	$c_{12}$	$c_{21}$	$c_{22}$	$c_o$	$c_{11}$	$c_{12}$	$c_{21}$	$c_{22}$
1	1	0	0.837		0.073		0	0.837		0.073	
	I+	0.270	0.687		0.031		0.378	0.603		0.031	
	I-	0.270	0.687		0.031		0.378	0.603		0.031	
	0	0.411	0.575		0.010		0.411	0.575		0.010	
	$H/R = 0.5$										
0.75	1	0	0.672	-0.045	0.059	-0.004	0	0.667	-0.040	0.057	-0.002
	I+	0.218	0.557	-0.046	0.025	-0.005	0.304	0.492	-0.046	0.012	-0.006
	I-	0.218	0.692	0.028	0.033	0.005	0.304	0.550	0.105	0.014	0.010
	0	0.380	0.580	0.024	0.011	0.002	0.352	0.525	0.100	0.010	0.007
	0.5	1	0	0.495	-0.076	0.044	-0.008	0	0.486	-0.068	0.040
I+		0.158	0.415	-0.077	0.019	-0.009	0.219	0.369	-0.076	0.009	-0.009
I-		0.158	0.702	0.054	0.036	0.010	0.219	0.474	0.237	0.014	0.023
0		0.347	0.588	0.045	0.012	0.003	0.286	0.453	0.226	0.010	0.016
0.25		1	0	0.291	-0.082	0.027	-0.009	0	0.283	-0.074	0.023
	I+	0.086	0.248	-0.081	0.012	-0.009	0.120	0.223	-0.079	0.006	-0.008
	I-	0.086	0.726	0.069	0.043	0.015	0.120	0.347	0.424	0.012	0.040
	0	0.310	0.608	0.058	0.014	0.005	0.212	0.331	0.405	0.009	0.028
	0.1	1	0	0.139	-0.056	0.014	-0.007	0	0.134	-0.051	0.011
I+		0.038	0.121	-0.054	0.006	-0.006	0.051	0.109	-0.052	0.003	-0.005
I-		0.038	0.765	0.054	0.054	0.013	0.051	0.202	0.609	0.009	0.055
0		0.286	0.641	0.046	0.018	0.004	0.163	0.192	0.581	0.006	0.039
$H/R = 1$											
1	1	0	0.837		0.073		0	0.837		0.073	
	I+	0.503	0.480		0.012		0.686	0.309		0.002	
	I-	0.503	0.480		0.012		0.686	0.309		0.002	
	0	0.738	0.259		0.001		0.738	0.259		0.001	
	0.75	1	0	0.676	-0.048	0.057	-0.003	0	0.660	-0.033	0.055
I+		0.416	0.392	-0.055	0.010	-0.007	0.565	0.254	-0.056	0.002	-0.007
I-		0.416	0.505	0.042	0.013	0.008	0.565	0.297	0.110	0.002	0.010
0		0.701	0.272	0.023	0.001	0.001	0.652	0.249	0.093	0.001	0.003

$\frac{\rho_2}{\rho_1}$	$\eta$	$H_2/H_1 = 0.5$					$H_2/H_1 = 2$				
		$c_o$	$c_{11}$	$c_{12}$	$c_{21}$	$c_{22}$	$c_o$	$c_{11}$	$c_{12}$	$c_{21}$	$c_{22}$
0.5	1	0	0.503	-0.084	0.041	-0.005	0	0.476	-0.057	0.037	-0.001
	I+	0.309	0.296	-0.090	0.007	-0.011	0.418	0.194	-0.088	0.001	-0.011
	I-	0.309	0.542	0.083	0.014	0.019	0.418	0.275	0.249	0.002	0.024
	0	0.658	0.293	0.045	0.001	0.001	0.549	0.230	0.209	0.001	0.008
0.25	1	0	0.303	-0.094	0.025	-0.007	0	0.274	-0.065	0.020	-0.001
	I+	0.175	0.184	-0.091	0.004	-0.010	0.236	0.122	-0.086	0.001	-0.010
	I-	0.175	0.611	0.109	0.017	0.032	0.236	0.224	0.440	0.002	0.043
	0	0.606	0.330	0.059	0.001	0.002	0.424	0.188	0.368	0.001	0.014
0.1	1	0	0.150	-0.066	0.015	-0.007	0	0.131	-0.050	0.009	-0.001
	I+	0.076	0.094	-0.060	0.003	-0.006	0.102	0.064	-0.054	0.000	-0.006
	I-	0.076	0.698	0.090	0.025	0.038	0.102	0.146	0.618	0.002	0.058
	0	0.569	0.377	0.048	0.001	0.002	0.335	0.122	0.517	0.001	0.019
$H/R = 2$											
1	1	0	0.837		0.073		0	0.837		0.073	
	I+	0.748	0.245		0.002		0.919	0.078		0.000	
	I-	0.748	0.245		0.002		0.919	0.078		0.000	
	0	0.955	0.042		0.000		0.955	0.042		0.000	
0.75	1	0	0.670	-0.042	0.055	-0.001	0	0.642	-0.015	0.055	-0.000
	I+	0.635	0.198	-0.069	0.002	-0.008	0.780	0.061	-0.076	0.000	-0.008
	I-	0.635	0.263	0.075	0.002	0.010	0.780	0.078	0.117	0.000	0.010
	0	0.940	0.045	0.013	0.000	0.000	0.892	0.042	0.063	0.000	0.001
0.5	1	0	0.498	-0.079	0.038	-0.001	0	0.446	-0.028	0.037	-0.000
	I+	0.487	0.148	-0.111	0.001	-0.012	0.598	0.044	-0.117	0.000	-0.012
	I-	0.487	0.292	0.164	0.002	0.024	0.598	0.077	0.270	0.000	0.024
	0	0.920	0.050	0.028	0.000	0.000	0.809	0.041	0.146	0.000	0.001
0.25	1	0	0.312	-0.103	0.020	-0.002	0	0.246	-0.037	0.018	-0.000
	I+	0.287	0.093	-0.108	0.001	-0.011	0.352	0.027	-0.105	0.000	-0.011
	I-	0.287	0.362	0.251	0.002	0.042	0.352	0.073	0.476	0.000	0.044
	0	0.893	0.062	0.043	0.000	0.000	0.698	0.039	0.257	0.000	0.003
0.1	1	0	0.173	-0.089	0.009	-0.002	0	0.116	-0.032	0.007	-0.000
	I+	0.128	0.052	-0.068	0.000	-0.006	0.157	0.015	-0.059	0.000	-0.006
	I-	0.128	0.491	0.247	0.003	0.058	0.157	0.062	0.647	0.000	0.060
	0	0.872	0.084	0.042	0.000	0.000	0.611	0.033	0.349	0.000	0.003

**Table 4.2:** Normalized values of effective masses in expression for base shear of two-layered systems with different  $H/R$  and  $H_2/H_1$

$\frac{\rho_2}{\rho_1}$	$H_2/H_1 = 0.5$					$H_2/H_1 = 2$				
	$\frac{m_o}{m_\ell}$	$\frac{m_{11}}{m_\ell}$	$\frac{m_{12}}{m_\ell}$	$\frac{m_{21}}{m_\ell}$	$\frac{m_{22}}{m_\ell}$	$\frac{m_o}{m_\ell}$	$\frac{m_{11}}{m_\ell}$	$\frac{m_{12}}{m_\ell}$	$\frac{m_{21}}{m_\ell}$	$\frac{m_{22}}{m_\ell}$
	$H/R = 0.5$									
1	0.299	0.660		0.027		0.299	0.660		0.027	
0.75	0.288	0.670	0.002	0.027	0.000	0.289	0.663	0.008	0.026	0.001
0.5	0.270	0.681	0.008	0.027	0.001	0.267	0.644	0.045	0.025	0.004
0.25	0.241	0.694	0.018	0.029	0.003	0.218	0.551	0.176	0.022	0.014
0.1	0.217	0.711	0.020	0.032	0.004	0.159	0.359	0.409	0.015	0.031
	$H/R = 1$									
1	0.547	0.432		0.014		0.547	0.432		0.014	
0.75	0.538	0.440	0.003	0.012	0.000	0.540	0.432	0.008	0.013	0.001
0.5	0.517	0.453	0.012	0.011	0.002	0.512	0.421	0.046	0.011	0.003
0.25	0.474	0.478	0.026	0.010	0.005	0.431	0.369	0.172	0.008	0.011
0.1	0.433	0.512	0.029	0.010	0.008	0.322	0.252	0.384	0.005	0.023
	$H/R = 2$									
1	0.762	0.227		0.007		0.762	0.227		0.007	
0.75	0.769	0.217	0.004	0.006	0.000	0.768	0.214	0.007	0.006	0.000
0.5	0.763	0.209	0.019	0.004	0.001	0.751	0.195	0.043	0.005	0.002
0.25	0.732	0.209	0.048	0.003	0.004	0.674	0.158	0.153	0.003	0.006
0.1	0.691	0.235	0.061	0.002	0.007	0.550	0.110	0.318	0.002	0.013



**Table 4.3: Normalized values of coefficients in expression for overturning moment at a section immediately above tank base of two-layered systems with different  $H/R$  and  $H_2/H_1$**

$\frac{\rho_2}{\rho_1}$	$H_2/H_1 = 0.5$					$H_2/H_1 = 2$				
	$\frac{m_0 h_0}{m_\ell h_\ell}$	$\frac{m_{11} h_{11}}{m_\ell h_\ell}$	$\frac{m_{12} h_{12}}{m_\ell h_\ell}$	$\frac{m_{21} h_{21}}{m_\ell h_\ell}$	$\frac{m_{22} h_{22}}{m_\ell h_\ell}$	$\frac{m_0 h_0}{m_\ell h_\ell}$	$\frac{m_{11} h_{11}}{m_\ell h_\ell}$	$\frac{m_{12} h_{12}}{m_\ell h_\ell}$	$\frac{m_{21} h_{21}}{m_\ell h_\ell}$	$\frac{m_{22} h_{22}}{m_\ell h_\ell}$
	$H/R = 0.5$									
1	0.238	0.703		0.037		0.238	0.703		0.037	
0.75	0.236	0.724	-0.016	0.037	-0.001	0.241	0.736	-0.032	0.037	-0.002
0.5	0.227	0.746	-0.028	0.038	-0.002	0.239	0.772	-0.064	0.038	-0.004
0.25	0.206	0.764	-0.029	0.039	-0.001	0.221	0.780	-0.058	0.037	-0.002
0.1	0.181	0.768	-0.016	0.041	0.001	0.177	0.643	0.110	0.032	0.011
	$H/R = 1$									
1	0.442	0.523		0.022		0.442	0.523		0.022	
0.75	0.446	0.538	-0.016	0.021	-0.001	0.453	0.542	-0.028	0.022	-0.001
0.5	0.439	0.557	-0.026	0.019	0.000	0.458	0.564	-0.054	0.021	-0.001
0.25	0.407	0.583	-0.023	0.017	0.004	0.434	0.573	-0.040	0.018	0.003
0.1	0.364	0.606	-0.008	0.017	0.008	0.353	0.483	0.118	0.014	0.013
	$H/R = 2$									
1	0.644	0.337		0.012		0.644	0.337		0.012	
0.75	0.663	0.331	-0.011	0.011	0.000	0.664	0.335	-0.017	0.012	-0.000
0.5	0.670	0.325	-0.011	0.009	0.001	0.679	0.330	-0.028	0.011	0.000
0.25	0.646	0.324	0.012	0.006	0.005	0.662	0.312	0.005	0.009	0.003
0.1	0.595	0.346	0.037	0.004	0.010	0.569	0.259	0.144	0.006	0.011

**Table 4.4: Normalized values of coefficients in expression for foundation moment of two-layered systems with different  $H/R$  and  $H_2/H_1$**

$\frac{\rho_2}{\rho_1}$	$H_2/H_1 = 0.5$					$H_2/H_1 = 2$				
	$\frac{m_0 h'_0}{m_\ell h'_\ell}$	$\frac{m_{11} h'_{11}}{m_\ell h'_\ell}$	$\frac{m_{12} h'_{12}}{m_\ell h'_\ell}$	$\frac{m_{21} h'_{21}}{m_\ell h'_\ell}$	$\frac{m_{22} h'_{22}}{m_\ell h'_\ell}$	$\frac{m_0 h'_0}{m_\ell h'_\ell}$	$\frac{m_{11} h'_{11}}{m_\ell h'_\ell}$	$\frac{m_{12} h'_{12}}{m_\ell h'_\ell}$	$\frac{m_{21} h'_{21}}{m_\ell h'_\ell}$	$\frac{m_{22} h'_{22}}{m_\ell h'_\ell}$
	$H/R = 0.5$									
1	0.292	0.687		0.013		0.292	0.687		0.013	
0.75	0.271	0.696	0.015	0.012	-0.000	0.254	0.652	0.076	0.011	0.000
0.5	0.244	0.708	0.032	0.011	-0.000	0.204	0.586	0.195	0.009	0.001
0.25	0.208	0.728	0.046	0.010	0.000	0.135	0.447	0.401	0.006	0.003
0.1	0.185	0.759	0.040	0.010	0.001	0.088	0.265	0.633	0.004	0.006
	$H/R = 1$									
1.0	0.526	0.451		0.015		0.526	0.451		0.015	
0.75	0.521	0.459	-0.000	0.013	-0.000	0.509	0.445	0.025	0.013	-0.000
0.5	0.505	0.471	0.006	0.011	0.000	0.469	0.425	0.088	0.011	-0.000
0.25	0.467	0.494	0.020	0.009	0.002	0.372	0.362	0.245	0.007	0.002
0.1	0.431	0.512	0.029	0.010	0.004	0.274	0.241	0.470	0.004	0.006
	$H/R = 2$									
1	0.676	0.305		0.011		0.676	0.305		0.011	
0.75	0.695	0.296	-0.008	0.010	0.000	0.692	0.295	-0.005	0.010	-0.000
0.5	0.704	0.285	-0.005	0.008	0.001	0.696	0.278	0.009	0.009	0.000
0.25	0.684	0.280	0.019	0.005	0.004	0.653	0.240	0.087	0.007	0.003
0.1	0.645	0.296	0.040	0.003	0.008	0.559	0.174	0.247	0.004	0.007

**Table 4.5: Normalized values of effective masses in expression for base shear of three-layered systems with different  $H/R$  and  $H_1 = H_2 = H_3 = H/3$**

$\rho_3/\rho_2/\rho_1$	$\frac{m_0}{m_\ell}$	$\frac{m_{11}}{m_\ell}$	$\frac{m_{12}}{m_\ell}$	$\frac{m_{13}}{m_\ell}$	$\frac{m_{21}}{m_\ell}$	$\frac{m_{22}}{m_\ell}$	$\frac{m_{23}}{m_\ell}$
			$H/R = 0.5$				
1/1/1	0.299	0.660			0.027		
1/2/3	0.252	0.674	0.028	0.004	0.026	0.003	0.000
1/3/5	0.229	0.672	0.044	0.008	0.027	0.005	0.001
			$H/R = 1$				
1/1/1	0.547	0.432			0.014		
1/2/3	0.495	0.450	0.032	0.004	0.010	0.003	0.001
1/3/5	0.459	0.462	0.050	0.009	0.008	0.004	0.001
			$H/R = 2$				
1/1/1	0.762	0.227			0.007		
1/2/3	0.757	0.193	0.035	0.005	0.004	0.001	0.001
1/3/5	0.731	0.189	0.058	0.012	0.003	0.002	0.001

**Table 4.6:** Normalized values of coefficients in expression for overturning moment at a section immediately above tank base of three-layered systems with different  $H/R$  and  $H_1 = H_2 = H_3 = H/3$

$\rho_3/\rho_2/\rho_1$	$\frac{m_0 h_0}{m_\ell h_\ell}$	$\frac{m_{11} h_{11}}{m_\ell h_\ell}$	$\frac{m_{12} h_{12}}{m_\ell h_\ell}$	$\frac{m_{13} h_{13}}{m_\ell h_\ell}$	$\frac{m_{21} h_{21}}{m_\ell h_\ell}$	$\frac{m_{22} h_{22}}{m_\ell h_\ell}$	$\frac{m_{23} h_{23}}{m_\ell h_\ell}$
$H/R = 0.5$							
1/1/1	0.239	0.703			0.037		
1/2/3	0.226	0.789	-0.057	-0.010	0.039	-0.003	-0.001
1/3/5	0.212	0.808	-0.054	-0.020	0.040	0.002	-0.002
$H/R = 1$							
1/1/1	0.442	0.523			0.022		
1/2/3	0.446	0.586	-0.049	-0.010	0.018	0.000	-0.001
1/3/5	0.424	0.609	-0.041	-0.020	0.017	0.002	-0.001
$H/R = 2$							
1/1/1	0.644	0.337			0.012		
1/2/3	0.692	0.323	-0.019	-0.010	0.008	0.001	-0.000
1/3/5	0.682	0.321	0.001	-0.018	0.006	0.003	-0.000

**Table 4.7: Normalized values of coefficients in expression for foundation moment of three-layered systems with different  $H/R$  and  $H_1 = H_2 = H_3 = H/3$**

$\rho_3/\rho_2/\rho_1$	$\frac{m_0 h'_0}{m_\ell h'_\ell}$	$\frac{m_{11} h'_{11}}{m_\ell h'_\ell}$	$\frac{m_{12} h'_{12}}{m_\ell h'_\ell}$	$\frac{m_{13} h'_{13}}{m_\ell h'_\ell}$	$\frac{m_{21} h'_{21}}{m_\ell h'_\ell}$	$\frac{m_{22} h'_{22}}{m_\ell h'_\ell}$	$\frac{m_{23} h'_{23}}{m_\ell h'_\ell}$
			$H/R = 0.5$				
1/1/1	0.292	0.687		0.013			
1/2/3	0.196	0.639	0.113	0.040	0.008	0.001	0.000
1/3/5	0.168	0.643	0.113	0.063	0.008	0.001	0.000
			$H/R = 1$				
1/1/1	0.526	0.451			0.015		
1/2/3	0.466	0.459	0.040	0.020	0.009	0.000	-0.000
1/3/5	0.429	0.467	0.056	0.034	0.008	0.001	-0.000
			$H/R = 2$				
1/1/1	0.678	0.305			0.011		
1/2/3	0.715	0.271	-0.000	0.001	0.007	0.001	-0.000
1/3/5	0.702	0.263	0.020	0.003	0.005	0.002	-0.000

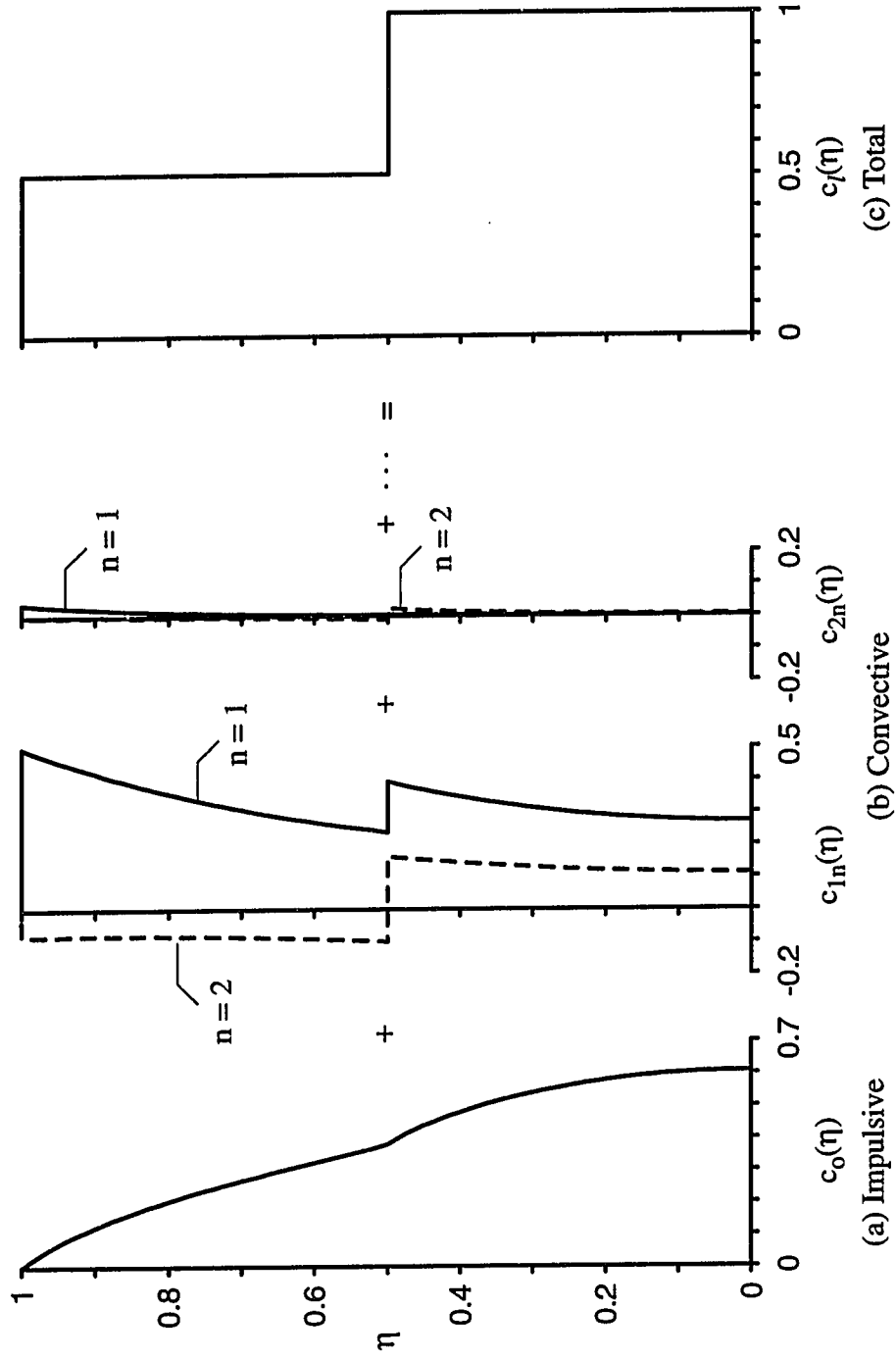


Figure 4.1 Interrelationship of coefficients for impulsive and convective components of wall pressure for two-layered system with  $H/R = 1$ ,  $H_2/H_1 = 1$  and  $\rho_2/\rho_1 = 0.5$

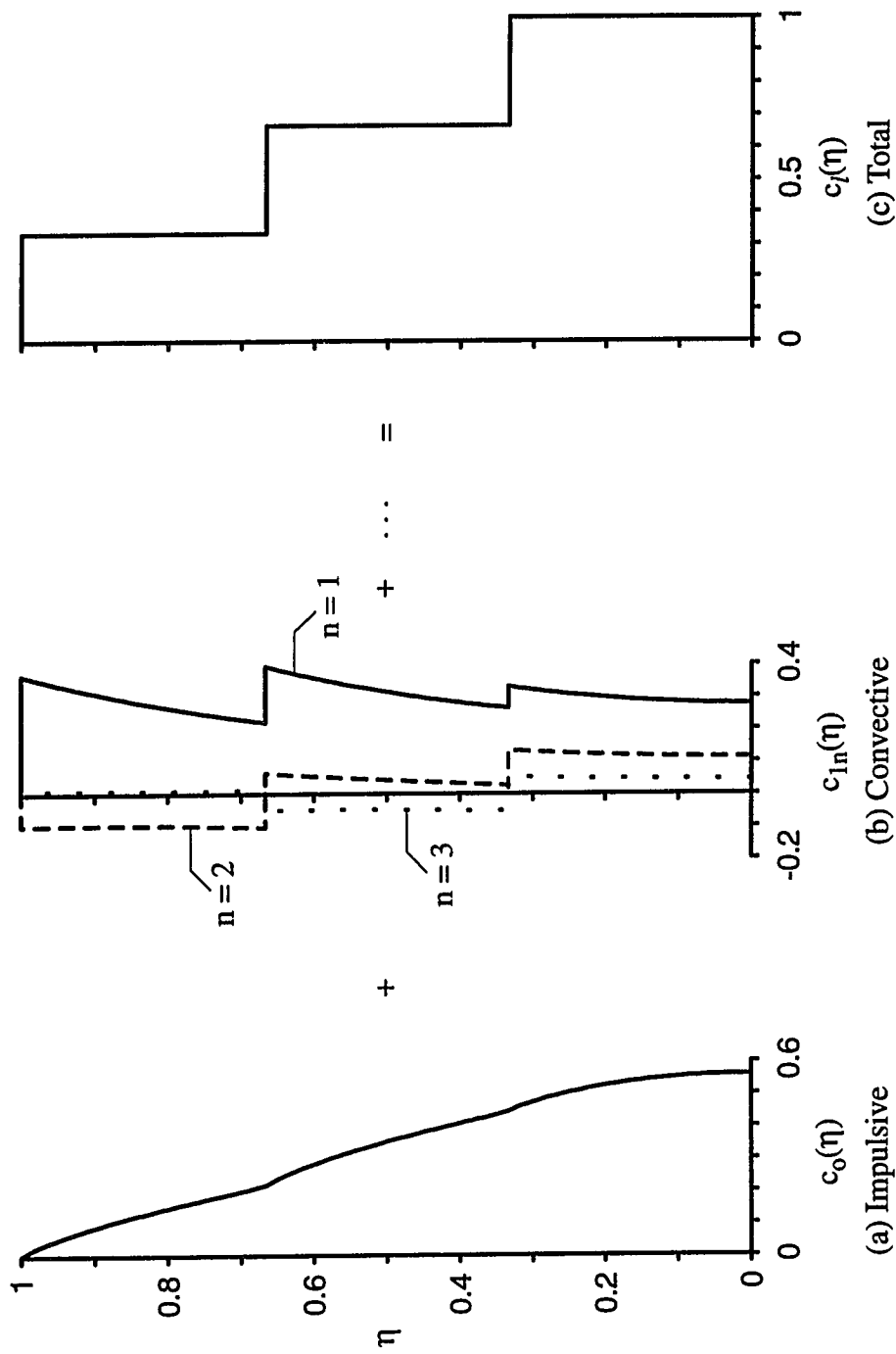


Figure 4.2 Interrelationship of coefficients for impulsive and convective components of wall pressure for three-layered system with  $H/R = 1$ ,  $H_1 = H_2 = H_3 = H/3$  and  $\rho_3/\rho_2/\rho_1 = 1/2/3$

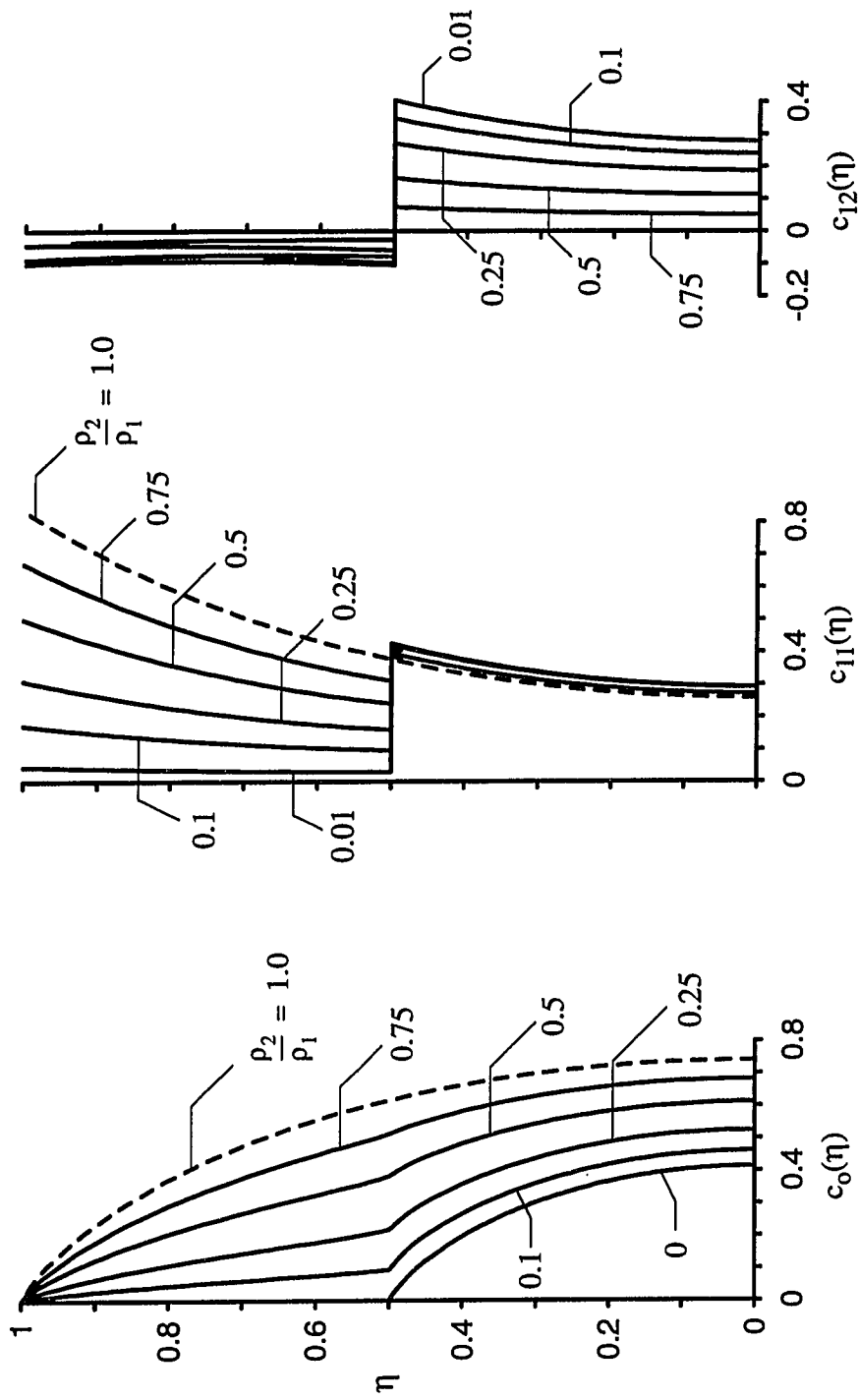


Figure 4.3 Effect of  $\rho_2/\rho_1$  on impulsive and fundamental convective pressure distributions for  $H/R = 1.0$ ,  $H_2/H_1 = 1$



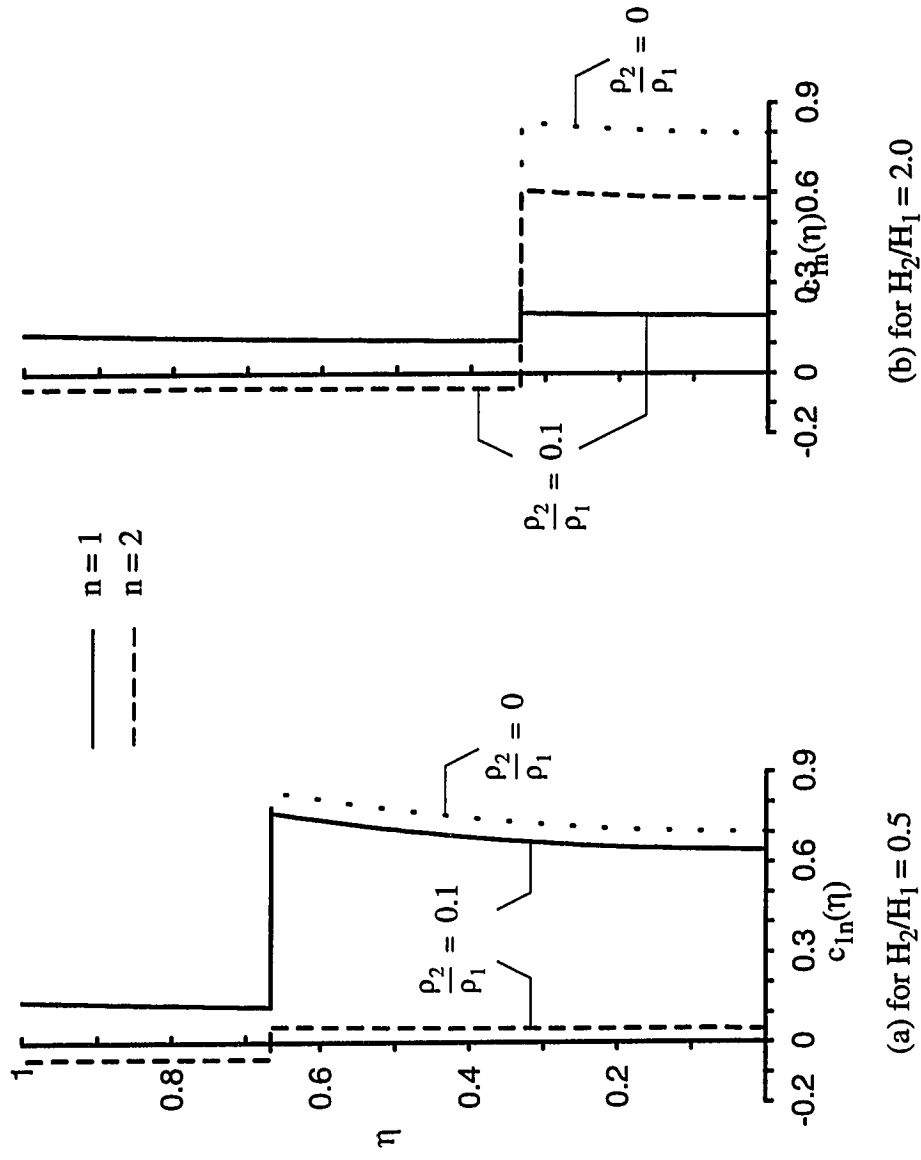


Figure 4.4 Effect of  $H_2/H_1$  on convective pressure coefficient  $c_{1n}(\eta)$  as  $\rho_2/\rho_1$  tends to zero; system with  $H/R = 1$

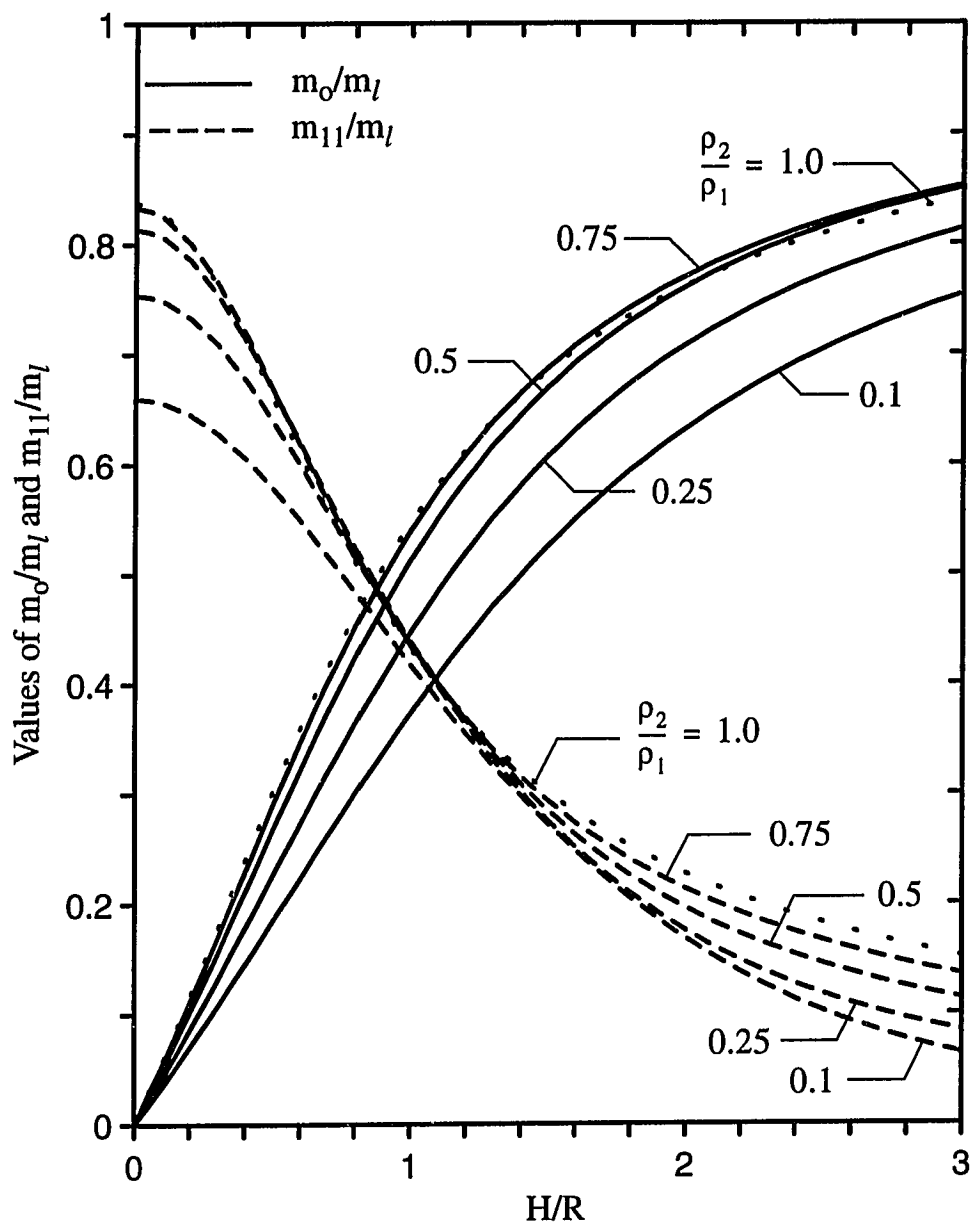


Figure 4.5 Impulsive and fundamental convective masses for two-layered systems with  $H_2/H_1 = 1$

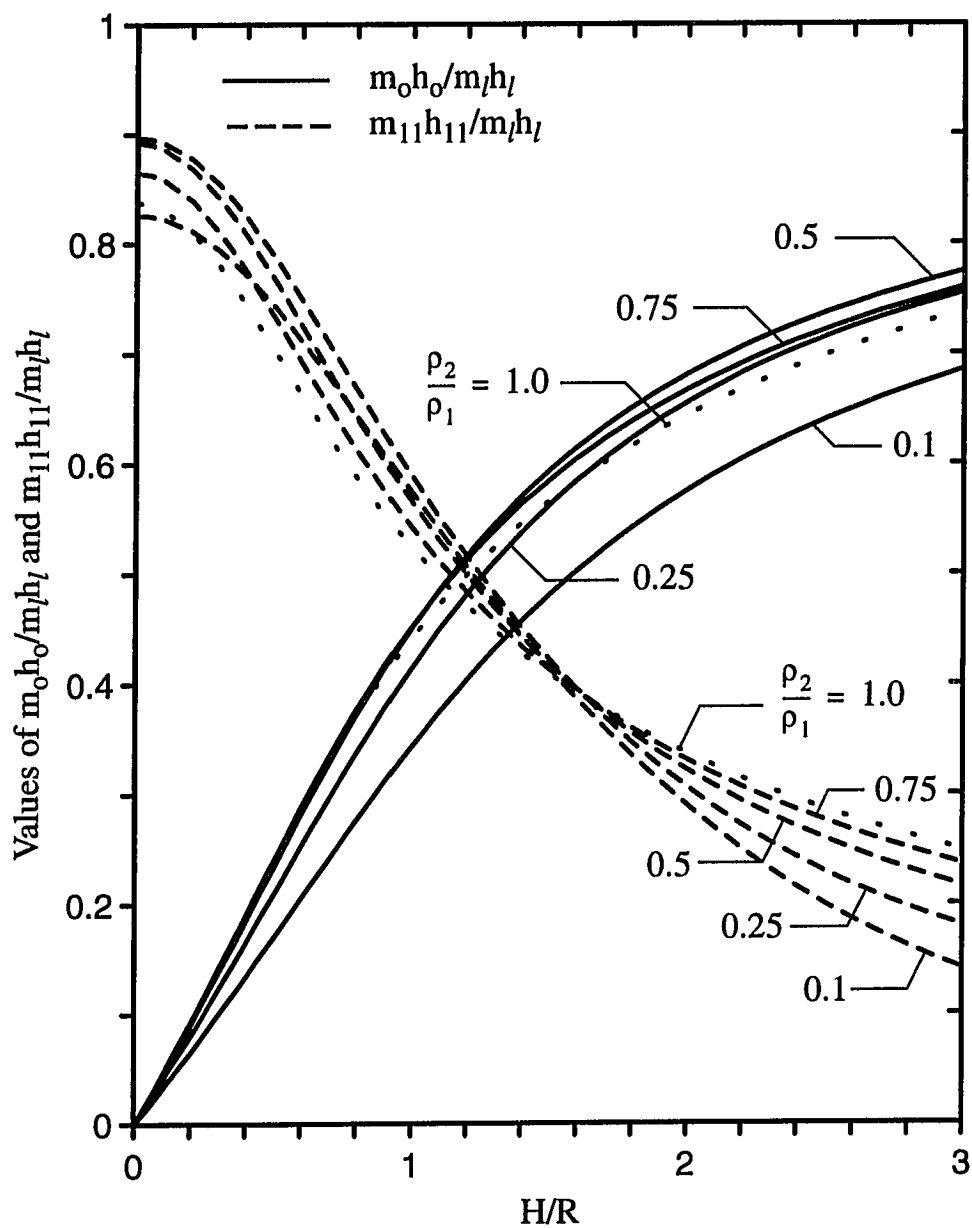


Figure 4.6 Normalized values of coefficients for impulsive and fundamental convective component of base moment for two-layered systems with  $H_2/H_1 = 1$

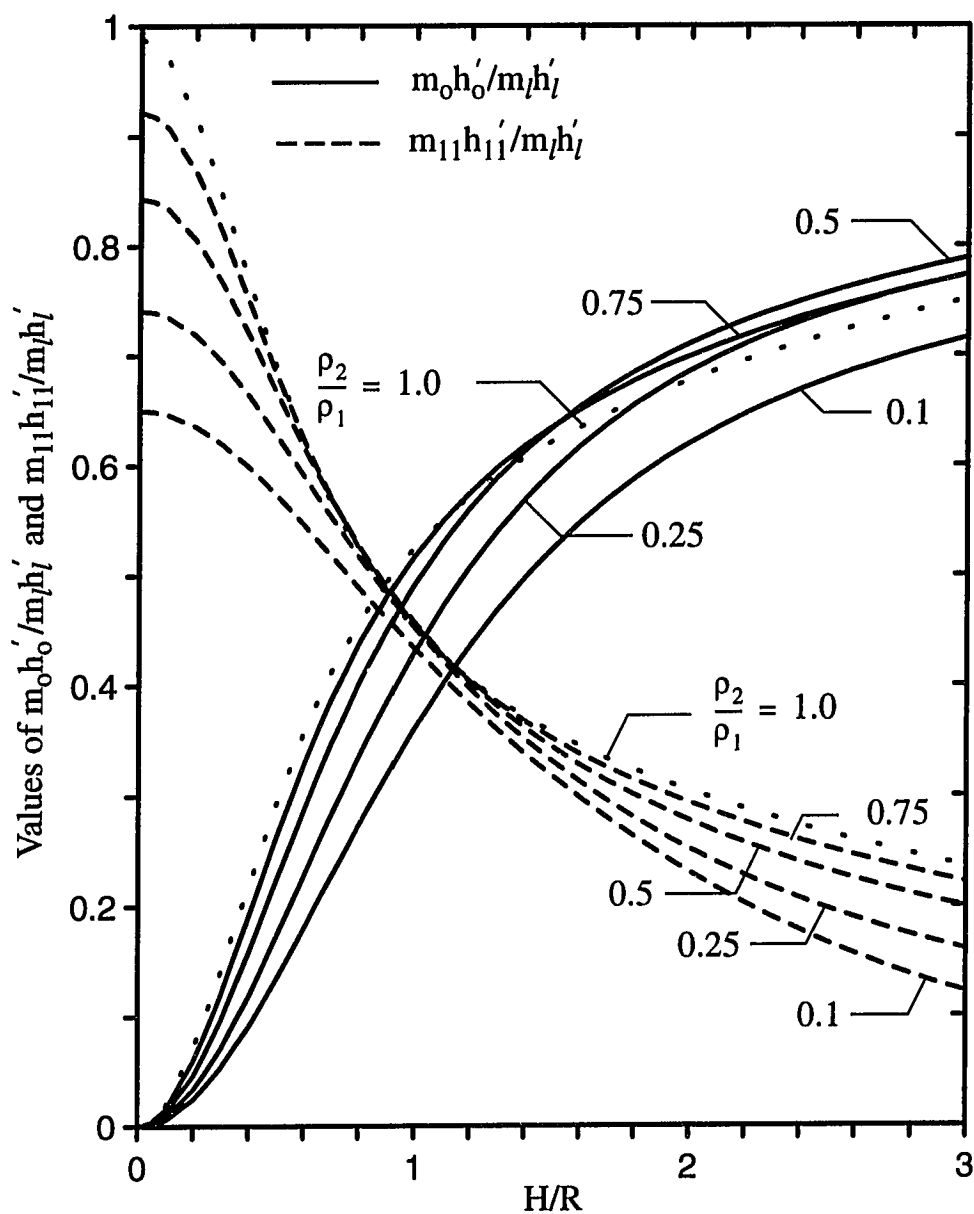


Figure 4.7 Normalized values of coefficients for impulsive and fundamental convective component of foundation moment for two-layered systems with  $H_2/H_1 = 1$

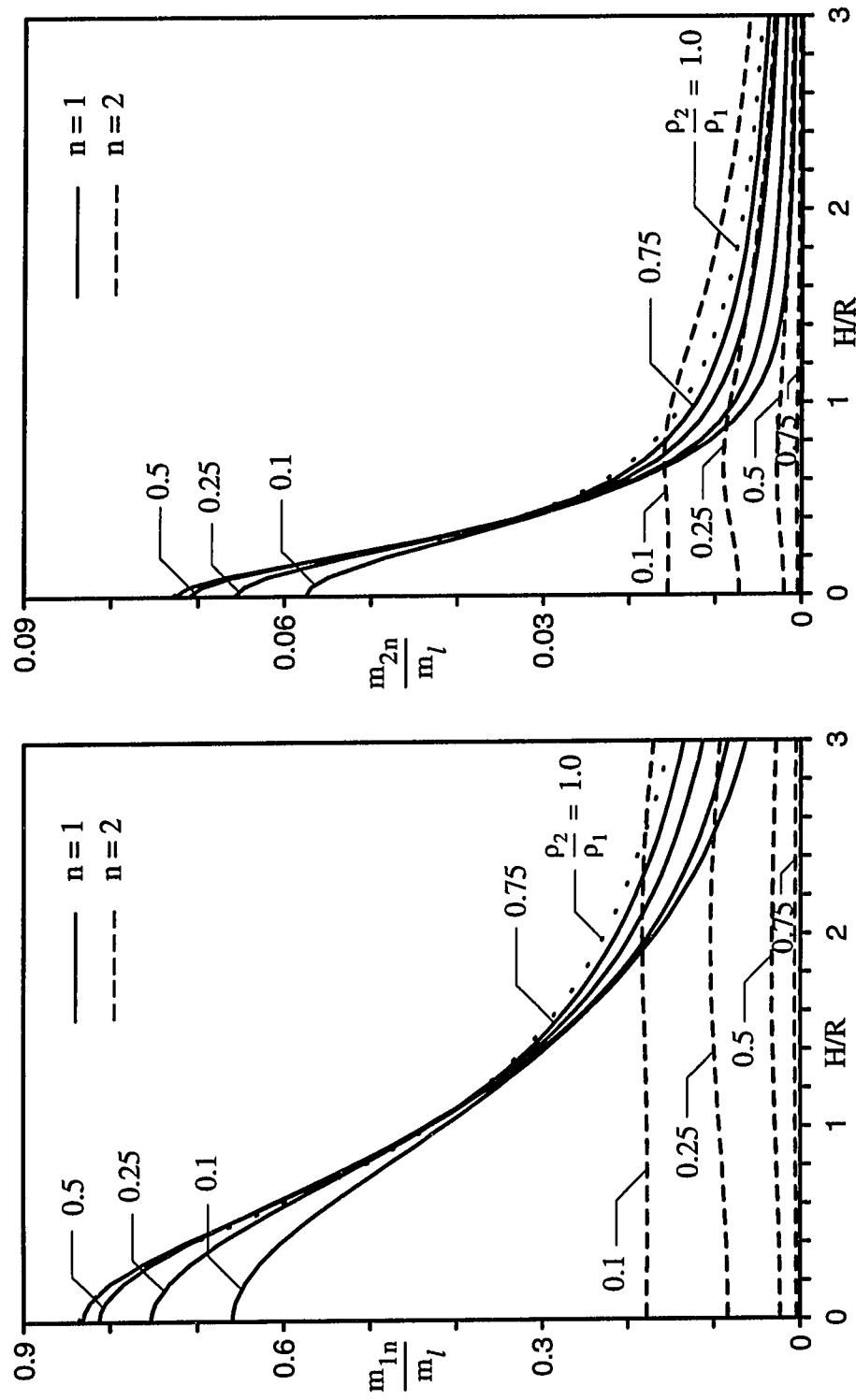


Figure 4.8 Convective masses for first two horizontal and two vertical modes of vibration of two-layered systems with  $H_2/H_1 = 1$

## Chapter 5

# Simplified Analysis of Layered Tank-Liquid Systems

### 5.1 Introduction

The evaluation of the exact response of systems containing layered liquids is based on relatively complex methods that require the development/readily accessibility to sophisticated programs for their implementation. The effort and complexity of the computations is further increased when effects of tank-wall flexibility need to be considered. In order to facilitate the preliminary design of both rigid and flexible layered systems, and develop an insight into their response characteristics, there is a need for simplified procedures that conveniently and accurately assess the hydrodynamic layered response. The study presented in this chapter is intended to be responsive to this need. The objectives of the study are two-fold :

- To propose a simple concept by which the natural frequencies associated with the dominant modes of vibration of a layered system can be readily assessed.
- To use the underlying concept to also estimate the impulsive response coefficients for rigid layered systems.

Since homogeneous tank-liquid systems have been the subject of several past studies and solutions for reference tank-liquid systems are well-established and readily available in the literature, it is desirable to base the proposed procedures for the layered systems on the solutions for such reference homogeneous systems. The validity of the proposed procedures is established by comparing the approximate solutions with their exact counterparts over a wide range of tank-liquid parameters.

Only the impulsive component is considered here. Since the convective component is generally associated with motions of significantly lower frequencies than the dominant frequencies of the excitation or the natural frequencies of the flexible tank-liquid system, it is assumed to be practically unaffected by tank-wall flexibility and can be evaluated from the rigid-tank expressions presented in Chapters 3 and 4.

## 5.2 Background

### 5.2.1 Rigid Tanks

The response of rigid tank-liquid systems is well-established and the expressions for the quantities of current interest are summarized in this section. The expressions are presented in a form that is applicable to both homogeneous and layered systems.

The instantaneous value of the impulsive pressure exerted on the tank wall,  $p_i = p_i(z, \theta, t)$ , is expressed as

$$p_i(z, \theta, t) = c_o(z) \ddot{x}_g(t) \rho_l R \cos \theta \quad (5.1)$$

where  $\rho_l$  is a measure of the mass density : for a homogeneous system, it is the liquid density, whereas for a layered system, it can be interpreted as the density of the bottom-most layer,  $\rho_1$ ;  $z$  is the vertical distance measured from the tank-base, and;  $c_o(z)$  is a dimensionless function that defines the heightwise variation of the impulsive pressure. It is a function of  $z$  and  $H/R$  for a homogeneous system, (Veletsos 1984), whereas for a layered system, it also depends on the relative layer densities,  $\rho_j/\rho_1$ , and relative layer heights,  $H_j/H$ , (see Chapter 4).

The impulsive tank forces are obtained by appropriate integrations of the pressure given by equation (5.1). The instantaneous value of the impulsive base shear,  $Q_{b,i}(t)$ , is given by

$$Q_{b,i}(t) = m_o \ddot{x}_g(t) \quad (5.2)$$

and the corresponding values of the bending moments immediately above and below the base are expressed in the form

$$M_i(t) = m_o h_o \ddot{x}_g(t) \quad (5.3)$$

and

$$M'_i(t) = m_o h'_o \ddot{x}_g(t) \quad (5.4)$$

respectively. The moment  $M_i(t)$  is due exclusively to the impulsive wall pressure, whereas  $M'_i(t)$  includes, in addition, the contribution of the pressure exerted on the tank base.  $m_o$  represents the impulsive component of the liquid mass, and  $h_o$  and  $h'_o$  are the heights at which this mass must be located to yield the correct base moments.

### 5.2.2 Flexible Tanks

In previous studies for flexible tanks containing homogeneous liquids, [65], a simple method has been presented to conveniently account for the effects of tank-wall flexi-

bility. For flexible tanks with  $H/R$  in the range between 0.25 and 1.0, the impulsive effects have been obtained from the relevant expressions for a rigid tank simply by replacing the ground acceleration term in these expressions by the pseudoacceleration function corresponding to the fundamental natural frequency of the tank-liquid system. For instance, the impulsive component of the base shear for the broad flexible system is expressed as

$$Q_{b,i}(t) = m_o A_i(t) \quad (5.5)$$

where  $m_o$  is the rigid-tank impulsive mass; and  $A_i(t)$  is the instantaneous pseudoacceleration of a single-degree-of-freedom oscillator, the natural frequency and damping of which are equal to those of the fundamental fixed-base natural mode of vibration of the tank-liquid system when subjected to the prescribed ground shaking.

The fundamental natural frequency,  $f_i$ , needed to compute  $A_i(t)$  is well-established for homogeneous systems and is given by

$$f_i = \frac{C_i}{2\pi H} \sqrt{\frac{E}{\rho}} \quad (5.6)$$

where  $H$  is the height of the liquid;  $E$  and  $\rho$  are the modulus of elasticity and the density of the material of the tank-wall respectively, and;  $C_i$  is a dimensionless frequency coefficient that depends on  $H/R$ ,  $h/R$ ,  $\rho_l/\rho$  and  $\nu$ .

The simplified approach has been based on the observation that, for all practical purposes, the impulsive pressure distribution for broad homogeneous systems is insensitive to the wall flexibility. The latter trend must also hold true for layered systems with broad aspect ratios and this has been verified in a recent study of two-layered systems, [58]. It follows that the simplified approach can be applied to broad layered systems too and that the crucial step in the extension to flexible tanks of the available information on impulsive effects in rigid tanks with layered liquids is the evaluation of the fundamental natural frequency of the tank-liquid system.

## 5.3 Flexible Layered Systems

### 5.3.1 Approximate Evaluation of Fundamental Natural Frequency

For a system with  $N$  uniform liquid layers of different thicknesses and mass densities, the desired frequency is determined from the corresponding frequencies of  $N$  subsystems, each containing a homogeneous liquid. The procedure is described by reference



to a three-layered cantilever system, for which the variation in liquid density is shown by the sketch at the extreme left of Fig. 5.1.

Referred to as subsystems  $A$ ,  $B$  and  $C$ , the three replacement systems are identified by the three rightmost diagrams in Fig. 5.1. For subsystem  $A$ , a homogeneous liquid of the density of the top layer,  $\rho_3$ , extends to the total height  $H$ ; for subsystem  $B$ , a homogeneous liquid of a density equal to the difference in the densities of the second and top layers,  $\rho_2 - \rho_3$ , extends to the top of the second layer,  $H_1 + H_2$ ; and for subsystem  $C$ , a homogeneous liquid of a density equal to the difference in the densities of the bottom and middle layers,  $\rho_1 - \rho_2$ , extends to the top of the bottom layer,  $H_1$ .

Let  $f_A$ ,  $f_B$  and  $f_C$  be the fundamental natural frequencies of the impulsive modes of vibration of subsystems  $A$ ,  $B$  and  $C$ , respectively, and let  $T_A$ ,  $T_B$  and  $T_C$  be the associated periods. The corresponding frequency of the actual layered system,  $f_i$ , may then be determined by application of a Dunkerley-type approximation from

$$\frac{1}{f_i^2} = \frac{1}{f_A^2} + \frac{1}{f_B^2} + \frac{1}{f_C^2} \quad (5.7)$$

and the corresponding natural period,  $T_i$ , may be determined from

$$T_i^2 = T_A^2 + T_B^2 + T_C^2 \quad (5.8)$$

Inasmuch as these expressions do not follow from an exact application of the Dunkerley approximation, the results obtained do not necessarily constitute a low-bound estimate of the desired frequency.

On expressing the frequency of the layered system in a manner similar to equation (5.6), and making use of equation (5.7), the frequency coefficient  $C_i$  for the layered system is expressed in the form

$$\frac{1}{C_i^2} = \frac{1}{C_A^2} + \frac{[(H_1 + H_2)/H]^2}{C_B^2} + \frac{[H_1/H]^2}{C_C^2} \quad (5.9)$$

$C_i$  is evaluated once the corresponding values of  $C_A$ ,  $C_B$  and  $C_C$  are known. These, in turn, can be evaluated directly from existing programs for systems that are partially filled with liquids of arbitrary homogeneous densities. It is more convenient, however, to evaluate  $C_A$ ,  $C_B$  and  $C_C$  from tabulated solutions for reference homogeneous systems. The latter evaluation involves making two approximations :

1. The frequency coefficient for a tank that is partially filled to a certain height can be taken to be the same as that for a fully filled tank of the same height.

This approximation is based on the observation that only the portion filled with liquid contributes significantly to the mass and stiffness properties of the system.

2. If the frequency coefficient for a homogeneous system with a specific  $h/R$  and  $\rho_l/\rho$  is taken as reference (denoted by the subscript *ref*), the value of the frequency coefficient for any other value of  $h/R$  and  $\rho_l/\rho$  is given by, [52],

$$C_i = (C_i)_{ref} \sqrt{\frac{(h/R)}{(h/R)_{ref}} \frac{(\rho_l/\rho)_{ref}}{(\rho_l/\rho)}} \quad (5.10)$$

The above expression is based on the assumption that the inertia effects of the tank itself are negligible compared to those of the contained liquid, a condition normally satisfied in practice.

Making use of equation (5.10), well-established solutions for reference systems can be used to evaluate the frequency coefficients for the homogeneous sub-systems,  $C_A$ ,  $C_B$  and  $C_C$ . The latter values are then substituted into equation (5.9) to determine  $C_i$  which, in turn, is used to evaluate the fundamental natural frequency of the three-layered system,  $f_i$ , from equation (5.6).

The basic principles that have been enunciated above can be easily applied to systems with any number of layers and similar expressions for the fundamental frequency can be obtained.

### 5.3.2 Approximate Evaluation of Second Natural Frequency

As shown in a later section, it is sometimes necessary to know the second natural frequency of vibration as well while approximately assessing the response of flexible tank-liquid systems and there is a need to have a simple method for evaluating this frequency for layered systems.

Making use of the fact that the frequency of a system vibrating in a certain mode is generally insensitive to inaccuracies in the representation of that mode, the method proposed above for evaluating the fundamental frequency is reapplied to evaluate the second natural frequency of the layered system. On repeating the steps shown before, the coefficient for the second natural frequency of vibration of the system is again given by equation (5.9), provided  $C_A$ ,  $C_B$  and  $C_C$  in that expression are now interpreted as the frequency coefficients for the second mode of vibration of the corresponding homogeneous sub-systems A, B and C. Solutions of the latter coefficients for

reference values of  $h/R$  and  $\rho_l/\rho$  are also readily available in the literature and equation (5.10) can again be conveniently used to relate them to corresponding frequency coefficients for arbitrary  $h/R$  and  $\rho_l/\rho$ .

### 5.3.3 Exact Evaluation of Natural Frequencies of Vibration

The validity of the proposed procedure for the natural frequencies of vibration of the layered system can only be established by comparing the approximate solutions with corresponding solutions obtained in an exact manner. The rigorous method for solving the free-vibrational problem is treated in this section. Attention is devoted to two and three-layered cantilever systems.

The procedure followed is based on the one formulated for homogeneous systems by Yang [82], with due provision made for the effects of the liquid layering. The analysis is implemented by making use of the Rayleigh-Ritz method. The axial, radial and tangential components of displacement,  $u$ ,  $v$ , and  $w$ , respectively, are expressed as linear combinations of the natural modes of vibration of a uniform, cantilever beam,  $\psi(z)$ , or of the first derivatives of the modes,  $\psi'(z)$ .

$$u = \sum_{i=1}^{N_1} U_i(t) \psi'(z) \cos\theta \quad v = \sum_{i=1}^{N_2} V_i(t) \psi(z) \sin\theta \quad w = \sum_{i=1}^{N_3} W_i(t) \psi(z) \cos\theta \quad (5.11)$$

where  $U_i(t)$ ,  $V_i(t)$  and  $W_i(t)$  are time-dependent coefficients with units of length indicating the degree of participation of each mode;  $N_1$ ,  $N_2$  and  $N_3$  are the number of terms used in the series expressions. Using equation (5.11) for the displacement components, the stiffness and mass properties of the tank-shell are computed in a manner identical to that for the homogeneous systems. The general principles followed in this evaluation have been extensively described in [55, 82] and are not repeated here.

Additionally, it is necessary to evaluate the participating modal masses of the layered liquid. The procedure to evaluate these masses for a three-layered cantilever system is presented in Appendix B. The liquid modal masses are combined with the appropriate values of the shell masses to form the mass matrix  $[M]$ . Using this and the previously established stiffness matrix  $[K]$ , the free-vibration problem is written in the form

$$[K]\{\hat{q}\} = \omega^2[M]\{\hat{q}\} \quad (5.12)$$

where  $\{\hat{q}\}$  is the vector of modal displacement ordinates, given by

$$\{\hat{q}\} = \{\hat{U}_1, \dots, \hat{U}_{N_1}, \hat{V}_1, \dots, \hat{V}_{N_2}, \hat{W}_1, \dots, \hat{W}_{N_3}\}^T \quad (5.13)$$

On solving the resulting characteristic equation, a total of  $(N_1 + N_2 + N_3)$  frequencies are obtained, of which only the first two solutions are of interest in the present study.

Using the same general scheme of the Rayleigh-Ritz method and Lagrange's approach, but a different method to compute the participating liquid modal masses, the free-vibrational problem for two-layered tank-liquid systems has also been studied in [57]. The solutions obtained therein have been restricted to  $N_1, N_2, N_3 \leq 9$  since numerical difficulties related to the precision with which integrals involving the shape functions  $\psi(z)$  and  $\psi'(z)$  can be evaluated have been encountered for values greater than 9. Such numerical problems have been resolved in the present study by using asymptotic expressions of the shape functions for large values of the arguments and the combination of  $N_1 = 10$ ,  $N_2 = 15$  and  $N_3 = 20$  has been successfully used for all the reported solutions. The larger number of approximating functions used in the present study naturally yield frequency values that are more accurate than those presented in [57].

#### 5.3.4 Numerical Results

Frequency coefficients for water-filled steel tanks with  $h/R = 0.001$ ,  $\nu = 0.3$  and  $\rho_l/\rho = 0.127$  are readily available in the literature (Haroun and Housner 1981, Veletsos 1984) and are taken as reference values in the present study for computing the frequency coefficients of the homogeneous sub-systems.

#### Two-layered systems

Approximate frequency coefficients for the fundamental mode of vibration of two-layered systems with equal layer thicknesses ( $H_1/H = H_2/H = 0.5$ ) are evaluated by the procedure demonstrated for the three-layered system and are compared with corresponding exact values in Fig. 5.2. The exact values are shown as solid lines while the approximate values are shown as dashed lines. The results are evaluated for steel tanks with  $h/R = 0.001$ ,  $\nu = 0.3$  and are plotted as a function of  $H/R$  for values of  $\rho_2/\rho_1$  ranging from 0.25 to 1. The liquid in the top layer is taken as water so that  $\rho_2/\rho = 0.127$ . Exact and approximate solutions for the equal-layered case considered and for additional values of  $H_1/H$  are also presented in Table 5.1. Similar solutions for the second mode of vibration are presented in Table 5.2 for two-layered steel tanks containing water in the top-layer. The results are obtained for values of  $H/R$  ranging from 0.5 to 2,  $\rho_2/\rho_1$  ranging from 0.25 to 1 and  $H_1/H$  ranging from

0.25 to 0.75. Similar studies have also been made for two-layered systems with the bottom layer taken as water, i.e.,  $\rho_1/\rho = 0.127$ . The following representative trends are worth noting :

1. For the fundamental frequency coefficients, the agreement between the exact and the approximate values is good over the entire range of parameters considered. For most cases, the errors are less than 3% to 4% and, as expected, the approximate values are not necessarily on the lower side. Relatively large errors that range between 4% and 6% occur for  $H_1/H \approx 0.25$  or  $1/3$  and  $\rho_2/\rho_1 = 0.25$ . The increased errors can be attributed to the fact that for systems with small values of  $H_1/H$  and  $\rho_2/\rho_1$ , the true mode of the layered system and the corresponding modes of the component homogeneous systems differ substantially.
2. While the agreement between the results for the second frequency is still quite good over the entire range of parameters considered, the agreement is not as good as that for the fundamental frequency coefficients. This follows from the fact that the proposed procedure is an adaptation of the Dunkerley procedure which, in turn, is strictly valid for only the fundamental mode of vibration. The larger errors are in the range of 10 % to 14 % and are again associated with small values of  $H_1/H$  and  $\rho_2/\rho_1$ .

### Three-layered systems

Exact and approximate solutions for the fundamental frequency coefficients of three-layered systems with equal layer thicknesses are presented in columns (2) and (3) of Table 5.3. Similar results for the second mode are presented in columns (4) and (5). The tanks are assumed to be made of steel and the top layer is taken as water:  $h/R = 0.001$ ,  $\nu = 0.3$  and  $\rho_3/\rho = 0.127$ . The agreement in the results is again very good and the general trends of the results are found to be similar to those for the two-layered systems.

#### 5.3.5 Extension to Tall Tanks

While the layered natural frequencies have been estimated with a good degree of accuracy over a wide range of  $H/R$ , it should be noted that the simplified method for evaluating the hydrodynamic response quantities is strictly applicable for systems with broad aspect ratios ( $H/R \leq 1$ ). Simple extensions are proposed in this section to estimate the hydrodynamic response effects for tall layered systems as well.

A better estimate of the impulsive base shear of tall systems may be obtained by considering the contributions of the first two modes of vibration, i.e.,

$$Q_{b,i}(t) = m_1 A_1(t) + m_2 A_2(t) \quad (5.14)$$

where  $m_j$  ( $j = 1$  or  $2$ ) is the impulsive mass for the layered system responding in the  $j$ th natural mode of vibration; and  $A_j(t)$  is the corresponding instantaneous pseudoacceleration function of the system. In order to be able to use equation (5.14), it is necessary to know the values of  $m_1$  and  $m_2$ . A simple method to estimate  $m_1$  and  $m_2$  for tall systems can be derived by presuming that tank-wall flexibility should have a similar effect on the average modal pressure of a layered system as on that of a homogeneous system. The shear coefficients of the flexible layered and homogeneous systems can then be approximately related by

$$(m_j)^L = (m_o)^L \left( \frac{m_j}{m_o} \right)^H \quad (5.15)$$

where the superscripts  $L$  and  $H$  denote solutions for layered and homogeneous systems respectively;  $m_o$  and  $m_j$  represent the impulsive masses for a rigid tank and for the  $j$ th mode of vibration of a flexible tank respectively. Note that for broad tanks,  $(m_1/m_o)^H \approx 1$ , and equation (5.15) reduces to  $(m_1)^L = (m_o)^L$ . The expressions and solutions for the terms on the right-hand side of equation (5.15) are well-established and can be used to evaluate the modal masses of the layered system. Using the solutions for the first two modal masses and the associated solutions for the natural frequencies to evaluate the pseudoacceleration functions, the base shear  $Q_{b,i}(t)$  for tall tanks can be evaluated from equation (5.14).

In order to compute the impulsive wall and foundation moments for tall layered systems, the simplified approach can be applied in its original form. This is again based on the observation for homogeneous systems that the moment coefficients for tall systems are not significantly affected by tank-wall flexibility and only the fundamental modal contribution is sufficient for estimating the impulsive moments.

## 5.4 Rigid Layered Systems

### 5.4.1 Proposed Method of Analysis

The concept that has been proposed in the previous section can be directly extended to assess the impulsive response of a rigid layered system. The procedure is demonstrated in Fig. 5.3 for a three-layered system : Wall-pressure distributions for the

three homogeneous sub-systems  $A$ ,  $B$  and  $C$  defined in Fig. 5.1 are evaluated from well-established solutions (Veletsos 1984) and shown in the left part of the figure. They are then normalized with respect to the density of the bottom-most layer,  $\rho_1$ , and superimposed to obtain the layered pressure distribution shown in the right part of the figure.

Approximate wall-pressure distributions for a two-layered system with  $H/R = 1$ ,  $H_1 = H_2 = H/2$  and  $\rho_2/\rho_1 = 0.5$  and for a three-layered system with  $H/R = 1$ ,  $H_1 = H_2 = H_3 = H/3$  and  $\rho_3/\rho_2/\rho_1 = 1/2/3$  are compared with corresponding exact wall-pressure distributions in Fig. 5.4. The exact solutions are obtained from the expressions previously established in Chapter 4. Both the exact and approximate pressure distributions are expressed in terms of  $\rho_1$ . It is seen that the two sets of solutions are in good agreement and that the proposed approximation captures the significant trends of the true response. The approximate ordinates are, however, consistently smaller than the exact ones. The reason for this is as follows : In any layer  $j$ , the exact impulsive pressure  $p_{j,i}$  is expressed as a superposition of the effects due to the motion of the tank-wall and those due to the rocking motions of the bounding interfaces  $j - 1$  and  $j$ . In the method being proposed, the latter interfacial motions are replaced with the rocking motions induced in a series of homogeneous liquids having free-surfaces located at successive interfaces and densities that are equal to the difference in densities between adjacent layers. The true layer-to-layer interaction that causes the interfacial rocking motions is not fully represented by this replacement causing an under-estimation of the impulsive response.

The errors involved can be assessed by computing the ratios of the approximate and exact values for the impulsive components of the base shear, base moment and foundation moment. The ratios are plotted versus  $H/R$  in Fig. 5.6 for two-layered systems with equal-layer thicknesses ( $H_1/H = H_2/H = 0.5$ ) and values of  $\rho_2/\rho_1$  ranging from 0 to 1. Similar studies for other two-layered systems with representative values of  $H_1/H$  in the range from 0 to 1 are presented in Table 5.4. The following trends are worth noting :

1. Due to the under-estimation of the true response, the approximate solutions are on the unconservative side. The errors, however, are reasonably small for all the response quantities and tank-liquid parameters of interest. For most practical cases, the errors are in the order of 5% to 15% and for some isolated cases, they vary between 15% and 20%.

2. While the ratios for the base shear and moment above base are relatively independent of  $H/R$ , those for the moment below base are close to unity for tanks with broad aspect ratios. The latter trend follows from the fact that the foundation moment of broad tanks is dominated by the contribution of the pressure acting on the base and the lever arm of this pressure is nearly the same for both the approximate and the exact solutions.
3. The absolute error values increase as  $\rho_2/\rho_1$  decreases from 1 to about 0.25 and then decrease as  $\rho_2/\rho_1$  tends to 0. They behave similarly with varying  $H_1/H$ , i.e., increase as  $H_1/H$  decreases from 1 to about 1/3 and then decrease as  $H_1/H$  tends to 0. This trend follows from the fact that the approximate solution satisfies the limiting cases of  $\rho_2/\rho_1 = 0, 1$  and  $H_1/H = 0, 1$ .

Similar ratios evaluated for three-layered systems with equal layer thicknesses ( $H_1/H = H_2/H = H_3/H = 1/3$ ) are given in columns (2), (3) and (4) of Table 5.5. Three different values of  $H/R$  and ratios of layer densities are considered. It can be seen that the proposed approximation works quite well for three-layered systems too and the associated errors are generally in the range of 10% to 15%.

#### 5.4.2 Adjustment to Proposed Method

The concept used in the previous section identically satisfies the limiting cases and captures the significant trends of the exact layered response with an average error of about 10% that may be tolerable for many practical applications. Since the errors are, however, on the unconservative side, a further improvement may be deemed necessary. An empirical adjustment is proposed in this section in order to improve the accuracy of the approximate method.

The basis of the proposed adjustment is to appropriately increase the proportion of liquid in each layer that participates in the impulsive action. This follows from the fact that the unadjusted approximate method consistently under-estimates the response for each layer. The increase is accomplished herein by empirically weighting the density of each liquid layer. The empirical formula that relates the old and new density values is identified later. When the new density values are used, the contributions of the homogeneous systems used to approximate the layered response are altered. For instance, for a three-layered system, the density of system A is increased from  $\rho_3$  to  $\rho_3^*$ , that of system B is changed from  $(\rho_2 - \rho_3)$  to  $(\rho_2^* - \rho_3^*)$  and that of system C is decreased from  $(\rho_1 - \rho_2)$  to  $(\rho_1 - \rho_2^*)$ .



Based on numerical studies of several layered systems with  $0.3 \leq H/R \leq 3$ ,  $H_j/H \geq 0.2$  and  $\rho_j/\rho_1 \geq 0.2$ , the adjusted density,  $\rho_j^*$ , is empirically related to the corresponding unadjusted density,  $\rho_j$ , by the expression

$$\rho_j^* = \rho_1 \left( \frac{\rho_j}{\rho_1} \right)^{\alpha_j} \quad (5.16)$$

where  $\alpha_j$  is a dimensionless function of  $H_j/H$ ,  $\rho_j/\rho_1$  and  $H/R$ , given by

$$\alpha_j = 1 - 0.6 \frac{H_j}{H} \left( 1 - \frac{H_j}{H} \right) \sin \frac{\pi \rho_j}{\rho_1} \left( 1 + \sin \frac{\pi H}{4R} \right) \quad (5.17)$$

It can be seen from (5.17) that the factor  $\alpha_j$  varies between 0.7 and 1. It is equal to 1 when the relative layer density/height becomes zero or unity, i.e., for these cases, the adjustment for the layer under consideration reduces, as it should, to zero.

For the two-layered system with  $H/R = 1$ ,  $H_1 = H_2 = H/2$  and  $\rho_2 = 0.5 \rho_1$ , the value of the equivalent density  $\rho_2^*$  is determined from (5.16) to be  $0.597 \rho_1$ . Similarly, for the three-layered system with  $H/R = 1$ ,  $H_1 = H_2 = H_3 = H/3$ ,  $\rho_2 = 0.667 \rho_1$  and  $\rho_3 = 0.333 \rho_1$ , the values of the equivalent densities are determined to be  $\rho_2^* = 0.722 \rho_1$  and  $\rho_3^* = 0.414 \rho_1$ . The adjusted pressure distributions for these two systems are shown in Fig. 5.7. The corresponding unadjusted pressure distributions and the exact ones are also shown in the figure. It is seen that the suggested adjustment significantly improves the agreement in the pressure distributions. Similar improvements have been obtained on applying the adjusted approximate procedure to other layered systems with different tank-liquid parameters.

Ratios of the base shear, wall moment and foundation moment obtained by the adjusted and exact methods are plotted in Fig. 5.8 as a function of  $H/R$  for two-layered systems with  $H_2/H_1 = 1$  and values of  $\rho_2/\rho_1$  ranging from 0 to 1. Ratios for three-layered systems having equal-layer thicknesses are presented in columns (5), (6) and (7) of Table 5.5. Similar results for other two-layered and three-layered systems have also been extensively studied. The agreement between the adjusted and exact results is found to be very good. The errors are generally confined to a range of  $\pm 5\%$  and are usually much smaller than that. For isolated cases that are associated with very low values of  $H/R$  ( $\leq 0.3$ ) or unrealistic values of  $\rho_j/\rho_1$ ,  $H_j/H$  ( $\leq 0.2$ ), these errors rise up to about  $\pm 8\%$ .

### 5.4.3 Other Approximate Methods

It is of interest to compare the accuracy of the proposed method with those of other methods that could be used to estimate the impulsive response of rigid layered systems. The latter methods are also based on simple, rational principles that express the layered response in terms of corresponding solutions for homogeneous systems.

#### Method I

The layered system is replaced by an equivalent uniform system that has the same average mass density. Approximate values for the impulsive base shear, base moment and foundation moment of the layered system are then computed from existing solutions for the equivalent homogeneous system and compared with exact values in Fig. 5.8 for two-layered systems with equal layer thicknesses. It is seen that :

1. The errors are on the positive side, i.e., the proposed approximation over-estimates the response. This over-estimation is moderate for values of  $\rho_2/\rho_1$  in the range of 0.5 to 1, but increases significantly for smaller values of  $\rho_2/\rho_1$  and  $H/R$ .
2. The errors for the base shear are smaller than those for the base and foundation moments. The reason for this is as follows : The proposed method only represents the effects of layering in an average sense and, as a result, the trends of the exact and approximate pressure distributions are quite different. While the areas under the two sets of curves are in reasonably good agreement, causing an acceptable match for the base shear, the heights of the respective centroids from the tank-base and the respective pressure ordinates at the base are quite different, causing significant errors for the base and foundation moments.

#### Method II

A normalization scheme used in Chapter 4 is to represent the hydrodynamic response of the layered system as a fraction of that obtained by presuming the contained liquid to act rigidly. For example, the impulsive base shear is expressed as a fraction of the total shear of the system,  $m_l \ddot{x}_g(t)$ , and the impulsive base moment is expressed in terms of the moment induced by the entire liquid mass acting at the center of mass of the layered system,  $m_l h_l \ddot{x}_g(t)$ .

Based on the similarity of the normalized exact numerical solutions presented therein to the corresponding solutions for homogeneous systems, it can be assumed

that the fractions which relate the hydrodynamic effects for the layered system to the corresponding rigid effects are approximately equal to those for a homogeneous system with identical height-to-radius ratio. For example, the impulsive shear and base moment for any layered system with  $H/R = 0.5$  is taken as  $Q_{b,i}(t) \approx 0.3 m_l \ddot{x}_g(t)$  and  $M_i(t) \approx 0.24 m_l h_l \ddot{x}_g(t)$  respectively, where  $m_l \ddot{x}_g(t)$  and  $m_l h_l \ddot{x}_g(t)$  are the total shear and base moment for the given system, and 0.3 and 0.24 are the corresponding solutions (fractions) for a homogeneous system with  $H/R = 0.5$  (Veletsos 1984). The accuracy of this procedure is examined in Fig. 5.9, wherein the ratios of the approximate and exact coefficients for the impulsive component of the base shear, base moment and foundation moment are plotted as a function of  $H/R$  for two-layered liquids with  $H_1/H = H_2/H = 0.5$  and values of  $\rho_2/\rho_1$  ranging from 0 to 1. It is seen that :

1. The ratios for base shear are identical to those obtained by replacing the layered system with a uniform system of the same average mass density. This follows from the fact that the total shear of the layered system evaluated in Method II is equal to that of the replacement uniform system considered in Method I.
2. While the errors are reasonably small for base shears and base moments, they are substantial for the foundation moments of tanks with broad aspect-ratios ( $H/R \leq 1$ ). This is consistent with the findings in the previous chapter and follows from the fact that in this range of  $H/R$ , the fraction that relates the contribution of the impulsive pressure exerted on the base to the total rigid foundation moment is quite different for the layered and homogeneous systems.

## 5.5 Conclusions

With the information presented herein, the impulsive response of a layered system may be evaluated readily from existing solutions for homogeneous systems. Simple methods have been presented for evaluating the dominant frequencies of vibration of a flexible layered system and the impulsive response coefficients of a rigid layered system. The latter quantities have been shown to play an important role in the approximate assessment of the modal participation factors for both broad and tall flexible tanks. The principal conclusions of the study are as follows :

1. The first two natural frequencies of vibration of a layered system are accurately estimated by representing the layered system as a series of homogeneous sub-

systems of different liquid heights and densities. For realistic values of the tank-liquid parameters, the errors are typically in the range of 3% to 5%.

2. The proposed concept also enables the convenient evaluation of the impulsive response coefficients for rigid layered tank-liquid systems. The errors in this case typically vary between  $-5\%$  and  $-15\%$ . An empirical modification to the densities of the approximating homogeneous sub-systems further improves the accuracy to within  $\pm 5\%$ . Furthermore, this method compares favorably with other methods that could be used to approximate the rigid layered response.

**Table 5.1: Frequency coefficients for fundamental mode of vibration of two-layered systems with different  $H/R$  and  $H_2/H_1$ ; Systems with  $h/R = 0.001$ ,  $\rho_2/\rho = 0.127$  and  $\nu = 0.3$**

$\rho_2/\rho_1$	$H_1/H = 0.25$		$H_1/H = 1/3$		$H_1/H = 0.5$		$H_1/H = 2/3$		$H_1/H = 0.75$	
	Exact	Appr.	Exact	Appr.	Exact	Appr.	Exact	Appr.	Exact	Appr.
(1)	(2)	(3)	(4)	(5)	(6)	(7)	(8)	(9)	(10)	(11)
					$H/R = 0.5$					
1	0.0719	0.0719	0.0719	0.0719	0.0719	0.0719	0.0719	0.0719	0.0719	0.0719
0.75	0.0700	0.0699	0.0692	0.0691	0.0676	0.0674	0.0659	0.0657	0.0650	0.0648
0.5	0.0674	0.0665	0.0654	0.0644	0.0613	0.0605	0.0575	0.0570	0.0557	0.0554
0.25	0.0622	0.0586	0.0574	0.0545	0.0495	0.0481	0.0439	0.0432	0.0416	0.0411
					$H/R = 1.0$					
1	0.0875	0.0875	0.0875	0.0875	0.0875	0.0875	0.0875	0.0875	0.0875	0.0875
0.75	0.0850	0.0854	0.0840	0.0845	0.0820	0.0825	0.0801	0.0804	0.0791	0.0793
0.5	0.0817	0.0815	0.0793	0.0793	0.0745	0.0747	0.0701	0.0703	0.0680	0.0681
0.25	0.0757	0.0725	0.0703	0.0680	0.0610	0.0602	0.0540	0.0538	0.0512	0.0510
					$H/R = 2.0$					
1	0.0896	0.0896	0.0896	0.0896	0.0896	0.0896	0.0896	0.0896	0.0896	0.0896
0.75	0.0880	0.0882	0.0871	0.0876	0.0851	0.0860	0.0828	0.0839	0.0817	0.0826
0.5	0.0857	0.0856	0.0836	0.0838	0.0787	0.0798	0.0736	0.0750	0.0712	0.0723
0.25	0.0817	0.0789	0.0770	0.0749	0.0672	0.0671	0.0586	0.0593	0.0549	0.0555

**Table 5.2: Frequency coefficients for second mode of vibration of two-layered systems with different  $H/R$  and  $H_2/H_1$ ; Systems with  $h/R = 0.001$ ,  $\rho_2/\rho = 0.127$  and  $\nu = 0.3$**

$\rho_2/\rho_1$	$H_1/H = 0.25$		$H_1/H = 1/3$		$H_1/H = 0.5$		$H_1/H = 2/3$		$H_1/H = 0.75$	
	Exact	Appr.	Exact	Appr.	Exact	Appr.	Exact	Appr.	Exact	Appr.
(1)	(2)	(3)	(4)	(5)	(6)	(7)	(8)	(9)	(10)	(11)
					$H/R = 0.5$					
1	0.1284	0.1284	0.1284	0.1284	0.1284	0.1284	0.1284	0.1284	0.1284	0.1284
0.75	0.1247	0.1248	0.1230	0.1231	0.1200	0.1198	0.1175	0.1168	0.1162	0.1154
0.5	0.1179	0.1184	0.1136	0.1141	0.1078	0.1067	0.1027	0.1007	0.1000	0.0981
0.25	0.1021	0.1038	0.0965	0.0958	0.0881	0.0838	0.0790	0.0757	0.0751	0.0724
					$H/R = 1.0$					
1	0.1656	0.1656	0.1656	0.1656	0.1656	0.1656	0.1656	0.1656	0.1656	0.1656
0.75	0.1590	0.1606	0.1566	0.1588	0.1528	0.1552	0.1500	0.1513	0.1487	0.1493
0.5	0.1480	0.1520	0.1425	0.1475	0.1354	0.1391	0.1300	0.1312	0.1272	0.1274
0.25	0.1247	0.1326	0.1180	0.1241	0.1094	0.1105	0.1001	0.0994	0.0956	0.0946
					$H/R = 2.0$					
1	0.2114	0.2114	0.2114	0.2114	0.2114	0.2114	0.2114	0.2114	0.2114	0.2114
0.75	0.2002	0.2057	0.1968	0.2034	0.1923	0.1984	0.1896	0.1932	0.1884	0.1906
0.5	0.1833	0.1955	0.1757	0.1898	0.1671	0.1782	0.1623	0.1675	0.1599	0.1626
0.25	0.1507	0.1722	0.1404	0.1610	0.1313	0.1418	0.1239	0.1268	0.1196	0.1207

**Table 5.3: Frequency coefficients for first two modes of vibration of three-layered systems with different  $H/R$  and  $H_1 = H_2 = H_3 = H/3$ ; systems with  $h/R = 0.001$ ,  $\rho_3/\rho = 0.127$  and  $\nu = 0.3$**

$\rho_3/\rho_2/\rho_1$	Values of $C_i$ for first mode		Values of $C_i$ for second mode	
	Exact	Appr.	Exact	Appr.
(1)	(2)	(3)	(4)	(5)
		$H/R = 0.5$		
1/1/1	0.0719	0.0719	0.1284	0.1284
1/1.5/2	0.0608	0.0603	0.1077	0.1068
1/2/3	0.0538	0.0530	0.0950	0.0934
1/3/5	0.0450	0.0440	0.0794	0.0770
		$H/R = 1$		
1/1/1	0.0875	0.0875	0.1656	0.1656
1/1.5/2	0.0738	0.0744	0.1357	0.1387
1/2/3	0.0656	0.0658	0.1189	0.1217
1/3/5	0.0551	0.0549	0.0991	0.1007
		$H/R = 2$		
1/1/1	0.0896	0.0896	0.2114	0.2114
1/1.5/2	0.0775	0.0790	0.1682	0.1776
1/2/3	0.0699	0.0715	0.1454	0.1561
1/3/5	0.0601	0.0612	0.1201	0.1294

**Table 5.4: Ratios of approximate to exact values of impulsive component of base shear, base moment and foundation moment for rigid two-layered systems with different  $H/R$  and  $H_1/H$**

$\rho_2/\rho_1$	$H_1/H = 0.25$			$H_1/H = 0.5$			$H_1/H = 0.75$		
	$\frac{[Q_{b,i}]_a}{[Q_{b,i}]_e}$	$\frac{[M_i]_a}{[M_i]_e}$	$\frac{[M'_i]_a}{[M'_i]_e}$	$\frac{[Q_{b,i}]_a}{[Q_{b,i}]_e}$	$\frac{[M_i]_a}{[M_i]_e}$	$\frac{[M'_i]_a}{[M'_i]_e}$	$\frac{[Q_{b,i}]_a}{[Q_{b,i}]_e}$	$\frac{[M_i]_a}{[M_i]_e}$	$\frac{[M'_i]_a}{[M'_i]_e}$
	(2)	(3)	(4)	(5)	(6)	(7)	(8)	(9)	(10)
	$H/R = 0.5$								
1	1	1	1	1	1	1	1	1	1
0.75	0.967	0.973	0.972	0.964	0.960	0.971	0.982	0.974	0.986
0.5	0.933	0.943	0.945	0.932	0.921	0.948	0.970	0.955	0.978
0.25	0.903	0.912	0.925	0.920	0.894	0.941	0.971	0.953	0.980
	$H/R = 1.0$								
1	1	1	1	1	1	1	1	1	1
0.75	0.953	0.961	0.953	0.949	0.944	0.950	0.978	0.966	0.975
0.5	0.906	0.920	0.907	0.906	0.891	0.909	0.960	0.941	0.960
0.25	0.867	0.877	0.871	0.891	0.856	0.895	0.962	0.940	0.961
	$H/R = 2.0$								
1	1	1	1	1	1	1	1	1	1
0.75	0.949	0.962	0.957	0.949	0.942	0.947	0.974	0.960	0.965
0.5	0.897	0.919	0.912	0.907	0.886	0.900	0.957	0.931	0.942
0.25	0.855	0.872	0.871	0.894	0.850	0.877	0.959	0.928	0.941



**Table 5.5: Ratios of approximate to exact values of impulsive component of base shear, base moment and foundation moment for rigid three-layered systems with different  $H/R$  and  $H_1 = H_2 = H_3 = H/3$**

$\rho_3/\rho_2/\rho_1$	Unadjusted Values			Adjusted Values		
	$\frac{[Q_{b,i}]_a}{[Q_{b,i}]_e}$	$\frac{[M_i]_a}{[M_i]_e}$	$\frac{[M'_i]_a}{[M'_i]_e}$	$\frac{[Q_{b,i}]_a}{[Q_{b,i}]_e}$	$\frac{[M_i]_a}{[M_i]_e}$	$\frac{[M'_i]_a}{[M'_i]_e}$
(1)	(2)	(3)	(4)	(5)	(6)	(7)
$H/R = 0.5$						
1/1/1	1	1	1	1	1	1
1/1.5/2	0.934	0.925	0.949	1.004	1.014	1.017
1/2/3	0.915	0.899	0.937	1.005	1.014	1.025
1/3/5	0.906	0.882	0.934	0.993	0.993	1.020
$H/R = 1$						
1/1/1	1	1	1	1	1	1
1/1.5/2	0.909	0.898	0.911	0.989	1.002	0.991
1/2/3	0.885	0.865	0.888	0.987	0.999	0.990
1/3/5	0.875	0.846	0.879	0.975	0.975	0.978
$H/R = 2$						
1/1/1	1	1	1	1	1	1
1/1.5/2	0.904	0.889	0.899	0.983	1.003	0.996
1/2/3	0.875	0.850	0.866	0.977	0.996	0.989
1/3/5	0.861	0.825	0.848	0.961	0.964	0.964

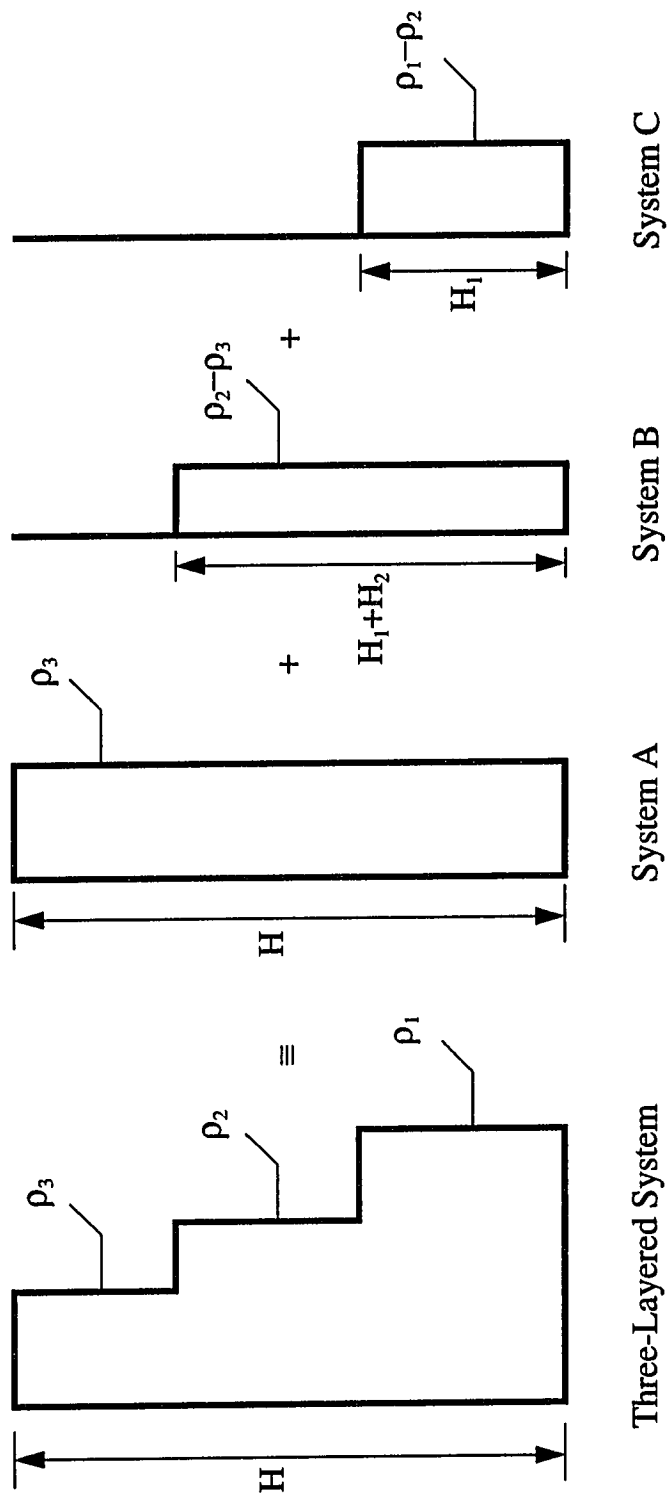


Figure 5.1 Proposed procedure for representing a three-layered system in terms of three homogeneous sub-systems A, B and C

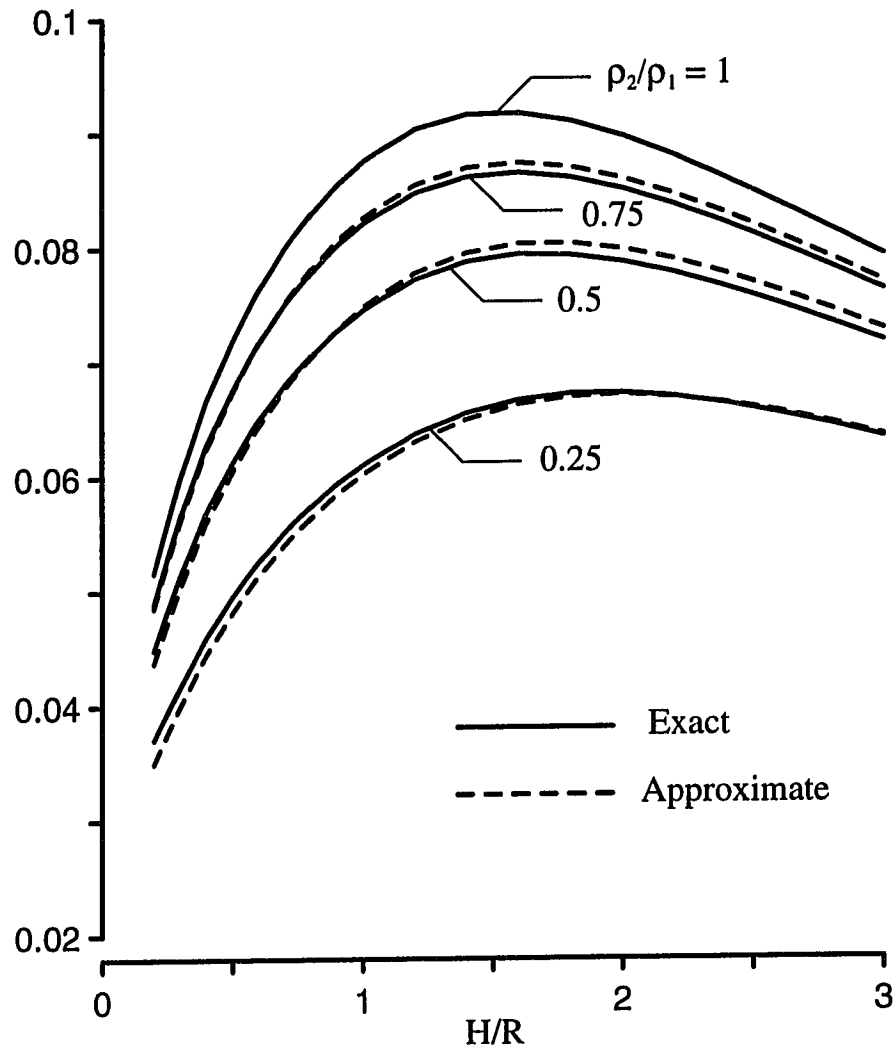


Figure 5.2 Frequency coefficient for fundamental mode of vibration of two-layered steel tanks with  $H_1=H_2=H/2$ ,  $\rho_2/\rho = 0.127$ ,  $h/R = 0.001$ ,  $\nu = 0.3$ .

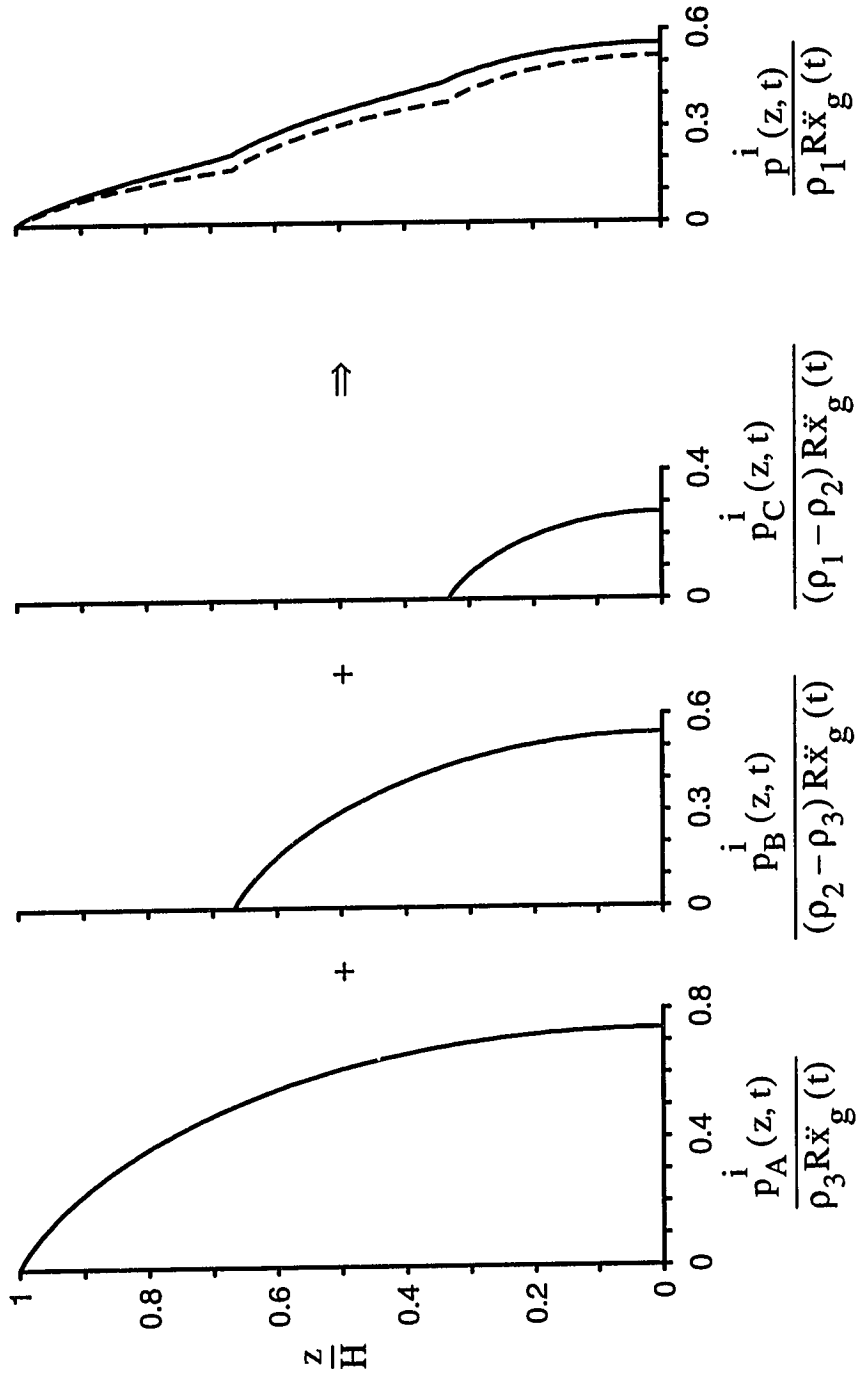


Figure 5.3 Proposed approximate procedure of evaluating the impulsive wall-pressure distribution for a three-layered system in terms of those for its homogeneous sub-systems

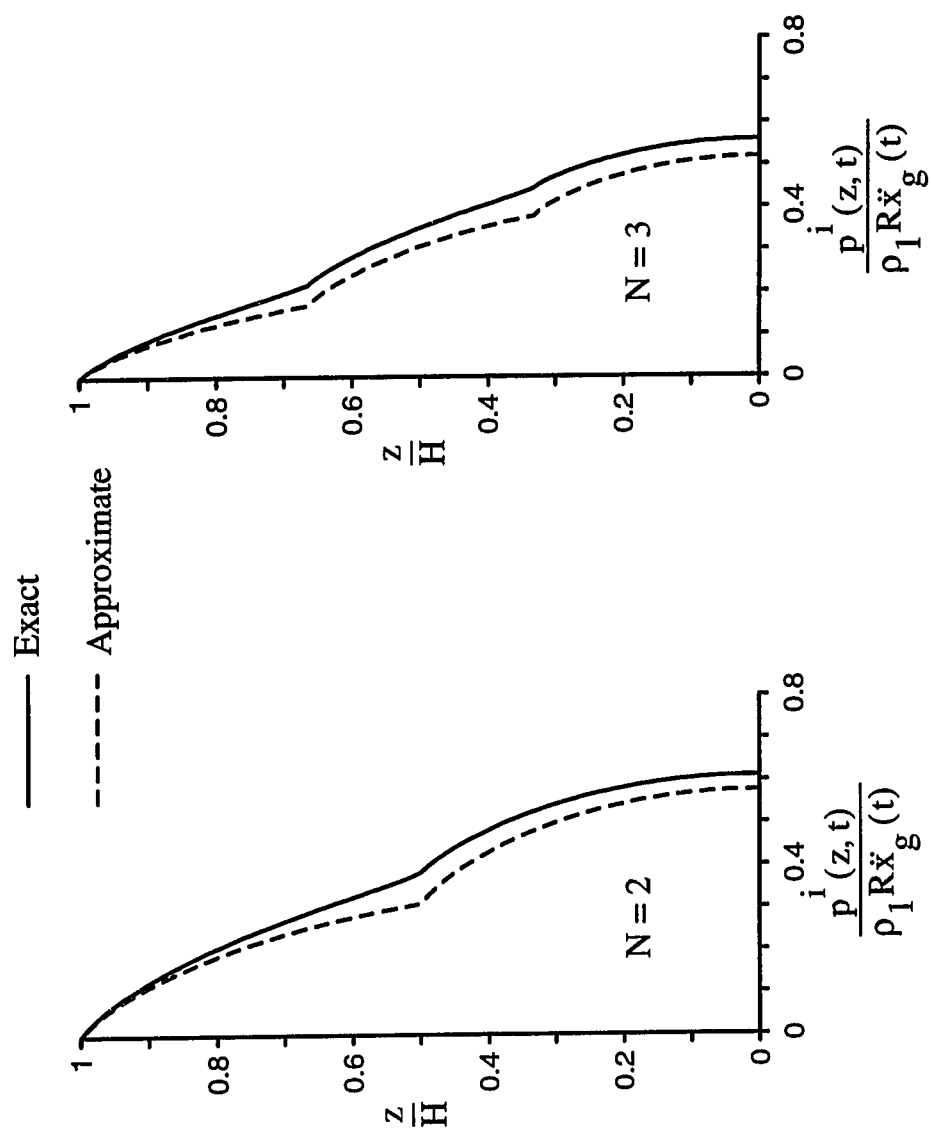


Figure 5.4 Approximate and exact impulsive wall-pressure distributions for two-layered system with  $H/R = 1$ ,  $H_1=H_2=H/2$ ,  $\rho_2/\rho_1=0.5$  and for three-layered system with  $H/R = 1$ ,  $H_1=H_2=H_3=H/3$ ,  $\rho_3/\rho_2/\rho_1=1/2/3$

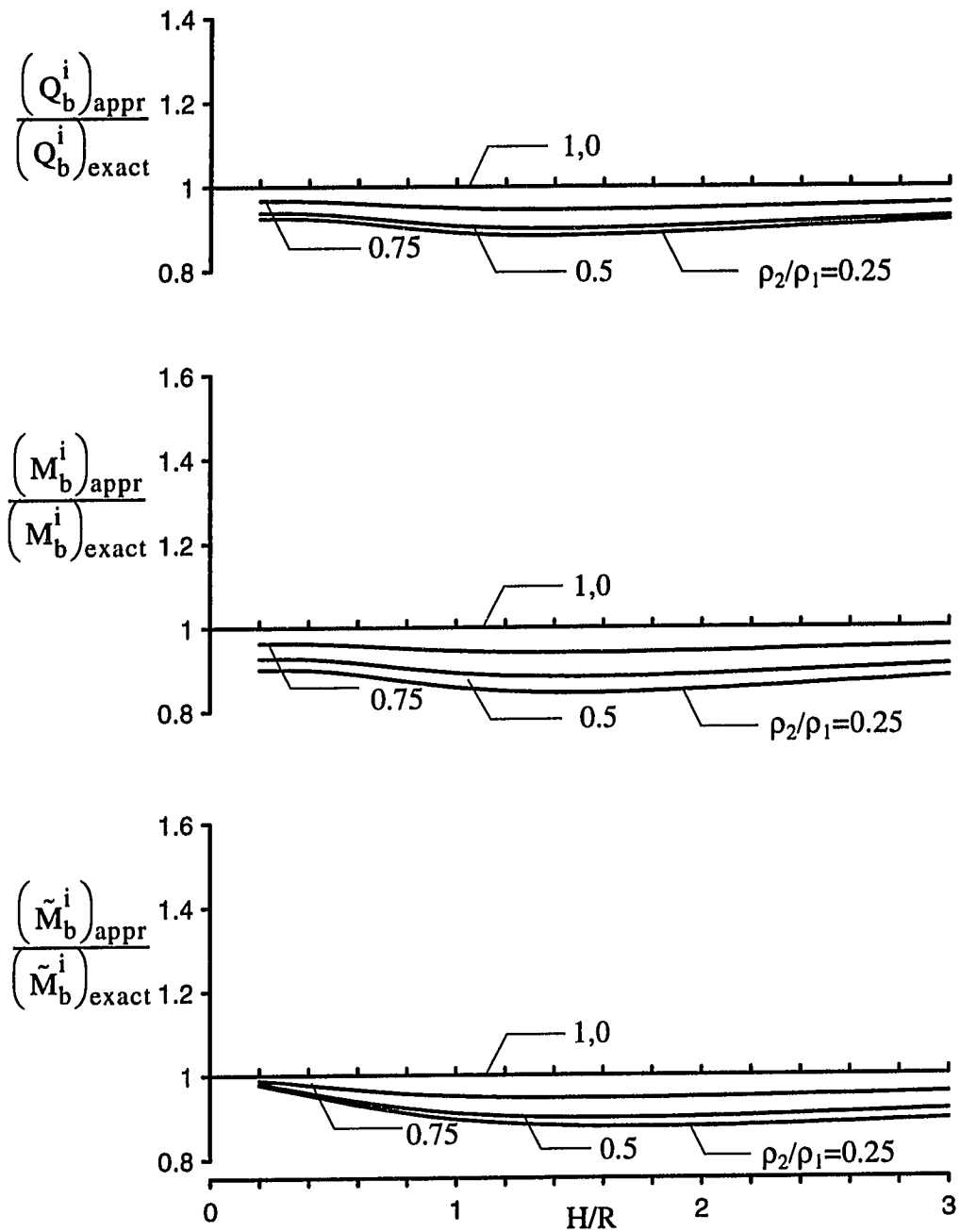


Figure 5.5 Ratios of approximate and exact impulsive base forces for two-layered systems with equal layer thicknesses; Approximate values computed by unadjusted proposed procedure

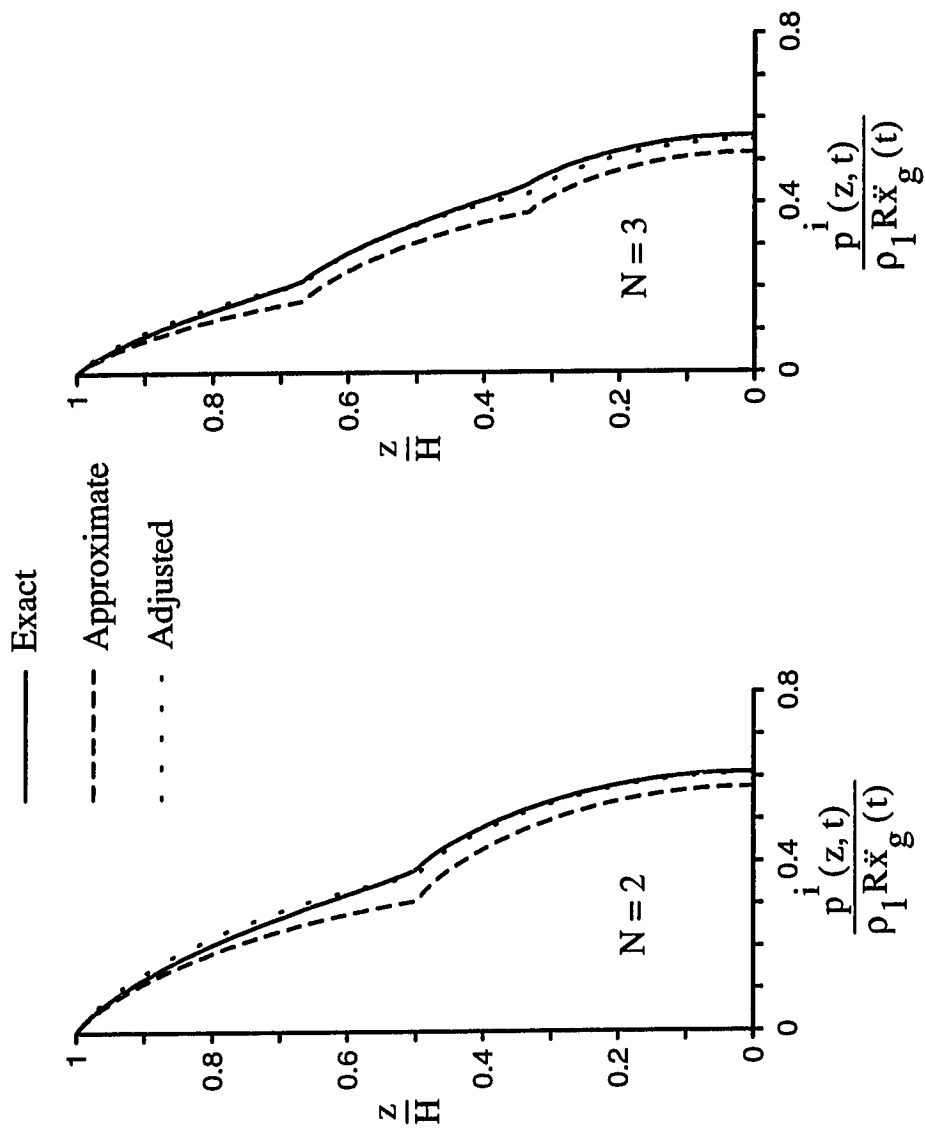


Figure 5.6 Approximate, adjusted and exact impulsive pressure distributions for two-layered system with  $H/R = 1$ ,  $H_1=H_2=H/2$ ,  $\rho_2/\rho_1=0.5$  and for three-layered system with  $H/R = 1$ ,  $H_1=H_2=H_3=H/3$ ,  $\rho_3/\rho_2\rho_1=1/2/3$

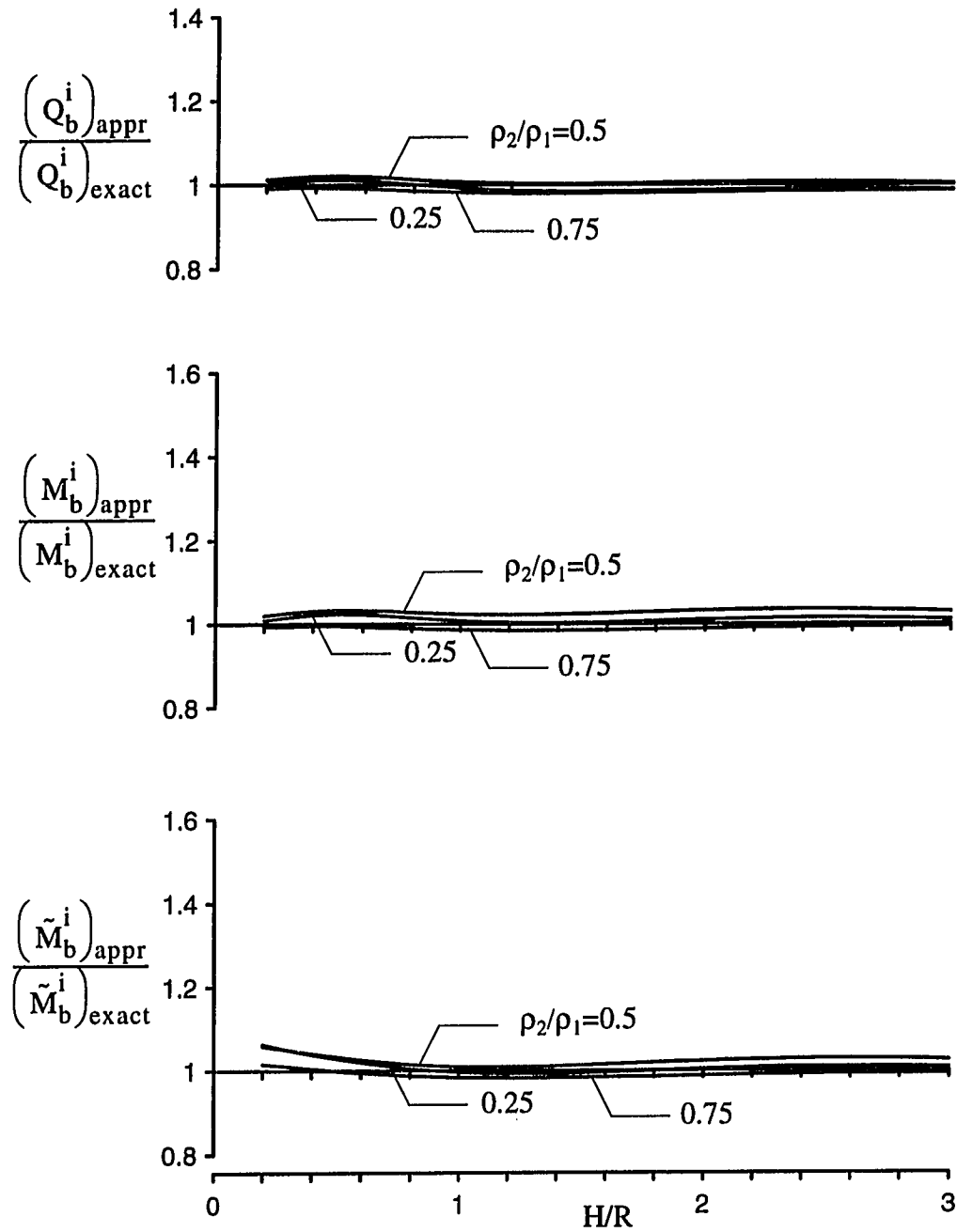


Figure 5.7 Ratios of approximate and exact impulsive base forces for two-layered systems with  $H_2/H_1=1$ ; Approximate values computed by adjusted proposed procedure



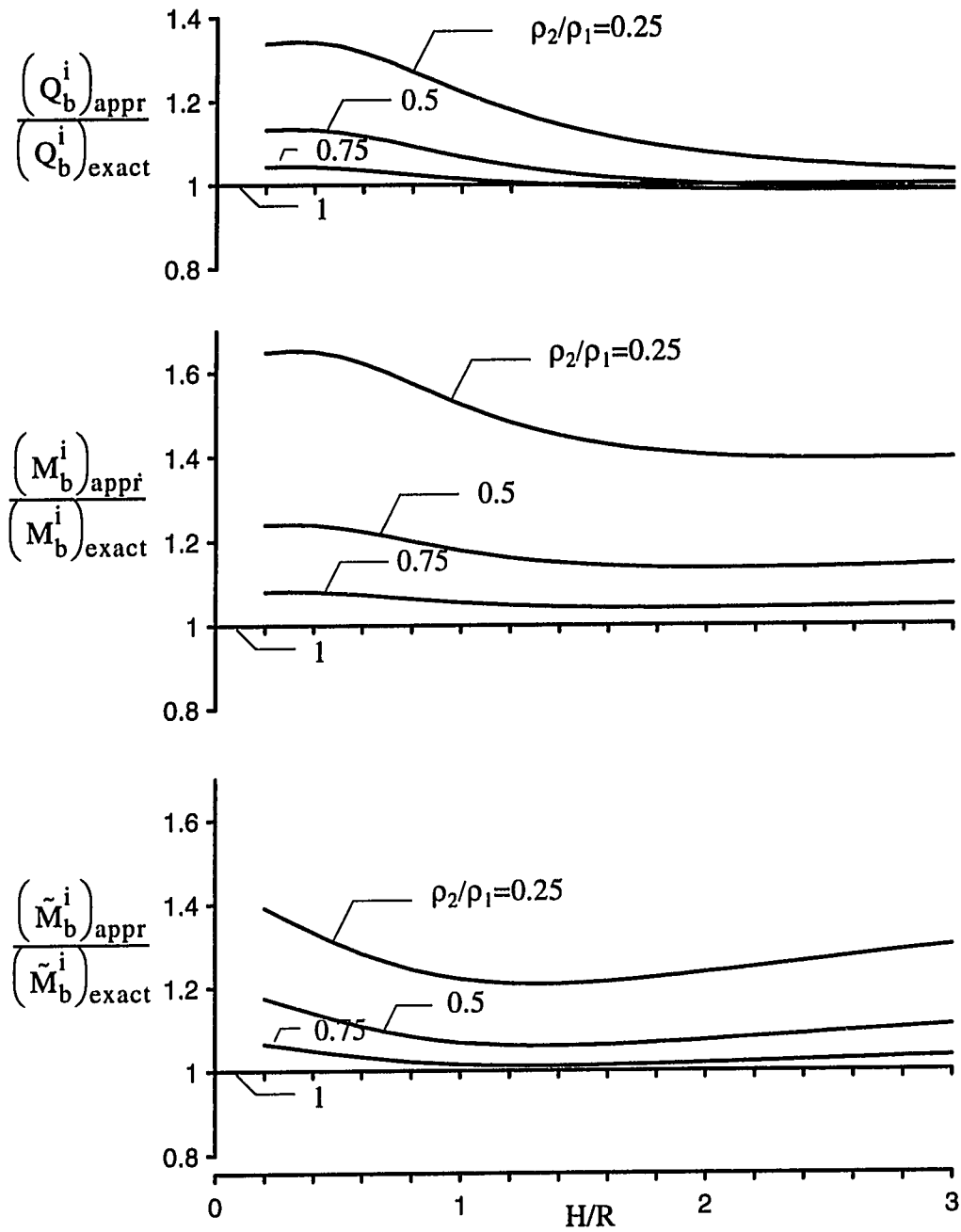


Figure 5.8 Ratios of approximate and exact impulsive base forces for two-layered systems with  $H_2/H_1=1$ ; Approximate values computed for a uniform liquid of the same average mass density

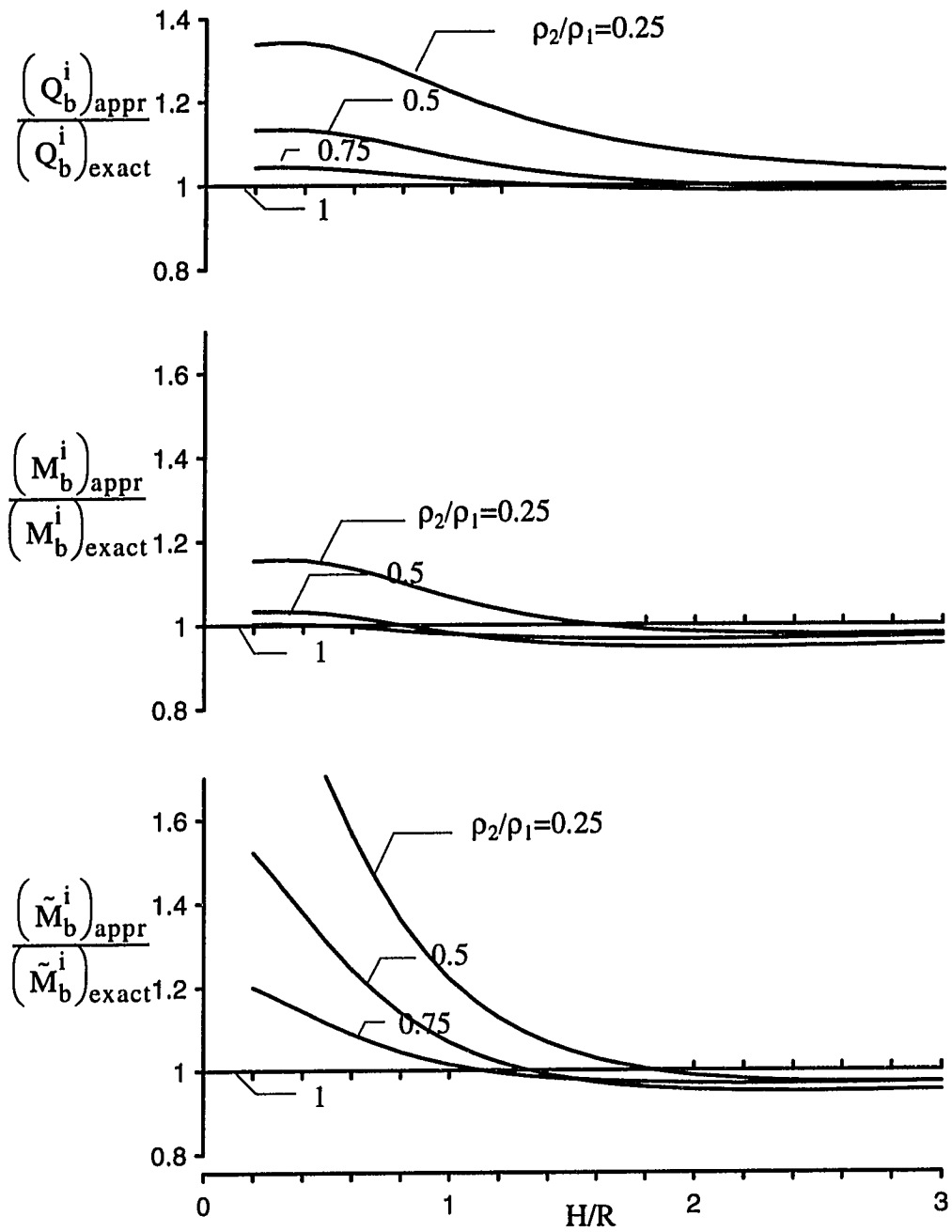


Figure 5.9 Ratios of approximate and exact impulsive base forces for two-layered systems with  $H_2/H_1=1$ ; Approximate values computed by using Method II

## Chapter 6

# Dynamic Response of Rigid Tanks with Inhomogeneous Liquids

### 6.1 Introduction

A sequel to the studies in Chapters 3, 4 and 5, the study reported herein is motivated by the need for improved understanding of the response to earthquakes of tanks in nuclear facilities that store high-level radioactive wastes. In some cases, the contents of these tanks cannot adequately be modeled as homogeneous liquids, and it is necessary to consider more complex representations such as continuously varying liquid densities.

For specific forms of such density variations, it is possible to obtain simple analytical solutions, and it is the purpose of this chapter to present such solutions for cylindrical tanks for which the density of the contained liquid increases exponentially from top to bottom. Some attention is also given to the interrelationship of the solutions obtained for the continuous variation and its discretized, multi-layered representation. The only known related study on this subject is the one reported by Chwang [11] for the limiting case of a straight wall retaining a slightly stratified liquid.

The governing equations of motion are first formulated for systems with an arbitrary vertical variation in liquid density, but the solutions presented are limited to the exponential variation. Both the free-vibrational characteristics of the system and its response to a horizontal ground shaking are studied. The response quantities examined include the vertical sloshing motions of the liquid at its free-surface, and the impulsive and convective components of the hydrodynamic wall pressures and associated tank forces. The impulsive effects reflect the action of the part of the liquid that may be considered to move in synchronism with the tank wall as a rigidly attached mass, whereas the convective effects represent the action of the part of the liquid undergoing sloshing motions. Comprehensive numerical solutions are presented which elucidate the effects and relative importance of the numerous parameters involved and

the relationship of these solutions to those obtained for an equivalent homogeneous system.

## 6.2 System Considered

The system investigated is shown in Fig. 6.1. It is a rigid, vertical, circular cylindrical tank of radius  $R$  that is filled to a height  $H$  with an inhomogeneous liquid the mass density of which increases continuously from top to bottom. The liquid is presumed to be incompressible, irrotational and inviscid, and only linear actions are examined. The tank is considered to be anchored to a rigid, horizontally moving base. Points within the tank-liquid system are specified by the cylindrical coordinates,  $r$ ,  $\theta$  and  $z$ , as shown in the figure. The heightwise variation of the liquid density,  $\rho(z)$ , is defined by

$$\rho(z) = \rho_o e^{-\beta(z/H)} \quad (6.1)$$

where  $\rho_o$  represents the density value at the tank base, and  $\beta$  is a dimensionless, positive decay factor. Fig. 6.2 shows the variations of  $\rho(z)$  for different values of  $\rho_1/\rho_o$ , where  $\rho_1$  represents the top value of the liquid density. The corresponding values of  $\beta$  are shown in parentheses.

The exciting motion is considered to be uniform over the tank base and to be directed along the  $\theta = 0$  coordinate axis. The acceleration of the base motion at any time  $t$  is denoted by  $\ddot{x}_g(t)$ , and the corresponding velocity and displacement are denoted by  $\dot{x}_g(t)$  and  $x_g(t)$ , respectively.

## 6.3 Governing Equations

### 6.3.1 Background Information

The response of the liquid is governed by the system of differential equations,

$$\frac{\partial^2 \phi}{\partial r^2} + \frac{1}{r} \frac{\partial \phi}{\partial r} + \frac{1}{r^2} \frac{\partial^2 \phi}{\partial \theta^2} - \frac{\partial^2 d}{\partial z \partial t} = 0 \quad (6.2)$$

and

$$\frac{\partial}{\partial z} \left( \rho \frac{\partial \phi}{\partial t} \right) + \rho \frac{\partial^2 d}{\partial t^2} - \frac{\partial \rho}{\partial z} g d = 0 \quad (6.3)$$

in which  $d = d(r, z, \theta, t)$  is the vertical sloshing displacement of the liquid at an arbitrary point and time, and  $\phi = \phi(r, z, \theta, t)$  is a velocity potential function which is

related to the hydrodynamic pressure,  $p = p(r, z, \theta, t)$ , by

$$p = \rho \frac{\partial \phi}{\partial t} \quad (6.4)$$

and to the radial and tangential components of liquid velocity,  $v_r$  and  $v_\theta$ , by

$$v_r = -\frac{\partial \phi}{\partial r} \quad v_\theta = -\frac{1}{r} \frac{\partial \phi}{\partial \theta} \quad (6.5)$$

Equations (6.2) and (6.3) are deduced from more general expressions presented by Yih [85] by expressing the latter in cylindrical coordinates and specializing them to the incompressible liquid considered herein. For a homogeneous liquid with  $\rho = \text{constant}$ ,

$$\frac{\partial d}{\partial t} = -\frac{\partial \phi}{\partial z} \quad (6.6)$$

and equation (6.2) reduces to the well-known Laplace's equation  $\nabla^2 \phi = 0$ .

The solutions of equations (6.2) and (6.3) must satisfy the continuity of radial velocities at the tank-wall, defined by

$$\left( \frac{\partial \phi}{\partial r} \right)_{r=R} = -\dot{x}_g(t) \cos \theta \quad (6.7)$$

the condition of no vertical motion at the tank-base, defined by

$$(d)_{z=0} = 0 \quad (6.8)$$

and the linearized pressure condition at the free liquid surface, defined by

$$\left( \frac{\partial \phi}{\partial t} - g d \right)_{z=H} = 0 \quad (6.9)$$

where  $g$  is the acceleration of gravity.

### 6.3.2 Equation of Motion in Terms of a Single Unknown

Following the approach used in the analysis of the layered system, the potential function  $\phi$  is expressed in the form

$$\phi(r, \theta, z, t) = -\dot{x}_g(t) r \cos \theta + \psi(r, \theta, z, t) \quad (6.10)$$

where the first term on the right side provides for the rigid body motion of the tank, and the potential function  $\psi$  provides for the relative motion of the liquid and tank. On substituting equation (6.10) into equations (6.2) and (6.3), one obtains

$$\frac{\partial^2 \psi}{\partial r^2} + \frac{1}{r} \frac{\partial \psi}{\partial r} + \frac{1}{r^2} \frac{\partial^2 \psi}{\partial \theta^2} - \frac{\partial^2 d}{\partial z \partial t} = 0 \quad (6.11)$$

and

$$\frac{\partial}{\partial z} \left( \rho \frac{\partial \psi}{\partial t} \right) + \rho \frac{\partial^2 d}{\partial t^2} - \frac{\partial \rho}{\partial z} g d = \frac{\partial \rho}{\partial z} r \ddot{x}_g(t) \cos \theta \quad (6.12)$$

The solutions of equations (6.11) and (6.12) may be obtained by the method of separation of variables in the form

$$d(r, z, \theta, t) = D(z, t) X(r) \cos \theta \quad (6.13)$$

$$\psi(r, z, \theta, t) = \Psi(z, t) X(r) \cos \theta \quad (6.14)$$

That the function  $X(r)$  in these two expressions must be the same follows from equation (6.12). On substituting equations (6.13) and (6.14) into equation (6.11), separating the resulting functions of  $r$  from those of  $z$  and  $t$ , and equating each set to  $-(\lambda/R)^2$ , where  $\lambda$  is a dimensionless constant, one obtains Bessel's differential equation for  $X(r)$  and the following relation between  $\Psi$  and  $D$  :

$$\Psi(z, t) = -\frac{R^2}{\lambda^2} \frac{\partial^2 D}{\partial z \partial t} \quad (6.15)$$

Next, on using the antisymmetry condition at  $r = 0$  and the continuity condition for radial velocities at  $r = R$ , the solution for  $X(r)$  can be shown to be given by any one of an infinity of Bessel functions of the first kind and first order. The  $m$ th of these functions may be expressed as

$$X_m(r) = B_m J_1 \left( \lambda_m \frac{r}{R} \right) \quad (6.16)$$

where  $B_m$  is a constant that remains to be determined, and  $\lambda_m$  is the  $m$ th root of the first derivative of  $J_1(\lambda)$ , the first three values of which are

$$\lambda_1 = 1.841 \quad \lambda_2 = 5.331 \quad \lambda_3 = 8.536 \quad (6.17)$$

Equation (6.16) effectively defines the radial variation of the displacement  $d$  when the liquid is oscillating in its  $m$ th horizontal mode of vibration. The displacement  $d$  at an arbitrary point and time is then determined from equation (6.13) as a linear combination of its modal components to be

$$d(\xi, \eta, \theta, t) = \sum_{m=1}^{\infty} D_m(\eta, t) \frac{J_1(\lambda_m \xi)}{J_1(\lambda_m)} \cos \theta \quad (6.18)$$

where the constant  $B_m$  in equation (6.16) has been absorbed into the function  $D_m$ ;  $\xi = r/R$  and  $\eta = z/H$  are dimensionless radial and vertical position coordinates;

and  $D_m(\eta, t)$  represents the instantaneous value of the vertical displacement of a liquid particle at the junction of the tank-wall and the  $\theta = 0$  plane when the liquid is vibrating in its  $m$ th horizontal natural mode. The corresponding expression for  $\psi$  is determined from equations (6.14), (6.15) and (6.16) to be

$$\psi(\xi, \eta, \theta, t) = - \sum_{m=1}^{\infty} \frac{R^2}{\lambda_m^2 H} \frac{\partial \dot{D}_m}{\partial \eta} \frac{J_1(\lambda_m \xi)}{J_1(\lambda_m)} \cos \theta \quad (6.19)$$

where a dot superscript denotes differentiation with respect to time.

On substituting equations (6.18) and (6.19) into equation (6.12) and making use of the orthogonality of the Bessel functions, the equation of motion for the system can be expressed solely in terms of the function  $D_m(\eta, t)$ , as

$$\rho \frac{\partial^2 \ddot{D}_m}{\partial \eta^2} + \frac{\partial \rho}{\partial \eta} \frac{\partial \ddot{D}_m}{\partial \eta} - \rho \left( \frac{\lambda_m H}{R} \right)^2 \ddot{D}_m + \frac{g \lambda_m}{R} \left( \frac{\lambda_m H}{R} \right) \frac{\partial \rho}{\partial \eta} D_m = -\epsilon_m \lambda_m \left( \frac{\lambda_m H}{R} \right) \frac{\partial \rho}{\partial \eta} \ddot{x}_g(t) \quad (6.20)$$

where

$$\epsilon_m = \frac{2}{\lambda_m^2 - 1} \quad (6.21)$$

Furthermore, on making use of equations (6.10), (6.18) and (6.19), the boundary conditions defined by equations (6.8) and (6.9) reduce to

$$(D_m)_{z=0} = 0 \quad (6.22)$$

$$\left( \frac{R^2}{\lambda_m^2 H} \frac{\partial \ddot{D}_m}{\partial \eta} + g D_m \right)_{z=H} = -\epsilon_m R \ddot{x}_g(t) \quad (6.23)$$

After determining the functions  $D_m = D_m(\eta, t)$  for different values of  $m$ , the displacement  $d$ , the potential functions  $\psi$  and  $\phi$ , and the hydrodynamic pressure  $p$  may be computed from equations (6.18), (6.19), (6.10) and (6.4), respectively.

For the system with the exponential variation in liquid density considered herein, equation (6.20) reduces to

$$\frac{\partial^2 \ddot{D}_m}{\partial \eta^2} - \beta \frac{\partial \ddot{D}_m}{\partial \eta} - \left( \frac{\lambda_m H}{R} \right)^2 \ddot{D}_m - \frac{g \lambda_m}{R} \left( \frac{\lambda_m H}{R} \right) \beta D_m = \epsilon_m \lambda_m \left( \frac{\lambda_m H}{R} \right) \beta \ddot{x}_g(t) \quad (6.24)$$

## 6.4 Free Vibration

On setting the right-hand side of equation (6.24) equal to zero and letting  $D_m(\eta, t) = \hat{D}_m(\eta) e^{i\omega_m t}$ , where  $i = \sqrt{-1}$  and  $\omega_m$  is the circular frequency of the  $m$ th horizontal

mode of vibration, one obtains

$$\frac{\partial^2 \hat{D}_m}{\partial \eta^2} - \beta \frac{\partial \hat{D}_m}{\partial \eta} + \left[ \frac{\beta \lambda_m H}{C_m^2 R} - \left( \frac{\lambda_m H}{R} \right)^2 \right] \hat{D}_m = 0 \quad (6.25)$$

in which  $C_m$  is a dimensionless factor related to  $\omega_m$  by

$$\omega_m = C_m \sqrt{\frac{g \lambda_m}{R}} \quad (6.26)$$

Similarly, the boundary conditions defined by equations (6.22) and (6.23) can be expressed as

$$(\hat{D}_m)_{\eta=0} = 0 \quad (6.27)$$

$$\left( \frac{\partial \hat{D}_m}{\partial \eta} - \frac{\lambda_m H}{C_m^2 R} \hat{D}_m \right)_{\eta=1} = 0 \quad (6.28)$$

With appropriate reinterpretations of the symbols involved, equations (6.25), (6.27) and (6.28) can be shown to be the same as those presented by Lamb [35] for the flow of inhomogeneous liquids in rectangular channels.

The nature of the solution of equation (6.25) depends on whether the roots of the associated characteristic equation are real-valued or complex, and this depends, in turn, on the value of  $C_m$ . For

$$C_m > \sqrt{\frac{\beta(\lambda_m H/R)}{\beta^2/4 + (\lambda_m H/R)^2}} \quad (6.29)$$

the roots are real, and on satisfying the boundary condition defined by equation (6.27), the solution can be written as

$$\hat{D}_m(\eta) = E_m e^{\beta\eta/2} \sinh \gamma_m \eta \quad (6.30)$$

where

$$\gamma_m = \sqrt{\frac{\beta^2}{4} + \left( \frac{\lambda_m H}{R} \right)^2 - \frac{\beta \lambda_m H/R}{C_m^2}} \quad (6.31)$$

and  $E_m$  is an arbitrary constant. Note that  $\gamma_m$  is a function of the still unknown frequency coefficient  $C_m$ . On making use of the second boundary condition defined by equation (6.28), it is found that  $\gamma_m$  and  $C_m$  are also interrelated by

$$C_m = \sqrt{\frac{\lambda_m H/R}{\beta/2 + \gamma_m / \tanh \gamma_m}} \quad (6.32)$$



and on substituting equation (6.32) into equation (6.31), one obtains the transcendental equation

$$\gamma_m^2 + \frac{\beta\gamma_m}{\tanh\gamma_m} + \frac{\beta^2}{4} - \left(\lambda_m \frac{H}{R}\right)^2 = 0 \quad (6.33)$$

It can be shown that equation (6.33) has a single positive root,  $\gamma_{m1}$ , and that this root exists only if

$$\frac{\beta^2}{4} + \beta - \left(\lambda_m \frac{H}{R}\right)^2 < 0 \quad (6.34)$$

With the value of  $\gamma_{m1}$  established, the displacement configuration for the  $m$ th horizontal and first vertical natural mode of vibration,  $\hat{D}_{m1}(\eta)$ , is determined from equation (6.30) by replacing the subscript  $m$  by  $m1$ , and the associated circular natural frequency,  $\omega_{m1}$ , and frequency coefficient,  $C_{m1}$ , are determined similarly from equations (6.26) and (6.32), respectively. It should be recalled that equations (6.30) and (6.32) are valid only as long as equation (6.34) is satisfied.

For values of  $C_m$  that are smaller than the right-hand member of equation (6.29), the roots of the characteristic equation are complex, and the counterpart of equation (6.33) becomes

$$\gamma_m^2 - \frac{\beta\gamma_m}{\tan\gamma_m} - \frac{\beta^2}{4} + \left(\lambda_m \frac{H}{R}\right)^2 = 0 \quad (6.35)$$

The latter equation has an infinity of roots,  $\gamma_{mn}$ , where  $n$  is an integer ranging from 2 to  $\infty$  when equation (6.34) is satisfied and from 1 to  $\infty$  when equation (6.34) is not satisfied. It follows that, for each horizontal mode of vibration, there is an infinity of vertical modes, each associated with a distinct frequency. Subject to the indicated qualification on  $n$ , the  $m$ th horizontal and  $n$ th vertical mode of vibration,  $\hat{D}_{mn}(\eta)$ , is given by

$$\hat{D}_{mn}(\eta) = E_{mn} e^{\beta\eta/2} \sin\gamma_{mn}\eta \quad (6.36)$$

where  $E_{mn}$  is an arbitrary constant, and the associated frequency,  $\omega_{mn}$ , may be expressed as

$$\omega_{mn} = C_{mn} \sqrt{\frac{g\lambda_m}{R}} \quad (6.37)$$

in which the dimensionless coefficient,  $C_{mn}$ , is determined from

$$C_{mn} = \sqrt{\frac{\lambda_m(H/R)}{\beta/2 + \gamma_{mn}/\tan\gamma_{mn}}} \quad (6.38)$$

For the intermediate case of  $C_m$  equal to the right-hand member of equation (6.29), the two roots of the characteristic equation are equal, and the mode can be shown to be given by equation (6.30) with the function  $\sinh \gamma_m \eta$  replaced by  $\eta$ .

For a homogeneous liquid for which  $\beta = 0$ , equation (6.33) yields

$$\gamma_m = \lambda_m \frac{H}{R} \quad (6.39)$$

which when substituted into equation (6.32), yields the well-established expression for the frequency coefficient (see, for example, [65])

$$C_m = \sqrt{\tanh \left( \frac{\lambda_m H}{R} \right)} \quad (6.40)$$

The associated mode of vibration is determined from equation (6.30) to be

$$\hat{D}_m(\eta) = E_m \sinh \left( \lambda_m \frac{H}{R} \eta \right) \quad (6.41)$$

The corresponding solutions from equations (6.35), (6.38) and (6.36) are trivial and are not considered.

### Orthogonality of Modes

The modal displacements defined by equations (6.30) and (6.36) satisfy the orthogonality relation

$$\int_0^1 [\beta + \delta(\eta - 1)] \rho(\eta) \hat{D}_{mr}(\eta) \hat{D}_{ms}(\eta) d\eta = 0 \quad \text{for } r \neq s \quad (6.42)$$

in which the term involving the delta function,  $\delta(\eta - 1)$ , accounts for the discontinuity in the liquid density value at the free-surface. The derivation of this equation follows well-established steps. Specifically, equation (6.25) for  $\hat{D}_{mr}(\eta)$  is multiplied through by  $\rho(\eta) \hat{D}_{ms}(\eta)$  and integrated from 0 to 1; the term involving the second derivative of  $\hat{D}_{mr}(\eta)$  in the resulting expression is integrated by parts; and use is made of the boundary condition defined by equation (6.28) to obtain

$$\begin{aligned} & \left[ \frac{\beta}{C_{mr}^2} - \frac{\lambda_m H}{R} \right] \int_0^1 \rho(\eta) \hat{D}_{mr}(\eta) \hat{D}_{ms}(\eta) d\eta = \\ & \frac{1}{C_{ms}^2} \rho_1 \hat{D}_{mr}(1) \hat{D}_{ms}(1) + \int_0^1 \frac{\rho(\eta)}{\lambda_m H/R} \frac{\partial \hat{D}_{mr}}{\partial \eta} \frac{\partial \hat{D}_{ms}}{\partial \eta} d\eta \end{aligned} \quad (6.43)$$

These steps are repeated by starting with the  $\hat{D}_{ms}(\eta)$  mode and multiplying through by  $\rho(\eta)\hat{D}_{mr}(\eta)$ . The resulting expression is then subtracted from equation (6.43) to obtain equation (6.42).

Equation (6.42) may also be deduced from the corresponding expression for the N-layered, discrete system examined in Chapter 3. The latter expression is

$$\{\hat{D}_{mr}\}^T [\mathcal{B}] \{\hat{D}_{ms}\} = 0 \quad (6.44)$$

where  $\{\hat{D}_{mr}\}$  and  $\{\hat{D}_{ms}\}$  are vectors of size  $N$  that define the amplitudes of the interfacial displacements; and  $[\mathcal{B}]$  is a matrix of size  $N \times N$  expressing the values of the density discontinuities at the interfaces. To obtain equation (6.42), one must : (1) replace the elements of the first  $(N - 1)$  rows of  $[\mathcal{B}]$  by  $(-\partial\rho/\partial\eta)d\eta$ , (2) replace the elements of the  $N$ th row by the density discontinuity at the top,  $\delta(\eta - 1)\rho(\eta)d\eta$ , and (3) express the inner products of the modal displacement vectors as an integral from 0 to 1 of the modal displacement functions.

## 6.5 Forced Vibration

With the natural frequencies and modes of vibration of the system established, its response to an arbitrary lateral excitation may be determined by modal superposition. In this approach, the modal displacements,  $D_m(\eta, t)$ , are expressed in the form

$$D_m(\eta, t) = \sum_{n=1}^{\infty} \hat{D}_{mn}(\eta) q_{mn}(t) \quad (6.45)$$

where  $q_{mn}(t)$  is a generalized time-dependent coordinate corresponding to the  $m$ th horizontal and  $n$ th vertical mode of vibration. Substituting equation (6.45) into equation (6.24), multiplying through by  $[\beta + \delta(\eta - 1)]\rho(\eta)\hat{D}_{mn}(\eta)$ , and making use of the orthogonality of the natural modes defined by equation (6.42), one finds that  $q_{mn}$  is governed by the differential equation

$$\ddot{q}_{mn}(t) + \omega_{mn}^2 q_{mn}(t) = -\epsilon_m \omega_{mn}^2 \Gamma_{mn} R \frac{\ddot{x}_g(t)}{g} \quad (6.46)$$

in which  $\Gamma_{mn}$  is a dimensionless factor given by

$$\Gamma_{mn} = \frac{\int_0^1 [\beta + \delta(\eta - 1)] \rho(\eta) \hat{D}_{mn}(\eta) d\eta}{\int_0^1 [\beta + \delta(\eta - 1)] \rho(\eta) \hat{D}_{mn}^2(\eta) d\eta} \quad (6.47)$$

The solution of equation (6.46) is given by

$$q_{mn}(t) = -\epsilon_m \Gamma_{mn} R \frac{A_{mn}(t)}{g} \quad (6.48)$$

where  $A_{mn}(t)$  represents the instantaneous pseudoacceleration of an undamped single-degree-of-freedom oscillator with a circular natural frequency  $\omega_{mn}$  subjected to the prescribed ground acceleration, and is given by

$$A_{mn}(t) = \omega_{mn} \int_0^t \ddot{x}_g(\tau) \sin[\omega_{mn}(t - \tau)] d\tau \quad (6.49)$$

The maximum value of  $A_{mn}(t)$  is the quantity displayed on a pseudoacceleration response spectrum. Substitution of equation (6.48) into equation (6.45) leads to

$$D_m(\eta, t) = -R \sum_{n=1}^{\infty} \delta_{mn}(\eta) \frac{A_{mn}(t)}{g} \quad (6.50)$$

where  $\delta_{mn}(\eta)$ , a dimensionless function corresponding to the  $m$ th horizontal and  $n$ th vertical mode of vibration, is given by

$$\delta_{mn}(\eta) = \epsilon_m \Gamma_{mn} \hat{D}_{mn}(\eta) \quad (6.51)$$

The latter function is the counterpart of the vector of displacement coefficients  $\{d_{mn}\}$  in the analysis of the layered system.

### 6.5.1 Vertical Sloshing Displacements

On substituting equation (6.50) into equation (6.18), the vertical displacement of the liquid at any point and time,  $d(\xi, \eta, \theta, t)$ , is found to be

$$d(\xi, \eta, \theta, t) = -R \sum_{m=1}^{\infty} \sum_{n=1}^{\infty} \delta_{mn}(\eta) \frac{J_1(\lambda_m \xi)}{J_1(\lambda_m)} \frac{A_{mn}(t)}{g} \cos\theta \quad (6.52)$$

As is true of the coefficients in the corresponding expressions for layered systems, the coefficients  $\delta_{mn}$  can be shown to satisfy the relations

$$\sum_{n=1}^{\infty} \delta_{mn}(\eta) = \epsilon_m \quad (6.53)$$

and

$$\sum_{m=1}^{\infty} \sum_{n=1}^{\infty} \delta_{mn}(\eta) = 1 \quad (6.54)$$

For a homogeneous liquid with  $\beta = 0$ , for which there is only one vertical mode of vibration for each horizontal mode, the quantities  $\hat{D}_{mn}(\eta)$ ,  $\Gamma_{mn}$ ,  $\delta_{mn}(\eta)$  and  $A_{mn}(t)$  are denoted by  $\hat{D}_m(\eta)$ ,  $\Gamma_m$ ,  $\delta_m(\eta)$  and  $A_m(t)$ , respectively. The free-surface value of  $\delta_m$  is then evaluated from equations (6.47) and (6.51) to be  $\delta_m(1) = \epsilon_m$ , and equation (6.52) reduces, as it should, to (see, for example, [65])

$$d(\xi, 1, \theta, t) = -R \sum_{m=1}^{\infty} \epsilon_m \frac{J_1(\lambda_m \xi)}{J_1(\lambda_m)} \frac{A_m(t)}{g} \cos \theta \quad (6.55)$$

### 6.5.2 Hydrodynamic Pressures

On substituting equation (6.19) into equation (6.10) and making use of equation (6.4), the hydrodynamic pressure may be expressed as

$$p(\xi, \eta, \theta, t) = \left\{ -\xi \ddot{x}_g(t) e^{-\beta \eta} - \frac{R}{H} \sum_{m=1}^{\infty} \frac{e^{-\beta \eta}}{\lambda_m^2} \frac{\partial \hat{D}_m(\eta, t)}{\partial \eta} \frac{J_1(\lambda_m \xi)}{J_1(\lambda_m)} \right\} \rho_o R \cos \theta \quad (6.56)$$

Furthermore, on substituting equation (6.50) into this expression, making use of the relation

$$\ddot{A}_{mn}(t) = \omega_{mn}^2 [\ddot{x}_g(t) - A_{mn}(t)] \quad (6.57)$$

which is obtained by substituting equation (6.48) into equation (6.46), and grouping terms with similar temporal variations, the hydrodynamic pressure can be expressed as the sum of two components : an impulsive component,  $p^i$ , given by

$$p^i(\xi, \eta, \theta, t) = - \left[ e^{-\beta \eta} \xi - \sum_{m=1}^{\infty} \sum_{n=1}^{\infty} c_{mn}(\eta) \frac{J_1(\lambda_m \xi)}{J_1(\lambda_m)} \right] \rho_o R \cos \theta \ddot{x}_g(t) \quad (6.58)$$

and a convective component,  $p^c$ , given by

$$p^c(\xi, \eta, \theta, t) = - \left[ \sum_{m=1}^{\infty} \sum_{n=1}^{\infty} c_{mn}(\eta) \frac{J_1(\lambda_m \xi)}{J_1(\lambda_m)} A_{mn}(t) \right] \rho_o R \cos \theta \quad (6.59)$$

in which

$$c_{mn}(\eta) = \frac{R}{H} \frac{e^{-\beta \eta}}{\lambda_m} C_{mn}^2 \frac{\partial \delta_{mn}(\eta)}{\partial \eta} \quad (6.60)$$

The impulsive component represents the effect of the portion of the liquid that may be considered to move as a rigid body in synchronism with the tank wall, while the convective component represents the effect of the liquid undergoing sloshing action. It should be observed that the pressures in equations (6.58) and (6.59) are expressed in terms of the base value of the liquid density,  $\rho_o$ , rather than the density value at the height being considered.

### Simplification for impulsive pressures

In the form presented in equation (6.58), the evaluation of the impulsive component of response requires the prior evaluation of the convective components. The impulsive component can also be evaluated independently of the convective by letting

$$e_m(\eta) = \sum_{n=1}^{\infty} C_{mn}^2 \delta_{mn}(\eta) \quad (6.61)$$

and rewriting equation (6.58) in the form of a single series as

$$p^i(\xi, \eta, \theta, t) = -e^{-\beta\eta} \left[ \xi - \frac{R}{H} \sum_{m=1}^{\infty} \frac{1}{\lambda_m} \frac{\partial e_m}{\partial \eta} \frac{J_1(\lambda_m \xi)}{J_1(\lambda_m)} \right] \rho_o R \cos \theta \ddot{x}_g(t) \quad (6.62)$$

It can be shown that the function  $e_m(\eta)$  may be determined without prior knowledge of the  $\delta_{mn}(\eta)$  functions from the differential equation

$$\frac{\partial^2 e_m}{\partial \eta^2} - \beta \frac{\partial e_m}{\partial \eta} - \left( \frac{\lambda_m H}{R} \right)^2 e_m = -\epsilon_m \beta \lambda_m \frac{H}{R} \quad (6.63)$$

subject to the boundary conditions

$$(e_m)_{\eta=0} = 0 \quad (6.64)$$

and

$$\left( \frac{\partial e_m}{\partial \eta} \right)_{\eta=1} = \epsilon_m \lambda_m \frac{H}{R} \quad (6.65)$$

Equation (6.63) is obtained by substituting equation (6.50) into equation (6.24), making use of the relation defined by equation (6.57), grouping the terms involving  $\ddot{x}_g(t)$ , and finally making use of equations (6.26) and (6.61). Equations (6.64) and (6.65) are derived by proceeding similarly with equations (6.22) and (6.23).

The solution of equation (6.63) is given by

$$e_m(\eta) = \frac{\epsilon_m}{\lambda_m H/R} \left[ b_1 e^{a_{m1} \eta} + b_2 e^{a_{m2} \eta} + \beta \right] \quad (6.66)$$

where

$$a_{m1,m2} = \frac{\beta}{2} \pm \sqrt{\frac{\beta^2}{4} + \left( \frac{\lambda_m H}{R} \right)^2} \quad (6.67)$$

$$b_1 = \frac{\beta a_{m2} e^{a_{m2}} + (\lambda_m H/R)^2}{a_{m1} e^{a_{m1}} - a_{m2} e^{a_{m2}}} \quad (6.68)$$

and

$$b_2 = -\frac{\beta a_{m1} e^{a_{m1}} + (\lambda_m H/R)^2}{a_{m1} e^{a_{m1}} - a_{m2} e^{a_{m2}}} \quad (6.69)$$

## Wall pressures

The impulsive and convective components of the hydrodynamic pressures induced against the tank-wall are determined from equations (6.62) and (6.59) by letting  $\xi = 1$ . The total wall pressure at an arbitrary height may be expressed in the form

$$p(1, \eta, \theta, t) = - \left[ c_o(\eta) \ddot{x}_g(t) + \sum_{m=1}^{\infty} \sum_{n=1}^{\infty} c_{mn}(\eta) A_{mn}(t) \right] \rho_o R \cos \theta \quad (6.70)$$

where the dimensionless function  $c_o(\eta)$  for the impulsive component of the pressure is determined from equation (6.62) to be

$$c_o(\eta) = e^{-\beta\eta} \left[ 1 - \frac{R}{H} \sum_{m=1}^{\infty} \frac{1}{\lambda_m} \frac{\partial e_m}{\partial \eta} \right] \quad (6.71)$$

and the corresponding functions for the convective components are determined from equation (6.60). From equations (6.60), (6.61) and (6.71), it now follows that

$$c_o(\eta) + \sum_{m=1}^{\infty} \sum_{n=1}^{\infty} c_{mn}(\eta) = e^{-\beta\eta} \quad (6.72)$$

For a homogeneous system ( $\beta = 0$ ), equation (6.66) yields

$$e_m(z) = \epsilon_m \frac{\sinh(\lambda_m z/R)}{\cosh(\lambda_m H/R)} \quad (6.73)$$

and equation (6.71) reduces, as it should, to the well-established expression (see, for example, [65])

$$c_o(z) = 1 - \sum_{m=1}^{\infty} \epsilon_m \frac{\cosh(\lambda_m z/R)}{\cosh(\lambda_m H/R)} \quad (6.74)$$

in which the  $m$ th term of the summation represents the coefficient  $c_m(z)$  for the convective component of the pressure.

### 6.5.3 Tank Forces

#### Base shear

The base shear or total hydrodynamic force exerted on the tank wall is obtained by integrating equation (6.70) over the tank-height. The result may be expressed in the form

$$Q_b(t) = m_o \ddot{x}_g(t) + \sum_{m=1}^{\infty} \sum_{n=1}^{\infty} m_{mn} A_{mn}(t) \quad (6.75)$$

where  $m_o$ , the impulsive component of the liquid mass, is given by

$$m_o = \left( \int_0^1 c_o(\eta) d\eta \right) \rho_o \pi R^2 H \quad (6.76)$$

and  $m_{mn}$ , the convective component associated with the  $m$ th horizontal and  $n$ th vertical sloshing mode of vibration, is given by

$$m_{mn} = \left( \int_0^1 c_{mn}(\eta) d\eta \right) \rho_o \pi R^2 H \quad (6.77)$$

From equations (6.76) and (6.77), and with the aid of equation (6.72), it can finally be shown that

$$m_o + \sum_{m=1}^{\infty} \sum_{n=1}^{\infty} m_{mn} = \left( \int_0^1 e^{-\beta\eta} d\eta \right) \rho_o \pi R^2 H = m_l \quad (6.78)$$

where  $m_l$  is the total mass of the contained liquid.

The integrals in equations (6.76) and (6.77) and those in the expressions for base moments presented in the following two sections can be evaluated readily. The resulting expressions are lengthy and are not presented, but comprehensive numerical solutions for both the base shear and base moment are given in later sections.

### Moment above base

The moment induced by the hydrodynamic wall pressure at a section of the tank immediately above its base may conveniently be expressed in the form

$$M(t) = m_o h_o \ddot{x}_g(t) + \sum_{m=1}^{\infty} \sum_{n=1}^{\infty} m_{mn} h_{mn} A_{mn}(t) \quad (6.79)$$

where the coefficient  $m_o h_o$  for the impulsive component is given by

$$m_o h_o = \left( \int_0^1 c_o(\eta) \eta d\eta \right) \rho_o \pi R^2 H^2 \quad (6.80)$$

and the coefficient  $m_{mn} h_{mn}$  for the convective component associated with the  $m$ th horizontal and  $n$ th vertical mode of vibration is evaluated from

$$m_{mn} h_{mn} = \left( \int_0^1 c_{mn}(\eta) \eta d\eta \right) \rho_o \pi R^2 H^2 \quad (6.81)$$

From the latter two expressions and from equation (6.72), it follows that

$$m_o h_o + \sum_{m=1}^{\infty} \sum_{n=1}^{\infty} m_{mn} h_{mn} = \left( \int_0^1 e^{-\beta\eta} \eta d\eta \right) \rho_o \pi R^2 H^2 = m_l h_l \quad (6.82)$$

where  $m_l h_l$  represents the moment above the tank base induced by an unit horizontal acceleration when the entire liquid is presumed to act as a rigid mass.



### Foundation moment

In addition to the moment defined by equation (6.79), the foundation moment,  $M'(t)$ , includes the effect of the hydrodynamic pressure exerted on the tank base. The latter effect is determined by appropriate integration of the base values of the hydrodynamic pressures defined by equation (6.58) or (6.62) and equation (6.59). The resulting expression may be written as

$$M'(t) = m_o h'_o \ddot{x}_g(t) + \sum_{m=1}^{\infty} \sum_{n=1}^{\infty} m_{mn} h'_{mn} A_{mn}(t) \quad (6.83)$$

where the coefficient  $m_o h'_o$  for the impulsive component of the moment is given by

$$m_o h'_o = m_o h_o + \left[ \frac{1}{4} - \frac{R}{H} \sum_{m=1}^{\infty} \frac{1}{\lambda_m^3} \left. \frac{\partial e_m}{\partial \eta} \right|_{\eta=0} \right] \rho_o \pi R^4 \quad (6.84)$$

and the coefficient  $m_{mn} h'_{mn}$  for the convective component associated with the  $m$ th horizontal and  $n$ th vertical mode of vibration is given by

$$m_{mn} h'_{mn} = m_{mn} h_{mn} + \left[ \frac{R}{H} \frac{C_{mn}^2}{\lambda_m^3} \left. \frac{\partial d_{mn}}{\partial \eta} \right|_{\eta=0} \right] \rho_o \pi R^4 \quad (6.85)$$

From equations (6.84) and (6.85), and with the aid of equations (6.61) and (6.82), it can further be shown that

$$m_o h'_o + \sum_{m=1}^{\infty} \sum_{n=1}^{\infty} m_{mn} h'_{mn} = m_l h_l + \frac{\rho_o \pi R^4}{4} = m_l h'_l \quad (6.86)$$

where  $m_l h'_l$  represents the foundation moment induced by a unit horizontal acceleration when the entire liquid is considered to act as a rigid mass. It should be kept in mind that the base pressure in this case increases linearly from zero at the center to  $\rho_o R \cos \theta$  at the junction of the base and wall.

## 6.6 Numerical Solutions

The numerical solutions presented in this section are for the free vibrational characteristics and for the response to horizontal base shaking of systems with different slenderness ratios,  $H/R$ , and different liquid density ratios,  $\rho_1/\rho_o$ .

### 6.6.1 Sloshing Frequencies and Modes

Mention has already been made of the fact that unlike a homogeneous liquid which for a prescribed horizontal mode of vibration has a single vertical mode, an inhomogeneous liquid has an infinite number of vertical modes, each with a distinct frequency.

Fig. 6.3 shows the variation with the density ratio  $\rho_1/\rho_o$  of the frequency coefficients  $C_{1n}$  for the fundamental horizontal and first three vertical modes of vibration of systems with  $H/R$  values in the range between 0.5 and 2. It is observed that the highest frequency coefficient  $C_{11}$  for the fundamental horizontal and vertical mode of vibration of the inhomogeneous system is smaller than that for the corresponding homogeneous system. However, the difference is quite small, especially for larger values of  $\rho_1/\rho_o$  and  $H/R$ . By contrast, the coefficients  $C_{1n}$  for  $n \geq 2$  are significantly smaller than those for  $n = 1$  and quite sensitive to variations in  $\rho_1/\rho_o$ . These trends may be explained by examining the modal displacement amplitudes,  $\hat{D}_{1n}(\eta)$ .

Fig. 6.4 shows the first three vertical modes of vibration corresponding to the fundamental horizontal mode for systems with  $H/R = 1$  and three values of  $\rho_1/\rho_o$  in the range between 0.1 and 1. Each mode is normalized such that its maximum amplitude is unity. It is observed that the  $n$ th vertical mode of vibration is associated with  $n - 1$  zero crossings. Since the vertical motion of the liquid is zero at these sections, the natural frequency of the system for this mode must equal that of a system with the same density distribution and a depth equal to the distance from the free surface to the uppermost level of zero amplitude. For  $n > 1$ , these effective depths are but small fractions of the total depth,  $H$ , and decrease with increasing  $\rho_1/\rho_o$ . The associated natural frequencies, which, based on equation (6.40) for a homogeneous liquid, are expected to be proportional to the effective liquid depth must, therefore, also be small and decrease with increasing  $\rho_1/\rho_o$ . For  $n = 1$ , on the other hand, the more rapid decays in the displacement amplitudes with depth are obtained for the smaller values of  $\rho_1/\rho_o$ . A decrease in  $\rho_1/\rho_o$  in this case is associated with a reduced effective depth for the system, and hence a reduced natural frequency. However, the differences are quite small, and for values of  $\rho_1/\rho_o$  in the range between 0.25 and 1, the fundamental natural frequencies of the inhomogeneous and homogeneous systems may be considered to be the same. These trends are representative of those obtained for the higher order horizontal modes of vibration (higher values of  $m$ ) as well.

Table 6.1 lists the values of  $\gamma_{mn}$  for the first two horizontal and first three vertical modes of vibration of systems with several combinations of  $H/R$  and  $\rho_1/\rho_o$ . For the

results marked with asterisks, the condition defined by equation (6.34) is not satisfied, and  $\gamma_{11}$  was evaluated from equation (6.35) rather than from equation (6.33). The frequency coefficients,  $C_{11}$ , and modes of vibration,  $\hat{D}_{11}(\eta)$ , for these cases must, therefore, be evaluated from equations (6.38) and (6.36) rather than from equations (6.32) and (6.30).

### 6.6.2 Sloshing Displacement Coefficients

Of special interest in practice is the sloshing motion of the liquid at its free surface, as the maximum surface displacement is needed to define the freeboard that must be provided to prevent the liquid from overflowing or impacting the roof. This displacement is obtained by letting  $\eta = 1$  in equation (6.52).

The displacement coefficients  $\delta_{1n}(1)$  for the fundamental horizontal and first three vertical modes of vibration are presented in Fig. 6.5. The results are plotted in a manner analogous to that employed in Fig. 6.3 as a function of the density ratio  $\rho_1/\rho_o$  for three values of  $H/R$  in the range from 0.5 to 2. These data along with corresponding data for additional systems and for the second horizontal mode of vibration are listed in Table 6.2. The following trends are worth noting :

1. The surface displacement coefficients are relatively insensitive to the value of  $H/R$  but increase substantially with decreasing  $\rho_1/\rho_o$ . The latter trend is consistent with that reported in Chapter 3 for layered systems, and is attributed to the fact that, the larger the variation in liquid density, the greater is the sloshing action induced.
2. The corresponding coefficients for the second horizontal mode of vibration,  $m = 2$ , are significantly smaller than those for the fundamental mode,  $m = 1$ , and the sum of the coefficients over  $n$  for each horizontal mode satisfies equation (6.53). Furthermore, when all the horizontal modes of vibration are considered, the algebraic sum of the coefficients, in agreement with equation (6.54), is unity.

It should be realized that the relative contributions of the various modes of vibration to the surface sloshing motion depend not only on the relative values of the displacement factors  $\delta_{mn}(1)$  but also on those of the corresponding pseudoaccelerations,  $A_{mn}(t)$ . The latter quantities depend, in turn, on the characteristics of the ground motion and the natural frequencies of the system itself.

### 6.6.3 Hydrodynamic Pressures

Shown in the left part of Fig. 6.6 are the heightwise variations of the function  $c_o(\eta)$  in equation (6.71) for the impulsive component of the hydrodynamic wall pressure. These plots are for a tank with  $H/R = 1$  and liquids with density ratios  $\rho_1/\rho_o$  in the range between 0.1 and 1. Also shown are the corresponding functions  $c_{11}(\eta)$  and  $c_{12}(\eta)$  for the fundamental horizontal and first two vertical sloshing modes. As would be expected (recall that the pressures are expressed in terms of the base value of the liquid density rather than that at the level being considered), the functions  $c_o(\eta)$  and  $c_{11}(\eta)$  decrease with decreasing  $\rho_1/\rho_o$ . Furthermore, consistent with the distributions of the modal displacement amplitudes displayed in Fig. 6.4, the function  $c_{1n}(\eta)$  for the  $n$ th vertical mode of vibration exhibits  $n - 1$  changes in sign.

The interrelationship of the hydrodynamic response for the inhomogeneous and homogeneous systems can be better appreciated by rewriting equation (6.70) for the wall pressure in the form

$$p(1, \eta, \theta, t) = - \left[ \bar{c}_o(\eta) \ddot{x}_g(t) + \sum_{m=1}^{\infty} \sum_{n=1}^{\infty} \bar{c}_{mn}(\eta) A_{mn}(t) \right] \rho_{av} R \cos \theta \quad (6.87)$$

where  $\rho_{av}$  represents the average value of the liquid density, given by

$$\rho_{av} = \frac{\rho_o (1 - e^{-\beta})}{\beta} \quad (6.88)$$

and the functions  $\bar{c}_o(\eta)$  and  $\bar{c}_{mn}(\eta)$  are related to the functions  $c_o(\eta)$  and  $c_{mn}(\eta)$  in equation (6.70) by

$$\bar{c}_o(\eta) = \frac{\rho_o}{\rho_{av}} c_o(\eta) \quad \text{and} \quad \bar{c}_{mn}(\eta) = \frac{\rho_o}{\rho_{av}} c_{mn}(\eta) \quad (6.89)$$

The variations of  $\bar{c}_o(\eta)$  and  $\bar{c}_{11}(\eta)$  are displayed in Fig. 6.7 for the values of  $\rho_1/\rho_o$  and  $H/R$  considered previously in Fig. 6.6. It is observed that these functions are still sensitive to variations in liquid density, but that for values of  $\rho_1/\rho_o$  in the range between 0.25 to 1, the areas under the individual curves are close to each other. It follows that, despite the indicated differences in the pressures themselves, the total hydrodynamic wall force or base shear for the inhomogeneous and homogeneous liquids can be interrelated simply. This matter is considered further in the following section.

#### 6.6.4 Hydrodynamic Tank Forces

Fig. 6.8 shows the variations with  $\rho_1/\rho_o$  and  $H/R$  of the impulsive and fundamental convective masses,  $m_o$  and  $m_{11}$ , in the expression for the hydrodynamic base shear. These masses are normalized with respect to the total liquid mass,  $m_l$ . Normalized values of the corresponding base moment coefficients,  $m_o h_o$  and  $m_{11} h_{11}$ , and of the foundation moment coefficients,  $m_o h'_o$  and  $m_{11} h'_{11}$ , are plotted in Figs. 6.9 and 6.10, respectively. It should be reemphasized that these three sets of normalized quantities express the hydrodynamic base shear and base moments as fractions of those computed on the assumption that the entire liquid acts as a rigid mass. The normalizing quantities are naturally different for tanks of different proportions and contents. The normalized values of  $m_o$  and  $m_{11}$  for additional systems, along with the corresponding values of  $m_{12}$ ,  $m_{21}$  and  $m_{22}$ , are presented in Table 6.3, and the normalized values of the base and foundation moment coefficients are presented in Tables 6.4 and 6.5.

Examination of the data presented in these figures and tables reveals the following trends :

1. For values of  $\rho_1/\rho_o$  in the range between 1 and about 0.25, the normalized values of  $m_o$  and  $m_{m1}$  may, for all practical purposes, be considered to be the same. This result, which is consistent with the prediction made from the pressure profiles displayed in Fig. 6.7, is generally valid over the entire range of  $H/R$  examined. Incidentally, the seismic response of systems normally encountered in practice is dominated by  $m_o$  and, to a lesser degree, by  $m_{11}$  and  $m_{21}$ . On recalling that within the range of  $\rho_1/\rho_o$  considered, the sloshing frequencies,  $\omega_{m1}$ , and the spectral values of the associated pseudoaccelerations,  $A_{m1}(t)$ , also are insensitive to variations in the density ratio, it is concluded that, when normalized with respect to the value computed on the assumption that the entire liquid in the tank acts as a rigid mass, the total hydrodynamic wall force or base shear for an inhomogeneous liquid is practically equal to that for a homogeneous liquid. The same is also true of the moment induced above the tank base. These two effects may, therefore, be evaluated from well-established procedures for homogeneous liquids. This approximation, however, is not adequate for the foundation moment, particularly for tanks with low values of  $H/R$  and  $\rho_1/\rho_o$ . The latter moment is dominated by the hydrodynamic pressures exerted on the tank base, and, as already demonstrated, these pressures may be substantially different for inhomogeneous and homogeneous systems.

2. For values of  $\rho_1/\rho_o$  less than about 0.25, the fraction of the liquid that acts impulsively is generally smaller for the inhomogeneous system than the homogeneous system. The large density gradients in this case increase the proportions of the liquid participating in the convective or sloshing actions. This increase, however, does not necessarily increase the convective force coefficients associated with the fundamental sloshing mode of vibration. For a given horizontal mode of vibration and a prescribed response, it is the sum of the coefficients for all the vertical modes that generally increases.

## 6.7 Approximation of Continuous Systems with Layered Systems

It is instructive to compare equation (6.19) for the continuous system with the corresponding expression for the discrete, layered system examined in Chapter 3. The potential function  $\psi_j$  for the  $j$ th layer of the latter system is given by

$$\psi_j = - \sum_{m=1}^{\infty} \frac{R}{\lambda_m} \left[ \frac{\dot{D}_{m,j} \cosh \lambda_m \eta_j - \dot{D}_{m,j-1} \cosh \lambda_m (\alpha_j - \eta_j)}{\sinh \lambda_m \alpha_j} \right] \frac{J_1(\lambda_m \xi)}{J_1(\lambda_m)} \cos \theta \quad (6.90)$$

where  $\alpha_j = H_j/R$  and  $\eta_j = z_j/R$ . Note that unlike the distance coordinate  $\eta$  employed in the analysis of the continuous system, which is normalized with respect to the liquid depth,  $H$ , the coordinate  $\eta_j$  is normalized with respect to the tank radius,  $R$ . Note further that as the layer-height,  $H_j = \Delta z$ , is decreased,  $\alpha_j = \Delta z/R$  tends to zero, the  $\cosh$  functions in equation (6.90) tend to unity, the  $\sinh$  function tends to  $\lambda_m \Delta z/R = \lambda_m (H/R) \Delta \eta$ , and equation (6.90) becomes the finite-difference counterpart of equation (6.19). It can similarly be shown that the equations of motion for the layered system (equation 28 of Chapter 3) are merely the finite-difference counterparts of equation (6.20). It follows that, contrary to the view expressed in [10], the representation of the continuous system as a multi-layered system is indeed a valid approximation. Additional relevant information on this subject may be found in [6] and [84].

### 6.7.1 Numerical Comparisons

The ability of the multi-layered systems considered in Chapters 3 and 4 to closely approximate the response of systems with continuous variations in liquid density is demonstrated in this section for a system with  $H/R = 1$  for which the density variation

is defined by equation (6.1). For the solutions presented herein,  $\beta$  is taken as 1.386 so that  $\rho_1/\rho_o$  is 0.25. For the discretized solutions, the liquid is approximated by  $N$  uniform layers of equal thicknesses and density values equal to those determined from the continuous distribution at mid-heights of the substitute layers. The convergence of the natural frequencies of sloshing motion for the system examined herein is studied in Table 6.6. The values of  $C_{11}$  through  $C_{23}$  for the continuous density variation are compared with those obtained for several discrete representations using values of  $N$  in the range between 5 and 50. It is clear that the results for the discrete representations converge quite rapidly to those for the continuous, and that good approximations are obtained with as few as 10, or even fewer, layers.

The convergence of the corresponding modes of vibration would not be expected to be as rapid but, as indicated in Fig. 6.11, good approximations are again obtained with only 10 layers. Defined by the maximum vertical displacements of the liquid at the layer interfaces, the indicated modes are for  $m = 1$  and  $n = 1, 2$  and 3. The displacements of points within a layer may be determined from the interfacial values either by interpolation or, more precisely, from the expression governing the response of the layer under consideration.

Comparisons similar to those presented in Table 6.6 are made in Table 6.7 for the coefficients  $d_{11}$  through  $d_{23}$  in the expression for the surface sloshing displacements of the liquid induced by horizontal base shaking (equation (3.54) of Chapter 3). The convergence rates for these results are again quite rapid.

Fig. 6.12 shows the heightwise variations of the impulsive component of wall pressure and of the convective components associated with the fundamental horizontal and first three vertical modes of vibration. The dashed lines represent the exact solutions for the continuous density variation, whereas the solid lines represent the solutions for the approximating layered systems with  $N = 10$  and  $N = 50$ . The results for both the layered and continuous systems are expressed in terms of the base value of the liquid density,  $\rho_o$ . It is seen that the impulsive pressures for the layered system with  $N = 10$  are practically indistinguishable from those of the continuous system. By contrast, the convective pressures of the layered system converge less rapidly, and a much larger number of layers is required to achieve comparable accuracy.

It is worth noting that both the natural frequencies and the modes of vibration of the discrete systems converge to those of the continuous system more rapidly than do the corresponding convective pressures. Two factors are responsible for the improved convergence : (1) Unlike the convective wall pressures that are discontinuous at the

interfaces, the modal displacements are continuous; and (2) the natural frequencies are relatively insensitive to inaccuracies in the corresponding modes of vibration.

Table 6.8 gives the normalized values of the impulsive and of the first six convective masses computed for layered systems with values of  $N$  ranging from 5 to 50. Also listed are the corresponding exact solutions for the continuous variation in density. Tables 6.9 and 6.10 give the corresponding moment coefficients for sections above and below the tank base, respectively. It can be seen that the solutions for the discrete systems do converge to those of the continuous system; that the rates of convergence of the results are quite rapid; and that good agreement is obtained with as few as ten uniform layers.

## 6.8 Conclusions

With the information presented herein, the free vibrational characteristics and the response to horizontal base shaking of rigid cylindrical tanks containing liquids of a density that decays exponentially with depth may be evaluated readily. The comprehensive numerical solutions that have been presented provide valuable insights into the underlying response mechanisms and into the effects and relative importance of the numerous parameters involved. The principal conclusions may be summarized as follows :

1. Unlike a homogeneous liquid, which for a given horizontal natural mode of vibration has a single vertical mode, the inhomogeneous liquid examined has an infinite number of such modes, each associated with a distinct frequency. The latter frequencies are smaller than the corresponding frequency of the homogeneous liquid.
2. For any horizontal mode of vibration, the  $n$ th vertical mode of the inhomogeneous liquid has  $n - 1$  zero crossings and its frequency decreases with increasing values of  $n$ .
3. For a specified horizontal mode of vibration, any two vertical modes satisfy the orthogonality relation defined by equation (6.42).
4. When normalized with respect to the pressures computed on the assumption that the entire liquid acts as a rigid mass, the coefficients in the expression for the impulsive and all convective components of the hydrodynamic wall pressures add up to unity. The same is also true of the corresponding coefficients for base shear and base moments in the tank.



5. The impulsive component of response may be obtained either by evaluating all the convective components and subtracting their sum from the response computed on the assumption that the entire liquid acts as a rigid mass, or, independently, without the prior evaluation of the convective effects.
6. When normalized with respect to the result computed on the assumption that the entire liquid in the tank acts as a rigid mass, the total hydrodynamic wall force or base shear for an inhomogeneous liquid with values of  $\rho_1/\rho_o$  in the range between 1 and 0.25 may be considered to be equal to that for a homogeneous liquid. The same is also true of the moment induced above the tank base. These two effects may, therefore, be evaluated from well-established procedures for homogeneous liquids. This approximation, however, may not be adequate for the foundation moment, particularly for broad tanks with high gradients in liquid density.
7. The finite-difference representations of the equations for the response of the continuous system examined here reduce to the same as the expressions for the response of the layered, discrete system studied in Chapters 3 and 4. The solutions for the latter systems may hence be used to accurately evaluate the responses of systems with arbitrary and continuous variations in liquid density.

**Table 6.1:** Values of  $\gamma_{mn}$  for systems with different  $H/R$  and  $\rho_1/\rho_o$ 

$\rho_1/\rho_o$	Values of $\gamma_{mn}$					
	$m = 1$			$m = 2$		
	$n = 1$	$n = 2$	$n = 3$	$n = 1$	$n = 2$	$n = 3$
$H/R = 0.5$						
1	0.9206			2.6657		
0.75	0.7025	3.2241	6.3277	2.5200	3.1947	6.3218
0.5	0.1668	3.3343	6.3894	2.3132	3.2691	6.3757
0.25	0.8285*	3.5080	6.4918	1.9514	3.3953	6.4662
0.1	1.2237*	3.7127	6.6212	1.4393	3.5596	6.5825
$H/R = 0.75$						
1	1.3809			3.9986		
0.75	1.2123	3.2171	6.3266	3.8547	3.1766	6.3157
0.5	0.9475	3.3194	6.3868	3.6520	3.2265	6.3613
0.25	0.1657	3.4837	6.4870	3.3038	3.3133	6.4386
0.1	0.9723*	3.6818	6.6141	2.8423	3.4320	6.5396
$H/R = 1$						
1	1.8412			5.3314		
0.75	1.6880	3.2090	6.3251	5.1876	3.1653	6.3098
0.5	1.4631	3.3017	6.3834	4.9849	3.1991	6.3472
0.25	1.0314	3.4537	6.4806	4.6383	3.2582	6.4112
0.1	0.3663*	3.6422	6.6045	4.1802	3.3400	6.4958
$H/R = 1.5$						
1	2.7618			7.9972		
0.75	2.6164	3.1931	6.3214	7.8533	3.1539	6.3007
0.5	2.4105	3.2655	6.3747	7.6506	3.1713	6.3254
0.25	2.0512	3.3886	6.4643	7.3040	3.2017	6.3678
0.1	1.5484	3.5497	6.5796	6.8459	3.2433	6.4246
$H/R = 2$						
1	3.6824			10.6629		
0.75	3.5385	3.1803	6.3172	10.5190	3.1489	6.2950
0.5	3.3358	3.2351	6.3648	10.3163	3.1593	6.3117
0.25	2.9861	3.3303	6.4453	9.9697	3.1773	6.3404
0.1	2.5208	3.4595	6.5502	9.5116	3.2016	6.3789

\*  $\gamma_{11}$  evaluated from equation (6.35) instead of equation (6.33).

**Table 6.2: Surface displacement coefficients for systems with different  $H/R$  and  $\rho_1/\rho_0$**

$\rho_1/\rho_0$	Values of $\delta_{mn}(1)$					
	$m = 1$			$m = 2$		
	$n = 1$	$n = 2$	$n = 3$	$n = 1$	$n = 2$	$n = 3$
$H/R = 0.5$						
1	0.8368			0.0729		
0.75	0.8790	-0.0514	0.0132	0.0762	-0.0038	0.0009
0.5	0.9451	-0.1345	0.0380	0.0814	-0.0101	0.0026
0.25	1.0787	-0.3113	0.1014	0.0925	-0.0242	0.0074
0.1	1.3039	-0.6319	0.2440	0.1121	-0.0509	0.0186
$H/R = 0.75$						
1	0.8368			0.0729		
0.75	0.8788	-0.0505	0.0126	0.0755	-0.0028	0.0007
0.5	0.9449	-0.1327	0.0365	0.0797	-0.0077	0.0020
0.25	1.0791	-0.3085	0.0982	0.0887	-0.0189	0.0059
0.1	1.3065	-0.6289	0.2383	0.1053	-0.0413	0.0156
$H/R = 1$						
1	0.8368			0.0729		
0.75	0.8778	-0.0487	0.0119	0.0750	-0.0021	0.0005
0.5	0.9429	-0.1286	0.0345	0.0782	-0.0056	0.0015
0.25	1.0766	-0.3017	0.0940	0.0850	-0.0138	0.0046
0.1	1.3055	-0.6205	0.2306	0.0974	-0.0307	0.0126
$H/R = 1.5$						
1	0.8368			0.0729		
0.75	0.8737	-0.0426	0.0100	0.0743	-0.0011	0.0002
0.5	0.9332	-0.1140	0.0298	0.0764	-0.0031	0.0008
0.25	1.0589	-0.2734	0.0835	0.0805	-0.0076	0.0027
0.1	1.2825	-0.5784	0.2107	0.0875	-0.0167	0.0080
$H/R = 2$						
1	0.8368			0.0729		
0.75	0.8684	-0.0351	0.0081	0.0739	-0.0007	0.0001
0.5	0.9195	-0.0949	0.0247	0.0755	-0.0019	0.0004
0.25	1.0290	-0.2316	0.0718	0.0784	-0.0046	0.0016
0.1	1.2301	-0.5035	0.1872	0.0830	-0.0101	0.0052

**Table 6.3:** Normalized values of effective masses in expression for base shear of systems with different  $H/R$  and  $\rho_1/\rho_0$

$\frac{\rho_1}{\rho_0}$	$\frac{m_0}{m_\ell}$	$\frac{m_{11}}{m_\ell}$	$\frac{m_{12}}{m_\ell}$	$\frac{m_{21}}{m_\ell}$	$\frac{m_{22}}{m_\ell}$
$H/R = 0.5$					
1	0.2999	0.6601		0.0271	
0.75	0.2926	0.6665	0.0015	0.0268	0.0001
0.5	0.2804	0.6713	0.0085	0.0265	0.0008
0.25	0.2559	0.6672	0.0320	0.0261	0.0030
0.1	0.2211	0.6396	0.0785	0.0256	0.0072
$H/R = 0.75$					
1	0.4391	0.5340		0.0182	
0.75	0.4320	0.5407	0.0016	0.0175	0.0001
0.5	0.4181	0.5476	0.0089	0.0165	0.0007
0.25	0.3866	0.5516	0.0331	0.0150	0.0027
0.1	0.3374	0.5405	0.0801	0.0135	0.0066
$H/R = 1$					
1	0.5475	0.4322		0.0137	
0.75	0.5435	0.4358	0.0016	0.0128	0.0001
0.5	0.5323	0.4401	0.0092	0.0117	0.0006
0.25	0.5009	0.4442	0.0341	0.0099	0.0021
0.1	0.4453	0.4408	0.0817	0.0080	0.0054
$H/R = 1.5$					
1	0.6858	0.3006		0.0091	
0.75	0.6887	0.2972	0.0016	0.0083	0.0001
0.5	0.6862	0.2927	0.0092	0.0072	0.0003
0.25	0.6656	0.2866	0.0344	0.0056	0.0013
0.1	0.6145	0.2802	0.0826	0.0039	0.0033
$H/R = 2$					
1	0.7627	0.2270		0.0068	
0.75	0.7698	0.2193	0.0015	0.0062	0.0000
0.5	0.7736	0.2092	0.0085	0.0052	0.0002
0.25	0.7640	0.1940	0.0320	0.0039	0.0008
0.1	0.7249	0.1789	0.0782	0.0025	0.0021

**Table 6.4: Normalized values of coefficients in expression for overturning moment at a section immediately above tank base of systems with different  $H/R$  and  $\rho_1/\rho_0$**

$\frac{\rho_1}{\rho_0}$	$\frac{m_0 h_0}{m_\ell h_\ell}$	$\frac{m_{11} h_{11}}{m_\ell h_\ell}$	$\frac{m_{12} h_{12}}{m_\ell h_\ell}$	$\frac{m_{21} h_{21}}{m_\ell h_\ell}$	$\frac{m_{22} h_{22}}{m_\ell h_\ell}$
$H/R = 0.5$					
1	0.2394	0.7031		0.0365	
0.75	0.2398	0.7244	-0.0190	0.0369	-0.0014
0.5	0.2388	0.7534	-0.0431	0.0376	-0.0030
0.25	0.2332	0.7980	-0.0753	0.0389	-0.0050
0.1	0.2200	0.8417	-0.0958	0.0410	-0.0057
$H/R = 0.75$					
1	0.3520	0.6053		0.0277	
0.75	0.3550	0.6236	-0.0185	0.0274	-0.0010
0.5	0.3566	0.6495	-0.0418	0.0270	-0.0022
0.25	0.3524	0.6919	-0.0722	0.0264	-0.0034
0.1	0.3357	0.7384	-0.0902	0.0258	-0.0032
$H/R = 1$					
1	0.4425	0.5235		0.0223	
0.75	0.4495	0.5368	-0.0177	0.0217	-0.0007
0.5	0.4559	0.5565	-0.0397	0.0208	-0.0015
0.25	0.4574	0.5908	-0.0677	0.0193	-0.0022
0.1	0.4429	0.6326	-0.0826	0.0175	-0.0016
$H/R = 1.5$					
1	0.5664	0.4094		0.0160	
0.75	0.5800	0.4134	-0.0152	0.0152	-0.0004
0.5	0.5954	0.4199	-0.0337	0.0141	-0.0008
0.25	0.6111	0.4333	-0.0556	0.0123	-0.0011
0.1	0.6101	0.4540	-0.0632	0.0100	-0.0004
$H/R = 2$					
1	0.6445	0.3367		0.0124	
0.75	0.6609	0.3346	-0.0124	0.0117	-0.0002
0.5	0.6811	0.3321	-0.0270	0.0107	-0.0005
0.25	0.7061	0.3294	-0.0428	0.0090	-0.0006
0.1	0.7181	0.3291	-0.0432	0.0069	-0.0001

**Table 6.5: Normalized values of coefficients in expression for foundation moment of systems with different  $H/R$  and  $\rho_1/\rho_o$**

$\frac{\rho_1}{\rho_o}$	$\frac{m_o h'_o}{m_\ell h'_\ell}$	$\frac{m_{11} h'_{11}}{m_\ell h'_\ell}$	$\frac{m_{12} h'_{12}}{m_\ell h'_\ell}$	$\frac{m_{21} h'_{21}}{m_\ell h'_\ell}$	$\frac{m_{22} h'_{22}}{m_\ell h'_\ell}$
$H/R = 0.5$					
1	0.2927	0.6869		0.0131	
0.75	0.2632	0.6616	0.0316	0.0118	-0.0001
0.5	0.2241	0.6212	0.0745	0.0101	0.0000
0.25	0.1668	0.5454	0.1381	0.0079	0.0005
0.1	0.1113	0.4470	0.1967	0.0058	0.0013
$H/R = 0.75$					
1	0.4369	0.5402		0.0148	
0.75	0.4120	0.5319	0.0178	0.0134	-0.0003
0.5	0.3729	0.5150	0.0468	0.0115	-0.0005
0.25	0.3028	0.4748	0.0994	0.0087	-0.0002
0.1	0.2195	0.4096	0.1595	0.0060	0.0006
$H/R = 1$					
1	0.5263	0.4508		0.0149	
0.75	0.5129	0.4465	0.0077	0.0135	-0.0004
0.5	0.4858	0.4373	0.0247	0.0117	-0.0006
0.25	0.4241	0.4133	0.0646	0.0089	-0.0005
0.1	0.3324	0.3695	0.1218	0.0060	0.0003
$H/R = 1.5$					
1	0.6226	0.3575		0.0131	
0.75	0.6266	0.3519	-0.0028	0.0120	-0.0003
0.5	0.6237	0.3428	-0.0006	0.0105	-0.0005
0.25	0.5960	0.3246	0.0184	0.0081	-0.0005
0.1	0.5246	0.2958	0.0629	0.0053	0.0001
$H/R = 2$					
1	0.6785	0.3048		0.0110	
0.75	0.6902	0.2972	-0.0061	0.0101	-0.0002
0.5	0.7003	0.2858	-0.0097	0.0089	-0.0004
0.25	0.6979	0.2652	-0.0023	0.0069	-0.0004
0.1	0.6571	0.2369	0.0301	0.0046	0.0001

**Table 6.6: Values of frequency coefficients  $C_{mn}$  for layered and continuous systems with  $H/R = 1$  and  $\rho_1/\rho_o = 0.25$**

$N$	$C_{11}$	$C_{12}$	$C_{13}$	$C_{21}$	$C_{22}$	$C_{23}$
5	0.9549	0.4136	0.2556	0.9999	0.4595	0.3631
10	0.9539	0.4049	0.2407	0.9999	0.4394	0.3345
20	0.9537	0.4027	0.2371	0.9999	0.4342	0.3273
30	0.9536	0.4023	0.2364	0.9999	0.4332	0.3260
50	0.9536	0.4021	0.2361	0.9999	0.4327	0.3253
Cont. System	0.9536	0.4019	0.2359	0.9999	0.4325	0.3249

**Table 6.7: Values of surface displacement coefficients  $d_{mn}$  for layered and continuous systems with  $H/R = 1$  and  $\rho_1/\rho_o = 0.25$**

$N$	$d_{11}$	$d_{12}$	$d_{13}$	$d_{21}$	$d_{22}$	$d_{23}$
5	1.0634	-0.2767	0.0681	0.0831	-0.0118	0.0029
10	1.0732	-0.2954	0.0872	0.0845	-0.0133	0.0041
20	1.0757	-0.3001	0.0923	0.0849	-0.0137	0.0044
30	1.0762	-0.3010	0.0933	0.0850	-0.0138	0.0045
50	1.0764	-0.3014	0.0938	0.0850	-0.0138	0.0045
Cont. System	1.0766	-0.3017	0.0940	0.0850	-0.0138	0.0046

**Table 6.8: Normalized values of effective masses in expression for base shear of a continuous system with  $H/R = 1$ ,  $\rho_1/\rho_o = 0.25$  and its N-layered approximation**

$N$	$\frac{m_o}{m_\ell}$	$\frac{m_{11}}{m_\ell}$	$\frac{m_{12}}{m_\ell}$	$\frac{m_{13}}{m_\ell}$	$\frac{m_{21}}{m_\ell}$	$\frac{m_{22}}{m_\ell}$	$\frac{m_{23}}{m_\ell}$
5	0.5022	0.4431	0.0338	0.0023	0.0099	0.0023	0.0001
10	0.5007	0.4439	0.0340	0.0026	0.0099	0.0022	0.0001
20	0.5004	0.4441	0.0341	0.0027	0.0099	0.0022	0.0001
30	0.5003	0.4442	0.0341	0.0027	0.0099	0.0022	0.0001
50	0.5003	0.4442	0.0341	0.0027	0.0099	0.0022	0.0001
Cont. System	0.5003	0.4442	0.0341	0.0027	0.0099	0.0021	0.0001

**Table 6.9: Normalized values of coefficients in expression for overturning moment at a section immediately above tank base for a continuous system with  $H/R = 1$ ,  $\rho_1/\rho_o = 0.25$  and its N-layered approximation**

$N$	$\frac{m_o h_o}{m_\ell h_\ell}$	$\frac{m_{11} h_{11}}{m_\ell h_\ell}$	$\frac{m_{12} h_{12}}{m_\ell h_\ell}$	$\frac{m_{13} h_{13}}{m_\ell h_\ell}$	$\frac{m_{21} h_{21}}{m_\ell h_\ell}$	$\frac{m_{22} h_{22}}{m_\ell h_\ell}$	$\frac{m_{23} h_{23}}{m_\ell h_\ell}$
5	0.4557	0.5861	-0.0645	-0.0023	0.0192	-0.0019	-0.0002
10	0.4565	0.5896	-0.0669	-0.0026	0.0193	-0.0021	-0.0002
20	0.4567	0.5905	-0.0675	-0.0026	0.0193	-0.0022	-0.0002
30	0.4567	0.5907	-0.0676	-0.0027	0.0193	-0.0022	-0.0002
50	0.4568	0.5908	-0.0676	-0.0027	0.0193	-0.0022	-0.0002
Cont. System	0.4568	0.5908	-0.0677	-0.0027	0.0193	-0.0022	-0.0002

**Table 6.10: Normalized values of coefficients in expression for foundation moment of a continuous system with  $H/R = 1$ ,  $\rho_1/\rho_o = 0.25$  and its N-layered approximation**

$N$	$\frac{m_o h'_o}{m_\ell h'_\ell}$	$\frac{m_{11} h'_{11}}{m_\ell h'_\ell}$	$\frac{m_{12} h'_{12}}{m_\ell h'_\ell}$	$\frac{m_{13} h'_{13}}{m_\ell h'_\ell}$	$\frac{m_{21} h'_{21}}{m_\ell h'_\ell}$	$\frac{m_{22} h'_{22}}{m_\ell h'_\ell}$	$\frac{m_{23} h'_{23}}{m_\ell h'_\ell}$
5	0.4541	0.4390	0.0619	0.0222	0.0095	-0.0005	0.0000
10	0.4391	0.4276	0.0651	0.0277	0.0092	-0.0005	0.0001
20	0.4313	0.4208	0.0653	0.0289	0.0090	-0.0005	0.0001
30	0.4287	0.4184	0.0652	0.0290	0.0090	-0.0005	0.0001
50	0.4266	0.4164	0.0650	0.0290	0.0090	-0.0005	0.0001
Cont. System	0.4234	0.4133	0.0646	0.0289	0.0089	-0.0005	0.0001



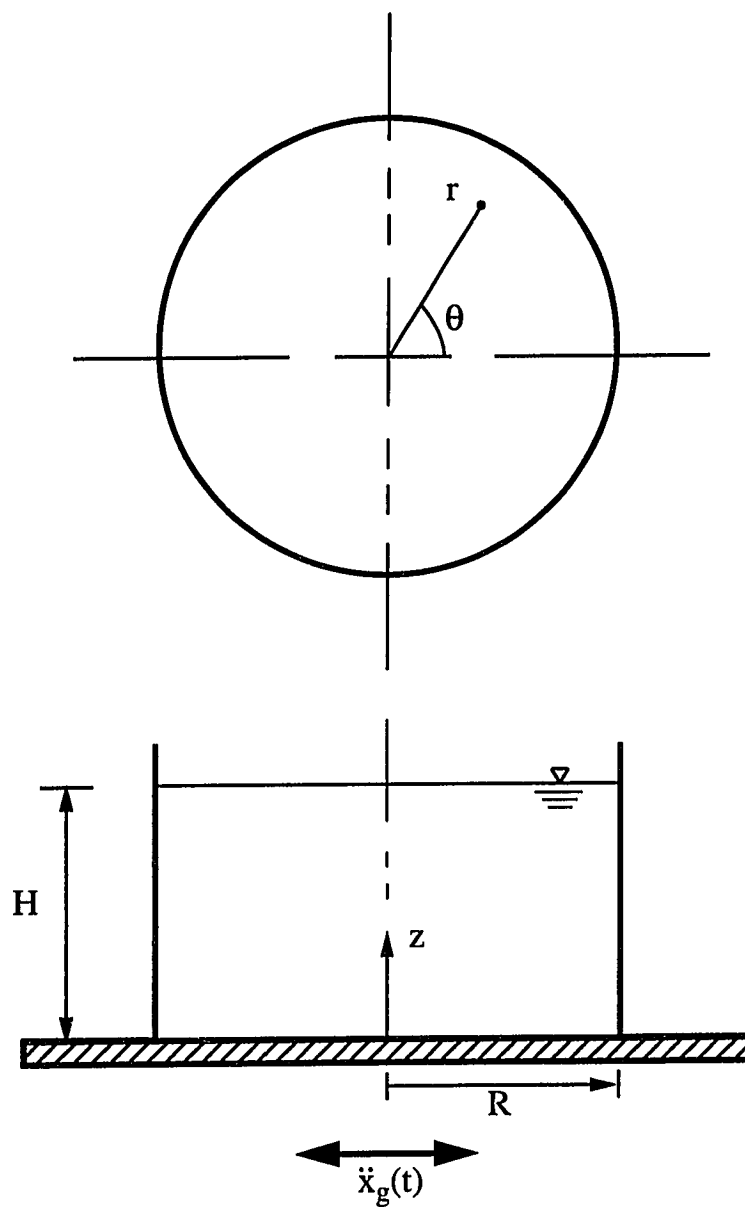


Figure 6.1 System Considered

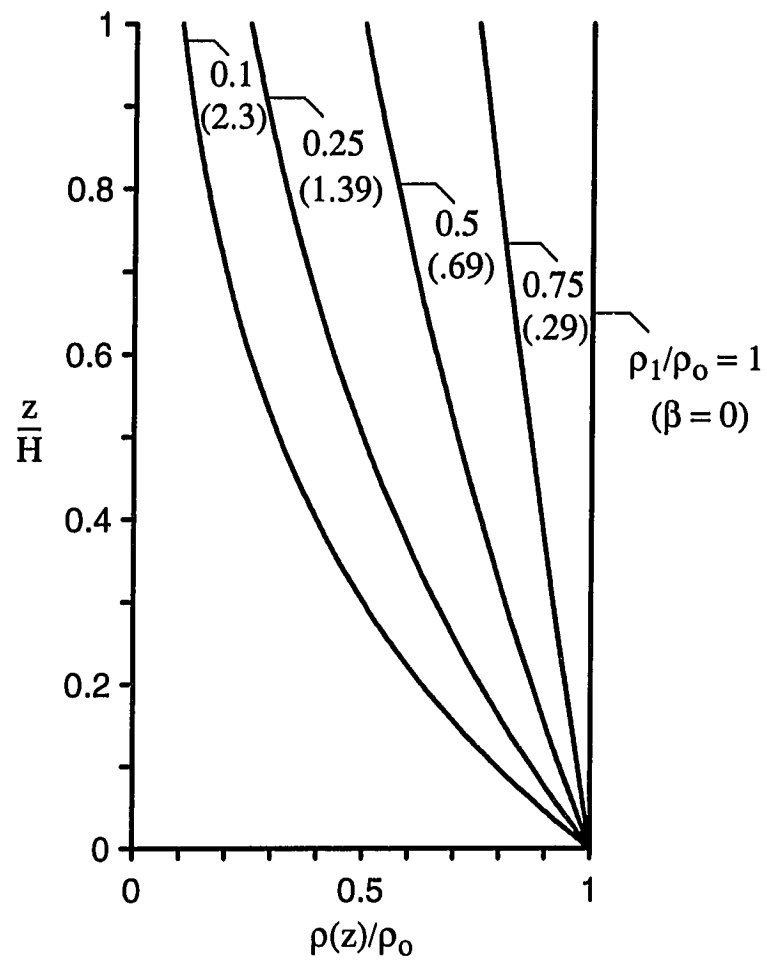


Figure 6.2 Vertical variations of liquid density for different values of  $\rho_1/\rho_0$  and  $\beta$

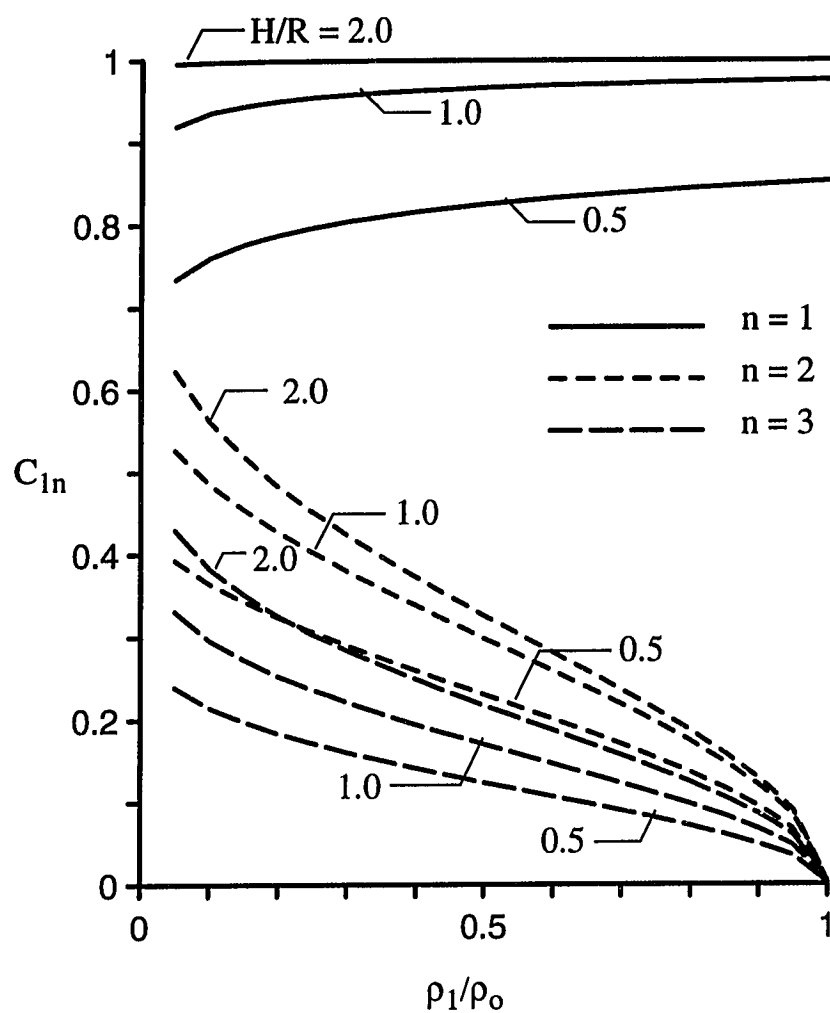


Figure 6.3 Frequency coefficients  $C_{1n}$  for the fundamental horizontal mode of vibration of systems with different values of  $H/R$  and  $\rho_1/\rho_0$

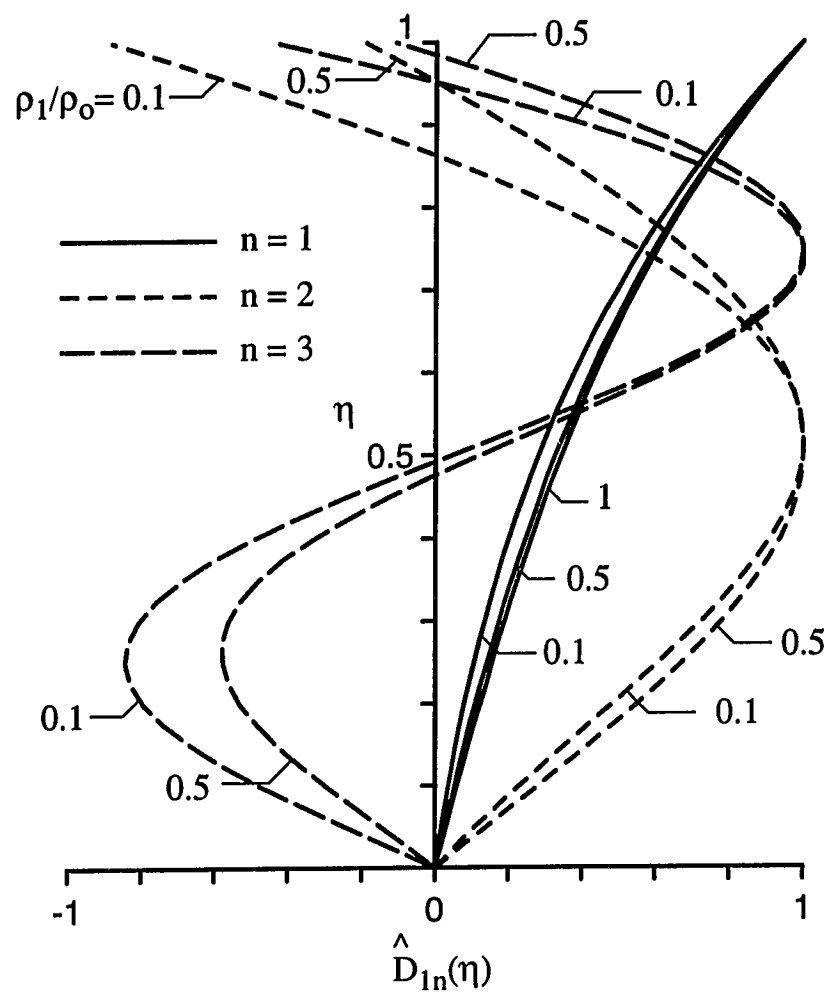


Figure 6.4 Vertical modes of vibration associated with fundamental horizontal mode of systems with  $H/R = 1$

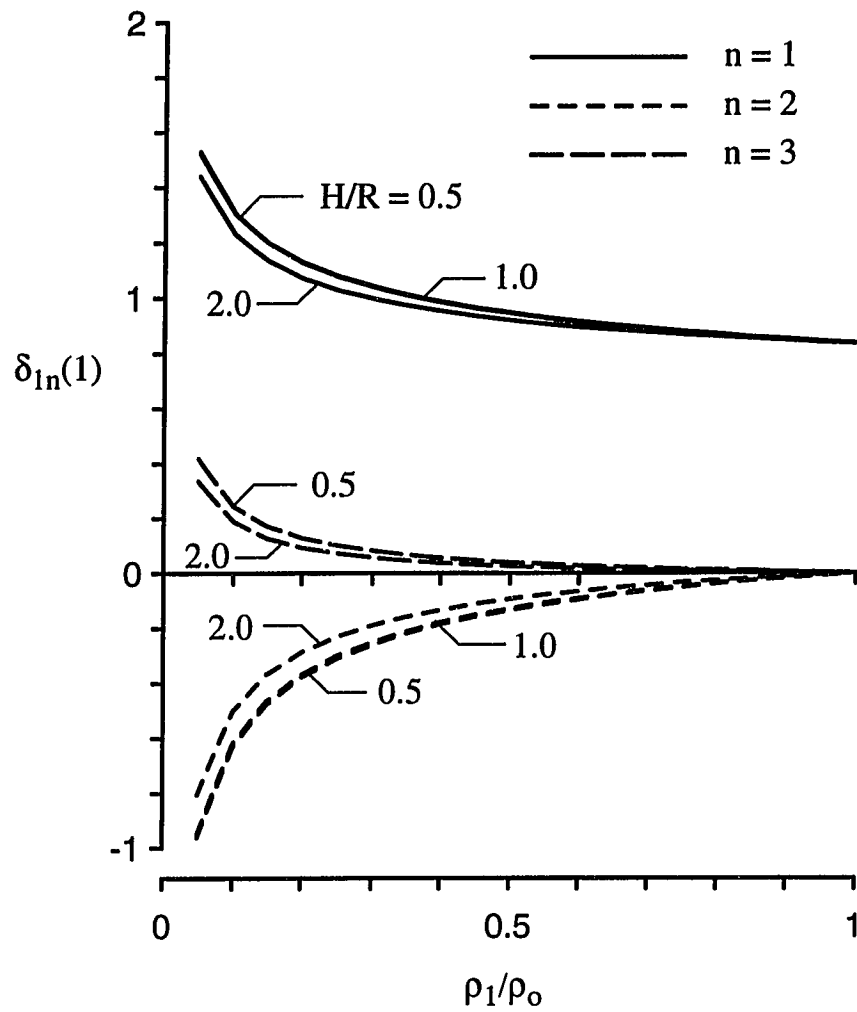


Figure 6.5 Surface displacement coefficients for fundamental horizontal mode of vibration of systems with different values of  $H/R$  and  $\rho_1/\rho_0$

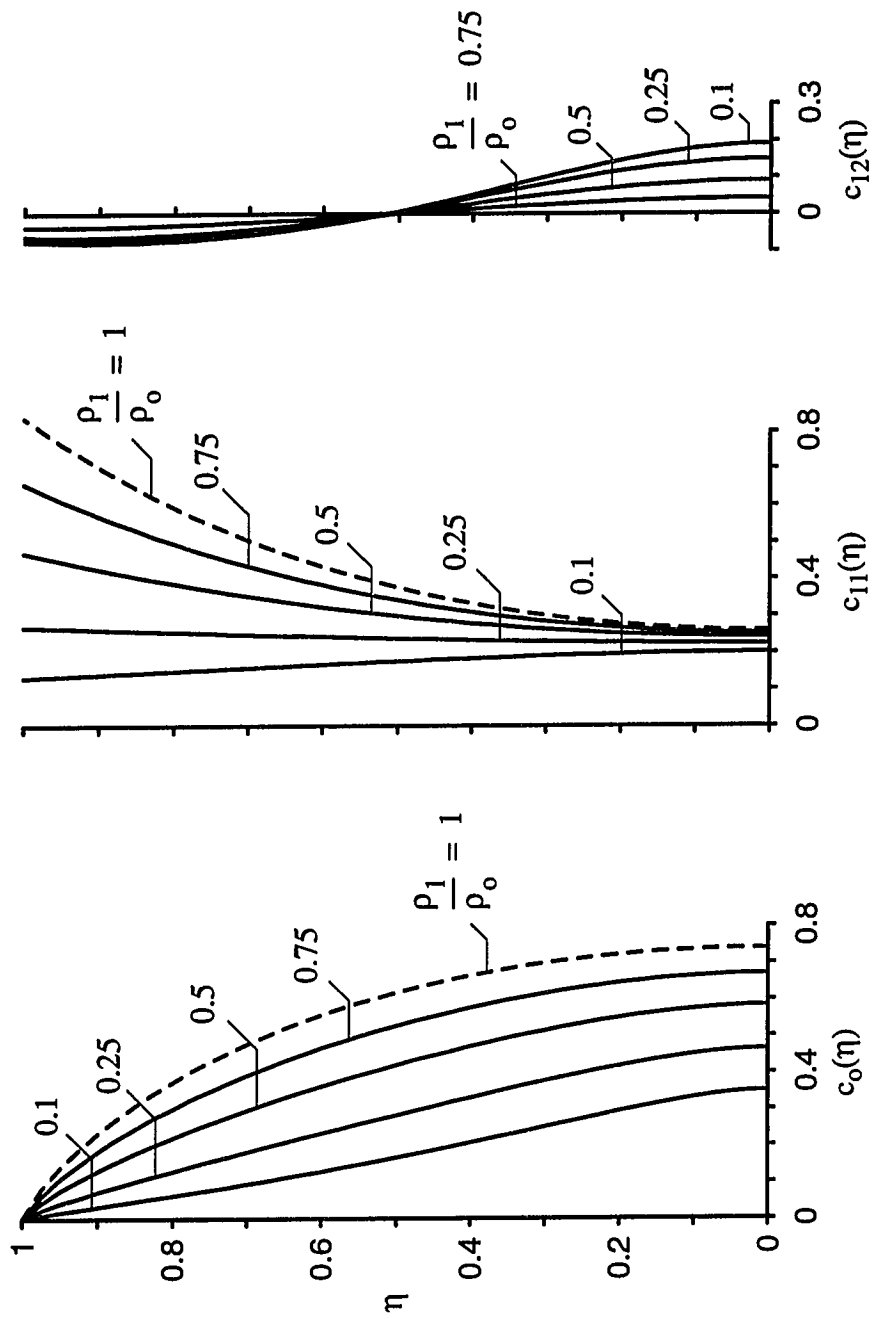


Figure 6.6 Effect of liquid density ratio  $\rho_1/\rho_0$  on coefficients for impulsive and convective components of wall pressure for systems with  $H/R = 1.0$

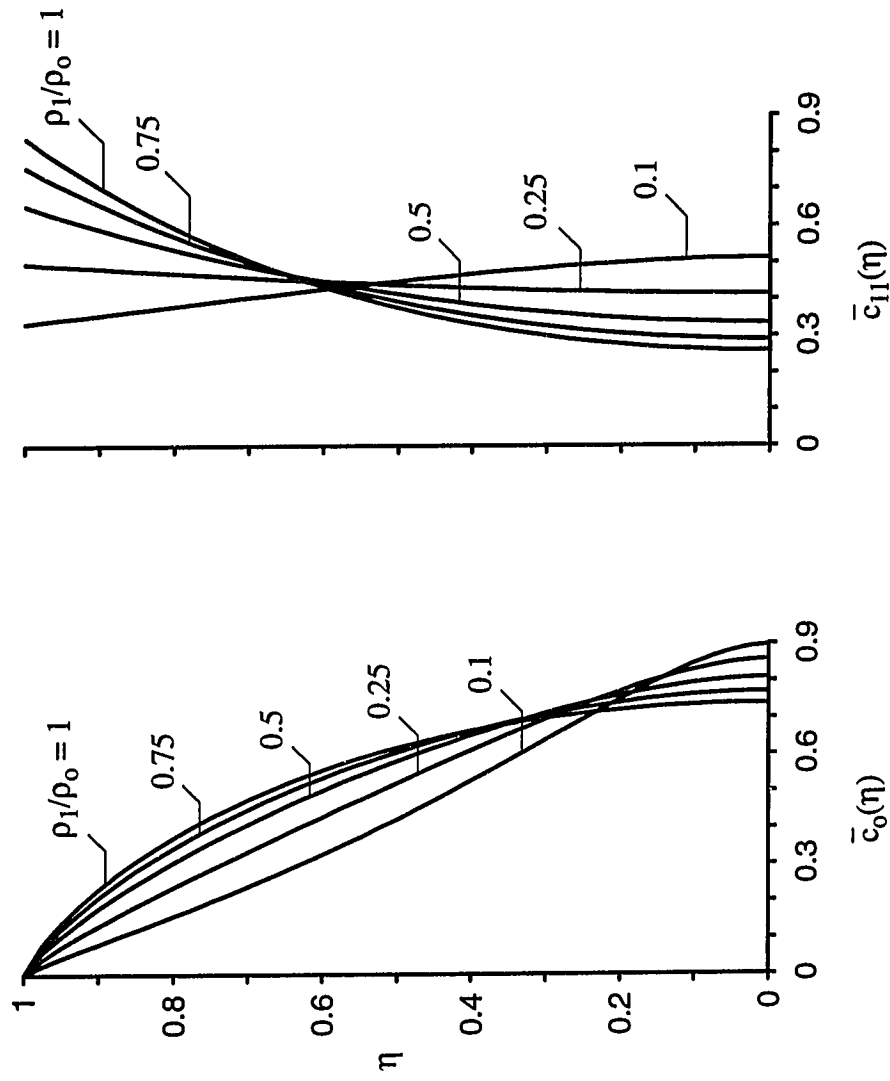


Figure 6.7 Coefficients  $\bar{c}_0(\eta)$  and  $\bar{c}_{11}(\eta)$  in expressions for impulsive and fundamental convective components of wall pressure for systems with  $H/R = 1.0$

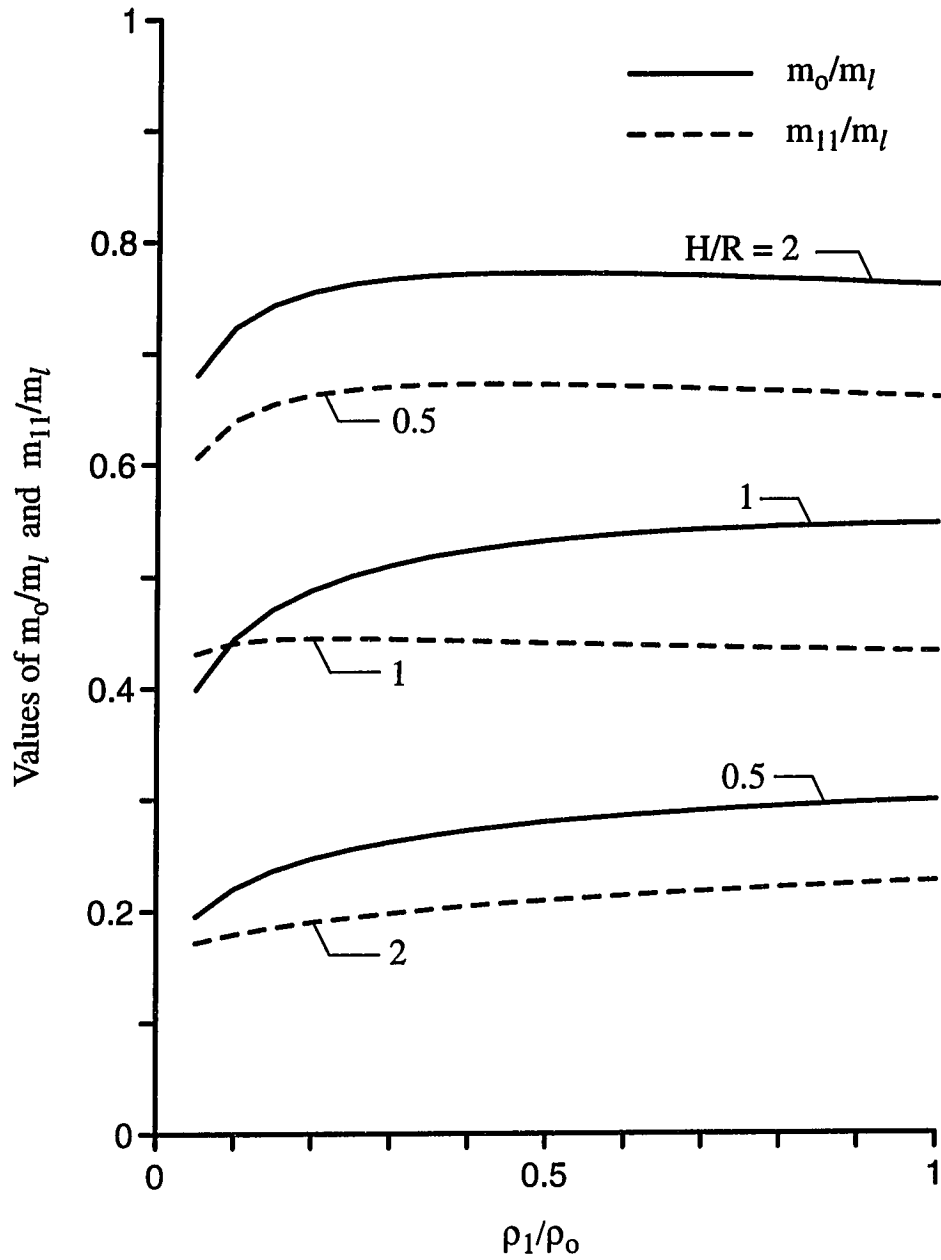


Figure 6.8 Normalized values of impulsive and fundamental convective masses for systems with different  $H/R$  and  $\rho_1/\rho_o$



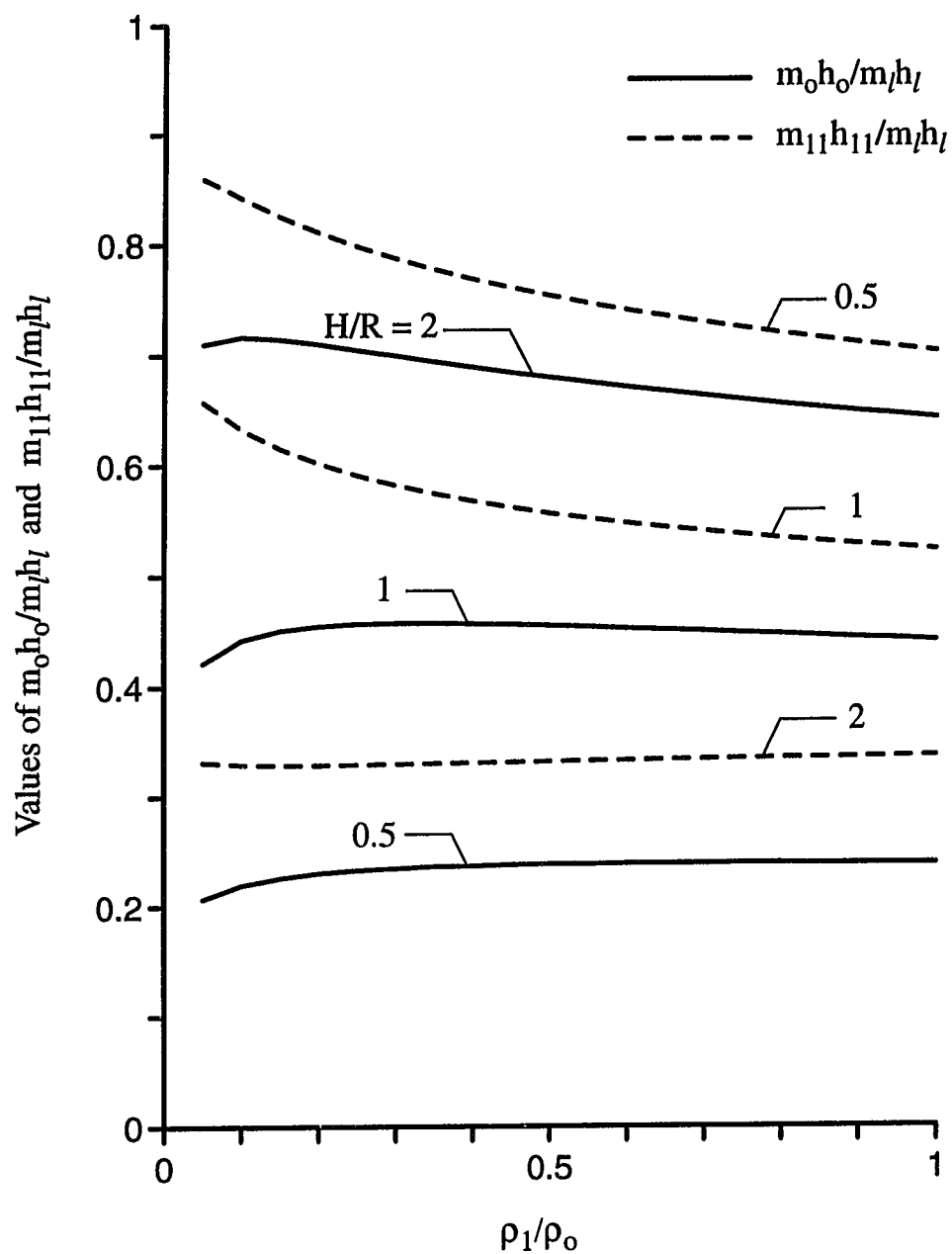


Figure 6.9 Normalized values of coefficients for impulsive and fundamental convective components of base moment for systems with different  $H/R$  and  $\rho_1 / \rho_0$

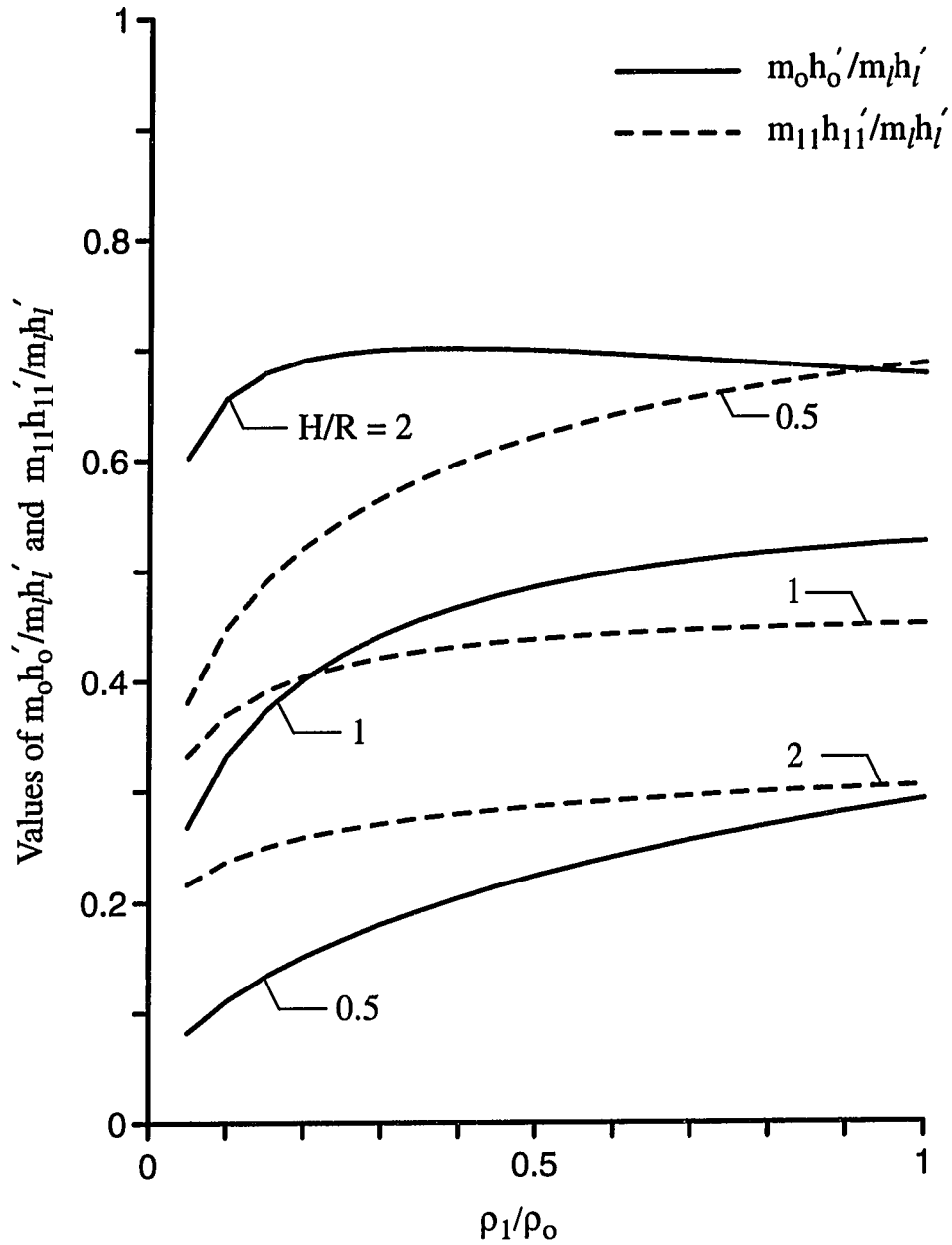


Figure 6.10 Normalized values of coefficients for impulsive and fundamental convective components of foundation moment for systems with different  $H/R$  and  $\rho_1 / \rho_o$

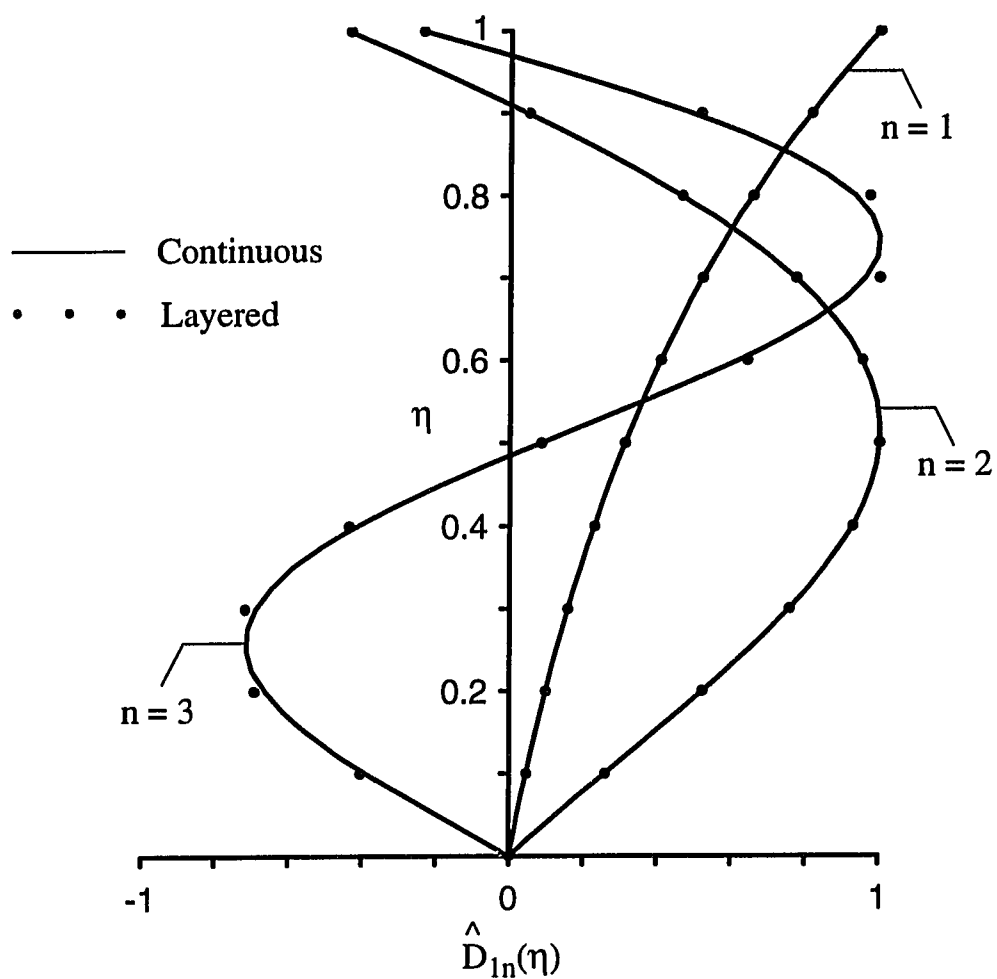
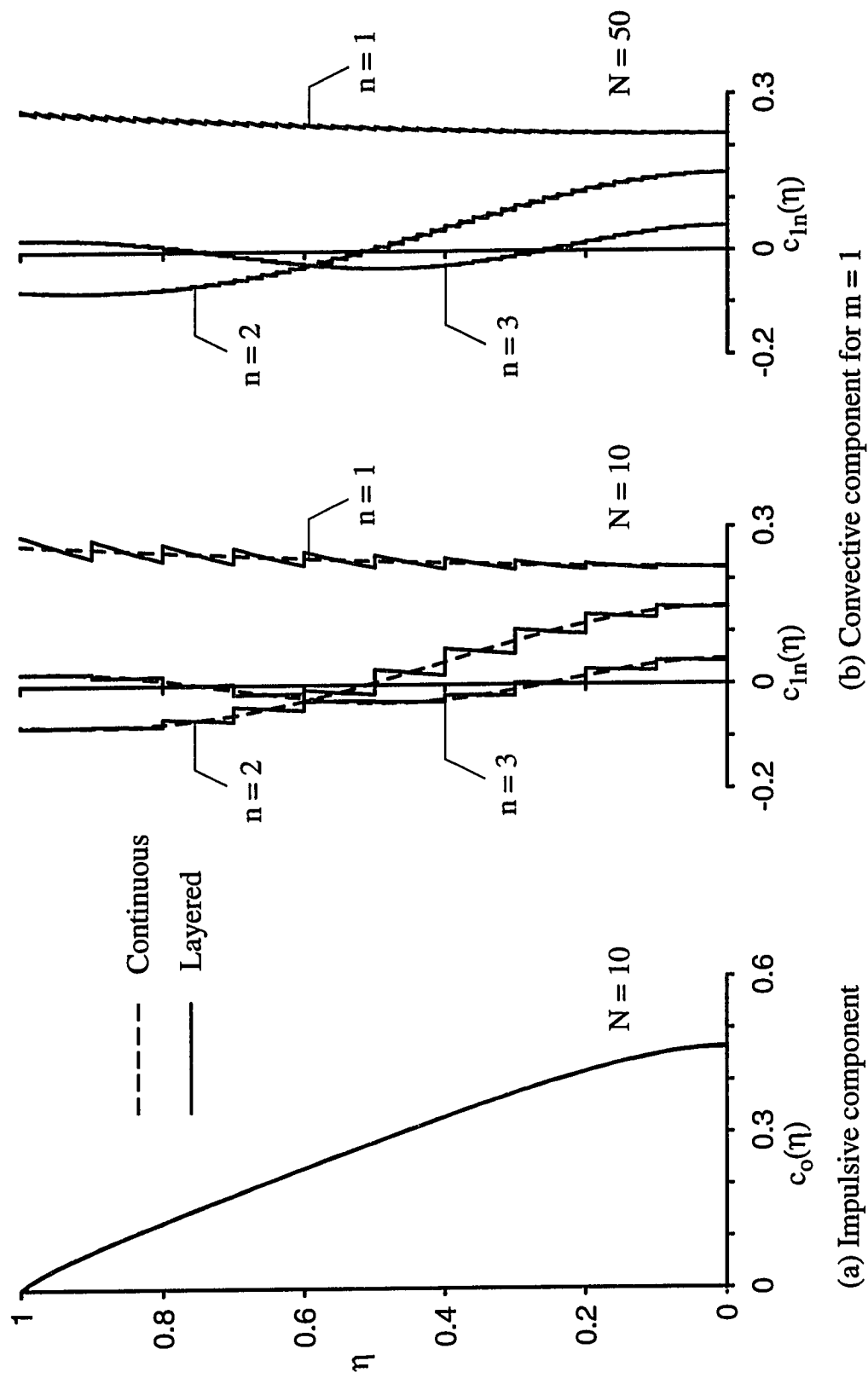


Figure 6.11 Configurations of vertical modal displacements for  $m=1$  and  $n=1, 2, 3$  for continuous system and its layered approximation;  $H/R = 1$ ,  $\rho_1/\rho_0 = 0.25$ ,  $N = 10$



(a) Impulsive component

(b) Convective component for  $m = 1$

Figure 6.12 Comparison of wall pressure distributions for continuous system with  $H/R = 1$  and  $\rho_1/\rho_o = 0.25$  with those of its layered approximations

## Chapter 7

# Effects of Basemat Flexibility for Vertically Excited Liquid Storage Tanks

### 7.1 Introduction

In the numerous studies to date that have dealt with the dynamic response of tank-liquid systems, it has been assumed that the foundation of the tank-liquid system is rigid. Previous studies and tests for actual buildings have, however, indicated that the assumption of rigid foundations may not be generally valid and that it may be necessary to take the foundation flexibility into consideration while computing the dynamic response, [25, 79, 81]. Such trends are also indicated in preliminary tests for buried high-level waste storage tanks, [42]. The objectives of this chapter are two-fold:

- To assess the adequacy of the rigid base assumption for liquid storage tanks subjected to vertical ground excitations, and
- To assess the effects that any deformation of the base-plate may have on the induced hydrodynamic effects in the tank.

In general, the problem considered requires taking into account the effects of fluid-structure-soil interaction, with due provision for the flexibilities of the tank-wall, base-plate and the soil medium. The intention of the present study is to obtain an engineering insight into the problem and suitable simplifications are made to enable an exploratory study. The soil is represented by a set of mutually independent Winkler springs and the effects of tank-wall flexibility are implicitly neglected. The model considered provides rigorously for the fluid-plate interaction effects while approximately accounting for the interaction of the base-plate and soil. The effects of these approximations on the results are also indicated in the study.

## 7.2 System Considered

The system considered is shown in Fig. 7.1(a). It is a vertical, circular cylindrical tank of radius  $R$  that is anchored to a flexible base plate. The thickness of the base plate is denoted by  $t_p$ , its density by  $\rho_p$ , the modulus of elasticity by  $E_p$ , and Poisson's ratio by  $\nu_p$ . The liquid height is denoted by  $H$  and its mass density by  $\rho_l$ . The mass density of the soil is denoted by  $\rho_s$ , its shear modulus by  $G_s$ , and Poisson's ratio by  $\nu_s$ . The free-field ground motion is considered to be a uniform, vertical excitation, the instantaneous acceleration of which is denoted by  $\ddot{x}_g(t)$ , and the corresponding velocity and displacement by  $\dot{x}_g(t)$  and  $x_g(t)$ , respectively. Points within the tank are defined by the cylindrical coordinates  $r$ ,  $\theta$  and  $z$ .

### 7.2.1 Model Considered

The simplified model of the system is shown in Fig. 7.1(b). The tank-wall and roof are considered to be rigid in axial vibration and their inertia is represented by a mass  $\bar{m}$  distributed along the circumference of the plate. For underground tanks,  $\bar{m}$  may also be considered to include the inertial effects of the soil surcharge and the surrounding soil.

The supporting soil is represented by a set of Winkler springs, the stiffness  $k$  of which is taken equal to the static vertical stiffness per unit area of a rigid footing resting on an elastic halfspace,

$$k = \frac{4 G_s}{\pi R(1 - \nu_s)} \quad (7.1)$$

This simplified representation for the soil makes no provision for the effects of plate-flexibility on the dynamic stiffness and more importantly, for the damping due to radiation. The nature of the induced damping and its effect on the magnitude of the induced response is also studied later.

The constraint offered by the wall at its junction to the base plate is represented by a rotational spring. Two cases are considered for the stiffness of this spring denoted by  $\mu$ : (1) Hinged case, ( $\mu = 0$ ), and (2) Fixed case, ( $\mu = \infty$ ).

## 7.3 Method of Analysis

Complicating the analysis for the model considered herein is the fact that the magnitude and distribution of the hydrodynamic liquid pressures induced on the plate are

unknown. The analysis is implemented herein by an energy procedure, making use of the Rayleigh-Ritz method in combination with Lagrange's equations of motion.

### 7.3.1 Deflection Configuration

The vertical component of the relative displacement,  $w = w(\xi, t)$ , is taken in the form

$$w(\xi, t) = w_0(t) + \sum_{n=1}^N w_n(t) \psi_n(\xi) \quad (7.2)$$

where  $\xi = r/R$ ;  $w_0(t)$  represents the rigid-body displacement of the plate relative to the free-field ground motion,  $x_g(t)$ ;  $w_n(t)$  are time-dependent generalized coordinates with units of length; and  $\psi_n(\xi)$  is the  $n$ th approximating function satisfying the geometric boundary conditions of the edge-supported plate.

For the hinged case,  $\psi_n(\xi)$  satisfies the conditions of zero displacement at the edge, finite displacement and zero slope at the center and is taken in the form,

$$\psi_n^h(\xi) = J_0(\alpha_n^h \xi) \quad (7.3)$$

where the superscript  $h$  denotes the hinged condition;  $J_0$  is the bessel function of first kind and zero order; and  $\alpha_n^h$  is the  $n$ th root of  $J_0(\alpha) = 0$ . The first three of these roots are

$$\alpha_1^h = 2.405 \quad \alpha_2^h = 5.520 \quad \alpha_3^h = 8.654 \quad (7.4)$$

For the fixed support,  $\psi_n(\xi)$  satisfies the conditions of zero displacement and zero slope at the edge, finite displacement and zero slope at the center. The shape function is taken in the same form as the  $n$ th mode-shape of a clamped circular plate,

$$\psi_n^f(\xi) = \frac{J_0(\alpha_n^f \xi)}{J_0(\alpha_n^f)} - \frac{I_0(\alpha_n^f \xi)}{I_0(\alpha_n^f)} \quad (7.5)$$

where the superscript  $f$  denotes the fixed condition;  $I_0$  is the modified bessel function of first kind and zero order, and  $\alpha_n^f$  is the  $n$ th root of

$$J_1(\alpha)I_0(\alpha) + J_0(\alpha)I_1(\alpha) = 0 \quad (7.6)$$

The first three of these roots are

$$\alpha_1^f = 3.196 \quad \alpha_2^f = 6.306 \quad \alpha_3^f = 9.439 \quad (7.7)$$

### 7.3.2 Strain Energy

The strain energy of the system includes two components : the energy stored in the springs,  $S_s$ , given by

$$S_s = \pi k R^2 \int_0^1 w(\xi, t)^2 \xi d\xi \quad (7.8)$$

and the energy of the deformed base-plate,  $S_p$ , given by

$$S_p = \frac{\pi D_p}{R^2} \int_0^1 \left[ \left( \frac{\partial^2 w}{\partial \xi^2} \right)^2 + \left( \frac{1}{\xi} \frac{\partial w}{\partial \xi} \right)^2 + 2\nu_p \left( \frac{\partial^2 w}{\partial \xi^2} \right) \left( \frac{1}{\xi} \frac{\partial w}{\partial \xi} \right) \right] \xi d\xi \quad (7.9)$$

where  $D_p = E_p t_p^3 / 12(1 - \nu_p^2)$ .

### 7.3.3 Kinetic Energy

The kinetic energy of the system includes three components : (1) the energy of the base-plate,  $T_p$ , given by

$$T_p = m_p \int_0^1 \dot{w}(\xi, t)^2 \xi d\xi \quad (7.10)$$

where  $m_p$  is the mass of the base-plate  $= \pi \rho_p t_p R^2$ . (2) the energy of the end-mass,  $T_{em}$ , given by

$$T_{em} = \frac{1}{2} m_{em} \dot{w}(1, t)^2 \quad (7.11)$$

where  $m_{em}$  is the total end-mass  $= 2\pi R \bar{m}$ , and (3) the kinetic energy of the liquid,  $T_l$ , given by

$$T_l = -\frac{\rho_l}{2} \int_S \phi \frac{\partial \phi}{\partial n} dS \quad (7.12)$$

where  $S$  refers to the bounding surfaces of the liquid;  $\phi$  is a velocity potential function describing the flow characteristics of the liquid;  $\partial \phi / \partial n$  describes the velocity normal to each surface. The derivation for  $\phi$  is summarized in Appendix C and the final expression is given by

$$\phi = \dot{w}_0(t) (H - z) + \sum_{n=1}^N \dot{w}_n(t) \left[ 2e_n (H - z) + R \sum_{m=1}^{\infty} \frac{2d_{nm}}{\lambda_m} \frac{J_0(\lambda_m \xi)}{J_0^2(\lambda_m)} \frac{\sinh \lambda_m (H - z)/R}{\cosh \lambda_m H/R} \right] \quad (7.13)$$

where

$$e_n = \int_0^1 \psi_n(\xi) \xi d\xi \quad (7.14)$$

$$d_{nm} = \int_0^1 \psi_n(\xi) J_0(\lambda_m \xi) \xi d\xi \quad (7.15)$$



and  $\lambda_m$  is the  $m$ th root of  $J_1(\lambda) = 0$ . The expressions for  $e_n$  and  $d_{nm}$  for the hinged and fixed conditions of edge-support are given in Appendix C. With  $\phi$  determined, the kinetic energy can be obtained from equation (7.12), as also indicated in Appendix C.

### 7.3.4 External Work

The external forces acting on the system include the distributed rigid-body inertias of the plate and liquid, and the concentrated inertia due to the end-mass. The external work done on the system is then given by

$$W_{ext} = - \left[ 2(m_l + m_p) \int_0^1 \left\{ w_0(t) + \sum_{n=1}^N w_n(t) \psi_n(\xi) \right\} \xi d\xi + m_{em} w_0(t) \right] \ddot{x}_g(t) \quad (7.16)$$

where  $m_l$  is the mass of the liquid  $= \pi \rho_l R^2 H$ . The negative sign indicates that the inertia forces and the displacement are in opposite directions.

### 7.3.5 Equations of Motion

The differential equations of motion for the system are obtained by repeated application of Lagrange's equation,

$$\frac{\partial}{\partial t} \left( \frac{\partial T}{\partial \dot{w}_i} \right) - \frac{\partial T}{\partial w_i} + \frac{\partial S}{\partial w_i} = \frac{\partial W_{ext}}{\partial w_i} \quad (7.17)$$

where  $i = 0, 1, \dots, N$ ; the dot superscript denotes differentiation with respect to time;  $T$  is the total kinetic energy  $= T_p + T_{em} + T_l$ ;  $S$  is the total strain energy  $= S_p + S_s$ ; and  $W_{ext}$  is the external work.

Substituting the relevant expressions into equation (7.17), and carrying out the indicated partial differentiations for  $i = 0, 1, \dots, N$ , the equations of motion can be written in matrix form as,

$$[M] \{\ddot{w}\} + [K] \{w\} = -[M] \{1, 0, \dots, 0\}^T \ddot{x}_g(t) \quad (7.18)$$

where  $\{w\}$  is the vector of generalized displacement coordinates and is given by

$$\{w\} = \{w_0, w_1, \dots, w_N\}^T \quad (7.19)$$

$[M]$  is the *mass matrix* of size  $(N + 1) \times (N + 1)$  and its elements are as follows:

$$m_{00} = m_t$$

$$m_{0i} = m_t(1 - \beta_{em})e_i \quad \text{for } i \neq 0$$

$$m_{ij} = m_t \left[ 2\beta_p g_{ij} + 4\beta_l \left( e_i e_j + \frac{R}{H} \sum_{m=1}^{\infty} \frac{\tanh \lambda_m H/R}{\lambda_m} \frac{d_{im} d_{jm}}{J_0^2(\lambda_m)} \right) \right] \quad \text{for } i, j \neq 0 \quad (7.20)$$

where  $m_t = (m_l + m_p + m_{em})$  is the total mass of the system;  $\beta_{em}$  is the ratio of the end-mass to the total mass  $= m_{em}/m_t$ ;  $\beta_p$  is the ratio of the plate mass to the total mass  $= m_p/m_t$ ;  $\beta_l$  is the ratio of the liquid mass to the total mass  $= m_l/m_t = 1 - \beta_p - \beta_{em}$ ;  $e_i$  and  $d_{im}$  are defined by equations (7.14) and (7.15) respectively; and  $g_{ij}$  is given by

$$g_{ij} = \int_0^1 \psi_i(\xi) \psi_j(\xi) \xi d\xi \quad (7.21)$$

For the hinged and fixed edge conditions considered,  $g_{ij}$  is evaluated to be

$$g_{ij}^h = \frac{J_1(\alpha_i^h) J_1(\alpha_j^h)}{2} \delta_{ij} \quad g_{ij}^f = \delta_{ij} \quad (7.22)$$

where  $\delta_{ij}$  represents the Kronecker delta symbol.

$$\delta_{ij} = \begin{cases} 1 & \text{for } i = j \\ 0 & \text{for } i \neq j \end{cases} \quad (7.23)$$

$[K]$  is the *stiffness matrix* of size  $(N+1) \times (N+1)$  and its elements are as follows:

$$k_{00} = \pi k R^2$$

$$k_{0i} = \pi k R^2 e_i \quad \text{for } i \neq 0$$

$$k_{ij} = 2\pi k R^2 \left[ \left( 1 + \frac{D_p}{k R^4} \alpha_i^2 \alpha_j^2 \right) g_{ij} + \frac{D_p}{k R^4} (\nu_p - 1) h_{ij} \right] \quad \text{for } i, j \neq 0 \quad (7.24)$$

where  $h_{ij}$  is given by

$$h_{ij} = \frac{\partial \psi_i}{\partial \xi} \frac{\partial \psi_j}{\partial \xi} \Big|_0^1 \quad (7.25)$$

For the hinged and fixed edge conditions considered, this reduces to

$$h_{ij}^h = \alpha_i \alpha_j J_1(\alpha_i) J_1(\alpha_j) \quad h_{ij}^f = 0 \quad (7.26)$$

## 7.4 Free Vibration

The equations of free-vibration are deduced from equation (7.18) by setting its right-hand side to zero, letting  $\{w(t)\} = \{\hat{w}\}e^{i\omega t}$  and solving the resulting characteristic value problem

$$[K]\{\hat{w}\} = \omega^2[M]\{\hat{w}\} \quad (7.27)$$

This results in a system of  $(N + 1)$  natural modes of vibration, and  $(N + 1)$  associated circular natural frequencies. The modes are real-valued and can be shown to satisfy the orthogonality relations

$$\{\hat{w}_p\}^T[M]\{\hat{w}_q\} = \{\hat{w}_p\}^T[K]\{\hat{w}_q\} = 0 \quad \text{for } p \neq q \quad (7.28)$$

### 7.4.1 Numerical Solutions

The circular natural frequency associated with the  $k$ th mode of vibration of the system can be conveniently expressed in the form

$$\omega_k = C_k \sqrt{\frac{\pi k R^2}{m_t}} \quad (7.29)$$

where  $C_k$  is a dimensionless frequency coefficient that depends on  $H/R$ ,  $D_p/kR^4$ ,  $\beta_{em}$ ,  $\beta_p$ ,  $\nu_p$  and the edge-support condition. The radial variation of the associated modal base plate displacement is evaluated by substituting  $\{\hat{w}_k\}$  into equation (7.2) and is expressed in the form

$$\hat{w}_k(\xi) = \hat{w}_{k,0} + \sum_{n=1}^N \hat{w}_{k,n} \psi_n(\xi) \quad (7.30)$$

where  $\hat{w}_{k,n}$  denotes the  $n$ th modal displacement amplitude associated with the  $k$ th mode of vibration.

For the solutions presented herein,  $H/R$  is considered to vary between 0.5 and 2, the relative plate mass  $\beta_p$  is taken to be in the order of 0.1 and the relative end-mass  $\beta_{em}$  is assumed to vary between 0 and 0.5. The larger values of  $\beta_{em}$  can be considered to be representative of tanks that are buried underground. The relative stiffness parameter,  $D_p/kR^4$ , is a function of several variables and has a wide range of variation. Using the value of  $k$  defined by equation (7.1),  $D_p/kR^4$  can be expressed in the form,

$$\frac{D_p}{kR^4} = \frac{\pi}{48} \frac{E_p}{G_s} \left( \frac{t_p}{R} \right)^3 \frac{1 - \nu_s}{1 - \nu_p^2} \quad (7.31)$$

On assuming  $t_p/R$  to vary between 0.03 and 0.075, using the relation  $G_s = \rho_s v_s^2$  with  $\rho_s = 3.416 \text{ lb/ft}^3$ , and the shear-wave velocity  $v_s$  assumed to vary between 400 ft/sec and 1200 ft/sec, taking  $\nu_s = 1/3$ , and assuming the material of the base-plate to be concrete, it is found that  $D_p/kR^4$  can vary between 0.02 and 0.00001, with most values typically in the range of 0.01 to 0.001.

The frequency coefficients for the first two modes of vibration are presented in Figs. 7.2 and 7.3 for the hinged and fixed conditions of edge-support respectively. The results are plotted as a function of  $\beta_{em}$  ranging from 0 to 0.5 and for values of  $D_p/kR^4$  ranging between 0.02 and 0.0005.  $H/R$  is taken as 1.0,  $\beta_p$  as 0.1 and  $\nu_p$  as 0.17. The associated modal displacement configurations are presented in Figs. 7.4 and 7.5 for values of  $D_p/kR^4 = 0.02$  and 0.001 respectively. The following trends can be noted from the data presented :

- The fundamental mode of vibration is typically associated with a significant rigid-body component of motion. For the case of zero end-mass ( $\beta_{em} = 0$ ), the system undergoes rigid-body motion irrespective of the plate flexibility or the edge-support condition and the associated frequency coefficient is unity. For increasing values of  $\beta_{em}$  and decreasing values of  $D_p/kR^4$ , the flexural component of the plate deformation increases, especially at the vicinity of the plate-edges and the associated frequency coefficient decreases monotonically from unity.
- The second mode of vibration is typically associated with a significant flexural component of motion. The associated frequency coefficient decreases significantly as the relative flexibility of the plate increases. For increasing values of  $\beta_{em}$  and decreasing values of  $D_p/kR^4$ , the central portion of the plate exhibits more uniform, rigid-body like motion and the frequency coefficient  $C_2$  tends to unity.
- The end-constraint condition has a tremendous influence on the free-vibrational characteristics of the system. The mode shapes are altered significantly by preventing the edge from rotating and the associated natural frequencies are increased significantly.

Numerical values of the fundamental and second frequency coefficients for the systems considered and for additional values of  $H/R$  are presented in Tables 7.1 and 7.2 respectively. Both the hinged and fixed conditions of edge-support are considered. It is seen that, in general, both frequency coefficients increase with increasing  $H/R$ .

However, the effect on the fundamental frequency coefficient is very slight and for all practical purposes,  $C_1$  can be considered to be independent of  $H/R$ .

#### 7.4.2 Further Simplification

As pointed out before, the evaluation of the added modal masses for the liquid is the issue complicating the analysis of the fluid-structure interaction problem. Frequently, this complication is resolved by simply assuming that the liquid inertia acts uniformly and lumping it with the plate inertia. This was the approach used in [42]. It is desirable to check the accuracy of such simplified solutions with the more exact solutions presented in the previous section.

The solution for this simplified problem can be obtained by solving exactly the governing differential equations of an equivalent elastically supported plate. The mass of this equivalent plate incorporates the original plate mass and the liquid mass. Such an exact solution also provides a means of checking the accuracy and the rate of convergence of the solutions obtained by the energy procedure. The latter solutions for this simplified problem are obtained by simply putting  $\beta_l = 0$  in the elements of the mass matrix.

The exact procedure for solving the free-vibration problem is shown in Appendix C. Frequency coefficients for the first two modes of vibration obtained by this exact method are shown in Tables 7.3 and 7.4 respectively.  $\beta_{em}$  is taken as 0.5,  $D_p/kR^4$  is taken equal to 0.02 and 0.001, and both hinged and fixed conditions of edge-support are considered in these tables. Approximate solutions obtained by the energy procedure are also included in these tables. The number of approximating functions used for these solutions are varied between 3 and 10. It is seen that :

- The values of the fundamental frequency coefficients evaluated for the equivalent plate are close to the corresponding frequency coefficients in Table 7.1 that were evaluated by accounting for the fluid-structure interaction effects. This follows from the fact that the first mode typically has a large rigid-body component and the liquid does behave more or less uniformly in this case. The frequency coefficients for the second mode, however, differ significantly from those in Table 7.2 and this follows from the fact that the second mode typically has a large flexural component and the associated liquid inertia is not generally uniform.
- The agreement in the results between the exact and the energy solutions is excellent. This is particularly true for the fixed case, where using only three

terms is sufficient to give satisfactory agreement for the frequency coefficients. The rate of convergence for the fundamental frequency is somewhat slower than that for the second frequency.

## 7.5 Forced Vibration

With the natural frequencies and modes of vibration of the system established, its response to an arbitrary lateral excitation may be obtained by the modal superposition method. In this approach, the vector  $\{w(t)\}$  of the generalized displacement amplitudes of the liquid is expressed as a linear combination of the characteristic vectors,  $\{\hat{w}_k\}$ , as

$$\{w(t)\} = \sum_{k=1}^{N+1} \{\hat{w}_k\} q_k(t) \quad (7.32)$$

in which  $q_k(t)$  is a generalized time-dependent coordinate corresponding to the  $k$ th mode of vibration. Substituting equation (7.32) into equation (7.18), premultiplying the resulting expression by  $\{\hat{w}_k\}^T$ , and making use of the orthogonality properties of the natural modes defined by equation (7.28), one obtains

$$\ddot{q}_k(t) + \omega_k^2 q_k(t) = -\Gamma_k \ddot{x}_g(t) \quad (7.33)$$

in which  $\Gamma_k$  is a dimensionless factor given by

$$\Gamma_k = \frac{\{\hat{w}_k\}^T [M] \{1, 0, \dots, 0\}^T}{\{\hat{w}_k\}^T [M] \{\hat{w}_k\}} \quad (7.34)$$

The solution of equation (7.33) is then given by

$$q_k(t) = -\frac{\Gamma_k}{\omega_k^2} A_k(t) \quad (7.35)$$

in which  $A_k(t)$  represents the pseudoacceleration function defined by

$$A_k(t) = \omega_k \int_0^t \ddot{x}_g(\tau) \sin \omega_k(t - \tau) d\tau \quad (7.36)$$

For a base-excited single-degree-of-freedom oscillator with a circular frequency  $\omega_k$ , the pseudoacceleration  $A_k(t)$  represents the product of the square of  $\omega_k$  and the deformation of the oscillator,  $U_k(t)$ , i.e.,  $A_k(t) = -\omega_k^2 U_k(t)$ . The maximum value of  $A_k(t)$  is the quantity displayed on a pseudoacceleration response spectrum.

From equations (7.32) and (7.35) one obtains,

$$\{w(t)\} = - \sum_{k=1}^{N+1} \Gamma_k \{\hat{w}_k\} \frac{A_k(t)}{\omega_k^2} = \sum_{k=1}^{N+1} \Gamma_k \{\hat{w}_k\} U_k(t) \quad (7.37)$$

From the latter part of equation (7.37), it can be shown that

$$\sum_{k=1}^{N+1} \Gamma_k \{\hat{w}_k\} = \{1, 0, 0, \dots, 0\}^T \quad (7.38)$$

The proof is as follows : Consider the limiting case of a very flexible system, i.e.,  $\omega_k \rightarrow 0$ . The relative base displacement for such a system is proportional to the ground displacement, i.e.,  $\{w(t)\} = -x_g(t) \{1, 0, \dots, 0\}^T$ . Similarly, the modal deformation  $U_k(t)$  for each of the  $(N+1)$  modes is equal to  $-x_g(t)$ . On substituting these relations into the latter part of equation (7.37), one obtains equation (7.38).

It is also desirable to compute the vector of modal acceleration amplitudes,  $\{\ddot{w}(t)\}$ . This may be obtained by double differentiating equation (7.37) with respect to time,

$$\{\ddot{w}(t)\} = - \sum_{k=1}^{N+1} \Gamma_k \{\hat{w}_k\} \frac{\ddot{A}_k(t)}{\omega_k^2} \quad (7.39)$$

Now, on substituting the relation  $\ddot{A}_k(t) = \omega_k^2 (\ddot{x}_g(t) - A_k(t))$  into the above expression and making use of equation (7.38), one obtains

$$\{\ddot{w}(t)\} = -\ddot{x}_g(t) \{1, 0, \dots, 0\}^T + \sum_{k=1}^{N+1} \Gamma_k \{\hat{w}_k\} A_k(t) \quad (7.40)$$

### 7.5.1 Hydrodynamic Pressure

The liquid pressure,  $p(r, z, t)$ , is given by

$$p(r, z, t) = \rho_l \ddot{x}_g(t)(H - z) + \rho_l \frac{\partial \phi}{\partial t} \quad (7.41)$$

where the term proportional to the ground acceleration is included since the velocity potential function  $\phi$  is only associated with the relative motion of the base plate. Now, on substituting equation (7.13) for  $\phi$  into equation (7.41), one obtains

$$p(\xi, \eta, t) = \rho_l H \left( \ddot{x}_g(t) + \ddot{w}_0(t) \right) (1 - \eta) + \sum_{n=1}^N \ddot{w}_n(t) \left( 2e_n(1 - \eta) + \frac{R}{H} \sum_{m=1}^{\infty} \frac{2d_{nm}}{\lambda_m} \frac{J_0(\lambda_m \xi)}{J_0^2(\lambda_m)} \frac{\sinh \lambda_m H/R (1 - \eta)}{\cosh \lambda_m H/R} \right) \quad (7.42)$$

where  $\eta = z/H$ . On substituting for  $\ddot{w}_0$  and  $\ddot{w}_n$  from equation (7.40) into the above expression and grouping together the terms that are proportional to each modal acceleration, equation (7.42) can be written in the form,

$$p(\xi, \eta, t) = \rho_l H \sum_{k=1}^{N+1} c_k(\xi, \eta) A_k(t) \quad (7.43)$$

where  $c_k(\xi, \eta)$  defines the heightwise and radial variations of the pressure distribution associated with the  $k$ th mode of vibration of the system and is given by

$$c_k(\xi, \eta) = \Gamma_k \left[ \hat{w}_{k,0}(1-\eta) + \sum_{n=1}^N \hat{w}_{k,n} \left\{ 2e_n(1-\eta) + \frac{R}{H} \sum_{m=1}^{\infty} \frac{2d_{nm}}{\lambda_m} \frac{J_0(\lambda_m \xi)}{J_0^2(\lambda_m)} \frac{\sinh \lambda_m H/R(1-\eta)}{\cosh \lambda_m H/R} \right\} \right] \quad (7.44)$$

It can be shown that the wall pressure coefficients must satisfy the relation

$$\sum_{k=1}^{N+1} c_k(1, \eta) = (1 - \eta) \quad (7.45)$$

The proof follows by considering the limiting case of a very rigid system, i.e.,  $\omega_k \rightarrow \infty$ . In this case,  $A_k(t) = \ddot{x}_g(t)$ . Substituting this into equation (7.43) and equating the resulting expression to the wall-pressure distribution for a rigid tank which is given by  $p_{rigid}(\eta, t) = \rho_l H \ddot{x}_g(t) (1 - \eta)$ , one obtains equation (7.45). In a similar manner, the base pressure coefficients can be shown to satisfy the relation

$$\sum_{k=1}^{N+1} c_k(\xi, 0) = 1 \quad (7.46)$$

### 7.5.2 Numerical Solutions

Hydrodynamic wall and base pressure distributions for the hinged and fixed conditions of edge-support are presented in Figs. 7.6 and 7.7 for values of  $D_p/kR^4 = 0.02$  and 0.001 respectively. The solutions are for values of  $\beta_{em}$  ranging from 0 to 0.5,  $H/R = 1.0$ ,  $\beta_p = 0.1$  and  $\nu_p = 0.17$ . Distributions for the fundamental mode are shown as solid lines while those for the second mode are shown as dashed lines. The following trends are worth noting :

- The first two modal pressure coefficients are the only dominant contributors to the response and higher modal terms can be neglected. Furthermore, the solutions presented approximately satisfy equations (7.45) and (7.46).



- For flexible plates with zero end-mass, the fundamental wall pressure tends to the linear rigid-tank distribution and the corresponding second modal pressure reduces to zero. Increasing values of  $\beta_{em}$  and decreasing values of  $D_p/kR^4$  cause a decrease in the fundamental modal pressure component and a corresponding increase in the second modal pressure component.
- The edge-support condition drastically alters the magnitudes of the pressure distributions. Clamping the edge of the plate results in solutions that are closer to the rigid-tank pressure distributions. For larger values of  $\beta_{em}$  and smaller values of  $D_p/kR^4$ , the hinged and clamped solutions vary by as much as 50 %.

Fundamental wall pressure distributions for the cases considered and for additional values of  $H/R$  are tabulated in Tables 7.5 and 7.6 for values of  $\beta_{em} = 0.3$  and  $0.5$  respectively. Since the pressure distributions are more or less linear from the top to roughly half the tank height, only values over the bottom half are tabulated. It is seen that the effect of increasing  $H/R$  is to decrease the fundamental modal component and to increase the second component. This follows from the fact that the effect of increasing the slenderness ratio is to increase the liquid pressures acting near the edge of the plate. This, in turn, can be interpreted as an increase in the end-mass ratio  $\beta_{em}$ , thereby reducing the fundamental modal pressure contribution.

### 7.5.3 Implication of Results

In order to understand the implications of the solutions presented, it is necessary to compare the response of the elastically supported systems with flexible base plates to that of similarly supported systems with rigid base plates. The hydrodynamic wall pressure for the latter systems,  $p_r = p_r(\eta, t)$ , is given by

$$p_r(\eta, t) = \rho_l H A_r(t) (1 - \eta) \quad (7.47)$$

where  $A_r(t)$  is the pseudoacceleration function corresponding to the natural frequency of the system,  $\omega_r = \sqrt{\pi k R^2 / m_t}$ .

For the purpose of establishing the relative magnitudes of the effects, it can be assumed that the natural frequencies are typically such that the spectral values of  $A_r(t)$  for the rigid systems and of  $A_1(t)$  and  $A_2(t)$  for the flexible systems fall in the amplified, nearly constant portion of the pseudoacceleration response spectrum. The maximum hydrodynamic wall pressure for the flexible system is then obtained by combining the first two modal terms of equation (7.43) by the sum-of-the-squares

rule,

$$p_{max}(1, \eta) = \rho_l H A_{max} \left( \sqrt{c_1(\eta)^2 + c_2(\eta)^2} \right) \quad (7.48)$$

where  $A_{max}$  is the spectral value of the modal pseudoaccelerations. Now, on making use of the relation  $c_1(\eta) + c_2(\eta) \approx (1 - \eta)$ , and comparing equation (7.48) with the maximum value of equation (7.47), it follows that the response of systems with flexible base-plates is generally smaller than the corresponding response of systems with rigid base-plates.

It should, however, be noted that the above conclusion has been based on the assumption of no radiational damping. The damping mechanisms for the rigid and flexible systems may be quite different and the corresponding responses may be significantly affected by the different damping values. It is necessary to provide for the effects of radiational damping and re-evaluate the implications of the results presented.

## 7.6 Incorporation of Damping

In general, the computation of the damping effects requires a precise evaluation of the tractions at the interface of the flexible plate and soil. The solution of the mixed-boundary value problem for this evaluation is quite complicated and is beyond the scope of this study. The intent of this section is to develop a simple and rational scheme by which the effects of radiational damping can be incorporated while retaining the essential features of the model previously considered.

### 7.6.1 Outline of method

The equation of motion for the undamped tank-liquid-soil system vibrating in the  $k$ th mode is rewritten as

$$m_k^* \ddot{U}_k(t) + k_k^* U_k(t) = -m_k^* \ddot{x}_g(t) \quad (7.49)$$

This equation is obtained by substituting equation (7.37) into equation (7.18), premultiplying the resulting expression by  $\Gamma_k \{\hat{w}_k\}^T$ , and using the orthogonality properties of the modes, defined by equation (7.28). The coefficients  $m_k^*$  and  $k_k^*$  are then given by

$$m_k^* = \frac{(\{\hat{w}_k\}^T [M] \{1, 0, \dots, 0\}^T)^2}{\{\hat{w}_k\}^T [M] \{\hat{w}_k\}} \quad k_k^* = \omega_k^2 m_k^* \quad (7.50)$$

On making use of the relation  $\ddot{U}_k(t) = -\ddot{x}_g(t) + A_k(t)$ , equation (7.49) reduces to the form  $m_k^* A_k(t) = -k_k^* U_k(t)$ . It follows that  $m_k^*$  represents the effective modal mass when the system responds to the vertical ground motion in the the  $k$ th mode of vibration and  $k_k^*$  represents the associated effective modal stiffness for the system. It can further be shown that

$$\sum_{k=1}^{N+1} m_k^* = m_t \quad \sum_{k=1}^{N+1} k_k^* = \pi k R^2 \quad (7.51)$$

The above relations are obtained by postmultiplying the transpose of equation (7.38) by  $[M]\{1, 0, \dots, 0\}^T$  and  $[K]\{1, 0, \dots, 0\}^T$  respectively.

With the effective modal masses and stiffnesses established, the elastically supported flexible system vibrating in the first and second modes ( $k=1,2$ ) is replaced by equivalent elastically supported rigid systems having identical values of  $m_k^*$  and  $k_k^*$ . This is tantamount to equating the total transmitted modal forces for the flexible and equivalent rigid systems or equating the total kinetic and strain energies for the two systems. It should be noted, however, that the displacements of the two systems are different : while the displacement of the equivalent rigid system is the motion of the SDOF oscillator defined by equation (7.49) and is equal to  $U_k(t)$ , the displacement of the flexible system is evaluated by substituting the  $k$ th term of equation (7.37) into equation (7.2) and varies over the length of the plate. The degree of agreement between the displacement values for the two systems forms a rough indicator of the accuracy of the equivalent replacement.

The types of equivalent rigid foundations used are based upon limiting trends revealed by the modal displacement configurations previously displayed in Figs. 7.4 and 7.5 for the flexible plate. Related studies for flexible circular and rectangular plates, [27, 28, 33, 38, 39, 47, 80], are used to verify the equivalent models. Previously established damping values for the equivalent rigid foundations are then used to compute the damping ratios  $\zeta_1$  and  $\zeta_2$  for the first two modes of the flexible system.

With the damping ratios defined, the hydrodynamic pressure is again evaluated from a two-mode expansion of equation (7.43), with the pseudoacceleration function  $A_k(t)$  given by

$$A_k(t) = \frac{\omega_k}{\sqrt{1 - \zeta_k^2}} \int_0^t \ddot{x}_g(\tau) \exp[-\zeta_k \omega_k(t - \tau)] \sin[\bar{\omega}_k(t - \tau)] d\tau \quad (7.52)$$

where  $\zeta_k$  is the modal damping and  $\bar{\omega}_k$  is the  $k$ th damped circular natural frequency of the system.

The remainder of this section deals with the evaluation of the damping ratios  $\zeta_1$  and  $\zeta_2$ .

### 7.6.2 Damping for fundamental mode of vibration

For increasing values of the end-mass and plate flexibility, the fundamental mode exhibits a large flexural component near the plate edges and the center of the plate does not move significantly. This indicates that in such cases, the elastically supported system vibrating in the fundamental mode essentially acts as a perimeter loaded plate and the central portion of the plate is ineffectively utilized. This suggests that the system can be modeled as an elastically supported ring foundation with a suitably defined radius. A similar replacement of a perimeter loaded flexible rectangular foundation by a rigid foundation with a hole in the center has also been suggested in [27]. The equivalent replacement is further corroborated by the close similarity between the impedance functions for edge-loaded flexible rectangular and circular plates (see References [27] and [39] respectively) to those for rigid ring foundations, [68].

The mass of the equivalent ring foundation is taken as  $m_1^*$  and its stiffness as  $k_1^*$ . The radius of the equivalent ring foundation,  $\Delta R$ , is then evaluated by equating the total stiffness due to the supporting Winkler springs to  $k_1^*$ , i.e.,

$$k (\pi R^2 - \pi R_i^2) = k_1^* \quad (7.53)$$

where  $k$  is defined by equation (7.1) and  $R_i$  is the inner radius of the ring foundation.

Values of the equivalent  $\Delta R/R$  obtained by use of equation (7.53) for edge-loaded plates ( $\beta_{em} = 1$ ), are presented in Table 7.7 for different values of  $D_p/kR^4$ . Both hinged and fixed conditions of edge-support are considered. Approximate values of  $\Delta R/R$  obtained by a visual comparison between the results for impedance functions presented in [27] and [39] with those in [68] are also included in the table. It should be noted that the latter comparisons are only available for the hinged case. The following trends are worth noting :

- For an infinitely rigid plate, the radius of the equivalent ring foundation reduces, as it should, to unity. As  $D_p/kR^4$  decreases, the radius of the equivalent ring tends to zero. For the hinged case, the results obtained from the present analysis match quite well with those obtained from the literature analysis for most values of  $D_p/kR^4$ , and the agreement deteriorates only for very small values of  $D_p/kR^4$ .
- Clamping the edge of the plate significantly increases the value of  $\Delta R/R$ , indicating that the radiational damping in this case is larger than that for the

hinged case and that, for many values of  $D_p/kR^4$ , the damping will not be significantly different from that for a rigid disc. This observation is further corroborated by the trends of the displacement configurations presented before and also by solutions available in the literature: Solutions presented by Lin [38] for clamped plates indicate that even for relatively flexible plates ( $D_p/kR^4 \approx 0.0025$ ), there is no significant reduction in the damping. On the other hand, recent solutions presented by Liou and Huang [39] for hinged plates indicate a significant reduction in the damping values even for relatively rigid plates ( $D_p/kR^4 \approx 0.05$ ).

With the dimensions of the equivalent ring foundation established, the damping due to the supporting Winkler medium is approximately evaluated from solutions for a ring foundation supported on an equivalent half-space. The properties of the equivalent half-space are taken such that the stiffness of the ring foundation resting on that half-space is  $k_1^*$ . Making use of previously established solutions, [68], the damping action of the medium is then represented by a dashpot coefficient  $c_1^*$  given by

$$c_1^* = \beta_1 (K_{st})_1 \frac{R}{v_s} \quad (7.54)$$

where  $\beta_1$  is the damping coefficient for the ring foundation and is a function of  $\Delta R/R$ ;  $(K_{st})_1$  is the static stiffness of the equivalent half-space, and is given by

$$(K_{st})_1 = k_1^*/\alpha_1 \quad (7.55)$$

where  $\alpha_1$  is the stiffness coefficient for the ring foundation and is a function of  $\Delta R/R$ .

The damping ratio  $\zeta_1$  is then evaluated to be

$$\zeta_1 = \frac{c_1^*}{2\sqrt{k_1^* m_1^*}} = \frac{\beta_1}{2\alpha_1} C_1 \sqrt{\frac{\pi k R^2}{m_t}} \frac{R}{v_s} = \frac{\beta_1}{2\alpha_1} C_1 \frac{\sqrt{1 - \beta_{em}}}{\sqrt{B}} \quad (7.56)$$

where  $C_1$  is the fundamental frequency coefficient, and  $B$  is a dimensionless mass ratio given by

$$B = \frac{1 - \nu_s}{4} \frac{(m_l + m_p)}{\rho_s R^3} = \frac{\pi(1 - \nu_s)}{4} \left( \frac{\rho_l H}{\rho_s R} + \frac{\rho_p t_p}{\rho_s R} \right) \quad (7.57)$$

Values of  $\zeta_1$  are presented in Table 7.8 for the hinged and fixed conditions of edge-support. The results are obtained for values of  $\beta_{em}$  ranging from 0 to 0.5, values of  $D_p/kR^4$  ranging between  $\infty$  and 0.001, and values of  $H/R$  equal to 0.5, 1 and

2. For these three values of  $H/R$ ,  $B$  is taken as 0.25, 0.45 and 0.9 respectively.  $\beta_p$  is taken as 0.1 and  $\nu_p$  as 0.17. The values of  $\alpha_1$  and  $\beta_1$  for the different values of equivalent  $\Delta R/R$  are obtained by interpolating between the values tabulated in [68] for the static case (zero exciting frequency). The following trends are worth noting :

- For  $\beta_{em} = 0$ , since the spring-supported flexible plate moves uniformly, the associated damping values are independent of the plate flexibility and are equal to that for a rigid disc. Furthermore, as anticipated, the values of  $\zeta_1$  for clamped plates are significantly larger than those for hinged plates and are not as sensitive to variations in the plate flexibility.
- For increasing values of  $\beta_{em}$  and decreasing values of  $D_p/kR^4$ ,  $\zeta_1$  decreases monotonically. The decrease is significant for the hinged case with values of  $\beta_{em}$  in the range of 0.3 to 0.5 and  $D_p/kR^4$  in the range of 0.002 to 0.001. Furthermore, for changing values of  $H/R$ ,  $\zeta_1$  is largely affected only by the respective changes in  $\sqrt{B}$ , i.e.,  $\zeta_1 \approx \zeta_1^* \sqrt{B^*/B}$ . This relation follows from the fact that the fundamental mode shapes and associated frequency coefficients are relatively insensitive to  $H/R$ .

### 7.6.3 Damping for second mode of vibration

For increasing values of the end-mass and plate flexibility, the second mode exhibits a relatively large rigid-body component of motion near the center of the plate and the edges do not move significantly. This indicates that in such cases, the system can be modeled as an elastically supported rigid disc with a suitably defined radius.

The suggested replacement may not be adequate for systems with small values of the end-mass or for relatively rigid systems since both the central part of the flexible plate and the edges participate in the motion. The agreement between the displacement values of the flexible and the equivalent disc systems in these cases may be expected to be quite poor. However, the contribution of the second mode is negligibly small in these cases and it is considered unnecessary to develop more sophisticated models for the modal damping values  $\zeta_2$ .

The mass of the equivalent disc is taken as  $m_2^*$  and its stiffness as  $k_2^*$ . The radius of the equivalent disc,  $R_{eq}$ , is then evaluated by equating the total stiffness due to the supporting Winkler springs to  $k_2^*$ , i.e.,

$$\pi k R_{eq}^2 = k_2^* \quad (7.58)$$

It can be shown that the equivalent radius,  $R_{eq}$ , evaluated from equation (7.58) is related to the radius of the equivalent ring foundation,  $\Delta R$ , evaluated from equation (7.53) by

$$R_{eq} + \Delta R \approx R \quad (7.59)$$

The above expression follows from the relation  $k_1^* + k_2^* \approx \pi k R^2$ .

With the dimensions of the equivalent disc defined, the damping due to the Winkler medium is approximately obtained from solutions for a disc foundation supported on an equivalent half-space, the properties of which are taken such that the stiffness of the disc foundation resting on that half-space is  $k_2^*$ . Making use of previously established solutions, [71], the damping action of the soil is then represented by a dashpot coefficient  $c_2^*$  given by

$$c_2^* = \beta_2 (K_{st})_2 \frac{R_{eq}}{v_s} \quad (7.60)$$

where  $\beta_2$  represents the damping coefficient for the equivalent disc foundation; and  $(K_{st})_2$  represents the static stiffness of the equivalent half-space and is given by  $(K_{st})_2 = k_2^*/\alpha_2$ , where  $\alpha_2$  represents the stiffness coefficient for the equivalent disc foundation.

The damping ratio for the second mode of vibration,  $\zeta_2$  is then evaluated to be

$$\zeta_2 = \frac{c_2^*}{2\sqrt{k_2^* m_2^*}} = \frac{\beta_2}{2\alpha_2} C_2 \sqrt{\frac{\pi k R^2}{m_t}} \frac{R_{eq}}{v_s} = \frac{\beta_2}{2\alpha_2} C_2 \frac{R_{eq}}{R} \frac{\sqrt{1 - \beta_{em}}}{\sqrt{B}} \quad (7.61)$$

Values of  $\zeta_2$  are presented in Table 7.9 for the combination of parameters considered before in Table 7.8. Both hinged and fixed conditions of edge-support are considered. It should be noted that for the second mode, values of  $\zeta_2$  are only defined for non-zero values of  $\beta_{em}$  and finite values of  $D_p/kR^4$ . It is seen that :

- For increasing values of  $\beta_{em}$  and decreasing values of  $D_p/kR^4$ , the damping ratios  $\zeta_2$  increase. This is related to the corresponding increase in the radii of the equivalent disc foundations. For values of  $\beta_{em}$  in the range of 0.3-0.5, values of  $\zeta_2$  may be even larger than the damping values for infinitely rigid plates presented in Table 7.8. This follows from the fact that even though the dashpot coefficient  $c_2^*$  for the flexible plate is smaller than that for a rigid disc, the value of the associated modal mass  $m_2^*$  in equation (7.61) is also smaller.
- The effect of increasing  $H/R$  is to decrease the damping value. Furthermore, the damping values for the fixed case are smaller than those for the hinged case and the latter results are more sensitive to variations in the parameters.

#### 7.6.4 Implication of results

The maximum hydrodynamic wall pressure for the rigid system is given by

$$p_{r,max}(1, \eta) = \rho_l H A_{r,max}(1 - \eta) \quad (7.62)$$

where  $A_{r,max}$  is the spectral pseudoacceleration value evaluated for the damping induced for a rigid disc. The corresponding value of the maximum hydrodynamic wall pressure for the flexible system is given by

$$p_{max}(1, \eta) = \rho_l H \left( \sqrt{(c_1(\eta) A_{1,max})^2 + (c_2(\eta) A_{2,max})^2} \right) \quad (7.63)$$

where  $A_{k,max}$  ( $k = 1, 2$ ) is the spectral pseudoacceleration value for the  $k$ th mode of vibration and is evaluated for a damping value  $\zeta_k$ .

The values of  $A_{1,max}$  and  $A_{2,max}$  are generally larger or are of the same order of magnitude as  $A_{r,max}$ . The values of  $c_1(\eta)$  and  $c_2(\eta)$  vary depending on the edge-support condition and the values of  $\beta_{em}$ ,  $H/R$  and  $D_p/kR^4$ , as shown in Tables 7.5 and 7.6. It follows that, depending on the relative magnitudes of the spectral pseudoacceleration values and the relative contributions of the modal pressure coefficients, the response of the flexible systems can be larger or smaller than the corresponding response of systems with rigid base-plates. Based on studies for several typical tank-liquid systems found in practice, it is found that base flexibility typically causes an increase when the modal components are combined by taking the numerical sum, but when they are combined by the SRSS rule indicated in equation (7.63), the hydrodynamic wall pressures for hinged systems are generally smaller than for corresponding rigid systems. The decrease in this case is typically in the order of 10 % to 20 %. On the other hand, for fixed systems, the fundamental modal response dominates the response and since the associated modal damping is reduced, the hydrodynamic wall pressures are smaller or larger than for the rigid case, with the range of variation about  $\pm 5$  %.

### 7.7 Conclusions

With the information presented herein, the free-vibrational characteristics and the hydrodynamic pressures induced in a vertically excited liquid storage tank with a flexible base may be evaluated readily. The principal conclusions of the study may be summarized as follows:



1. For systems having realistic values of plate-stiffnesses and soil parameters, the assumption that the base is rigid may not be necessarily true. Depending on the value of the superposed end-mass, the base-plate may undergo significant deformation and this, in turn, can influence the induced hydrodynamic effects.
2. The free-vibrational response of the flexible system consists of several modes of vibration and associated natural frequencies of vibration. Only the first two modes of vibration are, however, important in evaluating the response of the system. Their associated frequencies are, respectively, lower and higher than that for an elastically supported tank with a rigid base.
3. The first mode of vibration is typically associated with a significant rigid-body indentation of the plate. The flexural component of the plate deformation for this mode increases as the relative flexibility of the plate and the superposed end-mass increase. However, the bending is confined to the vicinity of the plate edges and the central portion of the plate does not move significantly.
4. The second mode of vibration is typically associated with a significant bending of the plate. As the relative flexibility of the plate and superposed end-mass increase, the central portion of the plate for this mode exhibits rigid-body like motion and the edges do not move much.
5. The constraint condition between the tank-wall and the base plate affects the response significantly. Clamping the edge of the plate effectively makes the system more rigid : it increases the natural frequencies, and renders the fundamental pressure distribution closer to a rigid-tank linear pressure distribution.
6. Damping effects for the two dominant modes of vibration have been evaluated approximately. The results for the fundamental mode have been obtained by replacing the flexible system vibrating in that mode by an equivalent ring foundation. Similarly, the results for the second mode have been obtained by replacing the flexible system vibrating in that mode by an equivalent disc foundation.

**Table 7.1: Values of frequency coefficients for fundamental mode of vibration for different values of  $H/R$ ,  $\beta_{em}$  and  $D_p/kR^4$ ;  $\beta_p = 0.1$**

$D_p/kR^4$	Hinged Edge				Fixed Edge			
	$\beta_{em}=0$	0.1	0.3	0.5	$\beta_{em}=0$	0.1	0.3	0.5
$H/R = 0.5$								
0.02	1	0.993	0.941	0.864	1	0.999	0.989	0.971
0.01	1	0.988	0.903	0.803	1	0.998	0.980	0.949
0.005	1	0.982	0.861	0.746	1	0.996	0.966	0.917
0.002	1	0.971	0.808	0.684	1	0.993	0.938	0.864
0.001	1	0.961	0.769	0.640	1	0.989	0.913	0.823
0.0005	1	0.950	0.728	0.598	1	0.985	0.885	0.781
$H/R = 1$								
0.02	1	0.994	0.944	0.868	1	0.999	0.990	0.972
0.01	1	0.990	0.910	0.809	1	0.998	0.981	0.950
0.005	1	0.985	0.872	0.753	1	0.996	0.968	0.920
0.002	1	0.977	0.821	0.690	1	0.994	0.944	0.870
0.001	1	0.970	0.781	0.646	1	0.991	0.922	0.830
0.0005	1	0.960	0.739	0.602	1	0.988	0.896	0.788
$H/R = 2$								
0.02	1	0.994	0.946	0.870	1	0.999	0.990	0.972
0.01	1	0.994	0.914	0.811	1	0.998	0.981	0.951
0.005	1	0.986	0.877	0.757	1	0.997	0.969	0.921
0.002	1	0.979	0.828	0.693	1	0.994	0.947	0.873
0.001	1	0.973	0.788	0.649	1	0.992	0.926	0.833
0.0005	1	0.964	0.745	0.604	1	0.989	0.901	0.791

**Table 7.2: Values of frequency coefficients for second mode of vibration for different values of  $H/R$ ,  $\beta_{em}$  and  $D_p/kR^4$ ;  $\beta_p = 0.1$**

$D_p/kR^4$	Hinged Edge				Fixed Edge			
	$\beta_{em}=0$	0.1	0.3	0.5	$\beta_{em}=0$	0.1	0.3	0.5
$H/R = 0.5$								
0.02	2.160	1.909	1.781	1.931	3.108	2.998	2.954	3.145
0.01	1.806	1.601	1.541	1.723	2.396	2.313	2.293	2.472
0.005	1.599	1.424	1.416	1.616	1.944	1.878	1.881	2.062
0.002	1.460	1.306	1.340	1.550	1.613	1.560	1.587	1.779
0.001	1.410	1.260	1.312	1.525	1.487	1.438	1.477	1.676
0.0005	1.384	1.230	1.293	1.508	1.419	1.369	1.415	1.618
$H/R = 1$								
0.02	2.766	2.223	1.925	2.027	3.984	3.639	3.355	3.435
0.01	2.312	1.860	1.656	1.800	3.071	2.806	2.600	2.695
0.005	2.048	1.647	1.509	1.681	2.492	2.276	2.125	2.240
0.002	1.870	1.495	1.410	1.602	2.068	1.885	1.778	1.917
0.001	1.806	1.425	1.367	1.567	1.906	1.730	1.637	1.791
0.0005	1.772	1.367	1.335	1.541	1.819	1.636	1.546	1.712
$H/R = 2$								
0.02	3.425	2.472	2.020	2.085	4.942	4.220	3.652	3.628
0.01	2.863	2.065	1.731	1.847	3.810	3.251	2.827	2.843
0.005	2.535	1.820	1.569	1.719	3.091	2.634	2.304	2.356
0.002	2.316	1.636	1.454	1.631	2.565	2.174	1.914	2.006
0.001	2.238	1.540	1.399	1.589	2.364	1.983	1.746	1.862
0.0005	2.196	1.456	1.357	1.558	2.257	1.857	1.631	1.767

**Table 7.3: Comparison of approximate fundamental frequency coefficients to corresponding exact solutions for elastically supported equivalent plate;  $\beta_{em} = 0.5$**

$D_p/kR^4$	No. of Terms	Hinged		Fixed	
		Energy Soln.	Exact Soln.	Energy Soln.	Exact Soln.
0.02	3	0.861	0.856	0.970	0.970
	5	0.858		0.970	
	10	0.857		0.970	
0.001	3	0.641	0.624	0.811	0.806
	5	0.627		0.807	
	10	0.625		0.806	

**Table 7.4: Comparison of approximate frequency coefficients for second mode of vibration with corresponding exact solutions for elastically supported equivalent plate;  $\beta_{em} = 0.5$**

$D_p/kR^4$	No. of Terms	Hinged		Fixed	
		Energy Soln.	Exact Soln.	Energy Soln.	Exact Soln.
0.02	3	1.774	1.761	2.714	2.714
	5	1.769		2.714	
	10	1.765		2.714	
0.001	3	1.431	1.430	1.490	1.490
	5	1.431		1.490	
	10	1.430		1.490	

**Table 7.5: Values of wall pressure coefficients for fundamental mode of vibration for different values of  $H/R$ , and  $D_p/kR^4$ ;  $\beta_{em} = 0.3$ ,  $\beta_p = 0.1$**

$\frac{z}{H}$	Hinged Edge				Fixed Edge			
	$\frac{D_p}{kR^4}=0.02$	0.005	0.002	0.001	$\frac{D_p}{kR^4}=0.02$	0.005	0.002	0.001
$H/R = 0.5$								
0	0.975	0.836	0.730	0.655	1.009	1.011	0.986	0.947
0.1	0.861	0.721	0.619	0.548	0.905	0.900	0.870	0.830
0.2	0.755	0.621	0.527	0.462	0.803	0.793	0.762	0.722
0.3	0.653	0.530	0.446	0.389	0.701	0.689	0.658	0.621
0.4	0.555	0.446	0.372	0.323	0.599	0.587	0.558	0.525
0.5	0.460	0.366	0.304	0.262	0.499	0.487	0.462	0.432
1	0	0	0	0	0	0	0	0
$H/R = 1$								
0	0.923	0.764	0.648	0.565	0.994	0.970	0.929	0.883
0.1	0.813	0.653	0.542	0.464	0.891	0.861	0.817	0.769
0.2	0.713	0.562	0.461	0.391	0.789	0.759	0.714	0.668
0.3	0.618	0.481	0.391	0.330	0.689	0.659	0.618	0.576
0.4	0.526	0.406	0.329	0.276	0.590	0.562	0.525	0.488
0.5	0.437	0.335	0.270	0.226	0.491	0.467	0.435	0.404
1	0	0	0	0	0	0	0	0
$H/R = 2$								
0	0.897	0.726	0.604	0.516	0.986	0.950	0.901	0.850
0.1	0.792	0.623	0.508	0.427	0.884	0.844	0.793	0.742
0.2	0.698	0.543	0.440	0.367	0.784	0.746	0.698	0.651
0.3	0.608	0.471	0.380	0.317	0.685	0.651	0.608	0.566
0.4	0.520	0.402	0.324	0.270	0.587	0.557	0.519	0.483
0.5	0.433	0.334	0.269	0.224	0.489	0.464	0.432	0.402
1	0	0	0	0	0	0	0	0

**Table 7.6: Values of wall pressure coefficients for fundamental mode of vibration for different values of  $H/R$ , and  $D_p/kR^4$ ;  $\beta_{em} = 0.5$ ,  $\beta_p = 0.1$**

$\frac{z}{H}$	Hinged Edge				Fixed Edge			
	$\frac{D_p}{kR^4}=0.02$	0.005	0.002	0.001	$\frac{D_p}{kR^4}=0.02$	0.005	0.002	0.001
$H/R = 0.5$								
0	0.854	0.683	0.596	0.536	0.990	0.942	0.874	0.812
0.1	0.748	0.583	0.500	0.444	0.886	0.835	0.766	0.706
0.2	0.651	0.498	0.422	0.371	0.784	0.732	0.666	0.610
0.3	0.561	0.422	0.355	0.310	0.684	0.634	0.573	0.521
0.4	0.475	0.353	0.295	0.256	0.584	0.539	0.484	0.438
0.5	0.392	0.289	0.240	0.207	0.486	0.446	0.399	0.360
1	0	0	0	0	0	0	0	0
$H/R = 1$								
0	0.785	0.586	0.490	0.428	0.967	0.886	0.797	0.724
0.1	0.683	0.491	0.401	0.344	0.864	0.780	0.692	0.621
0.2	0.594	0.418	0.337	0.286	0.764	0.683	0.600	0.534
0.3	0.512	0.355	0.283	0.239	0.666	0.591	0.516	0.457
0.4	0.434	0.298	0.236	0.199	0.469	0.503	0.437	0.385
0.5	0.359	0.244	0.193	0.162	0.473	0.417	0.361	0.317
1	0	0	0	0	0	0	0	0
$H/R = 2$								
0	0.748	0.534	0.433	0.370	0.954	0.856	0.757	0.678
0.1	0.652	0.449	0.356	0.299	0.853	0.755	0.658	0.582
0.2	0.572	0.387	0.305	0.254	0.755	0.664	0.575	0.506
0.3	0.497	0.334	0.262	0.218	0.660	0.578	0.499	0.438
0.4	0.425	0.285	0.223	0.185	0.565	0.494	0.426	0.374
0.5	0.353	0.236	0.185	0.154	0.471	0.411	0.354	0.311
1	0	0	0	0	0	0	0	0

**Table 7.7: Values of radii of equivalent ring foundation for fundamental mode of elastically supported flexible plate;  $\beta_{em} = 1.0$**

$D_p/kR^4$	Hinged		Fixed
	Present	Literature	
$\infty$	1	1	1
0.05	0.420	0.4-0.5	0.704
0.02	0.300	0.3-0.4	0.578
0.005	0.185	$\approx 0.2$	0.391
0.002	0.146	$\approx 0.1$	0.303
0.0002	0.082	$\approx 0.02$	0.169

**Table 7.8:** Values of effective damping  $\zeta_1$  for fundamental mode of vibration for different values of  $H/R$ ,  $\beta_{em}$  and  $D_p/kR^4$ ;  $\beta_p = 0.1$ ,  $\nu_p = 0.17$

$D_p/kR^4$	Hinged Edge				Fixed Edge			
	$\beta_{em}=0$	0.1	0.3	0.5	$\beta_{em}=0$	0.1	0.3	0.5
$H/R = 0.5, B = 0.25$								
$\infty$	0.784	0.744	0.656	0.554	0.784	0.744	0.656	0.554
0.02	0.784	0.738	0.612	0.465	0.784	0.743	0.648	0.538
0.005	0.784	0.729	0.540	0.381	0.784	0.740	0.632	0.502
0.002	0.784	0.718	0.492	0.338	0.784	0.738	0.608	0.464
0.001	0.784	0.708	0.457	0.307	0.784	0.735	0.587	0.435
$H/R = 1, B = 0.45$								
$\infty$	0.584	0.554	0.489	0.413	0.584	0.554	0.489	0.413
0.02	0.584	0.551	0.458	0.349	0.584	0.554	0.483	0.401
0.005	0.584	0.546	0.411	0.289	0.584	0.552	0.473	0.376
0.002	0.584	0.541	0.378	0.256	0.584	0.551	0.458	0.350
0.001	0.584	0.536	0.350	0.233	0.584	0.549	0.444	0.328
$H/R = 2, B = 0.9$								
$\infty$	0.413	0.392	0.346	0.292	0.413	0.392	0.346	0.292
0.02	0.413	0.389	0.325	0.248	0.413	0.391	0.342	0.284
0.005	0.413	0.386	0.293	0.206	0.413	0.391	0.335	0.266
0.002	0.413	0.383	0.271	0.183	0.413	0.389	0.325	0.249
0.001	0.413	0.381	0.252	0.166	0.413	0.389	0.316	0.234



**Table 7.9: Values of effective damping  $\zeta_2$  for second mode of vibration for different values of  $H/R$ ,  $\beta_{em}$  and  $D_p/kR^4$ ;  $\beta_p = 0.1$ ,  $\nu_p = 0.17$**

$D_p/kR^4$	Hinged Edge			Fixed Edge		
	$\beta_{em}=0.1$	0.3	0.5	$\beta_{em}=0.1$	0.3	0.5
$H/R = 0.5, B = 0.25$						
0.02	0.188	0.463	0.599	0.111	0.294	0.429
0.005	0.270	0.588	0.666	0.139	0.363	0.499
0.002	0.335	0.639	0.689	0.172	0.431	0.552
0.001	0.382	0.667	0.703	0.200	0.482	0.585
$H/R = 1, B = 0.45$						
0.02	0.150	0.355	0.459	0.098	0.244	0.346
0.005	0.193	0.440	0.509	0.113	0.288	0.394
0.002	0.227	0.480	0.527	0.130	0.331	0.431
0.001	0.256	0.505	0.539	0.145	0.367	0.458
$H/R = 2, B = 0.9$						
0.02	0.113	0.256	0.330	0.079	0.186	0.257
0.005	0.138	0.313	0.365	0.089	0.214	0.289
0.002	0.159	0.342	0.378	0.099	0.242	0.314
0.001	0.178	0.359	0.386	0.109	0.266	0.333

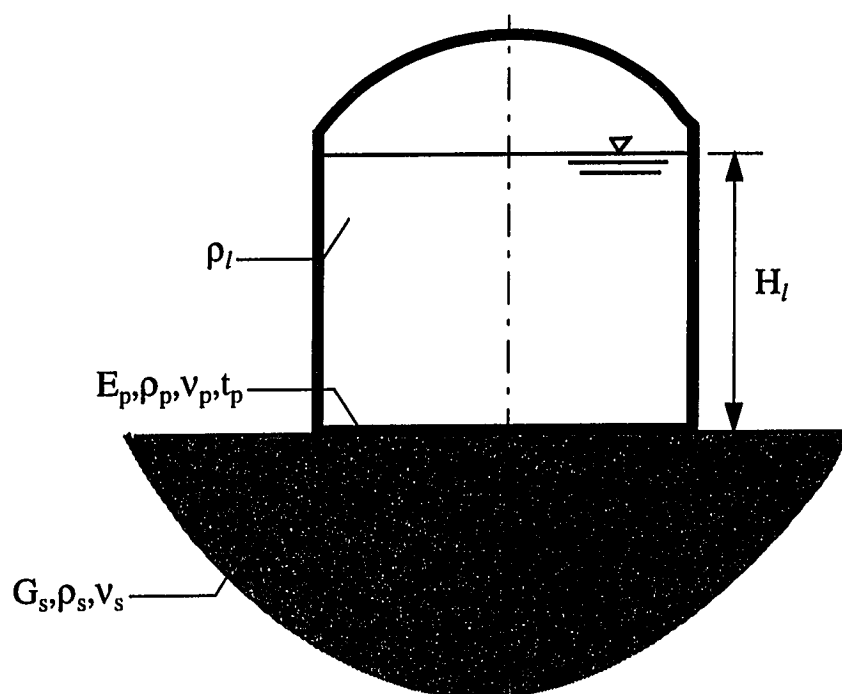


FIG. 7.1(a) System Considered

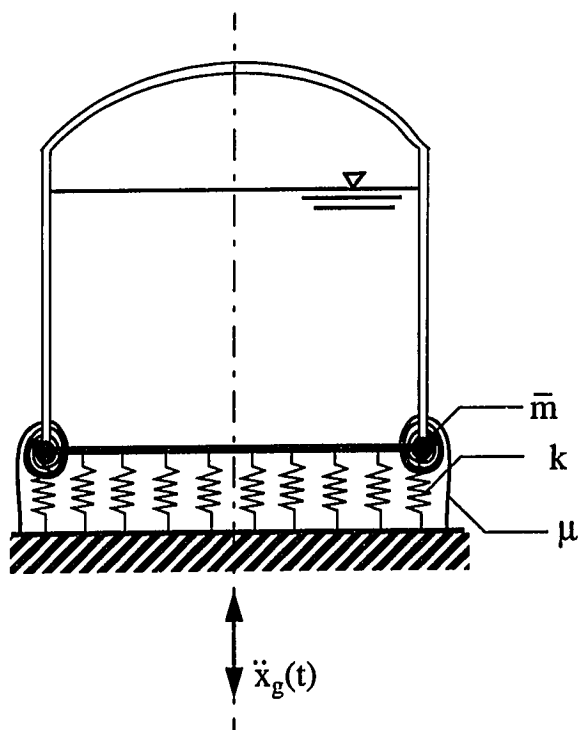


FIG. 7.1(b) Model Considered

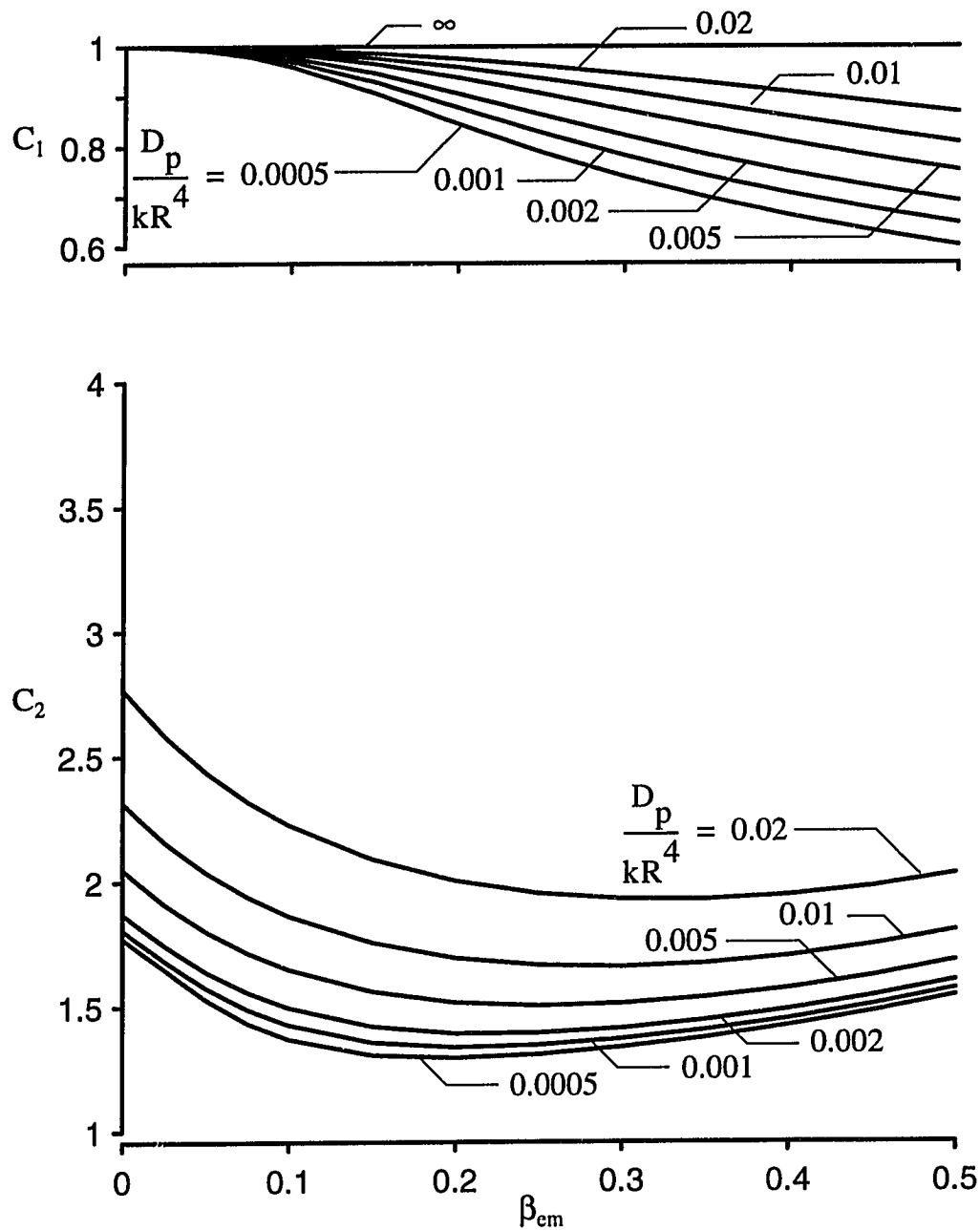


Figure 7. 2 Frequency coefficients for first two modes of vibration for elastically supported flexible base plate hinged at edge;  $H_l/R = 1.0$ ,  $\beta_p = 0.1$ ,  $\nu_p = 0.17$

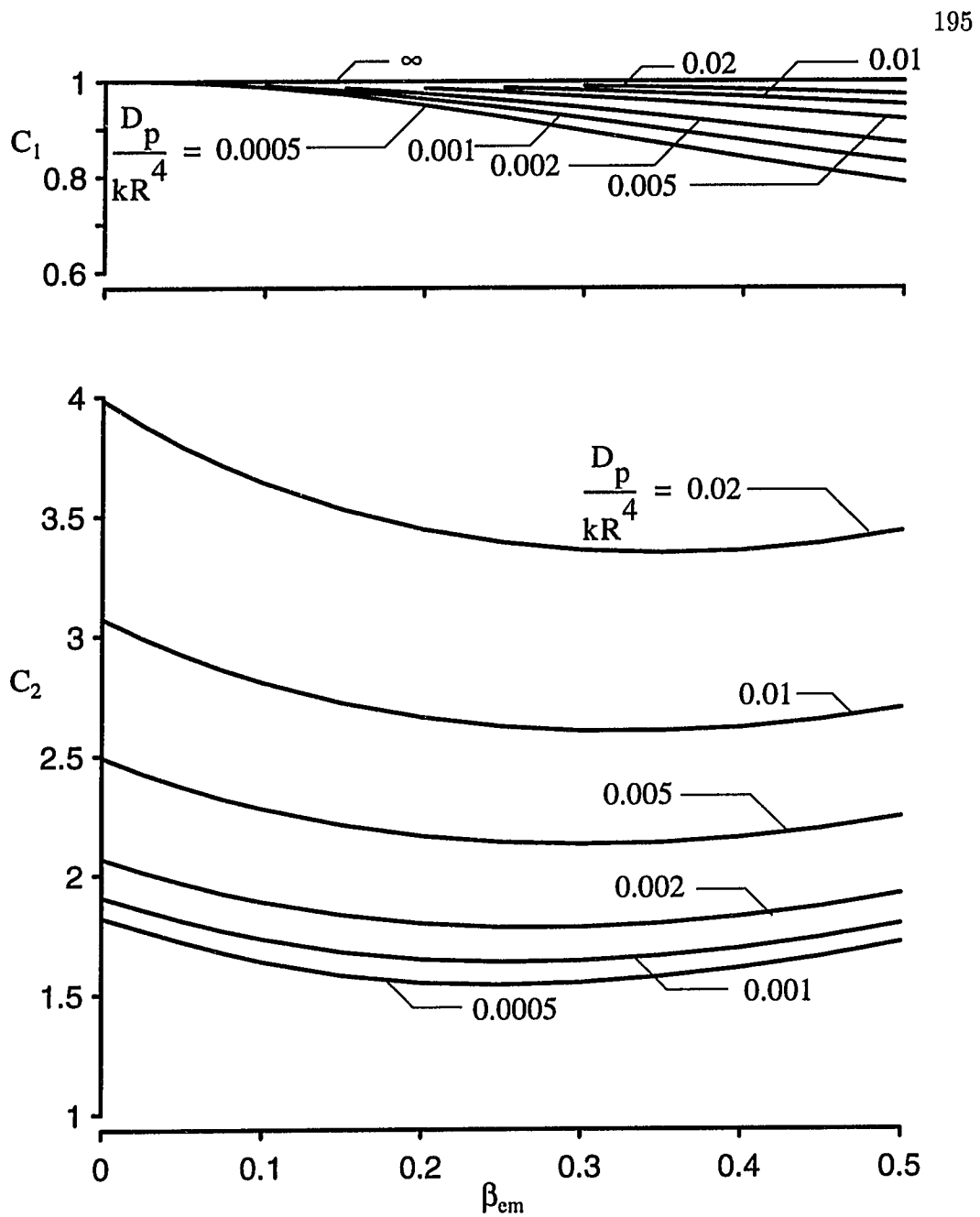


Figure 7.3 Frequency coefficients for first two modes of vibration for elastically supported flexible base plate clamped at edge;  $H_l/R = 1.0$ ,  $\beta_p = 0.1$ ,  $\nu_p = 0.17$

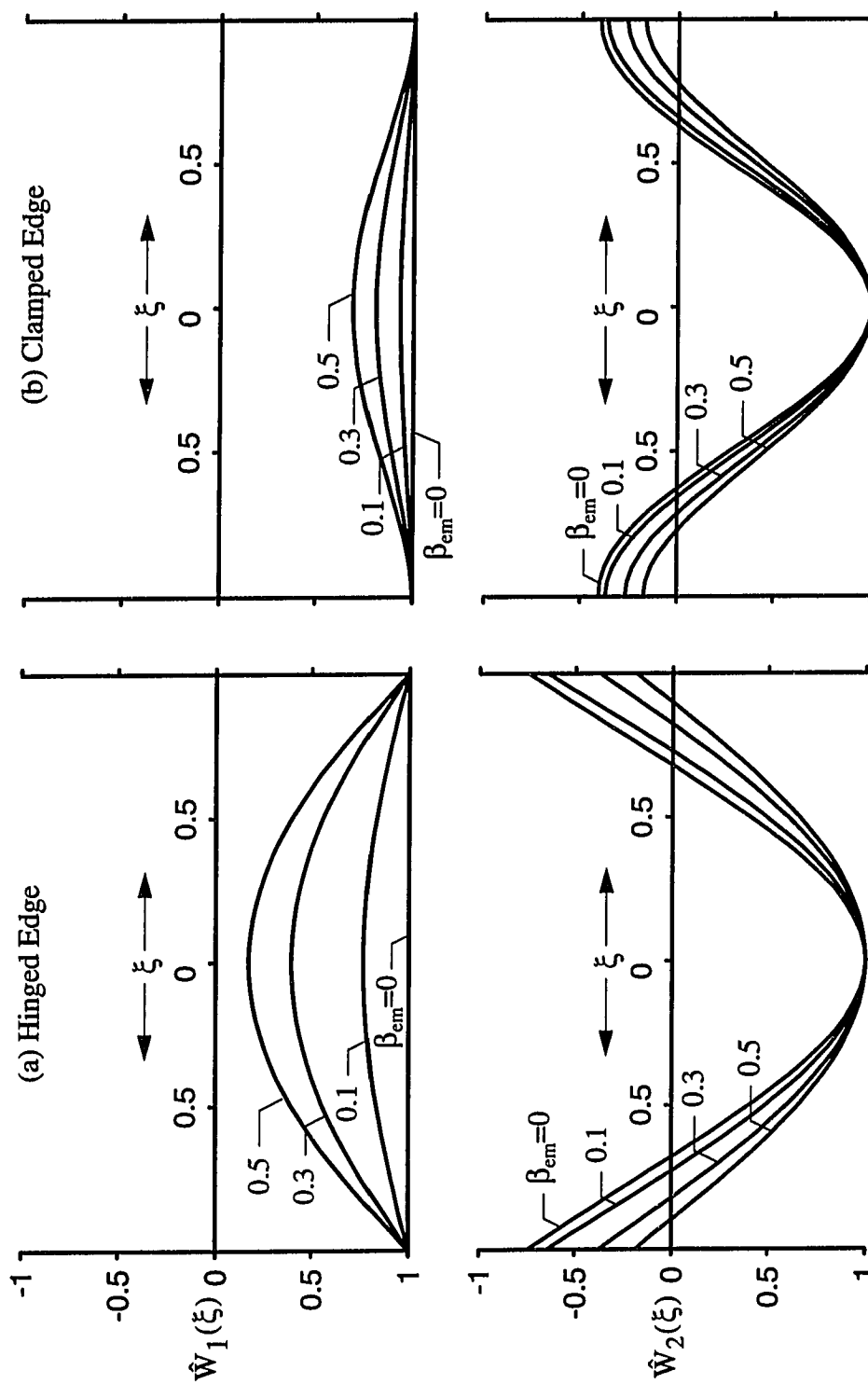


Figure 7.4 Modal displacement amplitudes for first two modes of vibration of elastically supported flexible plate;  
 $H_l/R = 1$ ,  $\beta_p = 0.1$ ,  $v_p = 0.17$ ,  $D_p/kR^4 = 0.02$

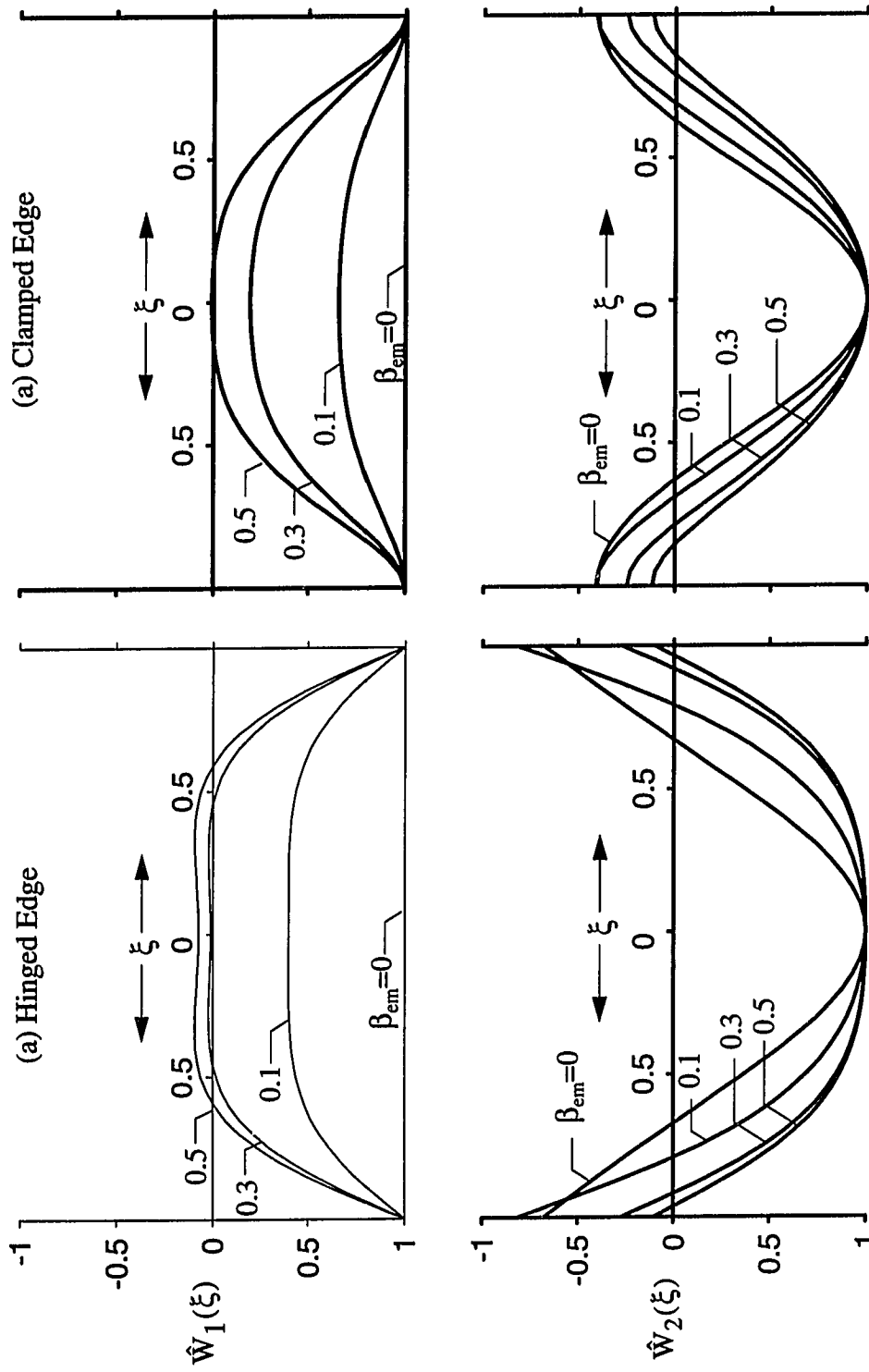


Figure 7.5 Modal displacement amplitudes for first two modes of vibration of elastically supported flexible plate;  
 $H_l/R = 1$ ,  $\beta_p = 0.1$ ,  $v_p = 0.17$ ,  $D_p/kR^4 = 0.001$

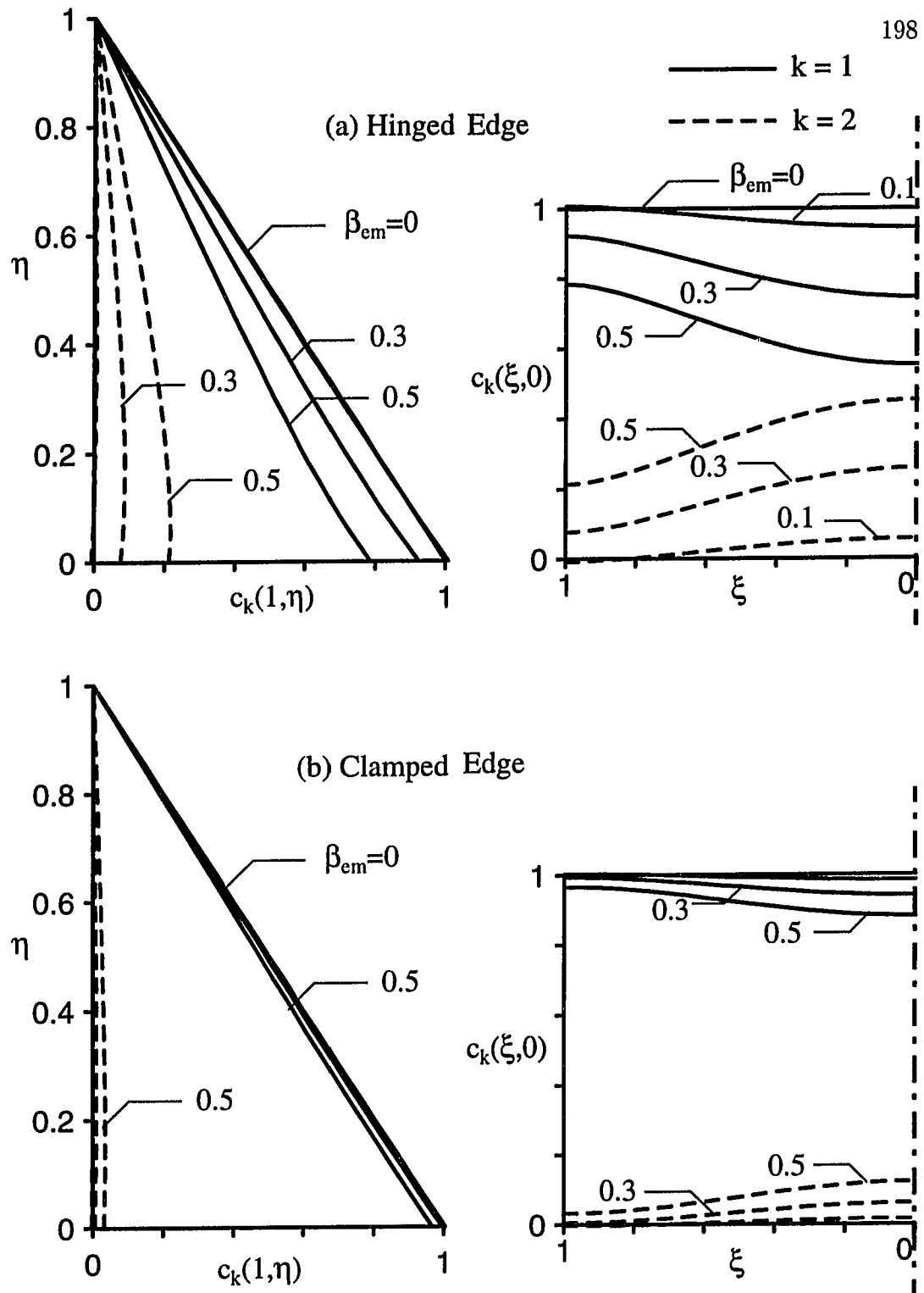


Figure 7.6 Wall and base pressure distributions for first two modes of vibration; Systems with  $H_l/R = 1.0$ ,  $\beta_p=0.1$ ,  $v_p=0.17$ ,  $D_p/kR^4 = 0.02$

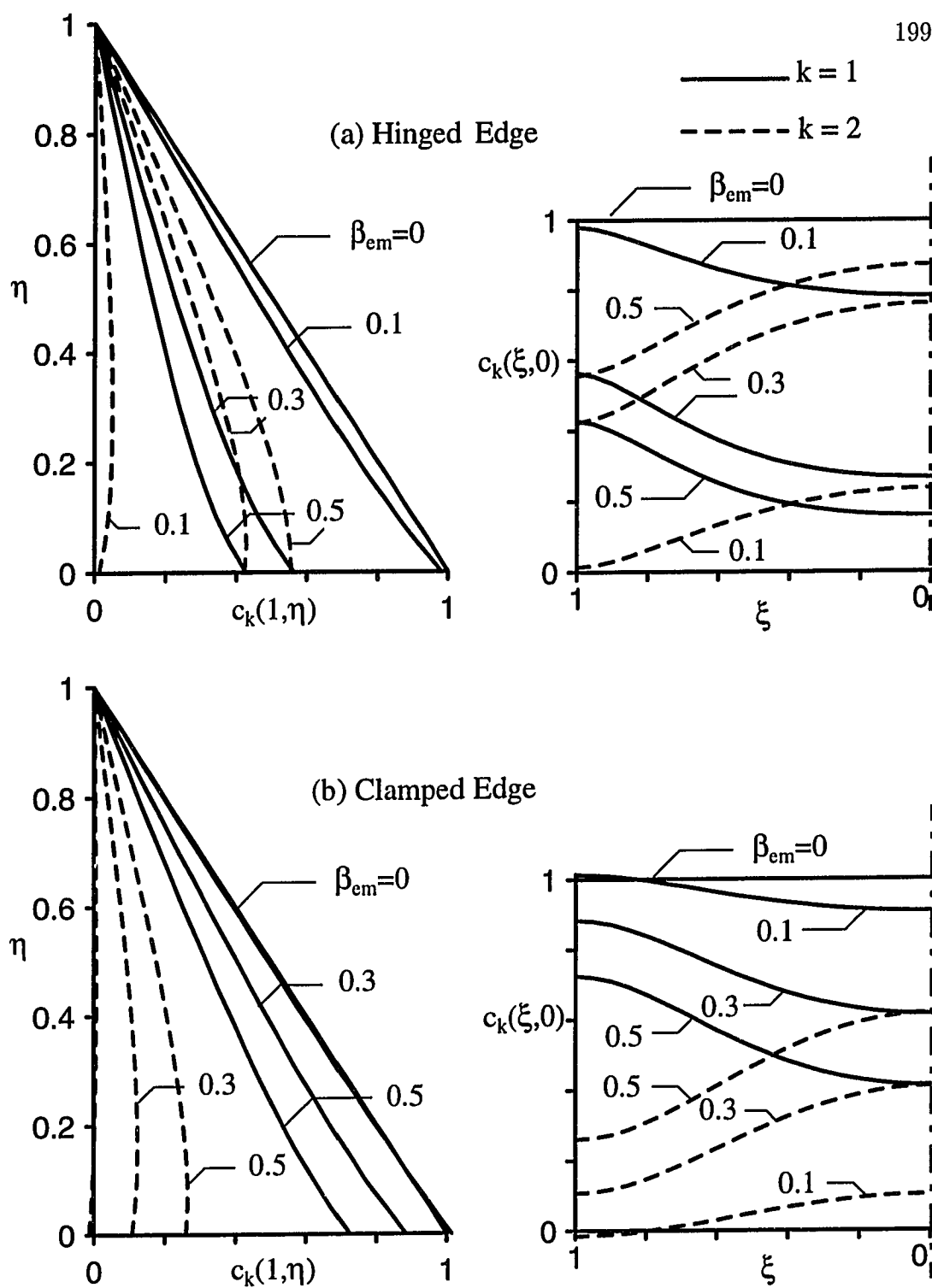


Figure. 7.7 Wall and base pressure distributions for first two modes of vibration; Systems with  $H_l/R = 1.0$ ,  $\beta_p=0.1$ ,  $v_p=0.17$ ,  $D_p/kR^4 = 0.001$



## Chapter 8

### Effects of Roof-Liquid Impact

#### 8.1 Introduction

The dynamic response of tank-liquid systems is generally assessed by allowing the contained liquid to slosh freely, i.e., by presuming the tank to have sufficient freeboard so that there is no contact between the sloshing liquid and the roof. In a number of tanks in nuclear facilities storing high-level radioactive wastes, however, the freeboard provided may be quite small, and the sloshing induced by a ground motion may cause the liquid to collide with the roof. This impact can induce localized high-magnitude pressures on the roof that vary rapidly with time. These pressures are, in turn, transmitted to the side-wall, and this may lead to significant forces acting over relatively small areas of the wall. Such collisions can occur repeatedly and may cause significant damage to the roof and tank thereby allowing the liquid contents to spill over.

There has been considerable interest in a variety of liquid-solid impact problems over the past six decades and a number of studies have been conducted in areas like seaplane landing, torpedo entry, ship slamming, wave impact on offshore platforms/tubular members, etc, [14, 29, 30, 41, 48, 49, 51, 63, 77, 78]. The pioneering contributions were made by Von Karman [77] and Wagner [78]. A survey of the early literature on the subject has been given by Szebehely and Ochi [54]. Many recent efforts have also been made to study the effects of sloshing impact in roofed tanks, [2, 4, 31, 34, 45, 46, 53, 83]. These exploratory studies have been both experimentally and numerically based, and the main focus has been to assess the impact pressures occurring at the junction of the tank-wall and roof.

There is need for further study of the roof-liquid impact problem. Many of the present studies have not been comprehensive and existing knowledge has been largely based on empirical/semi-analytical analyses. It is necessary to conveniently and rationally assess the peak impact forces and pressures that are induced on the tank-roof and make a critical investigation of the parameters controlling the response. It is also

necessary to estimate the impact effects that are transmitted to the tank-wall. For the embedded systems of current interest, the effects induced on the thin side-walls may frequently be of greater concern than those acting on the roof itself. The present study is intended to be responsive to these needs. The objectives of the study are :

- To provide rational estimates of the impact forces and pressures acting on the tank roof and also derive the spatial and temporal distributions of the impact effects that are transmitted to the tank-wall.
- To assess the importance of the wall impact effects by comparing them to previously established impulsive and convective effects.

The emphasis is placed on obtaining conservative, yet realistic estimates of the peak impact effects. The study is initially confined to two-dimensional motions in long, rectangular tanks and the results are then used to assess the corresponding effects in cylindrical tanks. The validity of the results is established by relating them to limited information available in the literature. Comprehensive numerical solutions are presented to elucidate the effects and relative importance of the parameters involved.

## 8.2 System Considered

The system considered is shown in Fig. 8.1. It is a vertical, cylindrical tank filled with liquid to a height  $H$ . The liquid is considered to be incompressible, inviscid and to be of uniform mass density  $\rho_l$ . The tank is of a circular cross-section of radius  $R$ . It is presumed to be anchored to a rigid moving plate at the base and to be covered by a rigid roof at the top.

The free-board distance between the mean liquid surface and the junction of the roof and tank wall is denoted by  $d_o$ . At any angle  $\theta$ , the instantaneous value of the theoretical wall displacement is denoted by  $d_w(\theta, t)$ . The maximum value occurs along  $\theta = 0$  and is denoted by  $d_{max}$ . Impact occurs for values of  $d_w(\theta, t) \geq d_o$ . The instantaneous length of the roof that is intersected by the rising free-surface is denoted by  $c_o(\theta, t)$  and the instantaneous half-angle of the impacted area is denoted by  $\theta_o(t)$ . Fig. 8.2 shows the maximum values of the impacted roof areas for different values of  $d_o/d_{max}$ .

The ground motion is considered to be horizontal and uniform and to be directed along the  $\theta = 0$  coordinate axis. The acceleration of the ground motion at any time,  $t$ , is denoted by  $\ddot{x}_g(t)$ , and the corresponding velocity and displacement are denoted by  $\dot{x}_g(t)$  and  $x_g(t)$ , respectively.

### 8.3 Background

Previous studies dealing with the tank roof-liquid impact problem have been both experimentally and numerically based, [2, 4, 31, 34, 45, 46, 53, 83].

*Experimental Studies* [4, 31, 34, 45, 83] : These have mainly focussed on measuring the peak impact pressures acting on the tank roof. Empirical/semi-analytical expressions have also been proposed in some of these studies to predict the peak impact pressure. A brief review of the more important conclusions are presented in this section.

The peak impact roof pressure induced on cone-roofs making an angle  $\alpha$  with the horizontal has been evaluated by Kobayashi [31] as

$$[p_r]_{max} = \rho_l \frac{\pi}{2} \cot \alpha v_o^2 \quad (8.1)$$

where  $v_o$  is the velocity at the instant of initial impact. Since equation (8.1) increases to infinity as  $\alpha \rightarrow 0$ , a different empirical formula has been proposed for flat roofs, [69, 31, 4],

$$[p_r]_{max} = 225 \rho_l v_o^{1.6} \quad (8.2)$$

where  $v_o$  is given in  $cm/sec$  and  $(p_r)_{max}$  is given in  $kgf/cm^2$  ( $1 \text{ } kgf/cm^2 = 14.23 \text{ } psi$ ).

Comparisons made by Yashiro et al in [83] between the peak pressures evaluated from equation (8.2) and experimentally measured pressures induced by water impacting a rigid flat roof have shown good agreement with one another. The experiments have been conducted for sinusoidal base excitations with a frequency equal to the fundamental sloshing frequency of the system. Limited information on the distributions of the pressures acting on the roof and tank-wall has also been provided in [83]. To eliminate the need to consider repeated impacts, the critical surface wave that induces maximum impact has been experimentally identified as that reaching a theoretical height  $d_w$  that is twice the available free-board  $d_o$ .

More recently, a series of experiments have been conducted by Kurihara et al [34] for the impact of waves in reactor vessels. Test results for three types of flat-roofed models placed on long-period large-amplitude shaking table have been provided for both sinusoidal and seismic ground motions. Furthermore, based on the test results, a semi-analytical formula has been proposed for the peak impact roof pressure,  $[p_r]_{max}$ ,

$$[p_r]_{max} = 6.63 \frac{(1 + d_o/H)(1 + d_o/H + 0.2R/H)}{(1 + d_o/H + 0.4R/H)^2} \rho_l R \frac{v_o^2}{d_o}$$

$$+ 0.35 \frac{(1 + d_o/H)}{(1 + d_o/H + 0.4R/H)} \rho_l R \omega_1 v_o \quad (8.3)$$

where  $\omega_1$  is the fundamental sloshing frequency of the liquid. While the peak roof pressures given by equation (8.3) match the experimental results in [34], they have not been in agreement with the values predicted by equation (8.2).

General impact between two-dimensional solids and liquids has been considered in a recent analytical study by Cointe [13]. Curvatures of both impacting surfaces have been considered. The impact effects have been evaluated by the method of matched asymptotic expansions and the maximum impact force has been conveniently expressed in the form,

$$F_{max} = 2 \pi \rho_l \frac{R_l R_s}{R_l + R_s} v_o^2 \quad (8.4)$$

where  $R_l$  and  $R_s$  are the radii of curvature of the liquid and solid respectively.

*Numerical studies* [2, 3, 46, 53] : A variety of methods including finite-difference and boundary-element techniques have been recently used for the roof-liquid impact problem. Such numerical techniques have also been used for other common solid-liquid impact problems and a comparative analysis for the liquid-cylinder impact problem has been presented in [26]. Currently, the most accurate and commonly used numerical methods are extensions of finite-difference based programs, SOLA-SURF and SOLA-VOF, originally developed for free-surface flows in [22, 23].

For the roof-liquid impact problem, the aim of the numerical studies has been to assess the entire time history of the liquid sloshing and to model the repeated impacts between the liquid and the tank roof. This has been accomplished by switching between zero velocity and zero pressure boundary conditions for the constrained and unconstrained liquid surfaces respectively. While this has generally resulted in meaningful displacement and velocity profiles over the entire time history, [46], very little information has been presented for the impact pressures/forces, and at the present time, there is no general consensus or expressions for the critical impact effects.

## 8.4 Method of Analysis

The method is formulated herein for long rectangular tanks having flat roofs and is subsequently extended to the cylindrical case. Suitable modifications are finally incorporated into the analysis to account for sloping roofs.

### 8.4.1 Fundamental Relations and Assumptions

For cylindrical tanks, the instantaneous value of the surface displacement is given by, (see for example, [65])

$$d(r, \theta, t) = R \sum_{m=1}^{\infty} \frac{2}{\lambda_m^2 - 1} \frac{A_m(t)}{g} \frac{J_1(\lambda_m r/R)}{J_1(\lambda_m)} \cos \theta \quad (8.5)$$

where  $J_1$  = the Bessel function of the first kind and first order;  $\lambda_m$  = the  $m$ th zero of the first derivative of  $J_1$ , of which the first three values are

$$\lambda_1 = 1.841 \quad \lambda_2 = 5.331 \quad \lambda_3 = 8.536 \quad (8.6)$$

$A_m(t)$  is the instantaneous pseudoacceleration of a simple oscillator, defined by

$$A_m(t) = \omega_m \int_0^t \ddot{x}_g(\tau) \sin \omega_m(t - \tau) d\tau \quad (8.7)$$

where  $\omega_m$  is the circular natural frequency of the  $m$ th horizontal sloshing mode of vibration, given by

$$\omega_m^2 = \tanh \left( \frac{\lambda_m H}{R} \right) \frac{\lambda_m g}{R} \quad (8.8)$$

In order to derive a simple and rational solution for the impact problem, it is necessary to develop an appropriate model for the design impinging wave. Accordingly, the following simplifications are made :

- The free-surface sloshing motion is predominantly harmonic in nature and the motion has a frequency that is approximately equal to the fundamental sloshing frequency of the system. This follows from the fact that for realistic tank-liquid systems and ground excitations, the fundamental mode of vibration predominates the sloshing response and the associated sloshing frequency is much lower than the dominant frequencies of the ground motion and of the tank-liquid system.
- The critical case for maximum impact is taken to be the cycle during which the wall displacement along the  $\theta = 0$  axis reaches its theoretical maximum,  $d_{max}$ . This assumption eliminates the need to consider repeated impacts and is believed to be more conservative than the recommendation made by Yashiro et al [83].  $d_{max}$  is given by the relation,

$$d_{max} = 0.837 R \frac{A_1}{g} \quad (8.9)$$

where  $A_1$  is the spectral value of the fundamental pseudoacceleration.

- The contributions of the higher modes are of increasing importance for evaluating the free surface velocity and acceleration. The maximum velocity,  $v_{max}$ , and the maximum acceleration,  $a_{max}$ , are evaluated herein by including the contribution of the second mode and combining by the SRSS rule,

$$v_{max} = R \sqrt{(0.837 \omega_1 \frac{A_1}{g})^2 + (0.073 \omega_2 \frac{A_2}{g})^2} \quad (8.10)$$

$$a_{max} = R \sqrt{(0.837 \omega_1^2 \frac{A_1}{g})^2 + (0.073 \omega_2^2 \frac{A_2}{g})^2} \quad (8.11)$$

Based on these assumptions, the kinematics of the design impinging wave for the cylindrical system can be expressed in the form,

$$\begin{aligned} d(r, \theta, t) &= d_{max} \frac{J_1(\lambda_1 r/R)}{J_1(\lambda_1)} \sin \omega_1 t \cos \theta \\ v(r, \theta, t) &= v_{max} \frac{J_1(\lambda_1 r/R)}{J_1(\lambda_1)} \cos \omega_1 t \cos \theta \\ a(r, \theta, t) &= a_{max} \frac{J_1(\lambda_1 r/R)}{J_1(\lambda_1)} \sin \omega_1 t \cos \theta \end{aligned} \quad (8.12)$$

As mentioned before, the impact study herein is based on a two-dimensional analysis and it is necessary to have equivalent 2-D expressions for the impinging wave. These are obtained herein by neglecting  $\cos \theta$  in the above expressions and replacing  $J_1(\lambda_1 r/R)/J_1(\lambda_1)$  by  $\sin \pi x/2R$ , i.e.,

$$\begin{aligned} d(x, t) &= d_{max} \sin \frac{\pi x}{2R} \sin \omega_1 t \\ v(x, t) &= v_{max} \sin \frac{\pi x}{2R} \cos \omega_1 t \\ a(x, t) &= a_{max} \sin \frac{\pi x}{2R} \sin \omega_1 t \end{aligned} \quad (8.13)$$

#### 8.4.2 Impact Effects for Flat Roofs

##### Long Rectangular Tanks

Impact commences at the instant when the wall-value of the displacement,  $d_w(t) = d(R, t)$ , becomes equal to the provided free-board,  $d_o$ . At any later time, the length of the roof that is covered by the rising free-surface,  $c_o(t)$ , is given by

$$\frac{c_o(t)}{R} = \frac{2}{\pi} \cos^{-1} \frac{d_o}{d_w(t)} \quad (8.14)$$

**Wetting Correction :** While  $c_o(t)$  is the intersection length between the roof and the rising free-surface, the actual impacted length  $c(t)$  will be larger because the liquid splashes and covers a larger portion of the roof. The splashing action occurs in such a manner that the volume of liquid which would have theoretically crossed the roof is conserved by a rearrangement of the free surface. This modification to  $c_o(t)$ , commonly referred to as the wetting correction, was first introduced by Wagner [78] in his studies of a wedge penetrating a quiescent free-surface. The impacted length,  $c(t)$ , is related to the intersection length,  $c_o(t)$ , by

$$c(t) = w(t) c_o(t) \quad (8.15)$$

where  $w(t)$  is the wetting correction factor.

It is shown in Appendix D that at initial stages of impact, the wetting correction factor for the two-dimensional case considered herein is equal to  $\sqrt{2}$ . At the final stages of impact, since the velocity with which the liquid strikes the roof is zero, there should be no splashing and the associated wetting correction factor should reduce to unity. On taking  $w(t)$  proportional to the instantaneous velocity of impact and satisfying the initial and final values for  $w(t)$ , one obtains

$$w(t) = 1 + (\sqrt{2} - 1) \frac{v_w(t)}{v_o} \quad (8.16)$$

where  $v_w$  is the instantaneous wall value of the sloshing velocity and  $v_o$  is the associated velocity at initial impact.

**Roof Impact Force :** In a manner analogous to that employed by Von Karman [77] and Wagner [78] in their studies for seaplane landing, and subsequently used for a variety of impact problems by a number of others, [14, 15, 29, 49, 50], the force of impact per unit normal width of the roof is given by the time rate of change of the fluid momentum associated with the impacted portion of the roof,

$$F_r(t) = \frac{\partial}{\partial t} [m(t) v_{av}(t)] = \frac{\partial m}{\partial t} v_{av}(t) + m(t) a_{av}(t) \quad (8.17)$$

where  $v_{av}(t)$  and  $a_{av}(t)$  are the vertical velocity and acceleration of impact respectively, averaged over the impacted length  $c(t)$ . The use of average values within the impacted region is generally valid since the impact phenomenon is very rapid, [30]. The relevant expressions for the average velocity and acceleration are given by

$$v_{av}(t) = v_w(t) \frac{\sin(\pi c(t)/2R)}{(\pi c(t)/2R)} \quad (8.18)$$

$$a_{av}(t) = a_w(t) \frac{\sin(\pi c(t)/2R)}{(\pi c(t)/2R)} \quad (8.19)$$

where  $v_w(t)$  and  $a_w(t)$  are evaluated by taking  $x = R$  in the appropriate expressions of equation (8.13).

$m(t)$  is the effective mass of liquid impacting with the roof. It is a measure of the liquid inertia that is affected by the impact with the roof and is commonly referred to as the ‘virtual mass’ or the ‘added mass’. As shown in Appendix D, the instantaneous value of  $m(t)$  for the two-dimensional roof-liquid impact problem is approximately given by the mass of liquid contained in a quarter circle of radius  $c(t)$ ,

$$m(t) = \rho_l \frac{\pi}{4} c(t)^2 \quad (8.20)$$

This expression is approximate since no provision has been made for the effects of the far-wall and of the tank-base. While these constraining boundaries tend to increase the value of  $m(t)$ , (see References [61, 64]), the increase is very slight for the small values of  $c(t)$  that are normally associated with maximum impact and can be conveniently neglected.

Using equation (8.20), the time derivative of  $m(t)$  is given by

$$\frac{\partial m}{\partial t} = \rho_l \frac{\pi}{2} c \frac{\partial c}{\partial t} \quad (8.21)$$

where  $\partial c/\partial t$  represents the velocity with which the roof is covered by the rising liquid and is obtained by differentiating equation (8.15) with respect to time.

The instantaneous value of the impact force,  $F_r(t)$ , is finally obtained by substituting equations (8.18), (8.19), (8.20) and (8.21) into equation (8.17). The maximum impact force is then found to occur at the instant of initial impact and to be given by

$$F_{r,max} = \rho_l \frac{4R^2}{\pi d_o} v_o^2 \quad (8.22)$$

The impulse-momentum approach outlined herein has also been used in the study by Kurihara et al [34] for evaluating the roof impact force. The significant exceptions in the latter study are that no wetting correction factor has been employed and the participating liquid mass  $m(t)$  has been estimated differently. The maximum roof force by Kurihara’s approach has been found to be

$$[F_{r,max}]_{Kurihara} = \rho_l \frac{14R^2}{\pi^2 d_o} v_o^2 \quad (8.23)$$



which is only about 11 % larger than that of equation (8.22). Another confirmation for the present approach is that equation (8.22) for the half-structure considered herein can be shown to be identical to one-half the value computed from Cointe's formula (equation 8.4) by putting  $R_s = \infty$  and  $R_l = \partial x^2 / \partial^2 d|_{x=R}$  in the latter equation.

The analytical prediction that the impact force rises instantaneously from zero to its finite maximum value is not in agreement with experimental data which indicate that the maximum force occurs after a small interval of time. Several factors can be attributed for the finite rise time, [12, 48] : (1) the formation of an air cushion between the roof and liquid surface, (2) free-surface deformation prior to impact, (3) entrapped air in the liquid, etc. These factors might also result in a reduction in the magnitude of the maximum force and the effect of these factors can be expected to become more significant as the free-board  $d_o$  decreases.

*Zero Free-Board* : For the limiting case of  $d_o = 0$ , the liquid acts impulsively and the force over the impacted portion of the roof can be conveniently evaluated from a pressure distribution that increases linearly from 0 at the center to  $\rho_l R \ddot{x}_g(t)$  at the tank-wall,

$$F_{limit}(t) = 0.5 \rho_l R^2 \ddot{x}_g(t) \quad (8.24)$$

It is of interest to check if the above result is in the same order of magnitude as the limiting value of the average impact force evaluated from equation (8.17). For the latter force, on assuming that a lamina of constant length  $R$  is introduced into the liquid, putting  $m = \rho_l \pi R^2 / 4$  and  $\partial m / \partial t = 0$ , one obtains

$$F_{limit}(t) = m a_{av}(t) = \frac{\pi}{4} \rho_l R^2 a_{av}(t) \quad (8.25)$$

where  $a_{av}$  is the average acceleration of the liquid. For rectangular tanks,  $a_{av}(t)$  is given by

$$a_{av}(t) = \frac{\int_0^R \ddot{d}(x, t) dx}{R} = R \sum_{m=1}^{\infty} \frac{16(-1)^{m+1}}{(2m-1)^3 \pi^3} \frac{\ddot{A}_m(t)}{g} \quad (8.26)$$

On using the relation  $\ddot{A}_m(t) = \omega_m^2 (\ddot{x}_g(t) - A_m(t))$ , and expressing  $\omega_m^2$  in a form similar to equation (8.8), one obtains

$$a_{av}(t) = \sum_{m=1}^{\infty} \frac{8(-1)^{m+1}}{(2m-1)^2 \pi^2} \tanh \frac{(2m-1)\pi H}{2R} (\ddot{x}_g(t) - A_m(t)) \quad (8.27)$$

Now,  $A_m(t)$  in the above equation can be taken as zero since the impact force for the limiting case of zero free-board theoretically occurs for zero sloshing. Equation (8.25)

is then written as

$$F_{limit} = \frac{2}{\pi} \rho_l R^2 \ddot{x}_g(t) \sum_{m=1}^{\infty} \frac{(-1)^{m+1}}{(2m-1)^2} \tanh \frac{(2m-1)\pi H}{2R} \quad (8.28)$$

A comparison of the roof force values obtained from equations (8.24) and (8.28) are presented below for values of  $H/R$  in the range from 0.3 to 2.

$H/R$	Values of $F_{limit}/\rho_l R^2 \ddot{x}_g(t)$	
	equation (8.24)	equation (8.28)
0.3	0.5	0.234
0.5	0.5	0.365
1.0	0.5	0.530
2.0	0.5	0.581

It is seen that while the impulse-momentum approach yields limiting results that are in good agreement with the exact results for tall tank-liquid systems with  $H/R \geq 1$ , the results are generally on the smaller side for broad tank-liquid systems. It should be noted, however, that for the latter systems, the previously neglected effects of the tank-base will be quite important. The virtual liquid mass for the lamina of length  $R$  considered herein will be significantly increased by the base-plate and this, in turn, should increase the associated roof force to the same order of magnitude as equation (8.24).

**Roof Impact Pressure :** The average impact pressure acting on the roof,  $p_r(t)$ , is given by

$$p_r(t) = \frac{F_r(t)}{c(t)} = \rho_l \frac{\pi}{2} \frac{\partial c}{\partial t} v_{av}(t) + \rho_l \frac{\pi}{4} c(t) a_{av}(t) \quad (8.29)$$

At the beginning stages of impact, since the analytical value of  $F_r$  is finite and  $c \rightarrow 0$ , it follows that  $p_{r,max} \rightarrow \infty$ . Alternately, the infinite pressure value follows from the fact that  $\partial c/\partial t \rightarrow \infty$  at the beginning stages of impact. In reality, there is no instantaneous infinite pressure and in a manner similar to the impact force, the maximum pressure occurs only after a short rise time.

The magnitude of the peak impact pressure and the rise time cannot be obtained by the simplifying assumptions involved in an irrotational, incompressible flow: The compressibility of the liquid may be important at the beginning of impact [7, 32], when the apparent growth velocity of the flat plate,  $\partial c/\partial t$ , is greater than the velocity of sound in the liquid. When the compressibility is taken into account, following the

suggestion of Von Karman [78] for flat plate-liquid impact, the peak pressure may be taken equal to the acoustic pressure of the liquid,

$$p_{r,max} = \rho_l c_s v_o \quad (8.30)$$

where  $c_s$  is the velocity of sound in the liquid. While the above equation accounts for the compressibility of the liquid and yields a finite value for the peak impact pressure, related studies dealing with flat body-water impact [76, 37] have shown that air cushioning may cause the impact pressure to reduce to about one-tenth of the value given by equation (8.30).

Other studies dealing with the impact of waves on flat offshore decks or walls, [9, 51], have shown that air entrainment can have a significant effect on the peak pressure, that the characteristics of this air entrainment are essentially random in nature, and that the magnitude, rise time for the peak pressure are also random in nature. In the absence of more sophisticated analyses that account for these factors, the peak pressure acting on the roof and its rise time need to be determined from equation (8.30) or from experimental observations, as in [34]. In the latter study, based on the experimental data, it has been proposed that the maximum pressure be considered to occur when the theoretical free-surface has crossed the roof to a height of  $1.05 d_o$ . This, in turn, corresponds to a value of  $c_o/R \approx 0.2$ . On making use of these values, the peak impact pressure has been obtained in the form of equation (8.3).

**Wall Impact Effects :** With the roof pressure established, the instantaneous value of the impact pressure at any point in the rectangular tank is obtained by solving for the associated potential function  $\phi$ . The derivation is shown in Appendix D and the final expression is given by

$$p(x, y, t) = p_r(t) \left[ \frac{c(t)}{2R} + \sum_{n=1}^{\infty} \frac{2}{n\pi} \frac{\cosh(n\pi y/2R)}{\cosh(n\pi H/2R)} \sin \frac{n\pi c(t)}{2R} \cos \frac{n\pi(x-R)}{2R} \right] \quad (8.31)$$

where  $p_r(t)$  is the impact pressure acting on the roof.

The wall impact effects per unit normal width of the rectangular tank can then be obtained by integrating the corresponding values of the wall pressures over the height  $H$ . For the near-wall ( $x = R$ ), the wall force is given by

$$F_{w,near}(t) = F_r(t) \left[ \frac{H}{2R} + \frac{R}{c(t)} \sum_{n=1}^{\infty} \frac{4}{n^2\pi^2} \tanh \frac{n\pi H}{2R} \sin \frac{n\pi c(t)}{2R} \right] \quad (8.32)$$

and the wall moment is given by

$$M_{w, near}(t) = F_r(t) H \left[ \frac{H}{4R} + \frac{R}{c(t)} \sum_{n=1}^{\infty} \frac{4}{n^2 \pi^2} \left\{ \tanh \frac{n\pi H}{2R} - \frac{2R}{n\pi H} \left( 1 - \frac{1}{\cosh n\pi H/2R} \right) \right\} \sin \frac{n\pi c(t)}{2R} \right] \quad (8.33)$$

Similarly, for the far-wall ( $x = -R$ ), the wall force is given by

$$F_{w, far}(t) = F_r(t) \left[ \frac{H}{2R} + \frac{R}{c(t)} \sum_{n=1}^{\infty} \frac{4(-1)^n}{n^2 \pi^2} \tanh \frac{n\pi H}{2R} \sin \frac{n\pi c(t)}{2R} \right] \quad (8.34)$$

and the wall moment is given by

$$M_{w, far}(t) = F_r(t) H \left[ \frac{H}{4R} + \frac{R}{c(t)} \sum_{n=1}^{\infty} \frac{4(-1)^n}{n^2 \pi^2} \left\{ \tanh \frac{n\pi H}{2R} - \frac{2R}{n\pi H} \left( 1 - \frac{1}{\cosh n\pi H/2R} \right) \right\} \sin \frac{n\pi c(t)}{2R} \right] \quad (8.35)$$

The total effects that are transmitted to the base are then given by

$$F_t(t) = F_{w, near}(t) - F_{w, far}(t) \quad M_t(t) = M_{w, near}(t) - M_{w, far}(t) \quad (8.36)$$

### Cylindrical Tanks

In order to simplify the problem, the approach followed herein is to extend the two-dimensional results to the three dimensional case after making suitable assumptions for the circumferential variations of the impact effects. The resulting expressions are approximate but are believed to be conservative estimates of the impact effects for cylindrical tanks. This follows from the well-established fact that the freedom for a liquid to move in three dimensions has the effect of reducing the participating liquid mass and consequently the impact, [61]. An approximate measure of the degree of conservatism of the approach is also provided.

**Geometry of Impacted Area :** From equation (8.12), the instantaneous value of the half-angle of the impacted area,  $\theta_o(t)$ , is evaluated to be

$$\theta_o(t) = \cos^{-1} \frac{d_o}{d_w(0, t)} \quad (8.37)$$

and for an angle  $\theta \leq \theta_o(t)$ , the instantaneous value of the intersection length,  $c_o(\theta, t)$ , is given by

$$\frac{c_o(\theta, t)}{R} = \frac{2}{\pi} \cos^{-1} \left( \frac{d_o}{d_w(0, t) \cos \theta} \right) \quad (8.38)$$

The associated value of the impacted length,  $c(\theta, t)$  is then given by

$$c(\theta, t) = w(\theta, t) c_o(\theta, t) \quad (8.39)$$

where the wetting correction factor,  $w(\theta, t)$ , is taken in the form

$$w(\theta, t) = 1 + (\sqrt{2} - 1) \frac{v_w(0, t) \cos \theta}{v_o} \quad (8.40)$$

where  $v_o$  is the wall-velocity at  $\theta = 0$  at the instant of impact.

**Roof Impact Force :** The impact force acting on the roof of the cylindrical tank is evaluated herein by assuming the roof pressure evaluated for the rectangular tank to have a cosine variation in the circumferential direction and then applying it over the impacted portion of the roof,

$$F_r(t) = \int_{-\theta_o(t)}^{\theta_o(t)} \int_{R-c(\theta, t)}^R p_r(t) \cos \theta r dr d\theta \quad (8.41)$$

**Wall Impact Pressure :** The impact pressure at any point of the cylindrical tank is obtained by the procedure shown in Appendix D and the final expression is given by

$$p(r, \theta, t) = \frac{p_r(t)}{\pi} \left[ \sum_{m=1}^{\infty} d_{m0}(t) \frac{J_0(\beta_{m0}\xi)}{J_0(\beta_{m0})^2} \frac{\cosh \beta_{m0} z / R}{\cosh \beta_{m0} H / R} + \sum_{n=1}^{\infty} \sum_{m=1}^{\infty} \frac{2 \beta_{mn}^2}{\beta_{mn}^2 - n^2} d_{mn}(t) \frac{J_n(\beta_{mn}\xi)}{J_n(\beta_{mn})^2} \frac{\cosh \beta_{mn} z / R}{\cosh \beta_{mn} H / R} \cos n \theta \right] \quad (8.42)$$

where,  $\xi = r/R$ ;  $J_n$  is the Bessel function of the first kind and the  $n$ th order;  $\beta_{mn}$  is the  $m$ th zero of  $J'_n(\beta) = 0$ ; and  $d_{mn}(t)$  is given by

$$d_{mn}(t) = \int_{-\theta_o(t)}^{\theta_o(t)} \int_{1-c(t)/R}^1 \xi J_n(\beta_{mn}\xi) \cos n \theta \cos \theta d\xi d\theta \quad (8.43)$$

**Wall Impact Forces :** With the wall impact pressure established, the associated internal tank forces can be computed by applying the wall pressure as a static load, and then using an appropriate shell theory. A simpler approach is to obtain an estimate of the peak impact effects by determining the total forces that are exerted on the wall. These total effects are obtained by appropriate integrations of the wall impact pressure given by equation (8.42).

The total impact force for the cylindrical system is given by

$$F_t(t) = \int_0^{2\pi} \int_0^H p(1, \theta, t) \cos \theta \, dz \, R \, d\theta = 4p_r(t)R^2 \sum_{m=1}^{\infty} \frac{\beta_{m1}}{\beta_{m1}^2 - 1} \frac{d_{m1}(t)}{J_1(\beta_{m1})} \tanh \frac{\beta_{m1}H}{R} \quad (8.44)$$

It should be noted that the infinite summation on  $n$  in equation (8.42) has reduced to  $n = 1$  in the above expression due to the orthogonality of the cosine functions. Furthermore, it should be noted that the  $\beta_{m1}$  factors are the same as the  $\lambda_m$  factors used in equation (8.5) and the first three values are given by equation (8.6).

The total impact moment for the cylindrical system is given by

$$M_t(t) = 4p_r(t)R^2H \sum_{m=1}^{\infty} \frac{\beta_{m1}}{\beta_{m1}^2 - 1} \frac{d_{m1}(t)}{J_1(\beta_{m1})} \left\{ \tanh \frac{\beta_{m1}H}{R} - \frac{R}{\beta_{m1}H} \left( 1 - \frac{1}{\cosh \beta_{m1}H/R} \right) \right\} \quad (8.45)$$

**Degree of Conservatism :** It is of interest to estimate the degree of conservatism inherent in extending the two-dimensional results to the three-dimensional case. This is established herein by solving a simple problem exactly for the three-dimensional case and comparing the result with the equivalent solution.

The problem considered is the axisymmetric impact of liquid on a circular disc of instantaneous contact radius  $c_o(t)$ . It has been previously shown that the wetting correction at the initial stages of impact for this case is  $w_o = 4/\pi$  (see [49]) and the associated virtual mass is  $m(t) = 4/3 \rho_l c(t)^3$  (see [43, 49]), where  $c(t) = w_o c_o(t)$ . Substituting these values into equation (8.17) and simplifying, the impact pressure at the initial stages of impact can be shown to be given by

$$p = \rho_l \frac{64 R^2}{\pi^4 d_o c_o} v_o^2 \quad (8.46)$$

The equivalent 2-D problem considered is the impact of liquid on a lamina of contact length  $2c_o(t)$ . Evaluating the associated impact length,  $2c(t) = 2\sqrt{2}c_o(t)$  and using equation (8.22), the two-dimensional impact pressure is given by

$$p_{eq} = \rho_l \frac{4 R^2}{\pi d_o \sqrt{2} c_o} v_o^2 \quad (8.47)$$

A comparison of equations (8.46) and (8.47) then reveals that the exact pressure value is about 73 % of the equivalent value.

### 8.4.3 Impact Effects for Sloping Roofs

This section deals with the impact on a roof that makes an angle  $\alpha$  with the horizontal. The analysis presented herein is, however, of more general value and can be extended

to assess the maximum impact effects for a roof with more general shape,  $y = h(x)$ . This is accomplished by defining an equivalent roof that is inclined at an angle  $\alpha_{eq}$ , given by  $\tan \alpha_{eq} = y_{max}/x_{max}$ , where  $y_{max}$  and  $x_{max}$  refer to the maximum height and projected length of the roof coming in contact with the rising liquid surface.

### Long Rectangular Tanks

Let  $s_o(t)$  refer to the instantaneous contact length between the sloping roof and the rising free-surface. The horizontal projection of this length,  $c_o(t) = s_o(t) \cos \alpha$ , is evaluated from the relation

$$d_w(t) \cos \frac{\pi c_o(t)}{2R} - d_o = \tan \alpha c_o(t) \quad (8.48)$$

For a more general roof shape, the right hand side in equation (8.48) is replaced by  $h(c_o)$ . The impacted length along the roof,  $s(t)$ , is then given by an expression similar to equation (8.15),

$$s(t) = w(t) s_o(t) = w(t) \frac{c_o(t)}{\cos \alpha} \quad (8.49)$$

where the wetting correction factor  $w(t)$  is taken in the form

$$w(t) = 1 + (\sqrt{2} - 1) \frac{v_w(t) \cos \alpha}{v_o} \quad (8.50)$$

**Impact Effects :** The impact effects are conveniently assessed herein by using the component of the liquid moving normal to the sloping roof. The roof impact force is defined in a manner similar to equation (8.17) as

$$F_r(t) = \frac{\partial}{\partial t} \left( \rho_l \frac{\pi}{4} s(t)^2 v_{n,av}(t) \right) = \rho_l \frac{\pi}{2} s(t) \frac{\partial s}{\partial t} v_{n,av}(t) + \rho_l \frac{\pi}{4} s(t)^2 a_{n,av}(t) \quad (8.51)$$

where  $v_{n,av}$  and  $a_{n,av}$  are the components of the average liquid velocity and acceleration normal to the sloping roof and are given by

$$v_{n,av}(t) = v_{n,w}(t) \frac{\sin(\pi s(t)/2R)}{(\pi s(t)/2R)} = v_w(t) \frac{\sin(\pi s(t)/2R)}{(\pi s(t)/2R)} \cos \alpha \quad (8.52)$$

and

$$a_{n,av}(t) = a_{n,w}(t) \frac{\sin(\pi s(t)/2R)}{(\pi s(t)/2R)} = a_w(t) \frac{\sin(\pi s(t)/2R)}{(\pi s(t)/2R)} \cos \alpha \quad (8.53)$$

respectively.

The average roof pressure is then given by

$$p_r(t) = \frac{F_r(t)}{s(t)} = \rho_l \frac{\pi}{2} \frac{\partial s}{\partial t} v_{n,av}(t) + \rho_l \frac{\pi}{4} s(t) a_{n,av}(t) \quad (8.54)$$

On evaluating  $\partial s/\partial t$  from equations (8.48) and (8.49), and substituting in equation (8.54), it can be shown that the maximum value of the roof pressure is given by

$$(p_r)_{max} = \rho_l \frac{\pi}{2} w_o \cot \alpha v_o^2 \quad (8.55)$$

where  $w_o$  is the wetting correction factor at initial stages of impact and is given by  $w_o = 1 + (\sqrt{2} - 1) \cos \alpha$ .

It is seen that, unlike the flat roof solutions, the maximum pressure induced on the sloping roof tends to a finite value. This follows from the fact that the growth velocities for the two roofs vary significantly at the initial stages of impact. While the growth rate for the flat roof is infinite, the corresponding rate for the sloping roof is finite,  $\partial s/\partial t = w_o v_o \operatorname{cosec} \alpha$ . It can further be noted that, with the exception of the  $w_o$  factor, equation (8.55) is identical to the one proposed by Kobayashi [31] (equation 8.1).

With the roof pressures evaluated, the wall pressures for the systems with sloping roofs can be evaluated by procedures similar to those used for flat-roofed systems. The vertical component of the roof pressure,  $p_r(t) \cos \alpha$ , acting over the horizontal projection of the impacted length,  $c(t) = s(t) \cos \alpha$ , is used in these computations. The final expression is similar to equation (8.31) and is not repeated here. The associated wall forces are finally obtained by appropriate integrations of the wall pressures.

### Cylindrical Tanks

The half-angle subtended by the horizontal projection of the impacted area is again given by equation (8.37). For an angle  $\theta \leq \theta_o(t)$ , the horizontal projection of the contact length,  $c_o(\theta, t)$ , is evaluated from the relation

$$d_w(0, t) \cos \theta \cos \frac{\pi c_o(\theta, t)}{2R} - d_o = \tan \alpha c_o(\theta, t) \quad (8.56)$$

The associated impact length,  $s(\theta, t)$ , is then defined by

$$s(\theta, t) = w(\theta, t) \frac{c_o(\theta, t)}{\cos \alpha} \quad (8.57)$$

where the wetting correction factor  $w(\theta, t)$  is taken in the form

$$w(\theta, t) = 1 + (\sqrt{2} - 1) \frac{v_w(0, t) \cos \alpha \cos \theta}{v_o} \quad (8.58)$$



**Impact Effects :** Applying the two-dimensional roof pressure values evaluated in the previous section over the impacted area of the cone-shaped roof, the roof impact force is given by

$$F_r(t) = \cos\alpha \int_{-\theta_o(t)}^{\theta_o(t)} \int_{\sqrt{R^2+H_r^2}-s(\theta,t)}^{\sqrt{R^2+H_r^2}} p_r(t) \cos\theta r dr d\theta \quad (8.59)$$

where  $H_r$  is the maximum height of the roof. The wall pressures for the systems considered can then be evaluated by applying the vertical component of the roof pressure,  $p_r(t) \cos\theta \cos\alpha$ , over the horizontal projection of the impacted area, and solving Laplace's equation in a manner similar to that indicated in Appendix D for flat-roofed systems. The associated wall forces can then be obtained by appropriate integrations of the wall pressures. The resulting expressions are quite similar to equations (8.42), (8.44) and (8.45) and are not repeated here.

## 8.5 Numerical Solutions

The numerical solutions presented in this section are for the impact pressures and forces induced on the roof and walls of rectangular and cylindrical tanks. Systems with both flat and sloping roofs are considered.

### 8.5.1 Impact Effects for Flat Roofs

It is desirable to suitably normalize the response quantities and present the results in terms of coefficients that are relatively insensitive to the tank-dimensions and wave properties. Since maximum impact effects for flat-roofed systems typically occur at or very close to the time of initial impact, the response quantities can be conveniently expressed in terms of the wave velocity at initial impact,  $v_o$ , and the corresponding wave displacement,  $d_o$ .

**Roof Effects :** Based on equation (8.22), the roof impact force for long rectangular tanks is expressed in the form

$$F_r(t) = c_{rf}(t) \rho_l R^2 \frac{v_o^2}{d_o} \quad (8.60)$$

Similarly, for the cylindrical system, the roof force is expressed in terms of  $\rho_l R^3 v_o^2/d_o$ .

The temporal variations of the normalized roof forces for rectangular and cylindrical tank-liquid systems are presented in Fig. 8.3 for a value of  $d_o/d_{max} = 0.5$ .

The time axis is normalized with respect to the fundamental period of sloshing,  $T_1$ , so that it varies between 0 and 0.25. The velocity-squared proportional slam term and the acceleration proportional inertia term are shown in the figure. The total roof force, evaluated herein as a numerical sum of the two terms, is also indicated. The following trends are worth noting:

- The slam term is predominant at the initial stages of impact and decreases rapidly with time. On the other hand, the inertia term is small at initial stages of impact and increases gradually with time.
- The time variation of the impact force for the cylindrical system is quite different from that for the long, rectangular system. While the latter force rises instantaneously from zero to a finite value and then decreases, the former force is zero at initial impact, increases rapidly to a maximum after a short rise time and then decreases slowly. These differing trends follow from the fact that the geometries of the impacted roof areas for the two systems are quite different. Such trends have also been demonstrated in studies by Miloh [44] for liquid impact of three-dimensional spheres and two-dimensional cylinders.
- As may be expected from equation (8.22), the maximum roof force coefficient for the rectangular system is  $4/\pi$ . On the other hand, the corresponding coefficient for the cylindrical system and the time of its occurrence,  $\Delta t_m$ , is a function of  $d_o/d_{max}$ . The variation of these quantities with  $d_o/d_{max}$  is studied in Table 8.1 for several values of  $d_o/d_{max}$  in the range between 0.1 and 0.9. The half-angle subtended by the impacted area corresponding to the maximum roof force,  $\theta_{o,m}$ , is also tabulated. The presented data are strictly valid for a tank with  $H/R = 1$ ,  $f_1 = 0.2$  Hz, but due to the normalization scheme used, the force coefficients depend mainly on  $d_o/d_{max}$  and are relatively insensitive to the other parameters. For most values of  $d_o/d_{max}$ , the following relations are found to be valid for estimating the cylindrical roof impact effects,

$$\begin{aligned}\frac{\Delta t}{T_1} &\approx 0.03 \frac{d_o}{d_{max}} \\ \theta_{o,m} &\approx 30 \text{ deg} \\ F_{r,max} &\approx (0.55 - 0.58) \frac{\rho_l R^3 v_o^2}{d_o}\end{aligned}\tag{8.61}$$

It is also of interest to know the roof pressures at the time of occurrence of the maximum impact force. These values, normalized with respect to  $\rho_l R v_o^2/d_o$ , are also

presented in Table 8.1 for the values of  $d_o/d_{max}$  previously considered. It is seen that for most cases, the roof pressure can be given by the relation,

$$p_{r,m} \approx 2 \frac{\rho_l R v_o^2}{d_o} \quad (8.62)$$

The critical roof pressures evaluated from equation (8.62) can be applied as static loads over the impacted area of the roof plate and a suitable computer program can be employed to obtain a detailed description of the stresses that are transmitted at the roof-wall junction. Large tensile stresses at this junction may cause the roof to separate from the wall, though this is not particularly of concern for the embedded tanks normally encountered in nuclear facilities.

**Wall Effects :** At the instant impact commences, the theoretical values of the wall forces and moments evaluated from equations (8.36) tend to infinity for rectangular tanks with flat roofs. However, in reality, the wall effects for the rectangular tank will also have finite maxima after a short rise time. The magnitudes of these maxima and rise times depend strongly on effects of liquid compressibility, air cushioning, air entrainment, etc., and are beyond the scope of this study. The present section is devoted to a discussion of the wall impact effects for cylindrical systems.

Based on the form suggested by equation (8.44), it is found convenient to express the total wall force for flat-roofed cylindrical systems in the form

$$F_t(t) = c_{wf}(t) \rho_l R^3 \frac{v_o^2}{d_o} \tanh \frac{\lambda_1 H}{R} \quad (8.63)$$

Similarly, based on equation (8.45), the total moment is expressed as

$$M_t(t) = c_{wm}(t) \rho_l R^3 H \frac{v_o^2}{d_o} \left\{ \tanh \frac{\lambda_1 H}{R} - \frac{R}{\lambda_1 H} \left( 1 - \frac{1}{\cosh \lambda_1 H/R} \right) \right\} \quad (8.64)$$

The temporal variations of the wall force and moment coefficients are presented in Fig. 8.4 for a cylindrical system with  $H/R = 1$  and  $d_o/d_{max} = 0.5$ . Approximate solutions for these coefficients obtained by applying the wall pressures for a rectangular system over an angle of  $2\theta_o(t)$  are also shown in the figure. Numerical values of the maximum wall force and moment coefficients for the system considered and for additional values of  $H/R$ ,  $d_o/d_{max}$  are presented in Tables 8.2 and 8.3 respectively. The associated times of occurrence,  $\Delta t_m$ , and the half-angles subtended by the associated impacted areas,  $\theta_m$ , are also tabulated. The following trends are worth noting:

- The magnitudes of the maximum force and moment coefficients are generally in the order of unity and decrease with increasing  $H/R$  and  $d_o/d_{max}$ . These maxima occur a short time after the initial impact and these times are generally smaller than those for the maximum roof force. Furthermore, the half-angle corresponding to the time of maximum impact is about 20 degrees.
- The approximate solutions obtained from the two-dimensional wall pressures are on the conservative side. For the system with  $H/R = 1$  considered in Fig. 8.4, the approximate procedure over-estimates the maximum force coefficients by about 28 % and the moment coefficients by about 18 %. The accuracy of the procedure is further found to deteriorate with increasing  $H/R$ . For a tank with  $H/R = 0.5$ , the errors for the force and moment coefficients are about 12 % and 8 % respectively and for  $H/R = 2$ , the over-estimation is by about 70 % and 40 % respectively.

It is also important to know the hydrodynamic wall impact pressures that correspond to the time of occurrence of the maximum wall impact effects. For the parameters of general interest, it is found that the pressure acting on the junction of the tank-wall and roof,  $p_{w,m}(H)$ , is given by

$$p_{w,m}(H) \approx (3 - 4) \frac{\rho_l R v_o^2}{d_o} \quad (8.65)$$

With this junction pressure established, the associated wall pressure distributions for the cylindrical system,  $p_{w,m}(z)$ , can be determined from equation (8.42). However, this expression is very cumbersome and time-consuming to evaluate and a simpler approach can be used to assess the vertical variation of the pressures. Based on the fact that the two-dimensional wall pressures yield reasonable estimates of the maximum wall effects for broad cylindrical tanks, the hydrodynamic wall pressures acting over the impacted portion for such systems are evaluated herein from equation (8.31) rather than from equation (8.42). The wall pressure distributions corresponding to the time of maximum impact are shown in Fig. 8.5 for two systems with  $H/R = 0.5$  and 1.0 respectively.  $d_o/d_{max}$  is taken as 0.5 in both cases. It is seen that the trends of the impact pressure distributions are quite similar to those for convective pressures. The pressures are a maximum at the top and decrease towards the base and the rate of decay increases with increasing  $H/R$ .

Once the critical wall pressures are known, they can be applied as radial loads on the shell and a suitable computer program can be employed to obtain a detailed

description of the stresses and displacements of the shell. It should be noted that for the small impact areas associated with the maximum wall impact forces, significant bending stresses may be induced due to the bulging of the shell wall.

**Numerical Comparisons :** In the form presented, it is not clear how the impact effects compare with the impulsive and convective effects and the relative magnitudes of these effects are ascertained in this section. The impulsive effects are associated with the portion that moves in synchronism with the flexible tank-wall and can be assumed to remain unaltered by the impact. The convective effects are associated with the portion that sloshes and will be reduced due to the impact. They are conveniently assessed herein by assuming the maximum liquid displacement to be  $d_o$ .

Two cylindrical tank-liquid systems that are representative of the storage systems used in nuclear facilities are considered. The system dimensions and the properties of the impacting wave are tabulated below. The wave kinematics are assessed from equations (8.9), (8.10) and (8.11). The maximum pseudoacceleration values in these expressions are evaluated from the response spectrum previously used in Chapter 3 (Figure 3.8),

Quantity	System 1	System 2
$H$	25 ft	35 ft
$R$	50 ft	35 ft
$f_1$	0.148 Hz	0.202 Hz
$d_{max}$	2.9 ft	3.8 ft
$v_{max}$	3.25 ft/s	5.2 ft/s
$a_{max}$	4.2 ft/s <sup>2</sup>	7.5 ft/s <sup>2</sup>

Values of the maximum impact wall forces and moments for the systems considered are presented in Table 8.4 for different values of  $d_o$ . The associated values of the impact pressures at the top and base are presented in Table 8.5. In order to enable direct comparisons with the other response effects, the values of the forces, moments and pressures are normalized with respect to  $m_l g$ ,  $m_l g H$  and  $\rho_l g R$  respectively. Similarly normalized impulsive effects and associated convective effects are also given in the tables. In evaluating the maximum impulsive effects, only the fundamental modal contribution of the flexible tank-liquid system is considered and the spectral value of the associated pseudoacceleration is taken as  $0.83g$ . The following trends are worth noting :

- The magnitude of the impact effects increase significantly with decreasing values of the free-board  $d_o$ . This trend follows from the fact that the maximum effects are proportional to  $v_o^2/d_o$ . On writing  $v_o$  as  $v_{max}\sqrt{1 - d_o^2/d_{max}^2}$ , it can be shown that, for an impacting wave with given displacement  $d_{max}$ , the effect of the free-board  $d_o$  on the maximum impact response is given by

$$F_{impact} \propto \frac{d_{max}}{d_o} - \frac{d_o}{d_{max}} \quad (8.66)$$

- The maximum impact effects are generally smaller than the corresponding impulsive effects. For System 1 with  $d_o = 0.3d_{max}$ , the impact effects are in the order of 60-90 % of the maximum impulsive effects. The corresponding range for system 2 is 40-70 %.
- Depending on the value of  $d_o$ , the impact effects are significantly larger or have the same order of magnitude as the maximum convective effects.
- For small values of  $d_o$ , the values of the impact pressures corresponding to the time of occurrence of the maximum wall effects can be much larger than the maximum impulsive or convective wall pressures. It should be remembered that these impact pressures act over relatively small lengths ( $2\theta_m \approx 40$  degrees) and may cause the flexible side-wall to bulge.

The total design forces for the tank-liquid system can be obtained by appropriately combining the impulsive, convective and impact effects. For the impacting wave considered herein, it is clear that the maximum impact and convective effects occur almost simultaneously. These are added numerically and their sum is then combined with the impulsive effects by taking the sum of the squares, i.e.,

$$\text{Total} = \sqrt{\text{Impulsive}^2 + (\text{Impact} + \text{Convective})^2} \quad (8.67)$$

The values of the design forces obtained by the above equation are also shown in Table 8.4.

### 8.5.2 Impact Effects for Sloping Roofs

The roof impact force coefficients,  $c_{rf}(t)$ , are presented in Figure 8.6 for rectangular and cylindrical systems with sloping roofs. The roof slope angle,  $\alpha$ , is varied between 0 and 0.3. Similar results for the total wall force and moment coefficients of cylindrical systems are presented in Figure 8.7. The results in the figures are for System 2 with

$d_o = 0.5d_{max}$ . These data, along with additional results for the roof force, wall force and wall moment coefficients are presented in Table 8.6 for values of  $d_o/d_{max}$  ranging between 0.3 and 0.7. Both Systems 1 and 2 are considered in the table. The properties of the systems and of the impacting waves have been tabulated in the previous section. The following representative trends are worth noting :

- The impact effects reduce significantly with increasing values of  $\alpha$ . The rapid decrease is related to the corresponding decrease in the value of the roof pressure. From equation (8.55), it is seen that the maximum roof pressure is proportional to  $\cot \alpha$ . For the flat-roof, this value tends to infinity, and as  $\alpha$  increases, it decreases rapidly. Furthermore, with increasing  $\alpha$ , the impacted roof area over which this pressure acts is reduced and this also causes the impact effects to decrease. For system 1, the decrease from the flat-roof solutions is in the range of 70 % to 95 % for  $\alpha$  ranging from 0.05 to 0.3. For system 2, the corresponding range is 55 % to 95 %.
- The maximum impact effects for the systems with sloping roofs do not occur at the initial stages of impact. The rise times are in the order of  $0.03T_1$  to  $0.1T_1$  for the cases considered.
- Unlike the flat roof solutions, the impact effects for both rectangular and cylindrical systems with sloping roofs behave similarly with time. The values start at zero, increase to a maximum and then decrease gradually with time. These trends follow from the fact that for both rectangular/cylindrical systems, the impact effects are induced by finite roof pressures acting over gradually increasing impact lengths/areas.

All the results presented herein for the sloping roofs have been normalized with respect to the factors used before for the flat roof. While this enables one to readily assess the relative magnitudes of the effects for different roof slopes, it should be noted that in the form presented, the results are sensitive to the assumed values of the tank-liquid parameters. This follows from the fact that the impact effects for the sloping roofs are not generally proportional to  $v_o^2/d_o$ , but to a more complex function that involves  $\alpha$ ,  $v_{max}$ ,  $d_{max}$  and  $d_o$ .

In order to get a better insight into the parameters affecting the impact effects for sloping roofed systems, a simplified analysis of the impact roof force in rectangular systems is undertaken. On considering only the dominant slam term in equation (8.51), writing  $s(t)$  in terms of equation (8.49), assuming the wetting correction factor

in this expression to be  $\sqrt{2}$  and using  $v_{n,av}(t) \approx v_w(t) \cos \alpha$ , the impact roof force can be written as

$$F_r(t) \approx \rho_l \frac{\pi}{\cos \alpha} c_o(t) \dot{c}_o(t) v_w(t) \quad (8.68)$$

where  $\dot{c}_o(t)$  is the rate of change of the projected length with time and is determined by differentiating equation (8.48),

$$\dot{c}_o(t) = \frac{v_w \cos \pi c_o / 2R}{\tan \alpha + \pi d_w / 2R \sin \pi c_o / 2R} \quad (8.69)$$

Simplifying the above expression and substituting it into equation (8.68), one obtains

$$F_r(t) \approx \rho_l \frac{\pi c_o v_w^2}{\cos \alpha (\tan \alpha + \pi^2 d_w c_o / 4R^2)} \quad (8.70)$$

For  $\alpha = 0$ , the maximum roof force occurs at initial impact and it is seen that equation (8.70) reduces to equation (8.22). However, for non-zero values of  $\alpha$ , the maxima occur at later times and the impact effects depend on the roof-slope angle,  $\alpha$ , the associated impact velocity  $v_{w,m}$ , the corresponding displacement,  $d_{w,m}$ , and the horizontal length,  $c_{o,m}$ , which from equation (8.48), depends on  $d_{w,m}$ ,  $d_o$  and  $\alpha$ . Therefore, the maximum impact effects induced on the sloping roof are largely affected by the values of  $\alpha$ ,  $d_o$ ,  $d_{w,m}$  and  $v_{w,m}$ . The latter two parameters depend in turn on the values of  $d_{max}$ ,  $v_{max}$  and the time  $t_m$  at which the maximum impact occurs.

A rough estimate of this rise time  $t_m$  can be obtained by the following simplified analysis : The cosine-shaped liquid surface is replaced by a flat surface of instantaneous height  $d_w(t)$  moving with a velocity  $v_w(t)$ . The horizontal projection of the impact length is then given by  $c_o(t) = (d_w(t) - d_o) \cot \alpha$ . The time of occurrence of the maximum impact force can then be obtained by equating the time-derivative of the force to zero. On defining the force approximately by equation (8.68) and differentiating, it can be shown that  $c_{o,m} = -v_{w,m}^2 \cot \alpha / 2 a_{w,m}$ . On equating the above expressions for  $c_o$ , and expressing  $d_w$ ,  $v_w$  and  $a_w$  as  $d_{max} \sin \omega_1(t)$ ,  $\omega_1 d_{max} \cos \omega_1 t$  and  $-\omega_1^2 d_{max} \sin \omega_1 t$  respectively, one obtains a quadratic expression for  $\sin \omega_1 t_m$ , the solution of which can be written as

$$\sin \omega_1 t_m \approx \frac{1}{3} \left[ \frac{d_o}{d_{max}} + \sqrt{\left( \frac{d_o}{d_{max}} \right)^2 + 3} \right] \quad (8.71)$$

It should be noted that the above analysis is valid only for relatively large values of  $\alpha$ . This restriction on  $\alpha$  is required because as  $\alpha$  decreases, the flat liquid surface



instantaneously comes in contact with a large portion of the roof and  $c_o$  tends to a very large value. The accuracy of the present analysis in estimating the time of maximum occurrence is found to be good for values of  $\alpha \geq 0.2$ . For values of  $\alpha$  ranging from 0 to 0.2, it is recommended that the time of occurrence for the maximum impact effects be estimated by using a linear interpolation between the time for initial impact and the time evaluated from equation (8.71).

With the time of maximum occurrence known,  $d_{w,m}$ ,  $v_{w,m}$  and  $c_{o,m}$  can be conveniently evaluated from the first two components of equation (8.13) and from equation (8.48). They are then substituted into equation (8.70) to obtain the maximum impact force.

## 8.6 Conclusions

With the information presented herein, the impact pressures and forces induced on the roofs and walls of tank-liquid systems can be evaluated readily. Effects for both rectangular and cylindrical systems have been evaluated and the influence of altering the roof slope has been studied. Comprehensive numerical solutions have been presented in a suitably normalized form and comparisons with well-established impulsive and convective solutions have been made. The principal conclusions of the study are as follows :

1. The impact force is comprised of two terms : a slam term that generally varies as the square of the velocity of impact and an inertia term that is proportional to the acceleration of impact. The slam term usually occurs during the early stages of impact and is the dominant contributor to the maximum impact response.
2. For a flat-roofed system, the maximum impact effects occur at the initial stages of impact and their magnitudes are proportional to the initial velocity of impact  $v_o$  and the free-board  $d_o$ .
  - The peak roof force for the cylindrical system is about  $0.57 \rho_l R^3 v_o^2 / d_o$ . The pressure corresponding to the time of occurrence of the maximum roof force is approximately  $2 \rho_l R v_o^2 / d_o$  and it acts over an area subtending a central angle of about 60 degrees.
  - The maximum wall effects are normalized so that the associated response coefficients are approximately unity. The pressures at the roof-wall junction corresponding to these maxima generally vary between  $3 - 4 \rho_l R v_o^2 / d_o$ , and the associated central angle is about 40 degrees.

- The magnitude of the maximum impact forces on the wall are generally larger than the convective effects but smaller than the impulsive effects. The impact effects increase rapidly with decreasing free-board and for a wave of given maximum displacement  $d_{max}$ , the impact response is proportional to  $(d_{max}/d_o - d_o/d_{max})$ . For small values of  $d_o$ , the values of the associated impact pressures at the roof-wall junction may be significantly larger than either the impulsive or convective pressure.
3. For a sloping-roofed system, the maximum impact pressure tends to a finite limit given by  $\rho_l \pi/2 \cot \alpha w_o v_o^2$ . The times of occurrence of the maximum impact forces are much larger than those for the flat-roofs. Furthermore, the magnitudes of the impact effects decrease significantly with increasing  $\alpha$ . The decrease depends strongly on the values of  $\alpha$ ,  $d_o$ ,  $d_{max}$  and  $v_{max}$ .

**Table 8.1:** Values of maximum roof impact effects for flat-roofed cylindrical tanks with different values of  $d_o/d_{max}$

$\frac{d_o}{d_{max}}$	$\frac{\Delta t_m}{T_1}$	$\theta_{o,m}$	$c_{rf,max}$	$\frac{p_{r,m}}{\rho_l R v_o^2 / d_o}$
0.1	0.002	29.1	0.578	2.04
0.2	0.005	29.8	0.577	1.96
0.3	0.008	29.5	0.575	1.98
0.4	0.011	29.6	0.570	1.96
0.5	0.014	29.2	0.563	1.99
0.6	0.018	28.8	0.551	2.01
0.7	0.021	27.4	0.528	2.12
0.8	0.023	24.3	0.483	2.44
0.9	0.020	18.2	0.387	3.36

**Table 8.2:** Values of maximum wall impact force for flat-roofed cylindrical tanks with different values of  $H/R$  and  $d_o/d_{max}$

$\frac{d_o}{d_{max}}$	$\frac{\Delta t_m}{T_1}$	$\theta_{o,m}$	$c_{wf,max}$
$H/R = 0.5$			
0.1	0.001	21.1	0.999
0.3	0.003	20.2	0.997
0.5	0.006	20.0	0.989
0.7	0.010	19.4	0.966
0.9	0.014	15.6	0.848
$H/R = 1$			
0.1	0.001	21.1	0.948
0.3	0.004	21.5	0.945
0.5	0.007	21.4	0.934
0.7	0.011	20.4	0.906
0.9	0.014	15.8	0.774
$H/R = 2$			
0.1	0.001	21.1	0.940
0.3	0.004	22.1	0.937
0.5	0.007	21.7	0.926
0.7	0.011	20.6	0.897
0.9	0.014	15.9	0.763

**Table 8.3:** Values of maximum wall impact moment for flat-roofed cylindrical tanks with different values of  $H/R$  and  $d_o/d_{max}$

$\frac{d_o}{d_{max}}$	$\frac{\Delta t_m}{T_1}$	$\theta_{o,m}$	$c_{wm,max}$
$H/R = 0.5$			
0.1	0.001	18.4	1.079
0.3	0.003	18.0	1.077
0.5	0.005	17.8	1.070
0.7	0.008	17.3	1.051
0.9	0.012	14.7	0.948
$H/R = 1$			
0.1	0.001	18.4	1.011
0.3	0.003	19.5	1.009
0.5	0.006	19.4	1.000
0.7	0.009	18.6	0.976
0.9	0.013	15.1	0.858
$H/R = 2$			
0.1	0.001	21.1	0.977
0.3	0.004	20.8	0.973
0.5	0.006	20.3	0.964
0.7	0.010	19.5	0.937
0.9	0.013	15.4	0.811

**Table 8.4: Comparison of maximum impact effects for representative flat-roofed cylindrical tanks with associated impulsive and convective effects**

Resp. Coefft	$\frac{d_o}{d_{max}}$	System 1				System 2			
		Impul.	Conv.	Impact	Comb.	Impul.	Conv.	Impact	Comb.
$\frac{Q_b}{m_{lg}}$	0.3		0.014	0.159	0.304		0.017	0.192	0.503
	0.5	0.250	0.023	0.078	0.270	0.457	0.028	0.094	0.473
	0.7		0.032	0.037	0.259		0.039	0.044	0.464
$\frac{M_b}{m_{lg}H}$	0.3		0.007	0.091	0.140		0.010	0.123	0.227
	0.5	0.100	0.012	0.044	0.115	0.184	0.017	0.061	0.200
	0.7		0.017	0.021	0.107		0.024	0.029	0.191

**Table 8.5: Comparison of impact pressures corresponding to time of occurrence of maximum wall forces with maximum impulsive and convective pressures**

Resp. Coefft	$\frac{d_o}{d_{max}}$	System 1			System 2		
		Impul.	Conv.	Impact	Impul.	Conv.	Impact
$\frac{p_w(H)}{\rho_{lg}R}$	0.3		0.017	1.191		0.033	2.135
	0.5	0	0.029	0.594	0	0.054	1.053
	0.7		0.041	0.291		0.076	0.529
$\frac{p_w(0)}{\rho_{lg}R}$	0.3		0.012	0.653		0.010	0.693
	0.5	0.344	0.020	0.322	0.614	0.017	0.339
	0.7		0.028	0.154		0.024	0.162

**Table 8.6: Values of maximum roof and wall impact effects for representative cylindrical tanks with sloping roofs with different values of  $\alpha$  and  $d_o/d_{max}$**

$d_o/d_{max}$	System 1			System 2		
	$C_{rf,max}$	$C_{wf,max}$	$C_{wm,max}$	$C_{rf,max}$	$C_{wf,max}$	$C_{wm,max}$
			$\alpha = 0$			
0.3	0.577	0.998	1.077	0.575	0.945	1.009
0.5	0.570	0.991	1.072	0.564	0.935	1.001
0.7	0.543	0.972	1.056	0.530	0.908	0.978
			$\alpha = 0.05$			
0.3	0.162	0.274	0.298	0.253	0.402	0.430
0.5	0.179	0.336	0.371	0.284	0.478	0.516
0.7	0.139	0.306	0.346	0.243	0.457	0.502
			$\alpha = 0.1$			
0.3	0.075	0.140	0.156	0.149	0.239	0.259
0.5	0.077	0.164	0.186	0.162	0.288	0.316
0.7	0.052	0.127	0.148	0.123	0.252	0.283
			$\alpha = 0.2$			
0.3	0.026	0.055	0.063	0.067	0.115	0.127
0.5	0.025	0.058	0.067	0.067	0.130	0.147
0.7	0.015	0.039	0.046	0.045	0.098	0.112
			$\alpha = 0.3$			
0.3	0.013	0.027	0.032	0.037	0.065	0.073
0.5	0.012	0.027	0.032	0.035	0.069	0.079
0.7	0.007	0.018	0.021	0.022	0.048	0.055

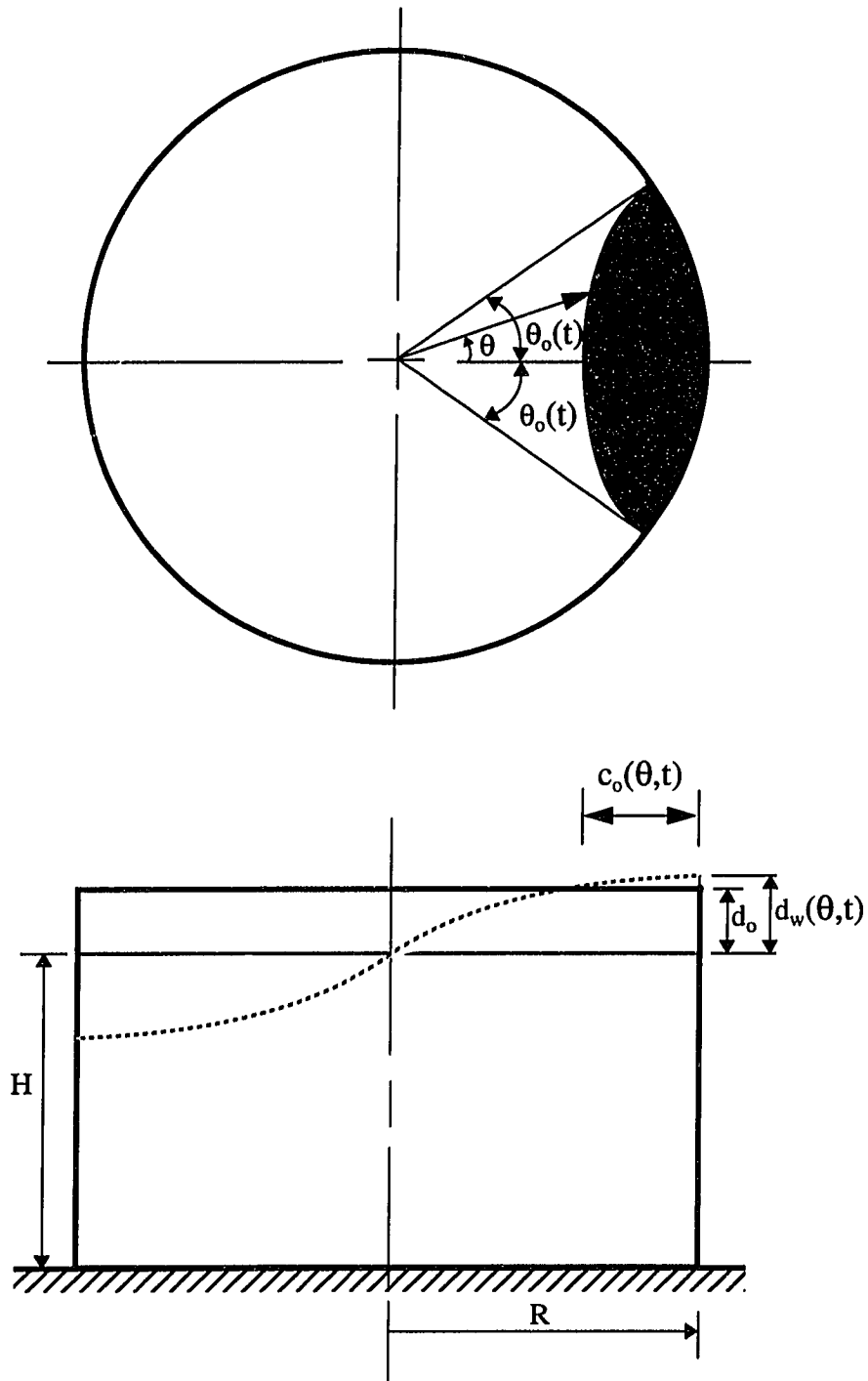


Figure 8.1 System Considered



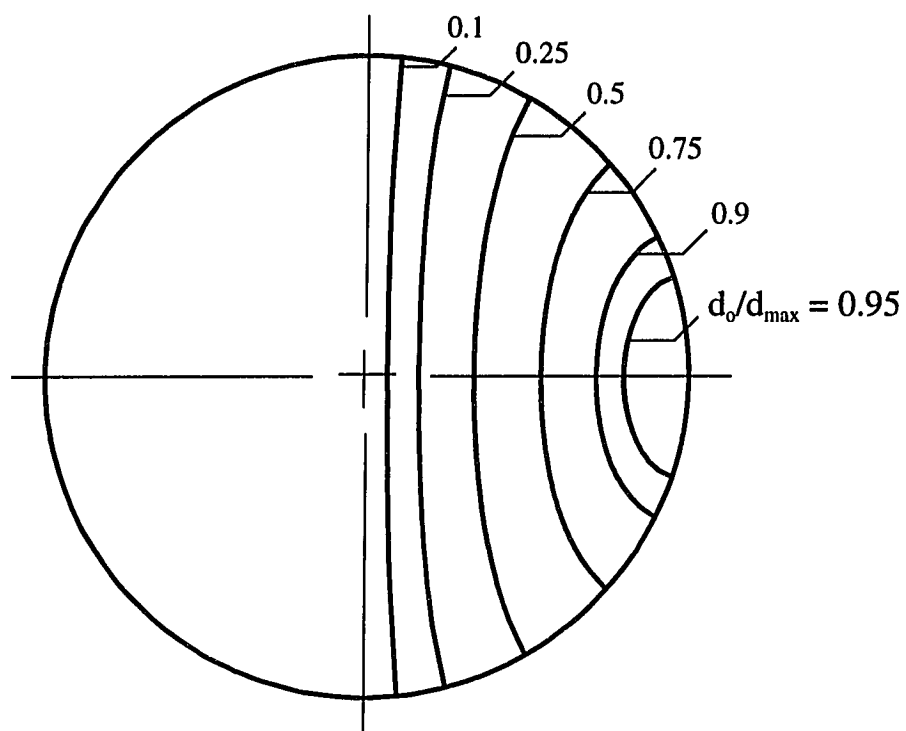


Figure 8.2 Impacted Roof Areas for Different Values of  $d_o/d_{max}$

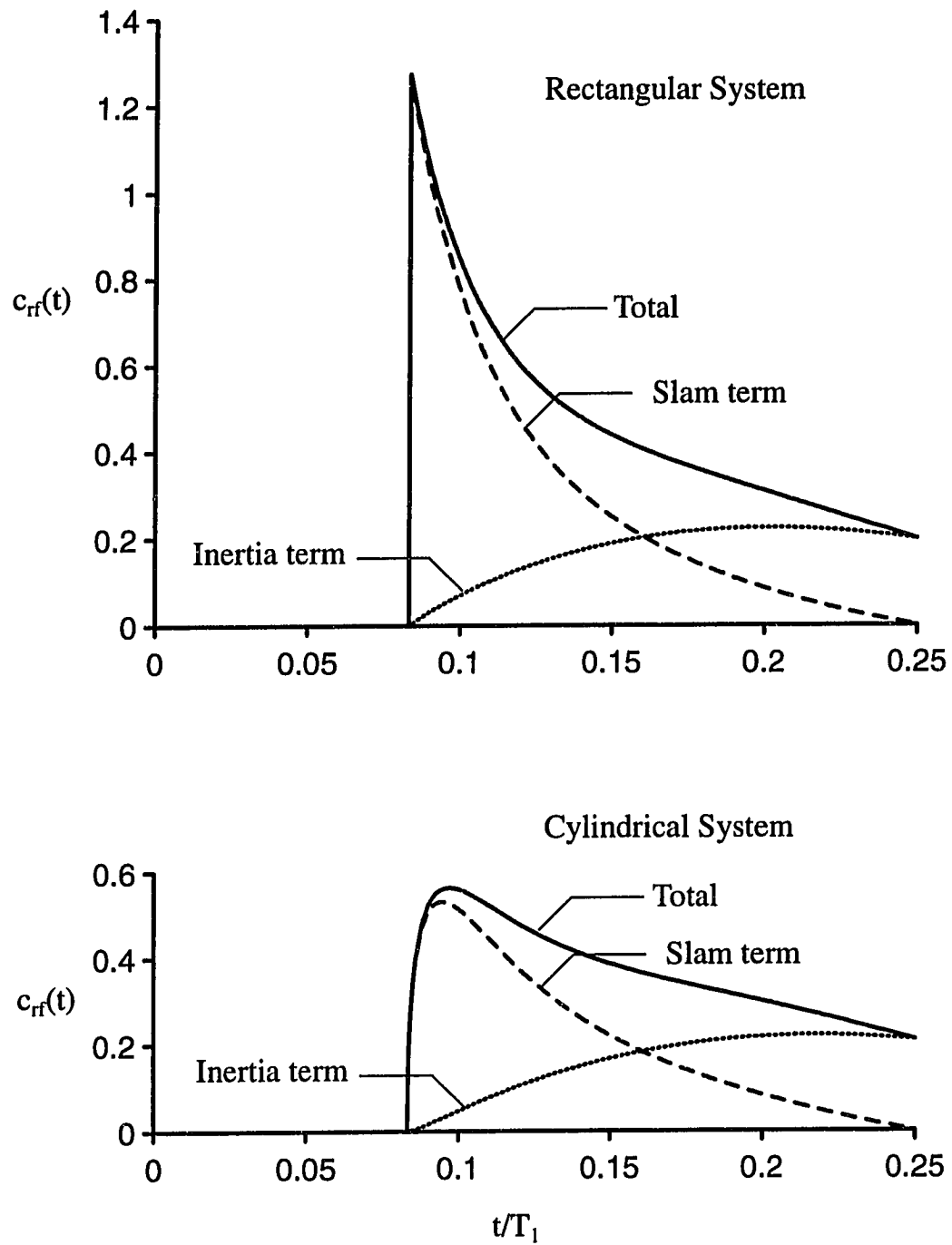


Figure 8.3 Variation of normalized roof impact force with time for flat-roofed rectangular and cylindrical systems with  $d_o/d_{max}=0.5$

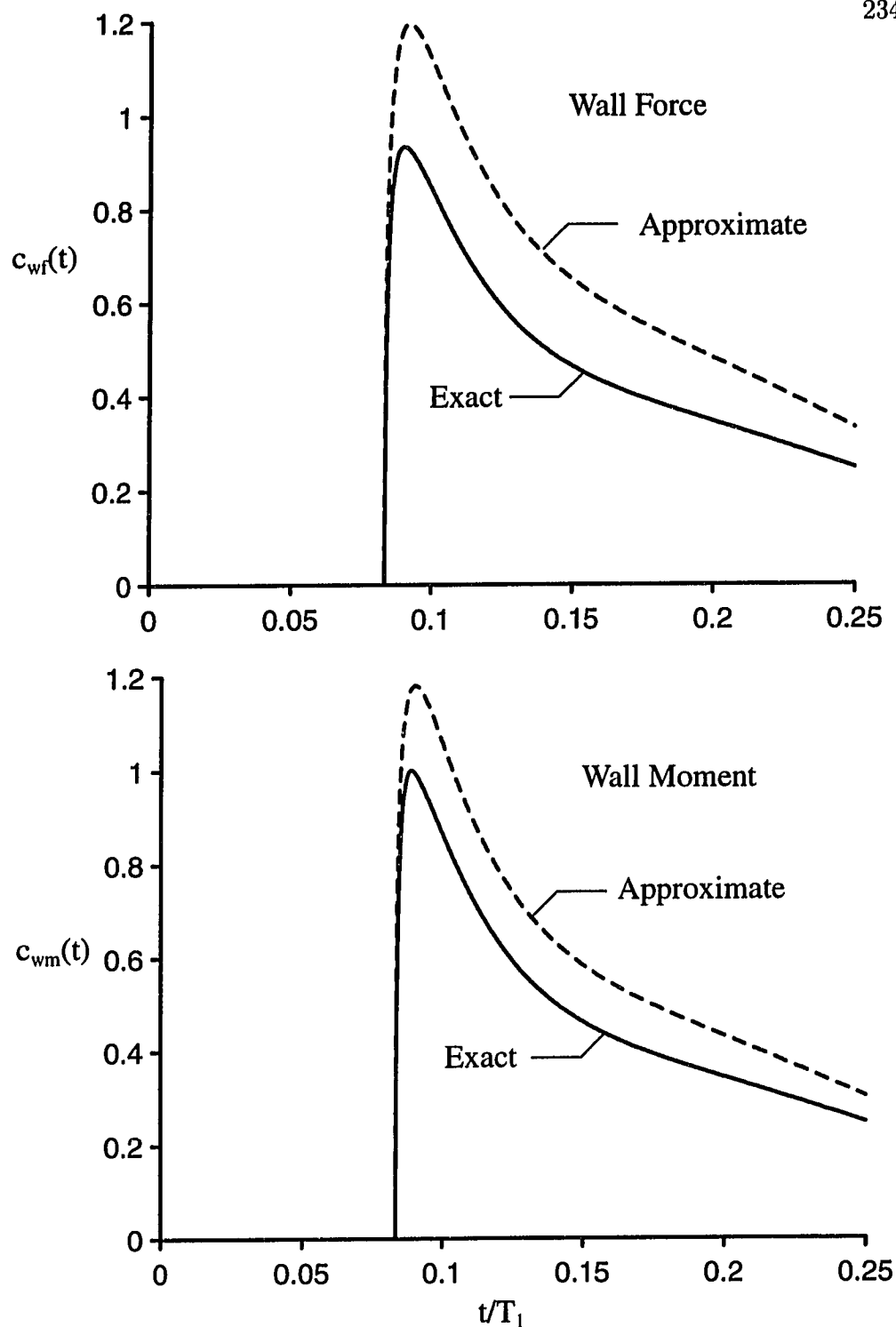


Figure 8.4 Variation of wall impact response coefficients with time for flat-roofed cylindrical system; Approximate solutions obtained from rectangular tank-wall pressure distributions;  $H/R = 1$ ,  $d_o/d_{max} = 0.5$

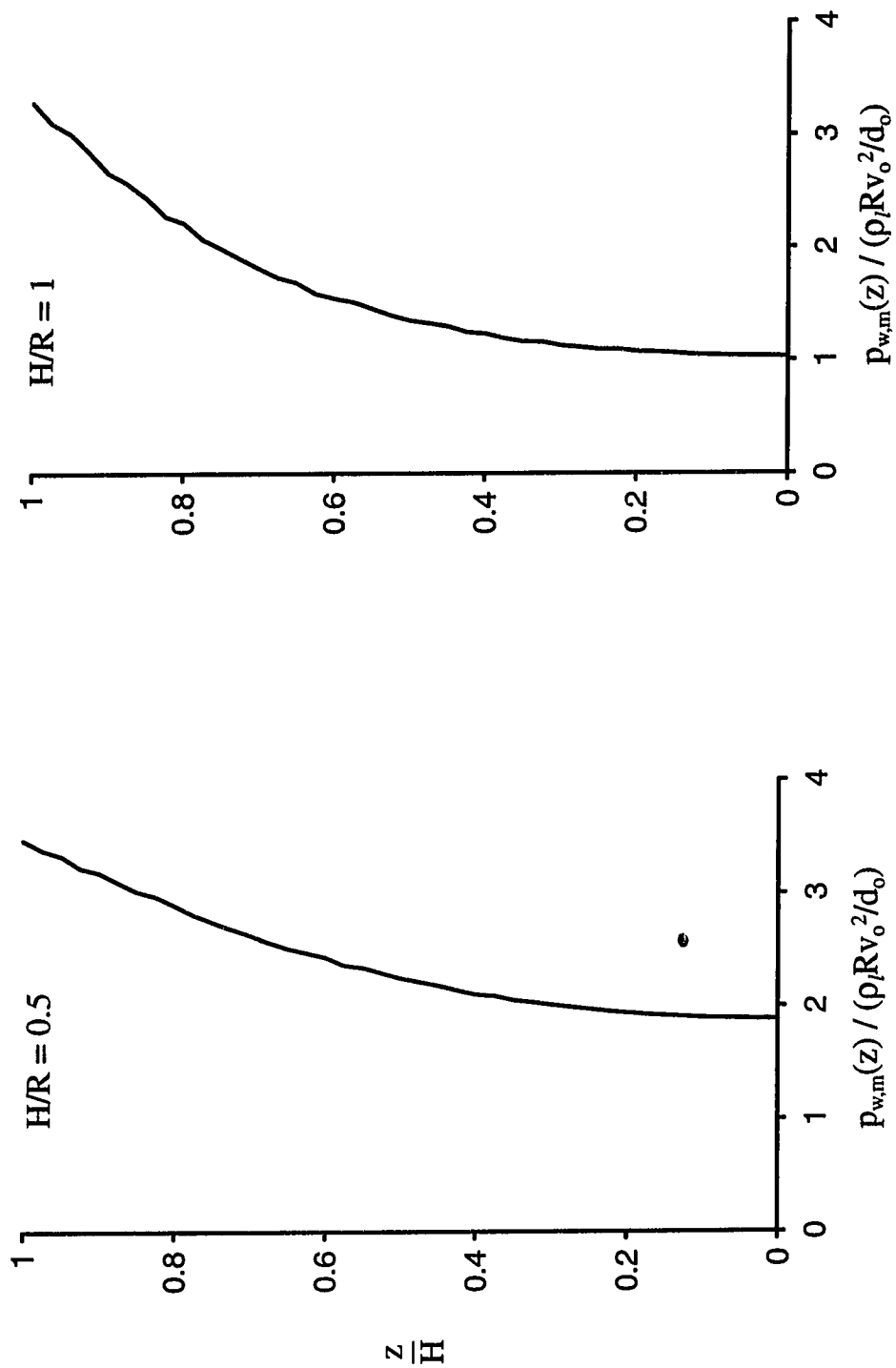


Figure 8.5 Wall pressure distributions corresponding to time of occurrence of maximum wall force for flat-roofed cylindrical systems with different values of  $H/R$  and  $d_o/d_{\max} = 0.5$

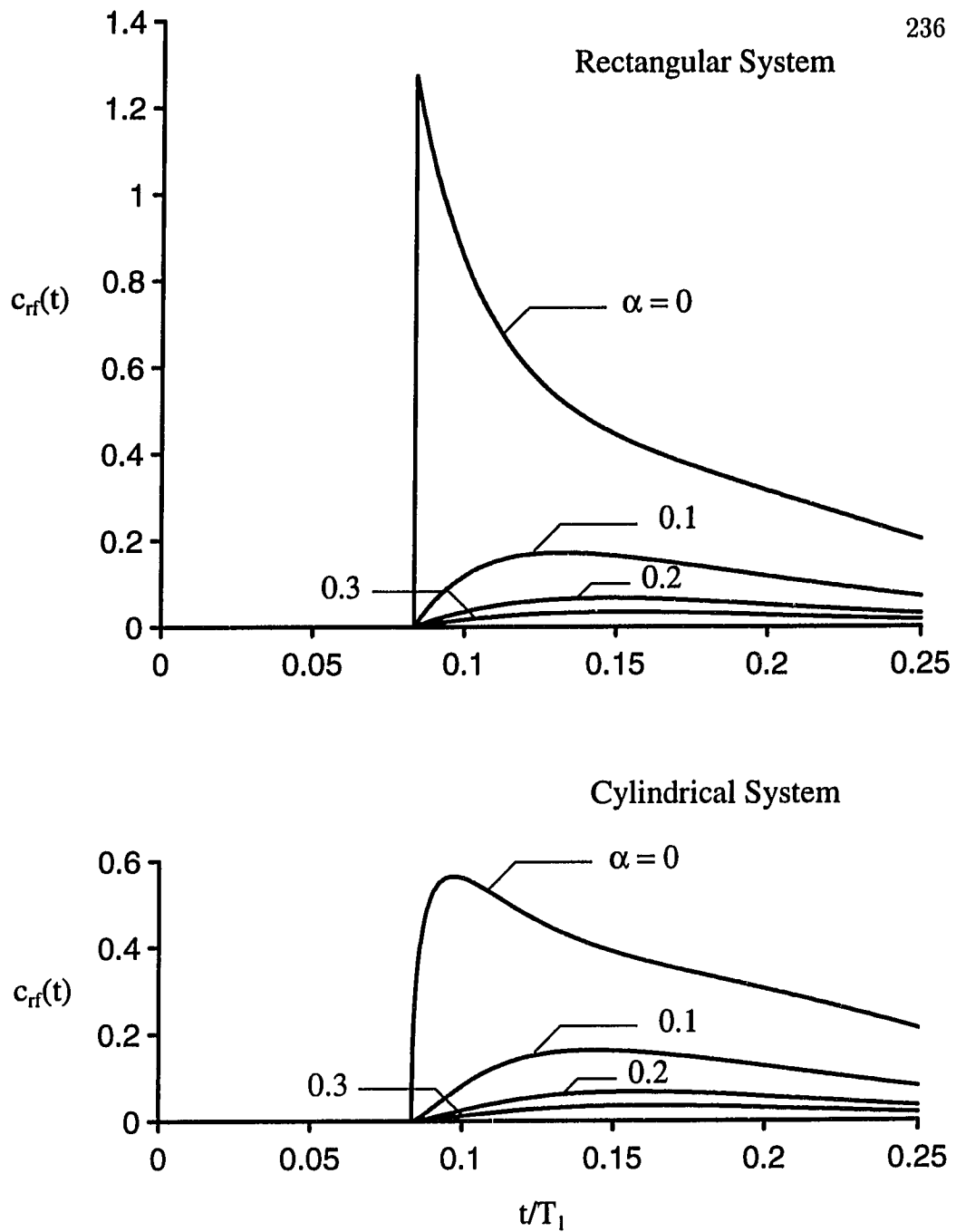


Figure 8.6 Comparison of roof impact forces for rectangular and cylindrical tanks with different angles of roof slope  $\alpha$ ; Tank-Liquid system considered is System 2;  $H = R = 35$  ft,  $d_{\max} = 3.8$  ft,  $v_{\max} = 5.2$  ft/s,  $d_0 = 0.5 d_{\max}$

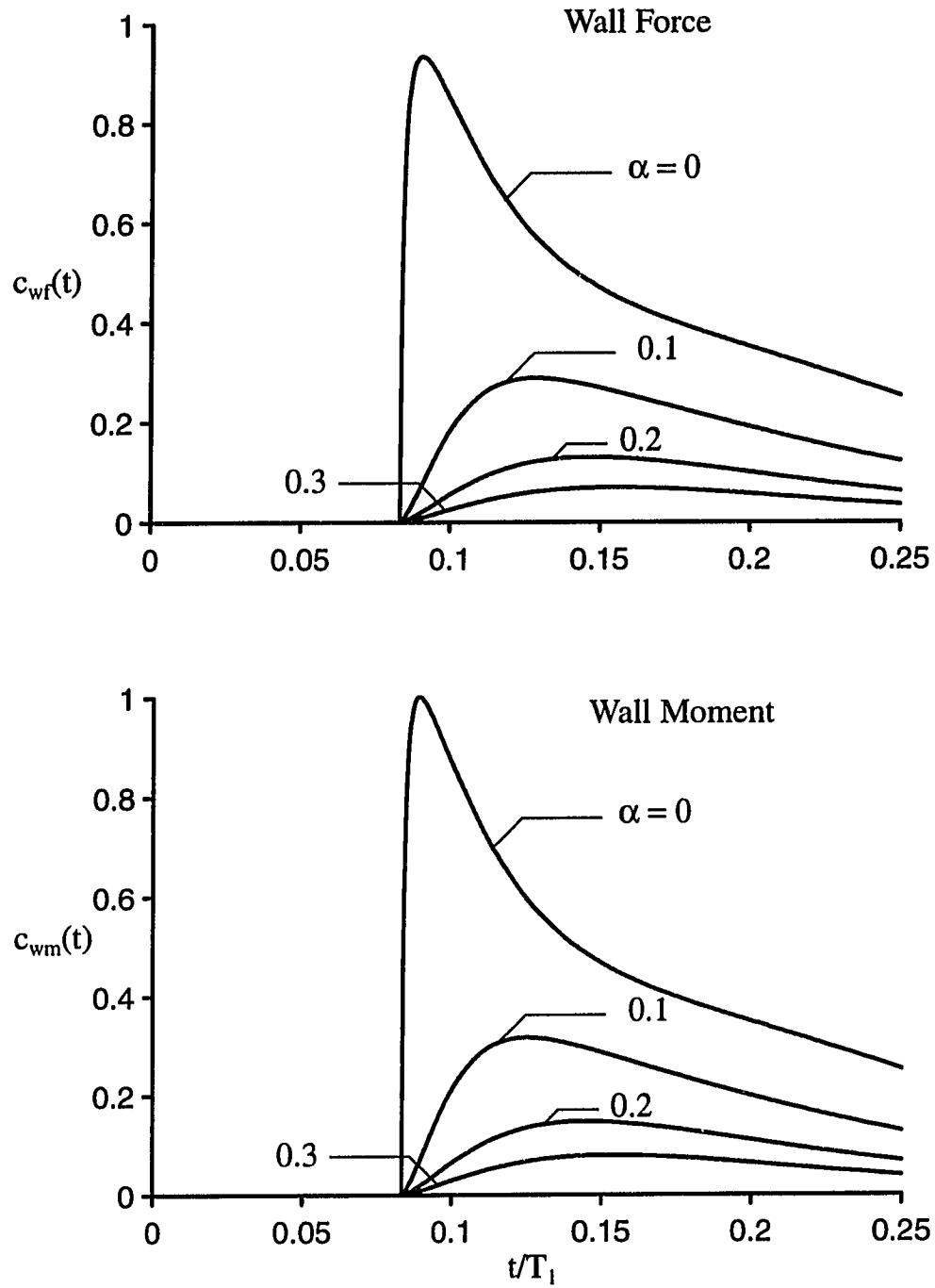


Figure 8.7 Comparison of wall impact response coefficients for cylindrical systems with different angles of roof slope  $\alpha$ ; Tank-liquid system considered is System 2;  $H = R = 35$  ft,  $d_{\max} = 3.8$  ft,  $v_{\max} = 5.2$  ft/s,  $d_0 = 0.5 d_{\max}$

## Bibliography

- [1] Abramson, H. N., (1966), The Dynamic Behavior of Liquids in Moving Containers with Application to Space Vehicle Technology, *NASA SP-106*
- [2] Amano, K., Koizumi, M., and Yamakawa, M., (1989), Three-dimensional analysis method for potential flow with a moving liquid surface using a boundary element method, *Proceedings of Sloshing and Fluid-Structure Vibration, Pressure Vessels and Piping Conference, ASME, Vol. PVP-157, Honolulu, Hawaii, pp. 127-132*
- [3] Arai, M., Cheng, L. Y., Inoue, Y., Sasaki, H., and Yamagishi, N., (1992), Numerical analysis of liquid sloshing in tanks of FPSO, *Proceedings of the second International Offshore and Polar Engineering Conference, San Francisco, USA, pp. 14-19*
- [4] Asai, O., (1979), Proposals for the earthquake-proof designs of cylindrical liquid storage tank with fixed roof (II)', *Pressure Engineering, Vol. 17, No. 4*
- [5] Bauer, M. F., (1964), Fluid Oscillations in the Containers of a Space Vehicle and Their Influence upon Stability, *NASA TR.R-187*
- [6] Benton, G. S., (1953), A general solution for the celerity of long gravitational waves in a stratified fluid, *Fluid Models in Geophysics, U.S. Government Printing Office, pp. 149-162*
- [7] Borg, S. F., (1959), Initial wedge impact on a compressible fluid, *Journal of Applied Physics, 30, pp. 1432-1436*
- [8] Burris, L., Steuneberg, R. K., and Miller, W. E., (1987), The application of electrorefining for recovery and purification of fuel discharged from the integral fast reactor, *AIChE Symposium Series, AIChE, New York, Vol. 83, No. 254.*
- [9] Chan, E. S., and Melville, W. K., (1987), Plunging wave forces on surface piercing structure, *Proc. 6th Int. Offshore Mechanics and Arctic Engineering Symp., Houston, pp. 61-72*

- [10] Chang, Y. W., (1994), Discussion of 'Sloshing response of layered liquids in rigid tanks' by A. S. Veletsos and P. Shivakumar, *Journal of Earthquake Engineering and Structural Dynamics*, Vol. 23, Nol 7, pp. 1596-1597
- [11] Chwang, A. T., (1981), Effect of stratification on hydrodynamic pressures on dams', *Journal of engineering mathematics*, Vol. 15, No. 1, 49-63
- [12] Cointe, R., and Armand, J. L., (1987), Hydrodynamic impact analysis of a cylinder, *Journal of Offshore Mechanics and Arctic Engineering*, ASME, Vol. 109, pp. 237-243
- [13] Cointe, R., (1989), Two-dimensional water-solid impact, *Journal of Offshore Mechanics and Arctic Engineering*, Vol. 111, No. 2, pp. 109-114
- [14] Fabula, A., (1957), Ellipse-fitting approximation of two-dimensional normal symmetric impact of rigid bodies on water, *Proceedings, Fifth Mid-Western Conference on Fluid Mechanics*, Univ. of Michigan Press, Ann Arbor, Mich.
- [15] Faltinsen, O., et al., (1977), Water Impact Loads and Dynamic Responses of Horizontal Circular Cylinders in Offshore Structures, *Proceedings, 9th Offshore Technology Conference*, OTC Paper 2741, Houston, TX.
- [16] Golub, G. H., and Van Loan, C. F., *Matrix Computations*, The Johns Hopkins University Press, II Edition, 1989, pp. 119 and 140.
- [17] Haroun, M. A., (1991), Implications of Observed Earthquake Induced Damage on Seismic Codes and Standards of Tanks, *Proceedings of Fluid-Structure Vibration and Sloshing, Pressure Vessels and Piping Conference*, ASME, Vol. PVP-223, San Diego, California, pp. 1-7
- [18] Haroun, M. A., and Abdel-Hafiz, E. A., (1986), A simplified seismic analysis of rigid base liquid storage tanks under vertical excitation with soil-structure interaction, *Journal of Soil Dynamics and Earthquake Engineering*, Vol. 5, pp. 217-225
- [19] Haroun, M. A., and Badawi, H. S., (1988), Seismic behavior of unanchored ground- based cylindrical tanks, *Proceedings of the 9th World Conference on Earthquake Engineering*, Tokyo-Kyoto, Japan, Vol. VI, pp. 643-648.



- [20] Haroun, M. A., and Housner, G. W., (1981), Seismic design of liquid storage tanks, *Journal of Technical Councils*, ASCE, Vol. 107, No. 1, pp.191-207.
- [21] Haroun, M. A., and Housner, G. W., (1982), Dynamic characteristics of liquid storage tanks, *Journal of the Engineering Mechanics Division*, ASCE, Vol. 108, No. EM5, pp. 783-800
- [22] Hirt, C. W., Nichols, B. D., and Pomeroy, N. C., (1975), SOLA-A numerical solution algorithm for transient fluid flows, *LA-5852*, Los Alamos Scientific Laboratory.
- [23] Hirt, C. W., and Nichols, B. D., (1981), Volume of fluid (VOF) method for the dynamics of free boundaries, *Journal of Computational Physics*, Vol. 39, pp. 201-225.
- [24] Housner, G. W., (1957), Dynamic pressures on accelerated fluid containers, *Bulletin of the Seismological Society of America*, Vol. 47, pp. 15-35
- [25] Hudson, D. E., (1977), Dynamic tests of full-scale structures, *Journal of Engineering Mechanics Division*, Vol. 103, No. EM6, pp. 1141-1157
- [26] Hydrodynamic Impact Analysis, (1978), *EPRI NP-824*, Electric Power Research Institute
- [27] Iguchi, M., and Luco, J. E., (1981), Dynamic response of flexible rectangular foundations on an elastic half-space, *Journal of Earthquake Engineering and Structural Dynamics*, Vol. 9, pp. 239-249
- [28] Iguchi, M., and Luco, J. E., (1982), Vibration of flexible plate on viscoelastic medium, *Journal of Engineering Mechanics*, ASCE, Vol. 108(6), pp. 1103-1120
- [29] Kaplan, P., and Silbert, M., (1976), Impact forces on platform horizontal members in the splash zone, *Proceedings, 8th Offshore Technology Conference*, OTC Paper No. 2498, Houston, TX.
- [30] Kaplan, P., (1987), Analysis and prediction of flat bottom slamming impact of advanced marine vehicles in waves, *Int. Shipbuilding Prog.*, vol. 34, no. 391, pp. 44-53
- [31] Kobayashi, N., (1980), Impulsive acting on the tank roofs caused by sloshing liquid, *Proceedings, 7th World Conference on Earthquake Engineering*, Vol. 5, pp. 315-322

- [32] Korobkin, A. A., (1985), Penetration of a blunt body into a slightly compressible liquid, *Journal of Applied Mechanics and Technical Physics*, Vol. 25, No. 5, pp. 751-757
- [33] Krenk, S., and Schmidt, H., (1981), Vibration of an elastic circular plate on an elastic half space - a direct approach, *Journal of Applied Mechanics*, American Society of Mechanical Engineers, Vol. 48, pp. 161-168
- [34] Kurihara, C., et al, (1992), Sloshing impact pressures of roofed liquid storage tanks, *Structural Engineering/Earthquake Engineering*, Vol. 8, No. 2, 95s-102s, Japan Society of Civil Engineers (Proc. of JSCE No. 432/I-16)
- [35] Lamb, H. (1945), *Hydrodynamics*, New York: Dover Publications
- [36] Lau T. D., and Zeng, X., (1992), Hydrodynamic Forces in Uplifting Cylindrical Tanks, *Proceedings of Fluid-Structure Vibration and Sloshing, Pressure Vessels and Piping Conference*, ASME, Vol. PVP-232, pp. 39-44
- [37] Lewison, G. and Maclean, W. M., (1968), On the cushioning of water impact by entrapped air, *Journal of Ship Research*, Vol. 12, No. 2, pp. 116 - 130
- [38] Lin, Y. J., (1978), Dynamic response of circular plates resting on viscoelastic half space, *Journal of Applied Mechanics*, American Society of Mechanical Engineers, Vol. 45, pp. 379-384
- [39] Liou, G. S., and Huang, P. H., (1994), Effect of flexibility on impedance functions for circular foundation, *Journal of Engineering Mechanics*, ASCE, Vol. 120(7), pp. 1429-1446
- [40] Malhotra, P. K., Veletsos, A. S., and Tang, H. T., (1992), Seismic Response of Partially Anchored Liquid Storage Tanks, *Proceedings of Seismic Engineering, Pressure Vessels and Piping Conference*, ASME, Vol. PVP-237-1, pp. 97-102
- [41] McDonald, D. T., Bando, K., Bea, R. G., and Sobey, R. J., (1990), Near surface wave forces on horizontal members and decks of offshore platforms, Coastal and Hydraulic Engg., Dept. of Civil Engineering, Univ. of California, Berkeley.

- [42] Miller, C. A., (1995), Effect of basemat flexibility on the vertical seismic response of buried high level waste tanks, White Paper submitted to Tank Seismic Expert Panel, *Brookhaven National Laboratory*
- [43] Milne-Thomson, L. M., *Theoretical Hydrodynamics*, New York : Macmillan, 4th Ed.
- [44] Miloh, T., (1981), Wave slam on a sphere penetrating a free surface, *Journal of Engineering Mathematics*, Vol. 15, No. 3, pp. 221-240
- [45] Minowa, C., (1994), Sloshing roof impact tests of a rectangular tank, *Sloshing, Fluid-Structure Interaction and Structural Response due to Shock and Impact Loads, PVP, Vol. 272*, ASME, New York, pp. 13-21
- [46] Navickas, J., Peck, J.C., Bass III R. L., Bowles E. B., Yoshimura, N., and Endo, S., (1981), Sloshing of fluids at high-fill levels in closed tanks, *Computers in flow predictions and fluid dynamics experiments*, ASME, Washington D.C., Nov. 15-20, pp. 191-198
- [47] Rajapakse, R. K., (1989), Dynamic response of elastic plates on viscoelastic half space, *Journal of Engineering Mechanics, ASCE*, Vol. 115(9), pp. 1867-1881
- [48] Sarpkaya, T., Wave impact loads on cylinders, (1978), *Proceedings, 10th Offshore Technology Conference*, OTC Paper No. 3065, Houston, TX.
- [49] Schiffman, M., and Spencer, D.C., (1951), The force of impact on a cone striking a water surface (vertical entry), *Comm. Pure Appl. Math.* 4, 4, pp. 379-417
- [50] Sedov, L., (1953), The impact of a solid body floating on the surface of an incompressible fluid, *ACSIL Translation No. 538*
- [51] Shih, R. W. K., and Anastasiou, K., (1992), A laboratory study of the wave-induced vertical loading on platform decks, *Proc. Instn. Civ. Engrs. Wat., Marit. and Energy*, 96, Paper 9778, pp. 19-33
- [52] Shivakumar, P., (1992), Dynamic response of liquid storage tanks subjected to coherent and incoherent ground motions, Thesis presented to Rice University at Houston, Texas, in partial fulfillment of the requirements for the degree of Master of Science

- [53] Su, T.C., and Kang, S. Y., (1984), Analysis of liquid impact on moving containers, Proceedings of the 12th Southeastern Conference on Theoretical and Applied Mechanics, Vol. 1, pp. 474-479.
- [54] Szebehely, V. G. and Ochi, M. K., (1966), Hydrodynamic impact and water entry, *Applied Mechanics Survey*, H. N. Abramson et al. Eds., Spartan, Washington, D. C., pp. 951-957
- [55] Tang, Y., (1986), Studies of dynamic response of liquid storage tanks, Thesis presented to Rice University at Houston, Texas, in partial fulfillment of the requirements for the degree of Doctor of Philosophy
- [56] Tang, Y., (1993), Dynamic response of a tank containing two liquids, *Journal of Engineering Mechanics*, ASCE, Vol. 119, No. 3, pp. 531-548.
- [57] Tang, Y. (1994), Free vibration analysis of a tank containing two liquids, *Journal of Engineering Mechanics*, ASCE, Vol. 120, No. 3, pp. 618-636.
- [58] Tang, Y., (1994), Computing response of tanks with two liquids, Technical Note, *Journal of Structural Engineering*, ASCE, Vol. 120, No. 12, pp. 3668-3674.
- [59] Tang, Y., and Chang, Y. W., (1993), The exact solutions to the dynamic response of tanks containing two liquids, *Report ANL/RE-93/2*, Argonne Nat. Lab., Argonne, Ill.
- [60] Tang, Y., Ma C. D., Chang W. Y., (1991), Sloshing Response in a Tank Containing two Liquids, Attachment # 2, *Proceedings of Fluid-Structure Vibration and Sloshing, Pressure Vessels and Piping Conference*, ASME, Vol. PVP-223, pp. 97-104
- [61] Taylor, J. L., (1930), Some hydrodynamical inertia coefficients, *Philosophical Magazine*, series 7, Vol. 9, pp. 161-183
- [62] Timoshenko, S. P., and Woinowsky-Krieger, S., Theory of Plates and Shells, *McGraw-Hill Book Co.*, New York, N.Y.
- [63] Trilling, L., (1950), The impact of a body on a water surface at an arbitrary angle, *Journal of Applied Physics*, 21, 2, pp. 161-170
- [64] Veklich, N. A., and Malyshev, B. M., (1988), The plane problem of the impact of a plate on a liquid strip of rectangular cross-section, *Journal of Applied Mathematics and Mechanics*, Vol. 52, No. 3, pp. 397-402

- [65] Veletsos, A. S., (1984), Seismic response and design of liquid storage tanks, *Guidelines for the Seismic Design of Oil and Gas Pipeline Systems*, Technical Council on Lifeline Earthquake Engineering, ASCE, New York, pp. 255-370 and 443-461
- [66] Veletsos, A. S., and Shivakumar, P. (1991), Hydrodynamic effects in tanks with different conditions of support, *Proceedings, Third DOE Natural Phenomena Hazards Mitigation Conference*, St. Louis, MO, U.S. Department of Energy, Washington, D.C., pp. 578-587
- [67] Veletsos, A. S., Shivakumar, P., Tang, Y. and Tang, H. T., Seismic Response of Anchored Steel Tanks, *Proceedings, Third Symposium on Current Issues Related to Nuclear Plant Structures, Equipment and Piping*, A. J. Gupta, Editor, North Carolina State University, Raleigh, NC, 1990, pp. X/2-2 to X/2-15
- [68] Veletsos, A. S., and Tang, Y., (1987), Vertical vibration of ring foundations, *Journal of Earthquake Engineering and Structural Dynamics*, Vol. 15, pp. 1-21
- [69] Veletsos, A. S., and Tang, Y., (1990), Soil-structure interaction effects for laterally excited liquid storage tanks, *Journal of Earthquake Engineering and Structural Dynamics*, Vol. 19, pp. 473-496.
- [70] Veletsos, A. S., Tang, Y., and Tang, H. T., (1992), Dynamic Response of Flexibly Supported Liquid Storage Tanks, *Journal of Structural Engineering*, ASCE, Vol. 118, No. 1, pp. 264-283.
- [71] Veletsos, A. S., and Verbic, B., (1973), Vibration of viscoelastic foundations, *Journal of Earthquake Engineering and Structural Dynamics*, Vol. 2, pp. 87-102
- [72] Veletsos, A. S., and Yang, J. Y., (1977), Earthquake response of liquid storage tanks, *Advances in Civil Engineering Through Engineering Mechanics*, Proceedings ASCE/EMD Specialty Conference, Raleigh, North Carolina, pp.1-24.
- [73] Veletsos, A. S., and Younan, A. H., (1994), Dynamic soil pressures on rigid cylindrical vaults, *Journal of Earthquake Engineering and Structural Dynamics*, Vol. 23, No. 6, pp. 645-669

- [74] Veletsos, A. S., and Younan, A. H., (1995), Dynamic modeling and response of rigid embedded cylinders, *Journal of Engineering Mechanics*, ASCE, Vol. 121, No. 9, pp. 1026-1035
- [75] Veletsos, A. S., and Younan, A. H., (1995), Dynamic soil pressures on vertical walls, State-of-Art paper, *Proceedings of Third International Conference on Recent Advances in Geotechnical Earthquake Engineering and Soil Dynamics*, University of Missouri, Rolla, MO, *in press*
- [76] Verhagen, J. H. G., (1967), The impact of a flat plate on a water surface, *Journal of Ship research*, Vol. 11, No. 4, pp. 211-223
- [77] Von Karman, T., (1929), The impact of seaplane floats during landing, *NACA TN 321*
- [78] Wagner, H., (1931), Landing of seaplanes, *NACA TM 622*
- [79] Whitman, R. V., Protonotarios, J. N., and Nelson, M. F., (1973), Case study of dynamic soil-structure interaction, *Journal of Soil Mechanics Division*, ASCE, Vol. 99, No. SM11, pp. 997-1009
- [80] Whittaker, W. L., and Christiano, P., (1982), Dynamic response of plate on elastic half-space, *Journal of Engineering Mechanics*, ASCE, Vol. 108(1), pp. 133-154
- [81] Wong, H. L., Luco J. E., and Trifunac, M. D., (1977), Contact stresses and ground motion generated by soil-structure interaction, *Journal of Earthquake Engineering and Structural Dynamics*, Vol. 5, pp. 67-79
- [82] Yang, J. Y., (1976), Dynamic behavior of fluid-tank systems, Thesis presented to Rice University at Houston, Texas, in partial fulfillment of the requirements for the degree of Doctor of Philosophy
- [83] Yashiro, T., et al, (1987), A study on non-linear sloshing of pool type LMFBR coolant, *Proceedings, 9th International Conference on Structural Mechanics in Reactor Technology*, North-Holland, Vol. E, pp. 459-464
- [84] Yih, C. S., (1960), Gravity waves in a stratified fluid', *Journal of Fluid Mechanics*, Vol. 8, 481-508
- [85] Yih, C. S., (1980), *Stratified Flows*, Academic Press Inc., New York

## Appendix A

### Hydrodynamic Effects for Rigid Layered Systems

#### A.1 Derivation of Equation (4.12)

On substituting equations (3.24) and (4.5) for  $\{D_m(t)\}$  and  $\{\ddot{D}_m(t)\}$  into equation (3.28), one obtains

$$[\mathcal{A}] R \left( \sum_{n=1}^N \omega_{mn}^2 \{d_{mn}\} \right) \frac{\ddot{x}_g(t)}{g} - [\mathcal{A}] R \left( \sum_{n=1}^N \omega_{mn}^2 \{d_{mn}\} \frac{A_{mn}(t)}{g} \right) + [\mathcal{B}] \lambda_m g \left( \sum_{n=1}^N \{d_{mn}\} \frac{A_{mn}(t)}{g} \right) = \epsilon_m \lambda_m \{s\} \ddot{x}_g(t) \quad (\text{A.1})$$

which on further dividing through by  $\lambda_m$ , grouping the terms with similar temporal variations, and making use of equations (3.45) and (4.10), can be written in the form

$$\left( [\mathcal{A}] \{e_m\} - \epsilon_m \{s\} \right) \ddot{x}_g(t) = \sum_{n=1}^N \left( C_{mn}^2 [\mathcal{A}] \{d_{mn}\} - [\mathcal{B}] \{d_{mn}\} \right) A_{mn}(t) \quad (\text{A.2})$$

Since the temporal variations of the two members of the latter equation are different, the equation can hold true only if the terms in parentheses on either side of the equation are equal to zero. On equating the left-hand member to zero, one obtains equation (4.12), and on doing the same with each of the right-hand members, one obtains the additional relation,

$$C_{mn}^2 [\mathcal{A}] \{d_{mn}\} = [\mathcal{B}] \{d_{mn}\} \quad (\text{A.3})$$

#### A.2 Derivation of Equation (4.40)

From equation (4.9) and the expressions for the elements of the matrix  $[\mathcal{A}]$  given in Reference 1, the difference in the convective pressure coefficients across the  $j$ th interface may be written as

$$\left[ \frac{\rho_j}{\rho_1} c_{mn,j}(\alpha_j) - \frac{\rho_{j+1}}{\rho_1} c_{mn,j+1}(0) \right] = C_{mn}^2 \left[ \mathcal{A}_{j,j-1} d_{mn,j-1} + \mathcal{A}_{j,j} d_{mn,j} + \mathcal{A}_{j,j+1} d_{mn,j+1} \right] \quad (\text{A.4})$$

On applying equation (A.4) to each of the  $N$  interfaces and normalizing the results in the form of equation (4.38), the difference in the interfacial values of the convective pressure coefficients can be written in vectorial form as

$$\left\{ c_{mn}^- - c_{mn}^+ \right\} = C_{mn}^2 [\mathcal{A}] \{d_{mn}\} \quad (\text{A.5})$$

and, by virtue of equation (A.3), as

$$\left\{ c_{mn}^- - c_{mn}^+ \right\} = [\mathcal{B}] \{d_{mn}\} \quad (\text{A.6})$$

On summing the latter expression over  $n$ , making use of equation (3.54) and the fact that  $\text{diag}[\mathcal{B}] = \{s\}$ , one obtains the desired equation (4.40). Finally, on summing equation (4.40) over  $m$  and making use of equation (3.55), one obtains the additional relation

$$\sum_{m=1}^{\infty} \sum_{n=1}^N \left\{ c_{mn}^- - c_{mn}^+ \right\} = \{s\} \quad (\text{A.7})$$



## Appendix B

### Modal Masses for Flexible Layered Systems

The distribution of the layer densities and heights for the three-layered cantilever system under consideration is as shown in Fig. 5.1. Let  $\phi_j^i$  be the impulsive potential function for the  $j$  th liquid layer ( $j = 1, 2, 3$ ) when the tank vibrates in the  $i$  th assumed mode of vibration,  $\psi_i(z)$ .  $\phi_j^i$  must satisfy Laplace's equation,

$$\nabla^2 \phi_j^i = 0 \quad (\text{B.1})$$

and it is subjected to the following boundary conditions :

(1) Zero velocity at the tank base

$$\left( \frac{\partial \phi_1^i}{\partial z_1} \right)_{z_1=0} = 0 \quad (\text{B.2})$$

(2) Continuity of radial velocity at the tank-wall

$$\left( \frac{\partial \phi_j^i}{\partial r} \right)_{r=R} = -\dot{W}_i(t) \psi_i(z) \cos \theta \quad (\text{B.3})$$

where  $z$  is the vertical distance measured from the tank-base;  $\psi_i(z)$  is the  $i$  th assumed beam mode and  $\dot{W}_i(t)$  is the associated generalized velocity coordinate.

(3) Zero impulsive pressure at the mean liquid surface

$$\left( \dot{\phi}_3^i \right)_{z_3=H_3} = 0 \quad (\text{B.4})$$

(4) Continuity of vertical velocities at the  $j$  th interface; and

$$\left( \frac{\partial \phi_j^i}{\partial z_j} \right)_{z_j=H_j} = \left( \frac{\partial \phi_{j+1}^i}{\partial z_{j+1}} \right)_{z_{j+1}=0} \quad (\text{B.5})$$

(5) Continuity of impulsive pressures at the  $j$  th interface,

$$\rho_j \left( \dot{\phi}_j^i \right)_{z_j=H_j} = \rho_{j+1} \left( \dot{\phi}_{j+1}^i \right)_{z_{j+1}=0} \quad (\text{B.6})$$

The solution for  $\phi_j^i$  is conveniently obtained herein by expressing  $\phi_j^i$  as the superposition of two component solutions as

$$\phi_j^i = \phi_h^i + \phi_{rj}^i \quad (\text{B.7})$$

where  $\phi_h^i$  is a velocity potential function associated with the motion of the tank-walls and  $\phi_{rj}^i$  is a corresponding function providing for the relative motion of the contained liquid and the tank-walls. This superposition approach is different from that followed in [57] for the two-layered systems, wherein the equations for each layer are solved directly. It is believed that the present approach is more simple to implement and is more readily extended to the case of arbitrary number of liquid layers.

The solution for  $\phi_h^i$  has been previously derived by Yang in his studies for homogeneous systems, [82], and is given by

$$\phi_h^i(r, z, t) = -\dot{W}_i(t) R \cos\theta \sum_{n=1}^{\infty} \frac{2}{\alpha_n} \frac{I_1(\alpha_n r/R)}{I_1'(\alpha_n)} d_{in} \cos\left(\frac{\alpha_n z}{R}\right) \quad (\text{B.8})$$

where  $I_1$  is the modified Bessel function of the first kind and first order;  $I_1'$  is the first derivative of  $I_1$ ;  $\alpha_n$  and  $d_{in}$  are given by

$$\alpha_n = (2n - 1) \frac{\pi}{2} \frac{R}{H} \quad (\text{B.9})$$

and

$$d_{in} = \frac{1}{H} \int_0^1 \psi_i(z) \cos\left(\frac{\alpha_n z}{R}\right) dz \quad (\text{B.10})$$

respectively.

On solving Laplace's equation for  $\phi_{rj}^i$  and making use of the homogeneous boundary conditions along the walls,  $\phi_{rj}^i$  can be written as

$$\phi_{rj}^i(\xi, \eta_j, t) = \dot{W}_i(t) R \cos\theta \sum_{m=1}^{\infty} \left[ P_{m,j}^i \cosh \lambda_m \eta_j + Q_{m,j}^i \sinh \lambda_m \eta_j \right] J_1(\lambda_m \xi) \quad (\text{B.11})$$

in which  $\xi = r/R$ ;  $\eta_j = z_j/R$ ;  $J_1$  is the Bessel function of the first kind and first order;  $\lambda_m$  = the  $m$ th root of  $J_1' = 0$ ; and  $P_{m,j}^i$  and  $Q_{m,j}^i$  are constants of integration that need to be determined from the boundary conditions. For  $j = 3$ , this results in a total of 6 unknowns. On satisfying equations (B.2) and (B.4) and the two components of equation (B.5), four of these unknowns can be eliminated. Then, on replacing the constants  $P_{m,j}^i$  and  $Q_{m,j}^i$  ( $j=1,2,3$ ) by equivalent constants  $A_m^i$  and  $B_m^i$ , one obtains

$$\phi_{r1}^i(\xi, \eta_1, t) = \dot{W}_i(t) R \cos\theta \sum_{m=1}^{\infty} \left[ A_m^i \frac{\cosh \lambda_m \eta_1}{\sinh \lambda_m H_1/R} \right] \frac{J_1(\lambda_m \xi)}{J_1(\lambda_m)}$$

$$\begin{aligned}\phi_{r2}^i(\xi, \eta_2, t) &= -\dot{W}_i(t) R \cos\theta \sum_{m=1}^{\infty} \left[ A_m^i \frac{\cosh\lambda_m(H_2/R - \eta_2)}{\sinh\lambda_m H_2/R} + B_m^i \frac{\cosh\lambda_m \eta_2}{\sinh\lambda_m H_2/R} \right] \frac{J_1(\lambda_m \xi)}{J_1(\lambda_m)} \\ \phi_{r3}^i(\xi, \eta_3, t) &= \dot{W}_i(t) R \cos\theta \sum_{m=1}^{\infty} \left[ B_m^i \frac{\sinh\lambda_m(H_3/R - \eta_3)}{\cosh\lambda_m H_3/R} \right] \frac{J_1(\lambda_m \xi)}{J_1(\lambda_m)}\end{aligned}\quad (\text{B.12})$$

The constants  $A_m^i$  and  $B_m^i$  are then evaluated by satisfying equation (B.6) at the two interfaces  $j = 1$  and  $j = 2$ . On substituting equations (B.7) and (B.8) into equation (B.6), multiplying through by  $\xi J_1(\lambda_m \xi) d\xi$ , integrating from 0 to 1, and making use of the relations

$$\int_0^1 \xi J_1^2(\lambda_m \xi) d\xi = \frac{\lambda_m^2 - 1}{2\lambda_m^2} J_1^2(\lambda_m) \quad \int_0^1 \xi J_1(\lambda_m \xi) I_1(\alpha_n \xi) d\xi = \frac{\alpha_n J_1(\lambda_m) I_1'(\alpha_n)}{\lambda_m^2 + \alpha_n^2} \quad (\text{B.13})$$

the resulting system of equations for  $A_m^i$  and  $B_m^i$  can be written in the form,

$$\begin{bmatrix} \frac{1}{\tanh\lambda_m H_1/R} + \frac{\rho_2/\rho_1}{\tanh\lambda_m H_2/R} & \frac{\rho_2/\rho_1}{\sinh\lambda_m H_2/R} \\ \frac{\rho_2/\rho_1}{\sinh\lambda_m H_2/R} & \frac{\rho_2/\rho_1}{\tanh\lambda_m H_2/R} + \rho_3/\rho_1 \tanh\lambda_m H_3/R \end{bmatrix} \begin{bmatrix} A_m^i \\ B_m^i \end{bmatrix} = \begin{bmatrix} X_m^i \\ Y_m^i \end{bmatrix} \quad (\text{B.14})$$

where

$$\begin{aligned}X_m^i &= \frac{2}{\lambda_m^2 - 1} \left( \frac{\rho_2}{\rho_1} - 1 \right) \sum_{n=1}^{\infty} \frac{2 d_{in} \cos\alpha_n H_1/R}{1 + \alpha_n^2/\lambda_m^2} \\ Y_m^i &= \frac{2}{\lambda_m^2 - 1} \left( \frac{\rho_2}{\rho_1} - \frac{\rho_3}{\rho_1} \right) \sum_{n=1}^{\infty} \frac{2 d_{in} \cos\alpha_n (H_1 + H_2)/R}{1 + \alpha_n^2/\lambda_m^2}\end{aligned}\quad (\text{B.15})$$

Solving for  $A_m^i$  and  $B_m^i$  from equation (B.14) and substituting in equation (B.12), one obtains  $\phi_{rj}^i$  ( $j=1,2,3$ ).

With the potential functions established, the participating modal mass can be computed by determining the kinetic energy of the liquid. The kinetic energy for the  $j$ th liquid layer,  $T_j$ , can be written as

$$T_j = -\frac{\rho_j}{2} \int_{S_j} \sum_{i=1}^{N_3} \phi_j^i \sum_{k=1}^{N_3} \frac{\partial \phi_j^k}{\partial n} dS_j \quad (\text{B.16})$$

where  $S_j$  refers to the bounding surfaces for the  $j$ th layer;  $\phi_j^i$  is given by equation (B.7); and  $\partial \phi_j^k / \partial n$  is the derivative of  $\phi_j^k$  in a direction normal to the boundary of the liquid.

In equation (B.16), it is not necessary to compute the energy components associated with the two bounding interfaces  $j-1$  and  $j$ . This follows from the fact that

the energy components associated with two adjacent layers along their common interface are of equal but opposite magnitudes (the interfacial pressures and velocities are equal but the normals are in opposite directions) and therefore cancel out each other. Furthermore, the components corresponding to the tank bottom and the mean liquid surface are zero. It follows that in order to compute the total kinetic energy, it is only necessary to compute the kinetic energy components associated with the wall of the tank.

The kinetic energy associated with the wall of the tank for the  $j$ th layer is evaluated by substituting equations (B.7), (B.8) and the appropriate component of (B.12) into equation (B.16). The total kinetic energy of the system,  $T$ , can then be expressed in the form

$$T = \sum_{j=1}^3 T_j = \frac{1}{2} \sum_{i=1}^{N_3} \sum_{k=1}^{N_3} m_{ik} \dot{W}_i \dot{W}_k \quad (\text{B.17})$$

where  $m_{ik}$  is the virtual mass of the layered liquid corresponding to the deflection functions  $\psi_i(z)$  and  $\psi_k(z)$ . It is expressed as a sum of the modal mass components for the individual liquid layers,

$$m_{ik} = \sum_{j=1}^3 m_{ik,j} = \sum_{j=1}^3 \rho_j \int_0^{H_j} \int_0^{2\pi} \left( \frac{\phi_h^i + \phi_{rj}^i}{\dot{W}_i} \right) \psi_k(z) \cos\theta R d\theta dz_j \quad (\text{B.18})$$

## Appendix C

### Vertically Excited Systems with Flexible Base

#### C.1 Velocity potential function $\phi$

$\phi$  is given by the solution of Laplace's equation

$$\nabla^2 \phi = 0 \quad (\text{C.1})$$

where, for the axisymmetric problem considered,

$$\nabla^2 = \frac{\partial^2}{\partial r^2} + \frac{1}{r} \frac{\partial}{\partial r} + \frac{\partial^2}{\partial z^2} \quad (\text{C.2})$$

The solution of equation (C.1) must satisfy the following boundary conditions :  
At the tank-base,

$$\left( \frac{\partial \phi}{\partial z} \right)_{z=0} = -\dot{w}(\xi, t) = -\dot{w}_0(t) - \sum_{n=1}^N \dot{w}_n(t) \psi_n(\xi) \quad (\text{C.3})$$

At the tank walls, the radial velocity must vanish (since the walls have been assumed to be rigid),

$$\left( \frac{\partial \phi}{\partial r} \right)_{r=R} = 0 \quad (\text{C.4})$$

and at the free-surface,

$$(\phi)_{z=H} = 0 \quad (\text{C.5})$$

where any sloshing action is implicitly neglected.

The solution of equation (C.1) is conveniently written in the form

$$\phi = \phi_0 + \sum_{n=1}^N \phi_n \quad (\text{C.6})$$

where  $\phi_0$  is associated with the relative rigid-body motion of the base plate and  $\phi_n$  is associated with the  $n$ th assumed mode of vibration of the base plate. It is clear that  $\phi_0$  is given by

$$\phi_0 = \dot{w}_0(t)(H - z) \quad (\text{C.7})$$

The solution for  $\phi_n$  is obtained by separation of variables,

$$\phi_n = \tilde{R}_n(r) \tilde{Z}_n(z) T(t) \quad (\text{C.8})$$

in which  $\tilde{R}$ ,  $\tilde{Z}$  and  $T$  are functions of  $r$ ,  $z$  and  $t$  respectively. On substituting equation (C.8) into equation (C.1), equating the expressions in  $r$  and  $z$  to  $-\lambda^2/R^2$  and  $+\lambda^2/R^2$  respectively, making use of the homogeneous boundary conditions along the walls and at the free-surface (equations (C.4) and (C.5) respectively), one obtains

$$\phi_n = A_{n0}(t)(H-z) + \sum_{m=1}^{\infty} A_{nm}(t) J_0(\lambda_m \xi) \sinh \frac{\lambda_m(H-z)}{R} \quad (\text{C.9})$$

where  $\xi = r/R$ ;  $\lambda_m$  is the  $m$ th root of  $J'_0(\lambda) = -J_1(\lambda) = 0$ . The first three of these roots are

$$\lambda_1 = 3.832 \quad \lambda_2 = 7.016 \quad \lambda_3 = 10.173 \quad (\text{C.10})$$

On solving for the unknown coefficients in equation (C.9) by putting  $(\partial\phi_n/\partial z)_{z=0} = -\dot{w}_n(t)\psi_n(\xi)$ , ( $n$ th component of equation C.3), one obtains

$$\phi_n = \dot{w}_n(t) \left[ 2e_n(H-z) + R \sum_{m=1}^{\infty} \frac{2d_{nm}}{\lambda_m} \frac{J_0(\lambda_m \xi)}{J_0^2(\lambda_m)} \frac{\sinh \lambda_m(H-z)/R}{\cosh \lambda_m H/R} \right] \quad (\text{C.11})$$

where  $e_n = \int_0^1 \psi_n(\xi) \xi d\xi$  and  $d_{nm} = \int_0^1 \psi_n(\xi) J_0(\lambda_m \xi) \xi d\xi$ . For the hinged and fixed conditions considered herein, these expressions are evaluated to be

$$e_n^h = \frac{J_1(\alpha_n^h)}{\alpha_n^h} \quad e_n^f = \frac{2J_1(\alpha_n^f)}{\alpha_n^f J_0(\alpha_n^f)} \quad (\text{C.12})$$

$$d_{nm}^h = \frac{\alpha_n^h J_0(\lambda_m) J_1(\alpha_n^h)}{(\alpha_n^h)^2 - \lambda_m^2} \quad d_{nm}^f = \frac{\alpha_n^f J_0(\lambda_m) J_1(\alpha_n^f)}{J_0(\alpha_n^f)} \left[ \frac{1}{(\alpha_n^f)^2 - \lambda_m^2} + \frac{1}{(\alpha_n^f)^2 + \lambda_m^2} \right] \quad (\text{C.13})$$

## C.2 Kinetic Energy

With the potential function  $\phi$  established,  $T_l$  can be computed from equation (7.12), where  $S$  refers to the surfaces of the base-plate, tank-walls and the free-surface of the liquid. This computation is further simplified by the fact that either  $\phi$  or  $\partial\phi/\partial n$  are zero for all surfaces except the base plate. On substituting for  $\phi$  and  $\partial\phi/\partial z$  at  $z = 0$ , one obtains

$$T_l = m_l \int_0^1 \left[ \dot{w}_0(t) + \sum_{n=1}^N \dot{w}_n(t) \left\{ 2e_n + \frac{R}{H} \sum_{m=1}^{\infty} \frac{2d_{nm}}{\lambda_m} \frac{J_0(\lambda_m \xi)}{J_0^2(\lambda_m)} \tanh \frac{\lambda_m H}{R} \right\} \right] \left[ \dot{w}_0(t) + \sum_{n=1}^N \dot{w}_n(t) \psi_n(\xi) \right] \xi d\xi \quad (\text{C.14})$$

### C.3 Free Vibration of Equivalent Plate : Exact Solution

The governing differential equation for the elastically supported equivalent plate is written as

$$D_p \left( \frac{1}{r} \frac{d}{dr} \left[ r \frac{d}{dr} \left\{ \frac{1}{r} \frac{d}{dr} \left( r \frac{dw}{dr} \right) \right\} \right] \right) + kw + \rho_p' \ddot{w} = 0 \quad (\text{C.15})$$

where  $\rho_p'$  is the equivalent mass density incorporating the effect of the original plate and the liquid. On assuming an exponential time variation for  $w$  and on suitably normalizing the above equation, one obtains

$$\frac{1}{\xi} \frac{d}{d\xi} \left[ \xi \frac{d}{d\xi} \left\{ \frac{1}{\xi} \frac{d}{d\xi} \left( \xi \frac{dw^*}{d\xi} \right) \right\} \right] = k^* [(C^*)^2 - 1] w^* \quad (\text{C.16})$$

where  $\xi = r/R$ ;  $w^* = w/R$ ;  $k^* = kR^4/D_p$ ; and  $(C^*)^2 = \omega^2 \rho_p'/k$  is a frequency coefficient. It should be noted that  $C^*$  differs from the coefficient  $C$  defined in equation (7.29). They are related by

$$C^2 = (C^*)^2 [1 - \beta_{em}] \quad (\text{C.17})$$

The boundary conditions for the normalized problem are as follows : At the center of the plate,

$$w^*|_{\xi=0} \text{ is finite } \quad \left. \frac{dw^*}{d\xi} \right|_{\xi=0} = 0 \quad (\text{C.18})$$

At the edge of the plate, the zero-shear condition is given by

$$\left. \frac{d^3 w^*}{d\xi^3} + \frac{1}{\xi} \frac{d^2 w^*}{d\xi^2} - \frac{1}{\xi^2} \frac{dw^*}{d\xi} + \frac{\beta_{em} k^* (C^*)^2 w^*}{2} \right|_{\xi=1} = 0 \quad (\text{C.19})$$

The second boundary condition at the plate edge depends on the edge-support condition. For the hinged case, the boundary condition is the condition of zero moment,

$$\left. \frac{d^2 w^*}{d\xi^2} + \nu_p \frac{1}{\xi} \frac{dw^*}{d\xi} \right|_{\xi=1} = 0 \quad (\text{C.20})$$

while for the fixed case, the boundary condition is the condition of zero slope,

$$\left. \frac{dw^*}{d\xi} \right|_{\xi=1} = 0 \quad (\text{C.21})$$

The solution to equation (C.16) depends on whether  $(C^*)^2$  is less than 1 or greater than 1.

### C.3.1 Case 1 : $(C^*)^2 < 1$

Following the procedure outlined in [62], the general solution for equation (C.16) is written as

$$w^* = D_1 ber(\epsilon\xi) + D_2 bei(\epsilon\xi) + D_3 ker(\epsilon\xi) + D_4 kei(\epsilon\xi) \quad (C.22)$$

where  $\epsilon$  is related to the natural frequency coefficient through the expression

$$\epsilon^4 = k^* \left( 1 - (C^*)^2 \right) \quad (C.23)$$

On making use of the boundary conditions at  $\xi = 0$ , one obtains

$$w^* = D_1 ber(\epsilon\xi) + D_2 bei(\epsilon\xi) \quad (C.24)$$

*Hinged Support* : On substituting the above expression into equations (C.19) and (C.20), two equations in  $D_1$  and  $D_2$  are obtained for the hinged case and are written as follows :

$$\begin{bmatrix} \epsilon ber'' + \nu_p ber' & \epsilon bei'' + \nu_p bei' \\ \epsilon^3 ber''' + \epsilon^2 ber'' - \epsilon ber' & \epsilon^3 bei''' + \epsilon^2 bei'' - \epsilon bei' \\ +\beta_{em} \frac{(k^* - \epsilon^4)}{2} ber & +\beta_{em} \frac{(k^* - \epsilon^4)}{2} bei \end{bmatrix} \begin{Bmatrix} D_1 \\ D_2 \end{Bmatrix} = \begin{Bmatrix} 0 \\ 0 \end{Bmatrix} \quad (C.25)$$

*Fixed Support* : The corresponding equations for the fixed case are obtained by substituting equation (C.24) into equations (C.19) and (C.21) and are written as :

$$\begin{bmatrix} ber' & bei' \\ \epsilon^3 ber''' + \epsilon^2 ber'' - \epsilon ber' & \epsilon^3 bei''' + \epsilon^2 bei'' - \epsilon bei' \\ +\beta_{em} \frac{(k^* - \epsilon^4)}{2} ber & +\beta_{em} \frac{(k^* - \epsilon^4)}{2} bei \end{bmatrix} \begin{Bmatrix} D_1 \\ D_2 \end{Bmatrix} = \begin{Bmatrix} 0 \\ 0 \end{Bmatrix} \quad (C.26)$$

In equations (C.25) and (C.26), the prime notation denotes differentiation with respect to  $\xi$ , and all functions and their derivatives are evaluated at  $\epsilon$ .

To avoid a trivial solution, the determinant of the coefficients in equations (C.25) and (C.26) must each equal zero. A single root for  $\epsilon$  is then obtained from the resulting equation by trial and error. With  $\epsilon$  determined, the fundamental frequency coefficient  $C_1^*$  can be determined from equation (C.23).

### C.3.2 Case II : $(C^*)^2 > 1$

In this case, the general solution for equation (C.16) can be written as

$$w^* = D_1 J_0(\epsilon\xi) + D_2 I_0(\epsilon\xi) + D_3 K_0(\epsilon\xi) + D_4 Y_0(\epsilon\xi) \quad (C.27)$$



where  $\epsilon$  is related to the natural frequency coefficient through the expression

$$\epsilon^4 = k^* \left( (C^*)^2 - 1 \right) \quad (\text{C.28})$$

On making use of the boundary conditions at  $\xi = 0$ , one obtains

$$w^* = D_1 J_0(\epsilon \xi) + D_2 I_0(\epsilon \xi) \quad (\text{C.29})$$

The solution procedure then follows that shown for Case I and matrix expressions similar to equations (C.25) and (C.26) can be written for the hinged and fixed cases with  $J_0$  and  $I_0$  functions replacing the *ber* and *bei* functions respectively. Several roots for  $\epsilon$  can then be evaluated for each of the determinant equations. The corresponding frequency coefficients for the second mode of vibration are then determined from equation (C.28). The lowest of these frequency coefficients corresponds to the second mode of vibration.

## Appendix D

### Effects of Roof-Liquid Impact

#### D.1 Background Information

For a general liquid-solid impact, if the impact is assumed to occur in a very short time and is therefore considered to be an impulse, the linearized boundary condition along the free-liquid surface can be written as  $\Phi = 0$ , where  $\Phi$  is the potential function induced in the liquid. Then, on using the symmetry property offered by the  $\Phi = 0$  surface, a section that is partially immersed in the liquid can be completed by adding its reflection in the free surface and then allowing the liquid to flow past the completed section. This approach, which was originally proposed by Von Karman [77] and refined by Wagner [78], can be used to evaluate the wetting correction factor as well as the virtual liquid mass that participates in the impacting action.

For the roof-liquid impact problem considered herein, using the principles outlined above, a liquid of uniform velocity  $v_{av}(t)$  is presumed to flow past a lamina of instantaneous length  $c(t)$  sticking out of a straight wall. For this lamina shape, the associated potential function can be conveniently determined by the method of conformal transformations, [43, 50]. The expression for  $\Phi$  along the surface of the lamina is given by

$$\Phi = v_{av}(t)\sqrt{c(t)^2 - X^2} \quad (\text{D.1})$$

and the associated velocity in a direction normal to the lamina is given by

$$v(t) = -\frac{\partial\Phi}{\partial Y} = \frac{v_{av}(t)}{\sqrt{1 - c^2/X^2}} \quad (\text{D.2})$$

where  $X$  and  $Y$  are the distance coordinates along and normal to the lamina respectively.

It should be noted that the model outlined above is approximate since the effects of the base plate of the tank and of the far-wall have not been incorporated. However, while these constraining boundaries will increase the participating liquid mass, the effects are negligibly small for realistic tank dimensions, (see [61, 64] for related information).

## D.2 Wetting Correction Factor

The wetting correction factor at the initial stages of impact,  $w_o$ , can be determined by evaluating the instantaneous vertical displacement induced on introducing the lamina into the liquid moving at a velocity  $v_o$ .

This displacement,  $\eta(X, t)$ , can be evaluated from the time integral of the velocity given by equation (D.2), which at the initial stages of impact, is written as

$$\eta(X, t) = \int_0^t \frac{v_o}{\sqrt{1 - c(\tau)^2/X^2}} d\tau = \int_0^{c(t)} \frac{v_o}{\sqrt{1 - c(\tau)^2/X^2}} \frac{d\tau}{dc(\tau)} dc(\tau) \quad (D.3)$$

The surface displacement at the edge of the lamina is then obtained by putting  $X = c(t)$  into the above expression

$$\eta(c(t), t) = \int_0^{c(t)} \frac{v_o}{\sqrt{1 - c(\tau)^2/c(t)^2}} \frac{\partial \tau}{\partial c(\tau)} dc(\tau) \quad (D.4)$$

where  $\partial c(\tau)/\partial \tau$  is evaluated by differentiating equation (8.15) with respect to time. At the initial stages of impact, one obtains

$$\frac{\partial c(\tau)}{\partial \tau} = w_o \frac{\partial c_o(\tau)}{\partial \tau} \quad (D.5)$$

where  $\partial c_o(\tau)/\partial \tau$  is evaluated by differentiating equation (8.14) with respect to time,

$$\frac{\partial c_o(\tau)}{\partial \tau} = \frac{2R}{\pi} \frac{v_w(\tau)}{d_w(\tau) \tan \pi c_o(\tau)/2R} \quad (D.6)$$

which, for the initial stages of impact, can be written as

$$\frac{\partial c_o(\tau)}{\partial \tau} = \frac{4R^2}{\pi^2} \frac{v_o}{d_o c_o(\tau)} \quad (D.7)$$

On substituting equation (D.7) into equation (D.5), and the resulting expression into equation (D.4), one obtains

$$\eta(c(t), t) = \frac{1}{w_o^2} \frac{\pi^2 d_o}{4R^2} \int_0^{c(t)} \frac{c(\tau)}{\sqrt{1 - c(\tau)^2/c(t)^2}} dc(\tau) = \frac{1}{w_o^2} \frac{\pi^2 d_o c(t)^2}{4R^2} \quad (D.8)$$

Alternatively, the surface displacement at the edge of the lamina can also be evaluated from the relation

$$\eta(c(t), t) = d_o - d(c(t), t) \quad (D.9)$$

and for initial stages of impact, this can be written in the form

$$\eta(c(t), t) \approx d_o \left( 1 - \cos \frac{\pi c(t)}{2R} \right) \approx \frac{\pi^2 d_o c(t)^2}{8R^2} \quad (\text{D.10})$$

From equations (D.8) and (D.10), it follows that

$$w_o = \sqrt{2} \quad (\text{D.11})$$

### D.3 Virtual Liquid Mass

The virtual liquid mass that participates in the impact is evaluated by determining the additional kinetic energy that is induced by introducing the lamina of length  $c(t)$  into the flow,

$$T = \frac{\rho_l}{2} \int_0^{c(t)} \Phi \frac{\partial \Phi}{\partial Y} dX \quad (\text{D.12})$$

On substituting for  $\Phi$  from equation (D.1), putting  $\partial \Phi / \partial Y = v_{av}(t)$  within the region of the lamina, and integrating, one obtains

$$T = \rho_l \frac{\pi}{8} c(t)^2 v_{av}(t)^2 \quad (\text{D.13})$$

On expressing  $T$  in the form  $T = \frac{1}{2} m(t) v_{av}(t)^2$ , it follows that

$$m(t) = \rho_l \frac{\pi}{4} c(t)^2 \quad (\text{D.14})$$

### D.4 Wall Pressures

#### D.4.1 Rectangular Tanks

Let  $\phi(x, y, t)$  be the velocity potential function induced in the tank due to the impact of the liquid against the roof. It should be noted that  $\phi$  will incorporate the effects of the conditions along the boundaries of the tank and is therefore different from the  $\Phi$  function defined for the lamina. The function  $\phi$  satisfies Laplace's equation,

$$\nabla^2 \phi = 0 \quad (\text{D.15})$$

and is related to the impact pressure by

$$p(x, y, t) = \rho_l \frac{\partial \phi}{\partial t} \quad (\text{D.16})$$

The boundary conditions to be satisfied by  $\phi$  are : (1) the velocity at the tank walls must be zero

$$\left. \frac{\partial \phi}{\partial x} \right|_{x=-R, R} = 0 \quad (\text{D.17})$$

(2) the velocity at the tank base must be zero, and

$$\left. \frac{\partial \phi}{\partial y} \right|_{y=0} = 0 \quad (\text{D.18})$$

(3) the condition at the top is

$$\begin{aligned} \left. \frac{\partial \phi}{\partial y} \right|_{y=H} &= v_{av}(t) \quad \text{for} \quad R - c(t) \leq x \leq R \\ \left. \frac{\partial \phi}{\partial t} \right|_{y=H} &= 0 \quad \text{for} \quad -R \leq x < R - c(t) \end{aligned} \quad (\text{D.19})$$

Any free-surface deformations in the non-impacted portion are implicitly ignored in the second part of equation (D.19). Furthermore, it is seen that the first part is a velocity condition while the second part is a pressure condition. This mixed-boundary value problem can be considerably simplified by using the previously established average pressure over the impacted portion. Equation (D.19) is therefore rewritten in the form,

$$\begin{aligned} \left. \frac{\partial \phi}{\partial t} \right|_{y=H} &= \frac{p_r(t)}{\rho_l} \quad \text{for} \quad R - c(t) \leq x \leq R \\ \left. \frac{\partial \phi}{\partial t} \right|_{y=H} &= 0 \quad \text{for} \quad -R \leq x < R - c(t) \end{aligned} \quad (\text{D.20})$$

where  $p_r(t)$ , the average roof impact pressure, is given by equation (8.29).

On separating the variables of  $x$  and  $y$ , substituting in equation (D.15) and satisfying equations (D.17) and (D.18), the solution for  $\phi$  is given by

$$\phi(x, y, t) = \sum_{n=0}^{\infty} B_n(t) \frac{\cosh(n\pi y/2R)}{\cosh(n\pi H/2R)} \cos \frac{n\pi(x-R)}{2R} \quad (\text{D.21})$$

where  $B_n(t)$  are arbitrary functions of time. On determining them by satisfying equation (D.20), the hydrodynamic impact pressure at any point and time can be written in the form

$$p(x, y, t) = p_r(t) \left[ \frac{c(t)}{2R} + \sum_{n=1}^{\infty} \frac{2}{n\pi} \frac{\cosh(n\pi y/2R)}{\cosh(n\pi H/2R)} \sin \frac{n\pi c(t)}{2R} \cos \frac{n\pi(x-R)}{2R} \right] \quad (\text{D.22})$$

### D.4.2 Cylindrical Tanks

Let  $\phi(r, \theta, z, t)$  be the velocity potential function induced in the cylindrical tank due to the impact of the liquid against the roof. The function  $\phi$  satisfies Laplace's equation and the boundary conditions are : (1) the velocity at the tank walls must be zero

$$\left. \frac{\partial \phi}{\partial r} \right|_{r=R} = 0 \quad (D.23)$$

(2) the velocity at the tank base must be zero, and

$$\left. \frac{\partial \phi}{\partial z} \right|_{z=0} = 0 \quad (D.24)$$

(3) the condition at the top is written as

$$\begin{aligned} \left. \frac{\partial \phi}{\partial t} \right|_{z=H} &= \frac{p_r(t)}{\rho_l} \cos \theta \quad \text{for} \quad R - c(\theta, t) \leq r \leq R; \quad -\theta_o(t) \leq \theta \leq \theta_o(t) \\ \left. \frac{\partial \phi}{\partial t} \right|_{z=H} &= 0 \quad \text{for} \quad r < R - c(\theta, t); \quad -\theta_o(t) \leq \theta \leq \theta_o(t) \\ \left. \frac{\partial \phi}{\partial t} \right|_{z=H} &= 0 \quad \text{for} \quad r \leq R; \quad \theta > |\theta_o(t)| \end{aligned} \quad (D.25)$$

where  $p_r(t)$  is taken to be the roof pressure evaluated for the two-dimensional case and is given by equation (8.29).

On separating the variables of  $r, z$  and  $\theta$ , substituting into Laplace's equation and satisfying equations (D.23) and (D.24), the solution for  $\phi$  can be written as

$$\phi = \sum_{n=0}^{\infty} \sum_{m=1}^{\infty} B_{mn}(t) \frac{J_n(\beta_{mn}\xi)}{J_n(\beta_{mn})} \frac{\cosh(\beta_{mn}z/R)}{\cosh(\beta_{mn}H/R)} \cos n\theta \quad (D.26)$$

where  $\xi = r/R$ ;  $J_n$  is the Bessel function of the first kind and the  $n$ th order; and  $\beta_{mn}$  is the  $m$ th zero of  $J'_n(\beta) = 0$ .  $B_{mn}(t)$  are determined by satisfying equation (D.25). On multiplying through by  $\xi J_n(\beta_{mn}\xi) \cos n\theta d\xi d\theta$ , integrating from 0 to 1 for  $\xi$  and from 0 to  $2\pi$  for  $\theta$ , and making use of the orthogonality properties of the Bessel functions and of the cosine functions, one obtains

$$\begin{aligned} p(r, \theta, t) &= \frac{p_r(t)}{\pi} \left[ \sum_{m=1}^{\infty} d_{m0}(t) \frac{J_0(\beta_{m0}\xi)}{J_0(\beta_{m0})^2} \frac{\cosh \beta_{m0}z/R}{\cosh \beta_{m0}H/R} + \right. \\ &\quad \left. \sum_{n=1}^{\infty} \sum_{m=1}^{\infty} \frac{2\beta_{mn}^2}{\beta_{mn}^2 - n^2} d_{mn}(t) \frac{J_n(\beta_{mn}\xi)}{J_n(\beta_{mn})^2} \frac{\cosh \beta_{mn}z/R}{\cosh \beta_{mn}H/R} \cos n\theta \right] \end{aligned} \quad (D.27)$$

where  $d_{mn}(t)$  for  $n = 0, \dots, \infty$  is given by

$$d_{mn}(t) = \int_{-\theta_o(t)}^{\theta_o(t)} \int_{1-c(t)/R}^1 \xi J_n(\beta_{mn}\xi) \cos n\theta \cos \theta d\xi d\theta \quad (\text{D.28})$$